Presynaptic AMPA receptor-mediated modulation of GABA release from cerebellar molecular layer interneurons

Mark Rigby

Department of Neuroscience, Physiology & Pharmacology
University College London
2013

Thesis is submitted for the degree of Doctor of Philosophy

Abstract

Presynaptic ionotropic glutamate receptors that modulate neurotransmitter release are widespread in the central nervous system, yet their regulation and mechanism of action are poorly understood. Indeed, their presumed dependence on transmembrane auxiliary proteins, which profoundly shape the behaviour of somatodendritic receptors, is an open question. The trafficking and function of postsynaptic α-amino-3-hydroxy-5-methyl-4-isoxazole propionic acid-type glutamate receptors (AMPARs) is regulated by transmembrane AMPAR regulatory proteins (TARPs). I examined the role of TARPs at presynaptic sites in cerebellar molecular layer interneurons (MLIs). The reduction in evoked GABA release triggered by glutamate spillover from climbing fibres, and the increased quantal release following AMPA application, were markedly attenuated in *stargazer* mice lacking the prototypical TARP stargazin (γ-2). 6-cyano-7-nitroquinoxaline-2,3-dione (CNQX), a partial agonist at TARP-associated AMPARs, had comparable effects on release that were also abolished in *stargazer* mice. These findings were replicated in dissociated Purkinje cells with adherent synaptic boutons, demonstrating the presynaptic locus of modulation. The absence of AMPAR-mediated effects in recordings from *stargazer* dissociated Purkinje cells, suggests that presynaptic AMPARs do not function without γ-2-association. This contrasts to postsynaptic and extrasynaptic AMPARs in MLIs that can function TARPless, or in association with TARP γ-7, respectively. Mechanistically, presynaptic AMPARs predominantly modulate release through regulation of voltage-gated Ca^{2+} channels (VGCCs). Pre-incubation of acutely dissociated Purkinje cells with either the specific VGCC blocker ω-Agatoxin-IVA, or the slow binding Ca^{2+} chelator, ethylene glycol-bis(2-aminoethylether)-N,N,′,N′-tetraacetic acid (EGTA), revealed that AMPARs mainly regulate the activity of P/Q- and/or N-type VGCCs coupled to the active zone in the microdomain. In addition, treatment with the Ca^{2+}-permeable AMPAR blocker, philanthotoxin-433, suggested that direct Ca^{2+} influx through the AMPAR channel may further contribute to effects on release at MLI – MLI boutons. My findings identify γ-2 as a crucial subunit for presynaptic AMPAR-mediated modulation of GABA release that occurs via regulation of VGCCs remote from active zones.

Declaration

I, Mark Rigby confirm that the work presented in this thesis is my own. Where information has been derived from other sources, I confirm that this has been indicated in the thesis.

Signed:

October 1, 2013

Acknowledgements

I would like to express my sincere gratitude to Professor Mark Farrant for his excellent guidance during my PhD. I have hugely benefited from his expertise in electrophysiological recordings.

My thanks to Professor Stuart Cull-Candy for his advice and support, I have valued his encouragement enormously.

I have had the great pleasure to work with many members of the Farrant and Cull-Candy laboratory who, by generously giving their time and assistance, have significantly contributed to my training. Dr Cécile Bats, Dr Jolenta Cheung, Dr Ian Coombs, Dr Rebecca Jones, Karolina Krol, Dr Tommy McGee, Dr Elizabeth Needham, Julia Oyrer, Dr Massimiliano Renzi, Dr Chris Shelley, Dr David Soto, Dorota Studniarczyk, Dr Steve Sullivan and Dr Marzieh Zonouzi, have all left their inimitable mark with me. I have thoroughly enjoyed their company.

Beyond the lab, many people have been extremely helpful. I would like to thank Dr Guy Moss, Dr David Benton and Dr Alan Robertson for advice on vibrodissociation, Dr Matthew Caldwell for his support with culturing cerebellar interneurons, Professor Tomoyuki Takahashi for his insightful comments on my data, Dr James Muir for his advice on antibodies, Dr Emmanuelle Chaigneau for her time and patience during collaborative experiments and Sahiba Chadha for her help with layouts and images.

Finally I would like to thank Professor David Attwell, Dr Alasdair Gibb, Professor Josef Kittler and Professor Patricia Salinas for their comments of the early PhD plan, and for their pastoral care throughout my 4 years.

The studies described in this thesis were conducted with funding from a Wellcome Trust 4 year studentship.

Contents

List of Figures

List of Tables

List of Abbreviations

Anatomy

CA1	Cornu Ammonis region 1
CA3	Cornu Ammonis region 3
CNS	Central nervous system
ER	Endoplasmic reticulum
MF	Mossy fibre
MLI	Molecular layer interneuron
NMJ	Neuro-muscular junction
SON	Supraoptic nucleus

Measures

µA	Microamp
µm	Micrometre
µM	Micromolar
µs	Microsecond
CV	Coefficient of variation
GΩ	Gigaohm
Hz	Hertz
EPP	Excitatory postsynaptic potential
EPSC	Excitatory postsynaptic current
IPSC	Inhibitory postsynaptic current
kDa	Kilodalton
kHz	Kilohertz
MΩ	Megaohm
mbar	Millibar
mm	Millimetre
mM	Millimolar

ms	Millisecond
mV	Millivolt
mEPP	Miniature excitatory postsynaptic potentials
mEPSC	Miniature excitatory postsynaptic currents
mIPSC	Miniature inhibitory postsynaptic current
mPSC	Miniature postsynaptic current
min	Minute
mOsmol/l	Number of osmoles per litre
n	Number of experiments
nA	Nanoampere
nm	Nanometre
P	Postnatal day
P	Probability
PPR	Paired-pulse ratio
pA	Picoampere
pC	Picocoulombs
pS	Picosiemens
pre-mIPSC	Presynaptic-miniature inhibitory postsynaptic current
r_s	Spearman's rank correlation coefficient
s	Second
SEM	Standard error of the mean
sIPSC	Spontaneous inhibitory postsynaptic current
V	Volts
X	Magnification

Miscellaneous

CICR	Calcium induced calcium release
DIANA	Divisive cluster analysis
GTP	Guanosine triphosphate
I_h	Hyperpolarisation-activated current
IP_3	Inositol trisphosphate
LTD	Long term depression

LTR	Long terminal repeats
mRNA	Messenger ribonucleic acid
RNA	Ribonucleic acid

Reagents

ACh	Acetylcholine
Agatoxin	ω-Agatoxin-IVA
AM	Acetoxymethyl etser
AMPA	α-amino-3-hydroxy-5-methyl-4-isoxazole propionic acid
BAPTA	1,2-bis(o-aminophenoxy) ethane-N,N,N′,N′-tetraacetic acid
BAPTA-AM	1,2-bis(o-aminophenoxy) ethane-N,N,N′,N′-tetraacetic acid acetoxymethyl ester
Ca^{2+}	Calcium
$CaCl_2$	Calcium chloride
Cd^{2+}	Cadmium
$CdCl_2$	Cadmium chloride
CGP 55845	(2S)-3-[[(1S)-1-(3,4-dichloro phenyl)ethyl]amino-2-hydroxypropyl] (phenylmethyl) phosphinic acid hydrochloride
CNQX	6-cyano-7-nitroquinoxaline-2,3-dione
CO_2	Carbon dioxide
CsOH	Cesium hydroxide
Cyclothiazide	6-chloro-3,4-dihydro-3-(2-norbornen-5-yl)-2H-1,2-4-benzothiadiazine-7-sulfonamide 1,1-dioxide
D-APV	D-(-)-2-Amino-5-phosphono pentanoic acid
EGTA	Ethylene glycol-bis(2-aminoethylether)-N,N,N′,N′- tetraacetic acid
EGTA-AM	Ethylene glycol-bis(2-aminoethylether)-N,N,N′,N′- tetraacetic acid acetoxymethyl ester
FM1-43	N-(3-triethylammoniumpropyl)-4-(4-(dibutylamino) styryl) pyridinium dibromide
GABA	γ-aminobutyric acid
$\gamma - dGG$	γ-D-glutamylglycine
Glucose	D-glucose
GYKI 52466	1-(4-aminophenyl)-4-methyl-7,8-methylenedioxy-5H-2,3- benzodiazepine hydrochloride

GYKI 53655	1-(4-aminophenyl)-3-methyl carbamyl-4-methyl-3,4-dihydro-7,8-methylenedioxy-5H-2,3-benzodiazepine hydrochloride
HEPES	4-(2-hydroxyethyl)piperazine-1-ethanesulphonic acid
KCl	Potassium chloride
Kgluconate	Potassium gluconate
L-AP4	L-(+)-2-Amino-4-phos phonobutyric acid
Mg^{2+}	Magnesium
MgATP	Magnesium adenosine triphosphate
$MgCl_2$	Magnesium chloride
Mn^{2+}	Manganese
Na^{+}	Sodium
NaATP	Sodium adenosine triphosphate
NaCl	Sodium chloride
$NaHCO_3$	Sodium bicarbonate
NaH_2PO_4	Sodium dihydrogen phosphate
NaOH	Sodium hydroxide
Na-pyruvate	Sodium pyruvate
NASPM	1-naphthyl acetyl spermine trihydrochloride
NBQX	2,3-dihydroxy-6-nitro-7-sulfamoyl-benzo[f]quinoxaline-2,3-dione
NMDA	N-methyl-D-aspartate
O_2	Oxygen
PhTx-433	(S)-N-[4-[[3-[(3-aminopropyl) amino] propyl] amino] butyl]-4-hydroxy-α-[(1-oxo- butyl)amino] benzenepropanamide tris (trifluoro acetate) salt
SR 95531	2-(3-carboxypropyl)-3- amino-6-(4 methoxyphenyl) pyridazinium bromide
TBOA	threo-β-Benzyloxyaspartic acid
TEACl	Tetraethylammonium chloride
TTX	Tetrodotoxin

Proteins

ABP	Adaptor binding protein
ADAR2	Adenosine deaminase acting on ribonucleic acid 2
AMPAR	α-amino-3-hydroxy-5-methyl-4-isoxazole propionic acid receptor

AP-2	Adapter protein 2
AP-4	Adapter protein 4
Arp2/3	Actin-related proteins 2/3
Arf1	Adenosine diphosphate-ribosylation factor-1
Arf6	Adenosine diphosphate-ribosylation factor 6
ATPase	Adenosine triphosphatase
CaMKII	Ca^{2+}/calmodulin-dependent protein kinase II
CaV	Voltage-gated calcium channel
CB1R	Endocannabinoid receptor 1
CI-AMPARs	Calcium-impermeable α-amino-3-hydroxy-5-methyl-4-isoxazole propionic acid receptor
CKAMP44	Cystine-knot AMPAR modulating protein 44
CNIH-2/3	Cornichon-2/3
CP-AMPARs	Calcium permeable α-amino-3-hydroxy-5-methyl-4-isoxazole propionic acid receptor
CTD	C-terminal domain
EAAT	Excitatory amino-acid transporter
eGFP	Enhanced green fluorescent protein
G-protein	Guanosine nucleotide-binding protein
$GABA_AR$	γ-aminobutyric acid A receptor
$GABA_AR$	γ-aminobutyric acid B receptor
GAD65	65-kD isoform of glutamic acid decarboxylase
GRASP-1	Glutamate receptor-interacting protein-associated protein-1
GRIP1	Glutamate receptor-interacting protein 1
GSG1L	Germ-cell-specific gene 1-like
GTPase	Guanosine triphosphatase
iGluRs	Ionotropic glutamate receptors
kif1A	Kinesin superfamily protein 1A
kif5	Kinesin superfamily protein 5
Kv	Voltage-gated potassium channel
LBD	Ligand binding domain
MAGUK	Membrane associated guanylate kinase
mGluR	Metabotropic glutamate receptor
Narp	Neuronal activity-regulated pentraxin

Nedd4	Neural precursor cell expressed developmentally down-regulated protein 4
Neto1 & 2	Neuropilin tolloid-like 1 and 2
NMDAR	N-methyl-D-aspartate receptor
NSF	N-ethylmaleimide-sensitive factor
NTD	N-terminal domain
PDZ	Post synaptic density protein, Drosophila disc large tumor suppressor, Zonula occludens-1 protein
PICK1	Protein interacting with PRKCA 1
PKA	Protein kinase A
PKC	Protein kinase C
PLC	Phospholipase C
PSD	Postsynaptic density
PSD-95	Postsynaptic density protein 95
RIM	Rab3-interacting molecule
RIM-BP	Rab3-interacting molecule-binding protein
SAP90	Synapse-associated protein 90
SAP97	Synapse-associated protein 97
SNAP	Soluble N-ethylmaleimide-sensitive factor attachment protein
SNARE	Soluble N-ethylmaleimide-sensitive factor attachment protein (SNAP) receptor
SynDIG1	Synapse differentiation-induced gene 1
TARP	Transmembrane amino-3-hydroxy-5-methyl-4-isoxazole propionic acid receptor regulatory protein
TMD	Transmembrane domain
TRPV1	Transient receptor potential vanilloid receptor 1
VGCC	Voltage-gated Ca^{2+} channel

Symbols

$\Delta I_{\text{whole cell}}$	Change in whole-cell current
μ	Mean
σ^2	Variance
C_m	Membrane capacitance
I	Average postsynaptic peak amplitude

m	Number of released quanta
N	Number of vesicles available for release
q	Quantal amplitude
p	Average probability of release
R_e	Series resistance
τ	Time constant
x	Number of quantal events over a given time

To my extended family

1 | Introduction

Presynaptic AMPARs modulate neurotransmitter release at a number of synapses in the central nervous system (CNS). In this thesis, I describe aspects of their function and regulation within one population of cells; the cerebellar molecular layer interneurons (MLIs). In order to place the study of presynaptic AMPARs into context, I begin the introduction by briefly discussing the history of glutamatergic neurotransmission before focusing on advances in the field of ionotropic glutamate receptors (iGluRs), and presynaptic neurotransmitter release. Given that the thesis focuses on presynaptic AMPARs in MLIs, I further introduce the cerebellar circuitry and features of MLIs, which regulate cerebellar output.

1.1 | A short history of synaptic transmission

Neurons consist of distinct axonal and dendritic compartments, emanating from the cell body typically with spatial polarity. Neurons are excitable and can communicate with one another either electrically through gap junctions in their membranes (Furshpan and Potter, 1959), or more commonly, through chemical transmission across a synaptic cleft, that can form when an axonal process comes within close contact with a postsynaptic target, typically a dendritic arborisation.

1.1.1 | Structural evidence for non-continuous synaptic connections

The origins of synaptic transmission can be traced back to Galvani who in the 1790s demonstrated that nerves could be electrically stimulated to produce muscle contraction in frog limbs (Piccolino, 1997). In the mid 1800s, a methylene blue staining technique allowed anatomists including Kuhne (1862), and Krause (1863) to describe an expanded nerve ending and a discrete junction between nerve and muscle (NMJ) (Cowan and Kandel, 2003). The theoretical foundations of the synapse are often credited to the Catalan physiologist Ramón y Cajal, who in 1891 rationalised "contacts" between the

Figure 1.1: Stained glass window depicting Sherrington's findings related to the synapse

Stained glass representing Sherrington's diagram of 'Two excitatory afferents with their fields of supraliminal effect in a motoneurone pool of a muscle'. Designed by Maria McClafferty and installed in Gonville and Caius Hall, Cambridge in 1992-3. Photo used with permission from Sahiba Chadha.

axon terminal and dendritic sites via a small gap, and predicted the direction of information transfer between neurons based wholly on sparse Golgi staining that revealed gross neuronal anatomy (Berlucchi, 1999). Though Cajal's theory of dynamic polarisation is the most commonly referred to, similar predictions were made in the same year by Arthur van Gehuchten, and both were preceded by the American psychologist William James who proposed his 'law of forward direction' in the late 19th century (Berlucchi, 1999). Empirical insight was later provided by Charles Sherrington in 1897, who showed using the spinal reflex arc that whilst axons conducted impulses in both directions, neuronal communication occurred in one direction (Berlucchi, 1999). Sherrington further discovered that communication involved a delay not reconcilable with the competing reticular theory of Camillo Golgi, in which the axons form a continuous link with dendrites through filamentous structures (Berlucchi, 1999). In 1897, with help from Arthur Verall, Sherrington conceived the term "synapse" which originated from the Greek meaning "the process of contact". Sherrington's interpretations must belong to an exclusive club which are summarised in stained glass (Figure 1.1). This view was supported by reports from Bayliss in 1924 and De Castro in 1930 who demonstrated the pre-ganglionic nerve fibre can degrade without affecting post-ganglionic nerve fibres (Tsuji, 2006). The theory of reticulurism was conclusively vanquished following visualisation of a synaptic space with a Janus green B dye employed by Couteaux in 1944, though this news took many years to attain worldwide recognition (Tsuji, 2006). This study was later confirmed by electron microscopic studies (De-Robertis and Bennett, 1955; Palade and Palay, 1954), which further showed the presence of synaptic vesicles concentrated within structures now referred to as active zones.

1.1.2 | Chemical transmission at synaptic connections

Fifty years before the existence of an inter-membranous synaptic gap was confirmed by anatomical evidence, the idea that chemical transmission could mediate information flow from nerves had been developed from pharmacological experiments on isolated organ preparations. The first mention of a chemical mediator resulted from observations of tubocurare-induced paralysis at the NMJ, where the electrophysiologist du Bois-Reymond

(1877) speculated that a "stimulatory secretion" or "powerful stimulatory substance" was released from the motor neuron to evoke muscle contraction (Sheperd, 2009). In support of this theory, a number of pioneering experiments using isolated organs demonstrated that exogenous application of substances could replicate nervous control over muscle. For example, in 1905 Elliott demonstrated adrenaline could mimic sympathetic nerve stimulation in an isolated heart preparation, and at the NMJ, Langley (1907) showed that nicotine produced muscle contraction (Rubin, 2007). Following the identification of acetylcholine (ACh) (Dale, 1914; Ewins, 1914), the crucial evidence for chemical transmission was provided by Loewi (1921) who elegantly demonstrated an ACh-like substance, released from the autonomic nervous system within one isolated heart preparation, could inhibit another isolated heart when connected by their perfusate (Rubin, 2007). Subsequent work by Dale, Vogt and Feldberg confirmed these findings in a number of NMJ preparations to show ACh was released from motor neurons following stimulation (Rubin, 2007).

Substantial progress in synaptic transmission was made following the development of microelectrodes, which provided the means for electrophysiological measures within or near neuronal structures, in addition to the microiontophoresis of small molecules. Concerns over the necessary speed of chemical transmission, as compared to the alternatively proposed electrical transmission (Eccles, 1945), were categorically quashed by electrophysiological experiments on the frog NMJ. Fatt and Katz (1952) demonstrated miniature excitatory postsynaptic potentials (mEPPs) resulted from spontaneous release of individual ACh quanta containing approximately 1000 molecules. By analysing fluctuations in the evoked EPP, del Castillo and Katz (1954) found that EPP amplitude was an integral of the individual mEPP amplitude, and concluded that action potentials drive synchronous release of numerous ACh quanta. In the same study, the EPP amplitude histogram was accurately described by a Poisson distribution, which predicted the number of quanta released, m, was a function of the number of vesicles available for release (N), and the average probability of release (p). The postsynaptic response to transmitter release is defined as q. These parameters are inferred from the average postsynaptic peak amplitude

(I) (Katz 1969), using the equation:

$$I = Npq \tag{1.1}$$

The quantal theory is fundamental to the analysis of synaptic parameters. In particular, it can inform an experimenter of the site of synaptic modulation. For example, a change in release probability will modulate m, whereas processes which modulate the postsynaptic receptor response to transmitter release will be represented as a difference in quantal amplitude, q.

Though great strides were initially made to describe synaptic transmission at peripheral synapses, little information was known about neurotransmitters, or their receptors, in the CNS. Contrary to sympathetic and parasympathetic transmission in the peripheral nervous system, cholinergic and adrenaline-like neurotransmitters were largely unable to replicate the rapid excitation and recovery observed in central neurons following stimulation (Lodge, 2009).

1.1.3 | Glutamatergic transmission in the CNS

With the use of sharp electrode recordings, the search for non-cholinergic, non-monoaminergic substances that mediated excitatory neurotransmission in the CNS led to the non-essential amino acid glutamate (Lodge, 2009). Glutamate is abundant throughout biology, both as a constituent of proteins, and as a key component of the Kreb's cycle for energy metabolism. Given these widespread functions, its suitability for neurotransmission was initially disputed when compared to more unusual substances like ACh (Watkins and Jane, 2006).

L-glutamate exists in high concentrations in the brain (Berl and Waelsh, 1958), and was shown to elicit convulsions in a report that may have been the first to suggest glutamate acts as a transmitter in the CNS (Hayashi, 1954). However, even after Curtis and colleagues showed application of glutamate, in addition to other amino acids, produced depolarisation and enhanced action potential firing of spinal neurons (Curtis et al., 1959), its role as a neurotransmitter was disputed.

Further studies demonstrated that the iontophoretic application of glutamate consistently evoked a response at sites on crustacean muscle where synapses were expected to be present (Takeuchi and Takeuchi, 1964). In addition to its endogenous release from stimulated axons, a mechanism was identified to terminate glutamate transmission. The reuptake of glutamate into neurons was demonstrated both in a population of synaptosomes, and within intact hippocampal mossy fibre (MF) terminals (Cowan and Kandel, 2003). Thus, further evidence which complied with Paton's original criteria for a neurotransmitter was accumulating (Paton, 1958).

To dismiss concerns that glutamate was acting non-specifically, knowledge of the receptors that mediated the excitatory effects of glutamate was required. This was gradually achieved following the synthesis of novel pharmacological agents which possessed greater selectivity for glutamate receptors. In the 1970s, excitatory responses could be elicited by novel compounds such as NMDA (Curtis and Watkins, 1963), kainate (Shinozaki and Konishi, 1970) and later by quisqualate (Shinozaki and Shibuya, 1974). However, without specific antagonists to block endogenous responses, excitatory CNS receptors were still tentatively grouped as 'aspartate-preferring' and 'glutamate-preferring' (Lodge, 2009).

Following improvements in ligand specificity, glutamate receptors were re-classified as NMDA or non-NMDA receptors, depending on their sensitivity to the antagonist D-α-aminoadipate (Davies and Watkins, 1979; Lodge, 2009). Mg^{2+} was also found to selectively block responses to NMDA (Lodge, 2009). Subsequently, non-NMDA receptors were further divided into quisialate and kainate sensitive receptors. The validity of the classification was confirmed by their relative sensitivities to the blockers glutamic acid diethyl ester, D-glutamylglycine (Davies and Watkins, 1981) and g-D-glutamylaminomethyl sulfonate (Davies and Watkins, 1985; Lodge, 2009). With the identification of specific glutamate receptors, it is was recognised that the vast majority of synaptic excitation in the CNS was mediated by glutamate (Watkins and Jane, 2006).

It was not until the systematic cloning of glutamate receptors around the beginning of the 1990s that glutamate receptor nomenclature began to reflect the families we have today (Figure 1.2) (Collingridge et al., 2008). Previous observations that a population

of glutamate receptors could couple to second messengers (Sladeczek et al., 1985), and GTP-binding regulatory proteins (Sugiyama et al., 1987), were validated by the family of metabotropic glutamate receptors (mGluRs), cloned in 1991 (Figure 1.2) (Hollmann and Heinemann, 1994; Masu et al., 1991). Their discovery helped to resolve strange observations previously found with "selective" glutamate receptor agonists and antagonists. For example, (±)-1-aminocyclopentane-trans-1,3-di carboxylic acid and L-(+)-2-amino-4-phosphonobutyric acid, respectively induced excitation and inhibition without being antagonised with the repertoire of NMDA or non-NMDA receptor blockers (Monaghan et al., 1989). Furthermore, the agonist activity of quisialate at mGluRs (Nicoletti et al., 1986; Sladeczek et al., 1985; Sugiyama et al., 1987), compromised the unique identity of quisialate receptors and prompted its change in name. Currently, receptors previously referred to quisialate are more appropriately identified by the more selective agonist, AMPA (though as AMPA and kainate both evoke gating of the other's namesake receptor, the pharmacologically based nomenclature is not perfect).

1.2 | Ionotropic glutamate receptors

iGluRs are tetrameric assemblies of individual subunits which, in mammals, are encoded by 18 genes (Traynelis et al., 2010). These 18 subunits are classified into groups by their sequence homology. Currently, there are seven NMDAR subunits (GluN-1, -2A-D and -3A-B), four AMPAR subunits (GluA1-4), two δ subunits (GluD1 and 2) and five kainate receptor subunits (GluK1-5) (Figure 1.2 *A*). In the endoplasmic reticulum (ER) a dimer of iGluR subunits pair up with another dimer to form the characteristic dimer of dimers structure (Ayalon and Stern-Bach, 2001) (Fig. 1.3 B). Depending on the receptor type, tetramers can comprise of identical subunits (homomers) or a combination of different subunits (heteromers). Generally, subunits do not assemble with subunits from other receptor subtypes (Traynelis et al., 2010).

iGluRs can bind up to four glutamate molecules at any one time to initiate gating and allow Na^+, K^+ and, depending on the channel selectivity, Ca^{2+} ions to flow across the cell membrane (Ascher and Nowak, 1988a,b). In neurons, where the Na^+/K^+ transporter ensures positive charge is concentrated extracellularly, iGluR activation acts to depolarise

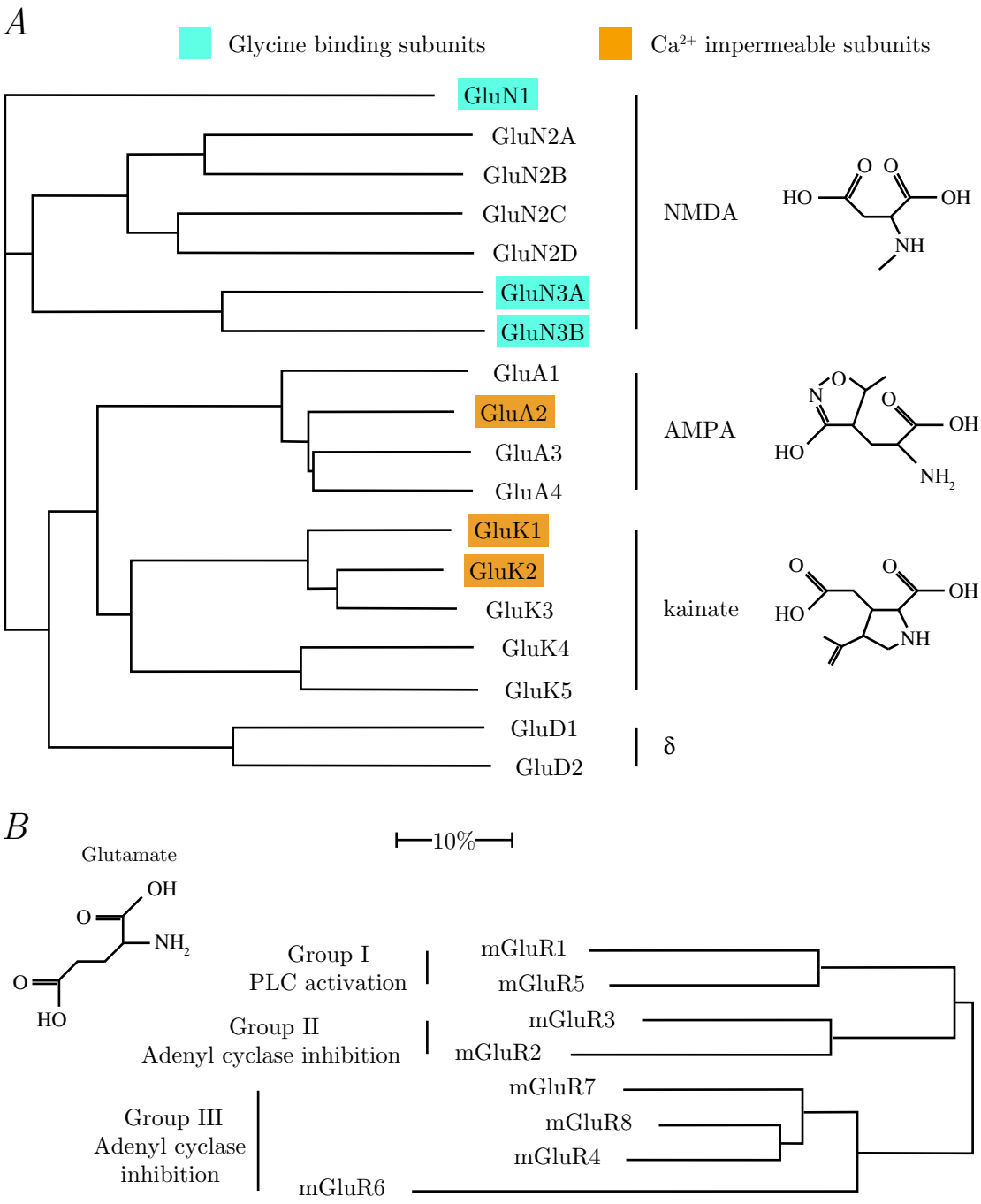

Figure 1.2: Dendrograms of iGluR and mGluR sequence homologies

Data refers to human sequences aligned by Swanson and Sakai (2009). Branch length demonstrates the difference between sequences. A distance of 0% indicates identical sequences, whereas 100% refers to an infinite difference between sequences. (*A*) The four families of iGluRs (NMDA, AMPA, kainate and *δ* receptors), differentiated by pharmacological profiles, show greater sequence homology to each other compared to members of other families. Orange boxes refer to subunits which, when edited from a glutamine to an arginine, are Ca^{2+}-impermeable. Green boxes refer to glycine-binding subunits. *B* Sequence homology grouping shows three groups of mGluRs.

the inside of the membrane relative to the outside. This is true for NMDA, AMPA and kainate receptors, but not for δ-1 or -2 glutamate receptors, which have no known endogenous ligand and thus have not been described to function as a ligand-gated ion channel (Araki et al., 1993; Lomeli et al., 1993; Yamazaki et al., 1992). Instead, δ-2 receptors are thought to play a role in synaptic formation and maintenance (Takeuchi et al., 2005), as well as AMPAR trafficking (Hirai et al., 2003). In the cerebellum, GluD2 promotes synapse formation through neurexin and cerebellin-1 signalling (Ito-Ishida et al., 2012), and binding of glial released D-serine was found to enhance synaptic AMPAR accumulation (Kakegawa et al., 2011).

The AMPA, NMDA, and kainate iGluRs mediate a majority of excitatory synaptic transmission in the CNS and can be differentiated not only by their pharmacology but also by their gating properties (Traynelis et al., 2010). AMPA and kainate receptors rapidly activate and desensitise, though kainate receptors exhibit a relatively longer recovery from desensitisation. NMDARs are activated by the co-agonism of glutamate and glycine (Figure 1.2) and exhibit a characteristically slow channel opening and a prolonged desensitisation (Zorumski et al., 1989). The ionic permeability also differs between iGluRs. Whilst all NMDAR subunit form tetramers that are permeable to Ca^{2+} (as well as Na^{+} and K^{+}), only AMPARs which lack the GluA2 subunit are calcium-permeable (CP), whereas those which contain the edited GluA2 subunit are calcium-impermeable (CI) (Burnashev et al., 1992) (subsection 1.3.3). Kainate receptors may also exhibit a limited Ca^{2+} permeability when assembled from the RNA edited GluK1 and 2 subunits (Traynelis et al., 2010) (Figure 1.2).

1.2.1 | The structure and gating mechanism of iGluRs is largely conserved

All subunits are comprised of four modular domains, the extracellular N-terminal domain (NTD), the ligand binding domain (LBD), the transmembrane domain (TMD), and the intracellular C-terminal domain (CTD) (Figure 1.3). The structure of glutamate receptor subunits can be traced back to bilobate structures in bacterial periplasmic glutamate-binding proteins (O'Hara et al., 1993; Quiocho and Ledvina, 1996). It is thought that the

transition to a glutamate binding channel occurred following the incorporation of a K^+ channel. Indeed, the iGluR pore closely resembles the pore of an inverted K^+ channel (Kuner et al., 2003), and furthermore, a K^+ channel that is activated by glutamate has been found in prokaryotes, which may reflect a transitional point in the evolution of iGluRs (Chen et al., 1999). Following the loss of K^+ selectivity and the insertion of a CTD, the present structure of glutamate cationotropic receptors is thought to be conserved in all eukaryotes (Tikhonov and Magazanik, 2009). The exception to this generalised structure is provided by the glutamate-gated anionic channels found in mollusc and nematode neurons as well as insect muscles, which permeate chloride ions and therefore contain a different TMD (Arena et al., 1991; Bolshakov et al., 1991; Cull-Candy and Usherwood, 1973).

The ∼380 amino acid NTD includes the R1 and R2 sequences which fold to form lobule structures linked by amino-acid loops (Figure 1.3 *B*) (Traynelis et al., 2010). This clamshell-like structure resembles the LBD of mGluRs (Karakas et al., 2009). The NTD promotes the correct formation of dimer and tetramer assemblies for export from the ER (Ayalon et al., 2005; Matsuda et al., 2005). For AMPAR and kaianate receptors, the interaction between NTDs on adjacent subunits are also important for the preferential heteromerisation of subunits (Kumar et al., 2011; Rossmann et al., 2011). Whilst the NTD is not involved in AMPAR gating or ligand binding (Pasternack et al., 2002), for NMDARs the NTD can modulate channel gating and agonist potency (Gielen et al., 2009; Yuan et al., 2009). Moreover, the NMDAR NTD is believed to provide regulatory sites for extracellular and intracellular signals such as N-Cadherin (Saglietti et al., 2007) and EphB tyrosine kinase receptors (Takasu et al., 2002), as well as the binding of allosteric ligands (Perin-Dureau et al., 2002).

Similar to the NTD, the LBD is comprised of a clamshell structure that forms from the discontinuous S1 and S2 amino acid sequences (Armstrong et al., 1998; Stern-Bach et al., 1994) (Figure 1.3 *A* & *B*). S1 corresponds to the 120 amino acids before the TMD M1 domain, and the S2 amino acid sequence is formed from the extracellular region positioned between the TMD M2 and M3 domains (Armstrong et al., 1998; Stern-Bach et al., 1994). Both sequences fold to form the extracellular lobes and are joined by

a flexible polypeptide linker (Armstrong et al., 1998). Crystal structures for all three subclasses of iGluRs show that the D1 and D2 domains form the glutamate binding pocket (Traynelis et al., 2010) (Figure 1.3 *B*). D1 sequences are highly conserved between different subunits. By contrast, residues in D2 demonstrate greater variability between subunits, this divergence is believed to underlie the selectivity of ligands for different iGluRs (Traynelis et al., 2010).

The LBD is connected by three short 9-17 amino acid linkers to the channel-forming TMD (Sobolevsky et al., 2009). The TMD consists of three α-helical structures that span the membrane (M1, M3 and M4) to form the outer and central cavities whereas the remaining M2 domain is membrane bound, with both extremities in the cytoplasm and forms the lining of the inner cavity (Traynelis et al., 2010) (Figure 1.3 *A* & *B*). M1 and M4 reside on the outer side of the TMD and do not contribute directly to the pore lining. The M4 domain of one subunit links to the M1,2 & 3 domains of adjacent subunits, an interaction thought to be required for efficient surface expression (Salussolia et al., 2011a). The AMPAR channel pore is formed from the TMDs. The M2 domain forms the cytoplasmic region of the channel, whilst a pre-M1, a C-terminal motif of M3 and an N-terminal motif of M4 contribute to the more extracellular pore regions (Chang and Kuo, 2008). When subunits tetramerise the individual M3 motifs come into close proximity to form the channel gate (Chang and Kuo, 2008). The steric occlusion confers impermeability to ions when closed and dilates following ligand binding.

An intracellular carboxyl terminal domain (CTD) is also preserved between all forms of iGluRs, though with marked divergence in the amino acid sequence and length (Traynelis et al., 2010). Due to the 'fluidity', the CTD has been difficult to crystalise, thus its structure is not well defined. However, from mutating specific regions of the amino acid sequence, the C-terminal is known to bind many intracellular proteins important for sub-cellular trafficking, membrane targeting and binding to intracellular regulatory proteins (Traynelis et al., 2010) (see section 1.3).

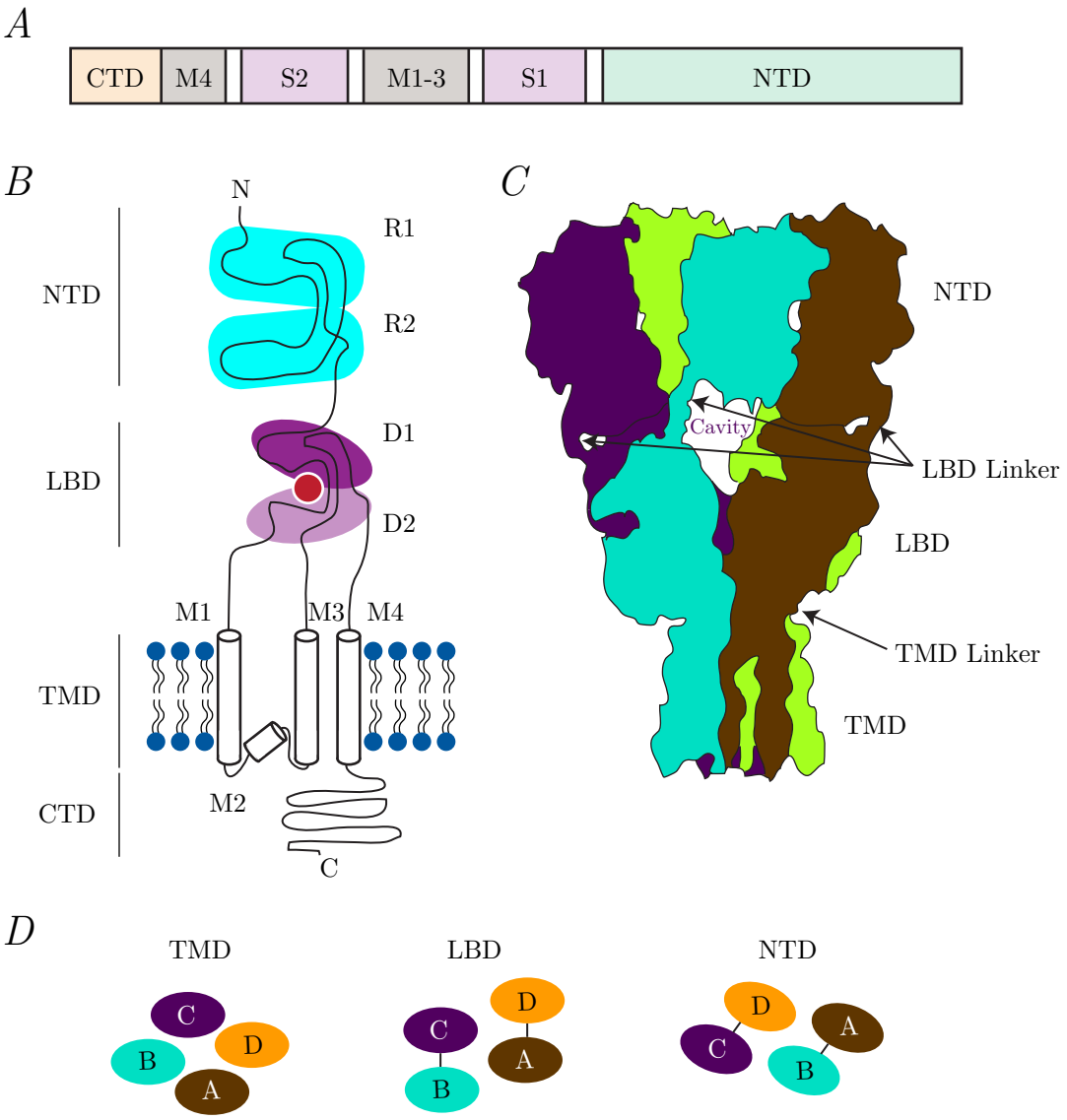

Figure 1.3: Structure and domain organisation of iGluRs

(*A*) Schematic illustration of the iGluR polypeptide chain divided into the N-terminal domain (NTD), S1 and S2 of the ligand binding domain (LBD), M1-4 α helices of the transmembrane domain (TMD) and the C-terminal domain. Depending on the subunit, the length can vary between 883-906 amino acids. (*B*) The folding of the amino acid sequence forms the distinctive lobule structures in the NTD and LBD. (*C*) Schematic of the domain organisation in the GluA2 ion channel resembling the crystal structure (Sobolevsky et al., 2009). The four subunits are represented in the different colours revealing the subunit positional swapping between domains, the cavity formed in the NTD and the relativity large size of the NTD compared to the LBD. (*D*) When the subunits are viewed from above, the TMDs show 4-fold symmetry whereas the NTDs and LBDs exhibit a 2-fold symmetry. The subunit swapping between domains can also be clearly demonstrated, where the rotation in the subunits give rise to different dimer formations in the NTD compared to the LBD. Figure based on an image from Traynelis et al. (2010)

1.2.2 | Tetrameric assembly and stoichiometry of iGluRs

Functional iGluR tetramers are assembled in the ER, and are only exported following correct protein folding and oligomerisation. The X-ray crystallographic structure of GluA2 NTD, LBD and TMD subunit domains (Sobolevsky et al., 2009) confirmed previous electron microscopic evidence (Midgett and Madden, 2008; Nakagawa et al., 2005; Tichelaar et al., 2004) suggesting the NTD and LBD exist in a dimer of dimers arrangement with a 2-fold rotational symmetry when viewed from above (Figure 1.3 *D*). By comparison, the TMD is thought to have a 4 fold symmetry, typical of K^+ channels, and thus confers a mismatch in symmetry between structural domains (Sobolevsky et al., 2009). Another strange structural property of iGluRs is their swapping of dimerised subunits between the NTD and LBD domains mediated by the conformation of the short flexible linking peptides (Sobolevsky et al., 2009) (Figure 1.3 *C* & *D*). This subunit crossover may help to secure the extracellular NTD. Beyond the individual NTDs and LBDs (Karakas et al., 2009; Kumar et al., 2009), the crystal structure of NMDA and kainate receptor subunits are not available. However, cysteine mutant cross-linking experiments demonstrate a similar subunit exchange is likely to be preserved in both cases (Das et al., 2010; Salussolia et al., 2011b).

iGluR subunits can assemble in a number of combinations to produce a diverse array of functional receptors. The subunit composition of NMDARs follow specific rules. NMDARs are obligatory heterotetrameric, requiring two glycine-binding GluN1 subunits to function (Ulbrich and Isacoff, 2008). This dimer can associate with two of the same, or two different members of the glutamate-binding GluN2 subfamily (2A, 2B, 2C, 2D) (Furukawa et al., 2005; Hatton and Paoletti, 2005). Alternatively, one glycine-binding GluN3A or 3B subunit can form a dimer with an individual GluN2 subunit (Yao et al., 2008). The coincident binding of glutamate to GluN2 and glyine (or D-serine) to the other subunits can produce channel gating (Johnson and Ascher, 1987). Interestingly, GluN1 and 3 can form an exclusively glycine activated NMDAR (Chatterton et al., 2002), though whether they can assemble in neurons remains unclear (Matsuda et al., 2003). It has been recently proposed that NMDAR assembly involves a rearrangement of subunits. GluN1-GluN2 heteromers are formed from the tetremerisation of GluN1 monomeric dimers and

GluN2 monomeric dimers, which then rearrange to form the GluN1-2 dimer of dimers before exit from the ER (Farina et al., 2011).

Compared to NMDARs, the subunit stoichiometry of AMPARs is less restricted. Functional AMPARs are formed from homomeric or heteromeric assemblies of either GluA1, 2, 3 and 4 (Nakagawa, 2010). Though homomeric GluA2 subunits can form in heterologous systems (Swanson et al., 1997), in the presence of other subunits, GluA2 subunits are preferentially incorporated into heteromers due to the presence of a charged arginine in the channel pore, which does not favour GluA2 subunits lying adjacent to one another (Greger et al., 2003). Like AMPARs, the low-affinity kainate receptor subunits GluK1, 2 and 3 can form either homomers or heteromers, however the high-affinity GluK4 and 5 subunits require tetramerisation with either GluK1, 2 or 3 (Contractor et al., 2011).

1.2.3 | Glutamate binding induces iGluR channel gating

Knowledge of the 3-dimensional structure further allows insight into how ligand binding translates into gating. The D1 lobes of each of the four LBDs connect back-to-back in the dimers within the tetramer (Armstrong and Gouaux, 2000). In response to agonist binding D2 moves relative to D1, which drives the separation and rotation of the short amino acid sequences linking D2 to M3 (Armstrong and Gouaux, 2000) (Figure 1.4). This rearrangement has been hypothesised to rotate the M3 TMD segments, to open the gate formed by individual subunits and allow cations to flow through the channel (Sobolevsky et al., 2009). Partial agonists are thought to produce less closure of the D1, D2 cleft, conferring less tension in the linkers, which results in a reduced pore opening (Armstrong and Gouaux, 2000; Jin et al., 2003).

Dissociation of glutamate from the cleft reverses the molecular processes following binding and returns the ion pore to a closed position with the M3 domains occluding the flow of cations. This process of deactivation relies on the stability of the contacts made between the D1 and D2 lobes when the cleft is closed (Maier et al., 2007; Robert et al., 2005) (Figure 1.4). For AMPARs the rate of deactivation can be attenuated by aniracetam which binds between the D1-D1 structures and prevents movement of the D1-D2 linker (Jin et al., 2005). Even when an agonist remains bound, iGluRs do not necessarily remain

in an open state but typically desensitise to produce a marked reduction in channel conductance. In AMPA and kainate receptors this occurs within a few milliseconds as a result of the unstable D1-D1 interface. The separation of the D1 lobes forces the D2 lobes closer together and relaxes the contortions in the linkers which force the TMDs apart (Armstrong et al., 2006). Just like deactivation, desensitisation of AMPARs can be blocked by channel potentiators such as 6-chloro-3,4-dihydro-3-(2-norbornen-5-yl)-2H-1,2-4-benzothiadiazine-7-sulfonamide 1,1-dioxide (cyclothiazide) which bind at the D1-D1 interface to prevent their separation (Jin et al., 2005).

1.3 | Postsynaptic AMPARs are subject to diverse regulatory factors

In the CNS, AMPARs mediate the majority of fast excitatory synaptic transmission, providing the initial, and at some synapses, the exclusive drive for postsynaptic depolarisation. Interestingly, their absolute requirement has been recently questioned, as kainate receptors appear to be homeostatically incorporated in to the postsynaptic density (PSD) in the absence of AMPARs (Yan et al., 2013). At glutamatergic synapses the postsynaptic parameter q, defined by Katz, can vary substantially depending on various factors that either influence biophysical features of the receptor, or regulate their delivery and/or stabilisation at synaptic sites.

1.3.1 | Interacting proteins deliver AMPARs to the postsynaptic density

A plethora of intracellular proteins interact with AMPARs to influence their transport from the ER, at either the cell body or the dendrites (Ju et al., 2004), to the PSD. Their vesicular exit is dependent on their subunit composition (Greger et al., 2002), as well as the AMPAR interacting proteins; synapse-associated protein 97 (SAP97) (Sans et al., 2001; Cai et al., 2002) and Protein interacting with PRKCA 1 (PICK1) (Greger et al., 2002). From the ER, AMPARs are trafficked to the dendrites within vesicles along actin based microtubules by kinesin motor proteins such as kif5 or kif1A under the

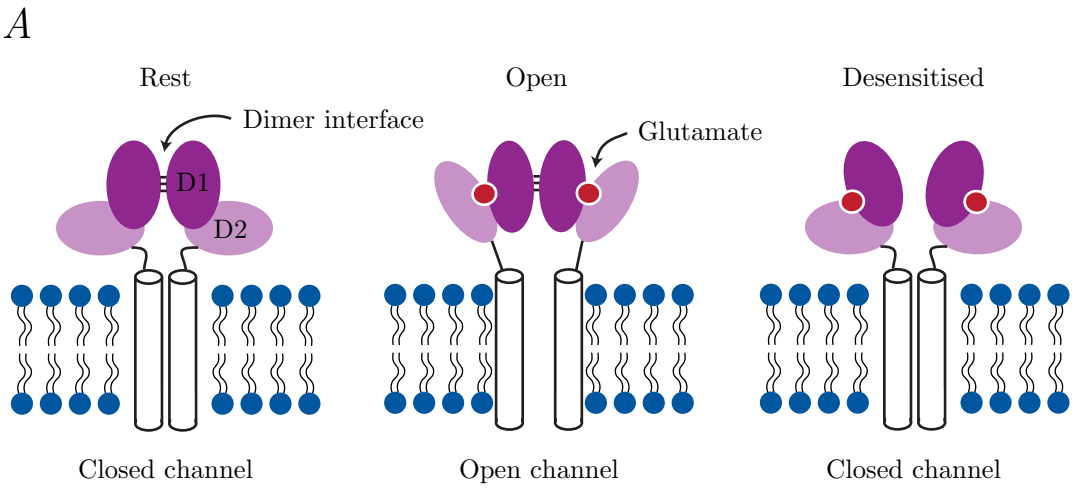

Figure 1.4: Activation and desensitisation of iGluRs

(*A*) Schematic illustration of the LBD and TMD of iGluR dimers in the resting, open and desensitised states. D1 and D2 segments of the LBD form the glutamate binding cleft. The binding of glutamate causes the D2 to close in greater proximity to D1. The subsequent movement in the linkers that bind S1 and S2 to the M1 and M3 TMD opens the channel (centre panel) (Armstrong and Gouaux, 2000). Breaking of the D1 interface (far right panel) causes relaxation of D2 and the LBD-TMD linkers which causes iGluR desensitisation (Armstrong et al., 2006) Figure adapted from Smart and Paoletti (2012).

direction of the AMPAR interacting protein; Glutamate receptor-interacting protein 1 (GRIP1) (Setou et al., 2002; Wyszynski et al., 2002; Shin et al., 2003). Microtubules are absent from dendritic spines (Kaech et al., 2001), instead the transport of AMPARs from intracellular endosomes in the dendritic cytoplasm to the membrane is likely mediated by the actin based motor proteins myosin-Va (Correia et al., 2008) or -Vb (Wang et al., 2008). Once at the membrane, the AMPAR containing vesicles fuse with the extrasynaptic membrane through the interactions of the vesicular SNARE [soluble N-ethylmaleimide-sensitive factor attachment protein (SNAP) receptor] SNAP-23 (Suh et al., 2010) and the target membrane SNARE syntaxin-4 (Kennedy et al., 2010). For GluA2, the membrane incorporation and stabilisation process also seems to require N-ethylmaleimide-sensitive factor (NSF) (Beretta et al., 2005; Araki et al., 2010).

Once in the membrane, AMPARs accumulate in the PSD through lateral diffusion (Adesnik et al., 2005; Yudowski et al., 2007) where they are stabilised through interaction with membrane scaffold proteins such as the PDZ motif-containing membrane associated guanylate kinases (MAGUKs) (Bats et al., 2007; Elias et al., 2006). Alternatively, extracellular proteins such as (Neuronal activity-regulated pentraxin) Narp have also been shown to stabilise AMPARs at the synapse (O'Brien et al., 1999). Furthermore, GluA1 subunits are thought to be secured at the synapses by actin filaments (Allison et al., 1998; Kim and Lisman, 1999, 2001) through interaction with protein 4.1N (Shen et al., 2000).

Their stabilisation in the membrane is finite; AMPARs are very mobile and can diffuse out of the PSD (Lüscher et al., 1999) either to the adjacently located endozytic zone (Blanpied et al., 2002; Lu et al., 2007), or more distant somatodendritic sites (Anggono and Huganir, 2012), where they can undergo endocytosis. AMPARs in this extrasynaptic membrane are bound to an intracellular clathrin lattice through the adapter protein-2 (AP-2) (Lee et al., 2002). Clathrin forms coats which invaginates the membrane and, through the oligomerisation of the GTPase dynamin (Praefcke and McMahon, 2004), pinches off to form vesicles containing AMPARs. The interacting protein PICK1 is though to promote endocytosis of GluA2-containing AMPARs through the disruption of actin polymerisation (Rocca et al., 2008) and interaction with the vesicle fusion protein, β-SNAP [Soluble N-ethylmaleimide-sensitive factor attachment protein] (Hanley et al., 2002). The PICK1-

AMPAR interaction can be regulated by NSF depending on local Ca^{2+} levels (Hanley et al., 2002).

The internalised AMPAR containing vesicles are referred to as early endosomes. These can mature to form late endosomes, which then fuse to the lysosomes for protein degradation. Alternatively, AMPARs can be recycled back to the membrane, either rapidly (Anggono and Huganir, 2012) or via recycling endosomes, the later process is regulated by GRIP1 (Braithwaite et al., 2002; Steiner et al., 2005). The fusion of early endosomes into recycling endosomes is mediated by GRIP-associated protein-1 (GRASP-1) interaction with the early endosome protein, Rab4, and the recycling endosome SNARE, syntaxin 13 (Hoogenraad et al., 2010). By retarding the actin-related protein-2/3 (Arp2/3)-mediated actin polymerisation (Rocca et al., 2008), PICK1 may slow the maturation of early endosomes and prolong the intracellular retention of CI-AMPARs (Citri et al., 2010). Recently, it was found that NMDAR-mediated postsynaptic depolarisation attenuated the activity of ADP-ribosylation factor-1 (Arf1), which under basal synaptic activity binds to PICK1; limiting its effects on Arp2/3-mediated actin polymerisation (Rocca et al., 2013).

1.3.2 | Auxiliary subunits

In contrast to the aforementioned AMPAR interacting proteins that bind relatively briefly under specific scenarios, AMPAR auxiliary subunits are loosely defined by their stable association with AMPARs, whose function they profoundly modify (Jackson and Nicoll, 2011b).

Over the past 15 years or so, a variety of auxiliary subunits have been shown to associate with iGluRs. For AMPARs, these include TARPs (Chen et al., 2000; Tomita et al., 2003), cornichons (CNIH-2/3) (Schwenk et al., 2009), cystine-knot AMPAR modulating protein 44 (CKAMP44) (von Engelhardt et al., 2010), synapse differentiation-induced gene 1 (SynDIG1) (Kalashnikova et al., 2010) and germ-cell- specific gene 1-like (GSG1L) (Schwenk et al., 2012; Shanks et al., 2012). Additionally, the auxiliary proteins neuropilin tolloid-like 1 and 2 (NETO1 and 2) have been found to associate with kainate and NMDA receptors (Ng et al., 2009; Straub et al., 2011; Zhang et al., 2009).

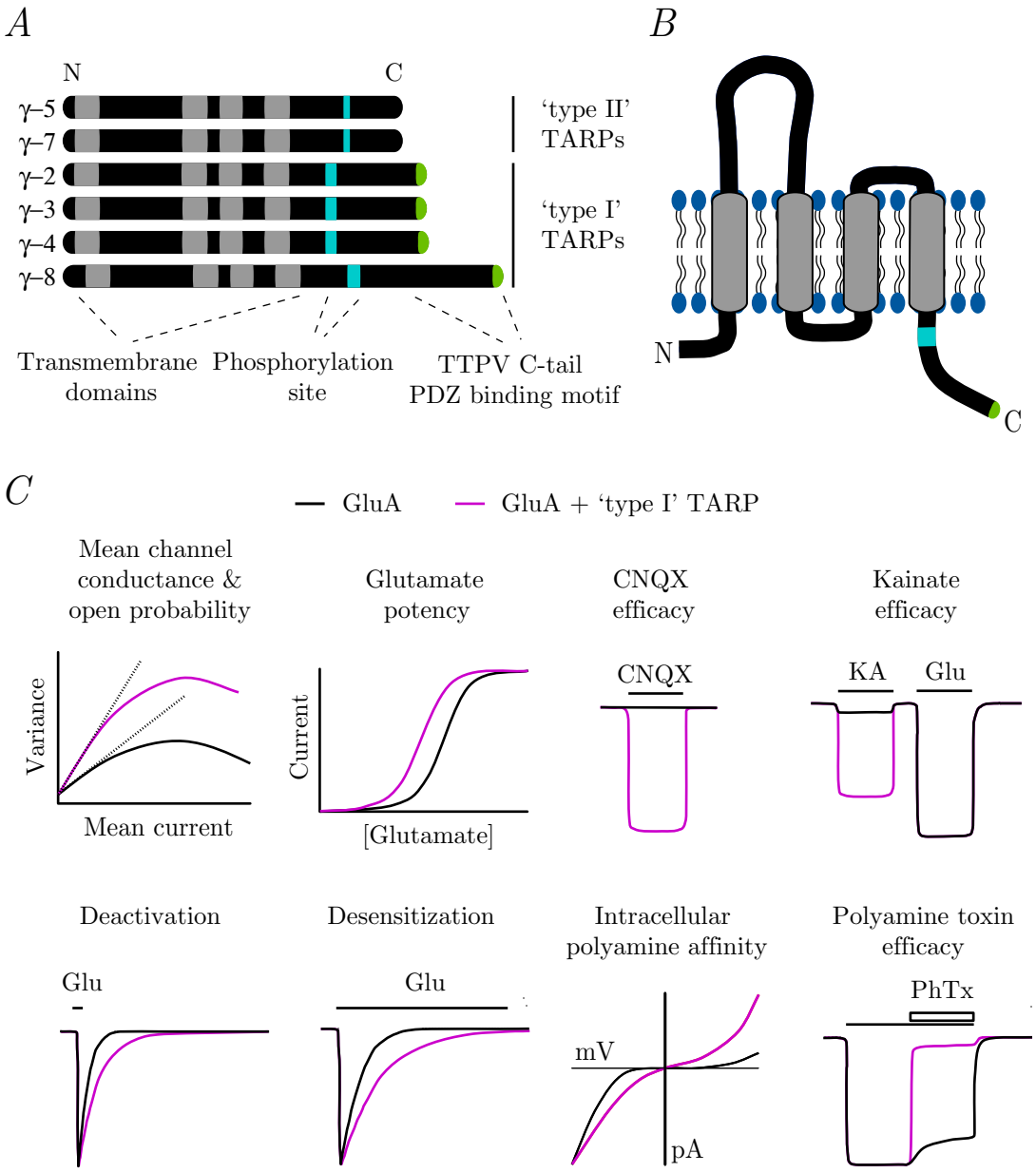

Figure 1.5: TARP structure and function

(*A* & *B*) The primary and secondary protein structure of TARPs. The structure consists of four transmembrane domains with intracellular N- and C-terminal regions. A PDZ binding motif at the C-terminus is important for stabilisation of AMPARs to MAGUKs at the synapse. The atypical 'type II' TARPs do not contain this motif. (*C*) Generalised representation of the effects of 'type I' TARP association on AMPAR biophysics and response to ligands. The effects mediated by an idealised AMPAR population are shown in the absence (black) and presence (blue) of TARP. 'Type I' TARP association enhances the mean single-channel conductance, increases glutamate potency, converts CNQX into a partial agonist, enhances the response to kainate, slows deactivation and desensitisation, attenuates block by polyamines and enhances the channel block by extracellular polyamine toxins. Figure modified from Jackson and Nicoll (2011b)

Of the identified iGluR auxiliary subunits, the best characterised are the TARPs, which stably associate with homo- or heteromeric assemblies of the pore-forming GluA1-4 AMPAR subunits. The prototypical TARP stargazin (γ-2) was identified from studies of the ataxic naturally occurring mutant *stargazer* (*stg*/*stg*) mouse (Hashimoto et al., 1999; Letts et al., 1998). Thus, six TARP isoforms, γ-2 (stargazin), -3, -4, -5, -7, and -8, with distinct though partially overlapping patterns of expression in the CNS (Fukaya et al., 2005), have been shown to differentially modulate trafficking, synaptic targeting, gating and pharmacology of AMPARs (Jackson and Nicoll, 2011b; Traynelis et al., 2010). Based on their structure, TARPs are grouped into the typical 'type I' TARPs and the atypical 'type II' TARPs (Figure 1.5). Unless specified, the studies described below refer to the effects of 'type I' TARPs on AMPAR function.

For an individual AMPAR, the stoichiometry of TARPs appears to be highly variable (Kim et al., 2010; Milstein et al., 2007; Shi et al., 2009). In heterologous cells, Shi et al. (2009) found they could achieve AMPAR responses when either zero, two or four TARPs were covalently linked to the tetramer. In cerebellar neurons however, a biochemical analysis revealed that, depending on expression levels, either 1, 2, 3 or 4 TARPs could produce functional AMPARs (Kim et al., 2010). A more recent study imaged GFP molecules tagged to individual TARP subunits (Hastie et al., 2013). Following the successive bleaching of single GFP molecules, it was shown that the number of TARPs associated with GluA1 homomers was dependent on expression level. This study further found that a maximum of four γ-2 or γ-3 subunits could associate with a single AMPAR, yet only 2 γ-4 subunits were found to be present at homomeric GluA1 AMPARs. Residues in the cytoplamic, transmembrane, and extracellular domains of both AMPARs and TARPs are thought to mediate their association (Traynelis et al., 2010).

The first point of contact between TARPs and AMPARs is thought to occur in the ER following AMPAR tetramerisation. The association is thought to promote both the exit of AMPARs from the ER (Bedoukian et al., 2006, 2008; Vandenberghe et al., 2005) and their delivery to the membrane (Chen et al., 2000; Tomita et al., 2003). Whilst this is true for 'type I' TARPs, an early study demonstrated that γ-5 and -7 were unable to promote AMPAR surface expression (Tomita et al., 2003). A study of AMPARs at the dendrites of

cerebellar Purkinje cells in culture and in acute slices, demonstrated that TARPs promote the dendrite-selective sorting of AMPARs from the ER through the interaction with adapter protein-4 (AP-4) (Matsuda et al., 2008a). Once at the membrane, TARPs further promote the synaptic accumulation of AMPARs (Cuadra et al., 2004; Ives et al., 2004). By mutating specific C-tail regions of the TARP and designing biomimetic divalent ligands that disrupt protein interactions, studies have shown a threonine-threonine-proline-valine (TTPV) motif, present in the TARP C-tail, promotes the targeting and stabilisation of AMPARs to the synapse through interaction with MAGUKs, including postsynaptic density protein 95 (PSD-95) and SAP97 (Chen et al., 2000; Bats et al., 2007; Howard et al., 2010; Sainlos et al., 2011).

In addition to their trafficking, the biophysical properties of AMPARs are markedly affected by TARP association (Figure 1.5). TARPs dramatically slow the deactivation (channel closure upon ligand removal) and desensitisation (channel closure in the continued presence of ligand) of AMPAR-mediated currents (Priel et al., 2005; Tomita et al., 2005; Turetsky et al., 2005). The effects vary depending on the TARP isoform; γ-4 and -8 decelerate deactivation kinetics to a greater extent than γ-2 and -3 (Cho et al., 2007; Milstein et al., 2007). Similarly, GluA-4 homomers associated with γ-4 desensitise slower that those associated with γ-8, which in turn desensitise more slowly than γ-2 or -3 associated AMPARs (Soto et al., 2009). TARP-association enhances the mean single-channel conductance, but not peak open probability, as measured by non-stationary fluctuation analysis of macroscopic currents (Jackson et al., 2011). For CP-AMPARs, mean single-channel conductance was uniformly enhanced by different TARP subtypes (Soto et al., 2007, 2009; Suzuki et al., 2008). By contrast, the extent to which mean single-channel conductance of heteromeric GluA2 containing CI-AMPARs was enhanced, depended on TARP subtype (Jackson et al., 2011). Intracellular polyamines such as spermine and spermidine are known to block CP-AMPARs when the membrane is depolarised. TARP association has been found to reduce the polyamine block and thus enhance both Ca^{2+} entry and the net flow of charge (Soto et al., 2007).

The modulation of the open AMPAR pore underlies TARP effects on mean single-channel conductance and kinetics. Upon glutamate binding, an AMPAR can open to between 2

and 4 distinct sub-conductance states (Shelley et al., 2012; Swanson et al., 1997; Tomita et al., 2005). In the presence of an agonist, TARP-association was shown to increase the probability that AMPAR channels reside at the higher sub-conductance levels (Jackson and Nicoll, 2011b). For homomeric GluA4 AMPARs, γ-2 increased the length of open channel bursts but did not alter the individual sub-conductance levels (Tomita et al., 2005). However, for GluA1 homomers associated with γ-2 and -4, the enhancement in the length of channel openings was accompanied by an approximate doubling of the individual conductance levels (Shelley et al., 2012).

The 'type II' TARPs; γ-5 and γ-7 demonstrate atypical effects on AMPAR gating. Kato et al. (2007) suggested that γ-5 enhanced glutamate affinity of GluA2-containing CI-AMPARs, but not of CP-AMPARs, The results of this study were later disputed by Soto et al. (2009), who reported that γ-5 does not regulate CI-AMPAR properties but selectively regulates long forms of GluA2-lacking CP-AMPARs. As with the 'type I TARPs', γ-5-associated AMPARs exhibited an increased mean single-channel conductance. However, this was accompanied with no significant effect on desensitisation or deactivation and by an unexpected attenuation of peak open probability (Soto et al., 2009). The same effects on decay kinetics and single-channel conductance are also characteristic of the other atypical TARP, γ-7 (Kato et al., 2007). A recent report suggests γ-7 selectively enhances the synaptic delivery of CP-AMPARs, and inhibits GluA2-containing CI-AMPARs from reaching the synapse (Studniarczyk et al., 2013).

TARPs have diverse effects on AMPAR pharmacology. For example, although traditionally characterised as a competitive antagonist, it has been found that CNQX acts as a partial agonist when AMPARs are associated with γ-2, -3, -4 or -8 (Menuz et al., 2007; Lee et al., 2010b), but not γ-7 (Bats et al., 2012). TARP-associated AMPARs further exhibit an increased response to the partial agonist kainate, though this does not appear to be the case for γ-5 (Kato et al., 2007). TARPs also increase the affinity of the AMPAR antagonist GYKI 53655 (Cokić and Stein, 2008), as well as modulating the affinity and efficacy of the AMPAR potentiators including cyclothiazide and 4-[2-(phenylsulfonylamino)ethylthio]-2,6-difluoro-phenoxyacetamide (Tomita et al., 2006). Without TARP-association, these channel potentiators enhance the deactivation and

desensitisation of flip splice variants of AMPAR subunits to a greater degree than the flop splice variants (Partin et al., 1994). TARP-association makes both splice variants equally sensitive to these potentiators (Tomita et al., 2006). By modulating the AMPAR mean single-channel conductance, TARPs are able to enhance the open channel block by polymaine toxins such as philanthotoxin-74 (Jackson et al., 2011). As the enhancement of channel conductance is TARP specific, the efficacy of polyamine toxin block is similarly dependent on the associated TARP (Jackson et al., 2011). However, channel block by the synthetic polyamine toxin 1-naphthyl acetyl spermine trihydrochloride (NASPM) was found to be reduced by association with the TARPs γ-2, -3 and -8, but not γ-4 (Kott et al., 2009).

As a distinct family of AMPAR auxiliary subunits, CNIH-2 and -3 act to chaperone AMPARs from the ER to the Golgi complex (Harmel et al., 2012; Shi et al., 2010). CNIHs remain bound to AMPARs to increase their membrane expression and slow desensitisation and deactivation kinetics of synaptic AMPARs in certain neurons and glia (Schwenk et al., 2009; Gill et al., 2011; Coombs et al., 2012). In hippocampal neurons CNIH-2/3 has similar effects on γ-8 associated AMPARs to suggest both subunits can mutually interact with the same AMPAR (Kato et al., 2010). CNIH-2/3 further modify AMPAR pharmacology, specifically by increasing the sensitivity to kainate in the presence of the AMPAR potentiator cyclothiazide (Coombs et al., 2012; Gill et al., 2011; Kato et al., 2010; Shi et al., 2010). CNIH-2/3 have greater effects on the gating of CP-AMPARs in comparison to CI-AMPARs. For example, CNIH-2/3 association increases single-channel conductance and glutamate potency, reduces intracellular polyamine channel block, and enhances Ca^{2+} permeability (Coombs et al., 2012). Further differences in subunit regulation by CNIHs were demonstrated in hippocampal neurons, where CNIH-2/3 appears to selectively bind to GluA1, with its association to GluA2 occluded by γ-8 association (Herring et al., 2013).

Other AMPAR auxiliary subunits are less well defined functionally; CKAMP44 association with AMPARs increases the rate of desensitisation and slows the recovery from desensitisation (von Engelhardt et al., 2010). In addition, SynDig1 binds to the AMPAR CTD, and potentially increases trafficking and accumulation at synapses in develop-

ing hippocampal neurons (Kalashnikova et al., 2010). However, a later study suggests that SynDIG1 increases both synaptic AMPA and NMDA receptor numbers exclusively through regulating excitatory synaptogenesis, rather than a direct influence on AMPAR gating, pharmacology, or surface trafficking (Lovero et al., 2013). Finally, in contrast to TARPs, and similar to CKAMP44, GSG1L slows AMPAR recovery from desensitisation (Shanks et al., 2012).

The picture of AMPAR auxiliary subunits is not about to get any simpler. A detailed quantitative proteomic screen has identified a further 21 potential AMPAR auxiliary subunits (Schwenk et al., 2012). Some of which are transmembrane proteins like those mentioned above, whereas others are suspected to be purely cytoplasmic proteins, or even secreted proteins that bind extracellularly.

1.3.3 | AMPAR properties are altered by post-transcriptional modifications

The editing and alternative splicing of AMPAR mRNA can fundamentally change AMPAR properties. The Ca^{2+} permeability of AMPARs is dependent on RNA editing of the GluA2 subunit. The molecular determinant of Ca^{2+} permeation is an individual amino acid located at the extracellular point of the M2 TMD, which forms the narrowest region of the open ion pore (Burnashev et al., 1996). mRNA encoding the GluA2 subunit undergoes post-transcriptional modification to replace the glutamine (Q) present at this residue position with an arginine (R) (Sommer et al., 1991). RNA editing is mediated by the adenosine deaminase acting on RNA 2 (ADAR2) enzyme (Higuchi et al., 1993; Melcher et al., 1996) and is almost 100% efficient (Cull-Candy et al., 2006).

Other features of GluA2-lacking CP-AMPARs which distinguish them from GluA2-containing CI-AMPARs include a relatively larger single-channel conductance (Swanson et al., 1997), faster kinetics (Geiger et al., 1995), sensitivity to intracellular polyamines at positive membrane potentials (Bowie and Mayer, 1995) and use- and voltage-dependent noncompetitive block by polyamine toxins (Blaschke et al., 1993; Herlitze et al., 1993; Kamboj et al., 1995; Koh et al., 1995; Strømgaard et al., 2005).

Further towards the C terminus, an arginine (R) situated between the M3 and M4 TMDs can be edited to a glycine (G) by ADAR-1 and -2 in the GluA-2, -3 and -4 subunits (Lomeli et al., 1994; Yang et al., 1997). R/G editing influences receptor assembly by prolonging GluA2 folding in the ER, which may be crucial for correct formation of heteromeric CI-AMPARs (Greger et al., 2006). In addition to their assembly, biophysical properties are modulated, whereby editing from R to G confers a more rapid recovery from desensitisation (Lomeli et al., 1994).

Downstream of the R/G residue an exon can be alternatively spliced to produce either the flip or flop AMPAR isoforms (Sommer et al., 1990). The splicing site refers to a 38 sequence of residues which differs in 9-11 individual amino acids (Sommer et al., 1990). Alternative splicing can occur in all four GluA subunits, which can heteromerise with different combinations of flip and flop subunit isoforms (Sommer et al., 1990). In addition to cell-type differences (Geiger et al., 1995), flip isoforms are predominantly expressed during development, whereas equal levels of either isoform occur in the adult brain (Monyer et al., 1991). The differentially spliced 38 amino acids sequence resides at the dimer interface within the LBD, just before the M4 TMD (Hollmann and Heinemann, 1994). Biophysical differences have been reported between the receptor variants depending on the AMPAR subunit. The flip variant of GluA-2, -3 and -4 desensitises slower and recovers from desensitisation faster than the flop variants (Mosbacher et al., 1994; Koike et al., 2000). In contrast, both isoforms of GluA1 homomers desensitise at equal rates (Mosbacher et al., 1994; Koike et al., 2000; Quirk et al., 2004). A more recent study reports that upon glutamate binding, the channels of both isoforms open at the same rate, but the flip channel undergoes closure at a faster rate (Pei et al., 2009).

1.3.4 | Post-translational modifications influence AMPAR trafficking and gating

At multiple stages in the lifetime of an AMPAR, enzymes can covalently attach functional groups at specific residues to modify receptor functions and increase receptor diversity. Post-translational modifications occur predominantly within the CTD, though residues in the intracellular loops between M1 and M2, as well as M2 and M3 TMDs are also subject

to modification (Lu and Roche, 2012; Traynelis et al., 2010).

Phosphorylation of AMPARs by several protein kinases present at the PSD modulates their synaptic targeting, internalisation and gating properties (Lu and Roche, 2012; Traynelis et al., 2010). The majority of studies that have investigated AMPAR phosphorylation have reported effects on their synaptic trafficking, particularly through the phosphorylation of serines in the CTD of GluA1 and 2 (Lu and Roche, 2012). For example, Protein kinase C (PKC) phosphorylation of the serine at residue 818 within the GluA1 CTD enhances its incorporation both at the synaptic (Boehm et al., 2006) and extrasynaptic membrane (Lin et al., 2009), the later mediated through promoting the binding to the actin-interacting protein 4.1N. Another GluA1 CTD serine positioned at amino acid 845 is subject to Protein kinase A (PKA) phosphorylation, which promotes the maintenance of GluA1 containing CP-AMPARs at perisynaptic sites (He et al., 2009), and increases GluA1 content at the PSD through increasing its incorporation (Lee et al., 2000) and decreasing endocytosis (Man et al., 2007). The GluA2 CTD contains two serine residues. Phosphorylation of ser880 by PKC enhances AMPAR endocytosis by modulating the binding of the GluA2 to GRIP1 and PICK1(Chung et al., 2000; Matsuda et al., 1999).

The post-translational regulation of AMPARs also occurs through phosphorylation of tyrosine residues. The GluA2 tyr876 is phosphorylated by Src tyrosine kinases to attenuate the interaction between CI-AMPARs and GRIP1 (Hayashi and Huganir, 2004). Phosphorylation of the same tyrosine was also reported to disrupt the interaction between GluA2 and BRAG2, a GTPase which promotes receptor endocytosis (Scholz et al., 2010). AMPAR Phosphorylation is not limited to the CTD, but also occurs in the intracellular sequence that forms a loop between the M1 and M2 TMDs. This structure has been implicated with efficient synaptic trafficking of GluA1 homomers and GluA1/2 heteromers (Lu et al., 2010). Such facilitation is attenuated when ser567, within the cytoplasmic loop, undergoes phosphorylation by Ca^{2+}/calmodulin-dependent protein kinase II (CaMKII) (Lu et al., 2010). Phosphorylation of AMPAR auxiliary subunits can further modify AMPAR trafficking. Opazo et al. (2010) found CaMKII-phosphorylation of γ-2 promoted the immobilisation of AMPARs at the PSD by reducing their lateral movement in the

membrane.

Phosphorylation of GluA1 CTD serines not only influences receptor trafficking, but also AMPAR gating mechanisms. For example, PKA enhances mean peak open probability by phosphorylating ser845 (Banke et al., 2000). In GluA1 homomers, ser831 is phosphorylated by either PKC or CaMKII to increase single-channel conductance (Barria et al., 1997a,b; Roche et al., 1996), whereas in GluA1/2 heteromers the same phosphorylation is dependent on receptor association with a member of the TARP family of auxiliary proteins (Kristensen et al., 2011).

Palmitoylation involves the addition of a palmitoyl group from palmitoyl-coenzyme A to cysteine residues, catalysed by palmitoyl acyl transferases (Dietrich and Ungermann, 2004). A cysteine in the M2 TMD and another in the CTD, conserved across all AMPAR subunits, are subject to palmitoylation (Hayashi et al., 2005). The palmitoylation of the cysteine in the M2 pore region both prevents receptor degradation, and confers a signal for retention in the Golgi apparatus until depalmitoylated by palmitoyl thioesterase (Hayashi et al., 2005). Palmitoylated of the cysteine in the CTD blocks interaction with protein 4.1N and thus increases the propensity for internalisation from the plasma membrane (Lin et al., 2009).

Ubiquitination of AMPARs acts a signal for their degradation. The mechanism involves the binding of either an individual or chain of ubiquitin molecules to lysine residues, catalysed by ubiquitin ligases (Pickart and Eddins, 2004). For the GluA1 subunit, a lysine at position 868 is ubiquitinated by ligases such as anaphase-promoting complex (Fu et al., 2011) and Nedd4 [neural precursor cell expressed developmentally down-regulated protein 4] (Lin et al., 2011). This predominantly occurs at the plasma membrane to promote endocytosis and lysosomal degradation (Schwarz et al., 2010). In contrast, GluA2 subunits are ubiquitinated following internalisation (Lussier et al., 2011), a process which does not involve either of the ligases responsible for GluA1 ubiquitination (Fu et al., 2011; Lin et al., 2011). To date, there have been no reports of GluA3 or GluA4 ubiquitination (Lin and Man, 2013).

1.4 | Neurotransmitter release

In addition to the amplitude of the postsynaptic response to a single quantum (q), Katz and colleagues described synaptic transmission to be a function of the number of independent release sites (N) and the probability of release (p) (Katz 1969). Before considering release probability and how it can be influenced, I address the subject of neurotransmitter release.

At presynaptic terminals, or en passant boutons, neurotransmitter can be released by several distinct mechanisms. I will largely ignore the slower forms of exocytosis including dense-core vesicular transmission of monoamines and neuropeptides (Bean et al., 1994), and release resulting from reversal of neurotransporters (Szatkowski et al., 1990). Instead, I will consider the probability of neurotransmitter release via the classically described vesicular synaptic transmission, which often occurs adjacent to specialised PSDs and typically involves a rapid rise and decay in neurotransmitter concentration.

1.4.1 | Active zones dock synaptic vesicles for release

In response to an action potential, neurotransmitter release can occur from axon terminals or boutons, which contain sites of release, termed active zones (Südhof, 2012). Although the pioneering studies mentioned earlier refer to a synapse as a point of contact between the axon and dendrites (subsection 1.1.1), the structural definition of a synapse is more appropriately fulfilled by the electron-dense pre- and post-synaptic membrane thickening, representing the active zone and PSD, respectively (Atwood and Karunanithi, 2002; Pfenninger et al., 1972). The active zone functions to anchor and prime synaptic vesicles for exocytosis across the cell membrane, position VGCCs in close apposition to the vesicles, and secure both vesicles and VGCCs to cell-adhesion proteins (Südhof, 2012).

The active zone cytomatrix is constituted of a number of proteins that provide specialised roles (Figure 1.6). The scaffolding Rab3-interacting molecule (RIM) proteins couple to VGCCs (Kiyonaka et al., 2007) and maintain the distribution of readily releasable and docked neurotransmitter vesicles through interaction with the vesicular membrane protein

Rab 3/27 (Han et al., 2011). RIM-binding proteins (RIM-BPs) connect VGCCs to RIMs (Hibino et al., 2002) and Munc-13 proteins prime the SNAREs for vesicle exocytosis (Augustin et al., 1999; Betz et al., 1997, 2001). In vertebrates, Bassoon and piccolo proteins are essential for the efficient transport of synaptic vesicles from the axon swelling interior within close proximity to the active zone (Mukherjee et al., 2010; Hallermann et al., 2010). Knockout studies have identified other proteins such as α-liprin, ELKS proteins and CAST as essential features of the active zone but their exact functions are perhaps too enigmatic to describe succinctly here.

The neurotransmitter vesicles which are primed at the active zone for immediate release are referred to as the readily releasable pool, and only comprise 1% of the total number of vesicles within an axonal varicosity (Rizzoli and Betz, 2005). They can be morphologically identified by electron microscopic imaging of FM1-43-stained vesicles (Schikorski and Stevens, 2001). For example, in cultured hippocampal neurons, from a total number of 40-800 synaptic vesicles, typically only 0-15 are docked ready for release (Branco et al., 2010; Murthy et al., 2001; Schikorski and Stevens, 2001).

1.4.2 | Action potentials drive neurotransmitter release across the synapse

Within 0.5 ms of a propagating action potential invading an axonal swelling, VGCCs open in response to membrane depolarisation (Borst and Sakmann, 1996, 1998). Experiments from the calyx of Held, a large presynaptic structure in the auditory brainstem, have reported that the Ca^{2+} concentration from VGCC opening can vary between 10-100 mM within a local domain, at least 10,000 fold greater than resting levels (Bollmann et al., 2000; Schneggenburger and Neher, 2000; Wang et al., 2008). As the time of diffusion is proportional to the square of distance (Einstein, 1905), the rapid speed of synaptic transmission stipulates that local VGCC mediated Ca^{2+} influx and the presynaptic elements that mediate synaptic vesicle release, should be in close proximity. Indeed, electron microscopic studies at the frog NMJ have suggested a distance of $\sim$ 20 nm (Harlow et al., 2001). At some central synapses, an equivalent distance is proposed given the attenuated action potential-driven release observed following application of the fast

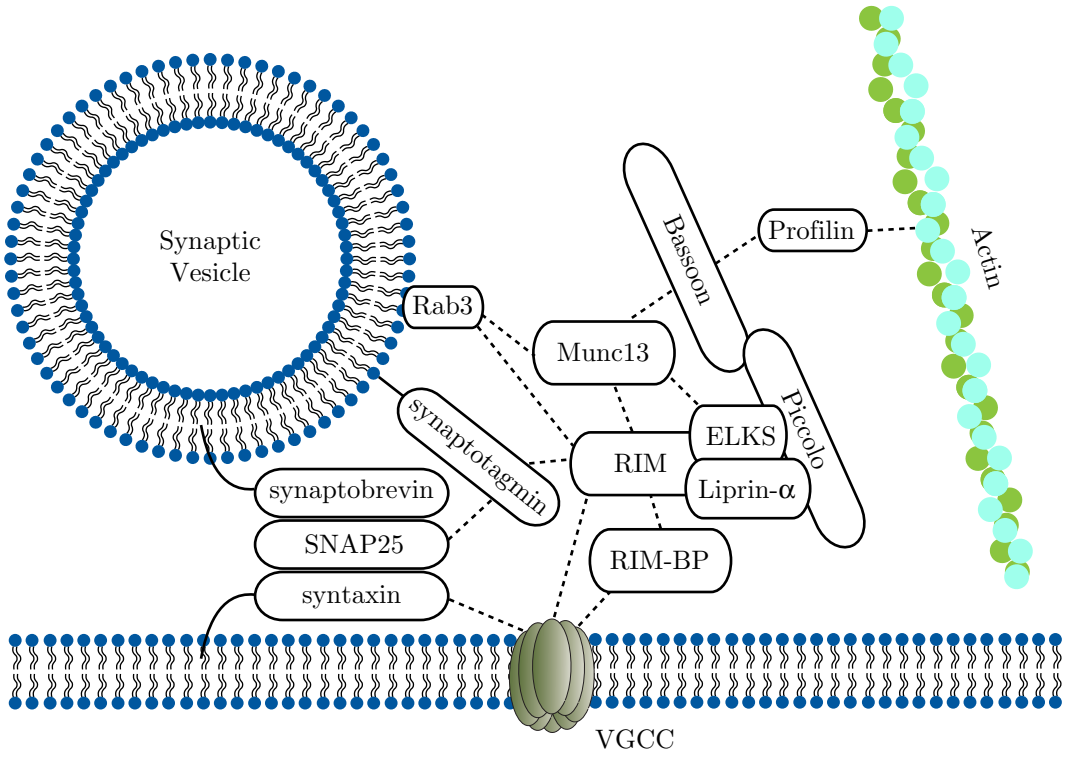

Figure 1.6: Organisation of the active zone

Schematic representation of proteins involved in the fusion of synaptic vesicles at the active zone. Dotted lines refer to proteins that interact with one another. VGCCs open to allow the influx of Ca^{2+} in close proximity to the Ca^{2+} sensor synaptotagmin. Its binding of Ca^{2+} promotes the conformation changes in the three SNAREs; synaptobrevin, SNAP25 and syntaxin that mediate vesicle exocytosis. The Rab proteins attach synaptic vesicles to the active zone protein complex by binding RIM, which itself binds to MUNC13, ELKS and liprins. RIM also stabilises VGCCs to the active zone through its direct binding, and through the binding of RIM-BP. Figure based on an image from Südhof (2012).

Ca^{2+} chelator; BAPTA [1,2-bis(o-aminophenoxy)ethane-N,N,N',N'-tetraacetic acid], but not the slow buffer; ethylene glycol-bis(2-aminoethylether)-N,N,N',N'- tetraacetic acid (EGTA) (Christie et al., 2011; Rozov et al., 2001). Thus, at certain synapses, VGCCs are contained within the active zone matrix, a configuration referred to as nanodomain coupling (<100 nm) (Eggermann et al., 2012) (Figure 1.6). The efficacy of action potential-driven release is subject to the fourth power of external Ca^{2+} concentration (Dodge and Rahamimoff, 1967). Such effective cooperativity between Ca^{2+} and neurotransmitter release means that just 1 or 2 VGCCs are required to release a single vesicle (Bucurenciu et al., 2010; Shahrezaei et al., 2006). Nanodomain coupling of VGCCs is not a requisite for action potential-dependent release; at other CNS synapses, VGCCs which transform cell spiking into release are positioned >100 nanometers away from the active zone in the microdomain (Goswami et al., 2012; Ohana and Sakmann, 1998). It is thought that this configuration produces a relatively delayed global rise in Ca^{2+} levels within the varicosity to promote release.

Ca^{2+} influx at the active zone predominantly occurs through the P/Q- (Cav2.1) and N- (Cav2.2) type high threshold-VGCCs (Llinás et al., 1992), though R-type (Cav2.3) and L-type (Cav 1.1-1.4) VGCCs may also be tightly coupled to active zones at specific synapses (Brandt et al., 2005; Gasparini et al., 2001; Li et al., 2007; Moser and Beutner, 2000). There are even some rare examples where low-threshold T-type VGCCs (Cav3.1-3.3) have been shown to mediate release. For example, at the ribbon synapse in retinal bipolar cells (Pan et al., 2001) and at a subset of glutamatergic terminals in the entorhinal cortex (Huang et al., 2011b). Not only does the type of VGCC at presynaptic terminals change, but so do their number. By taking outside-out patches of membrane from the release face of the calyx of Held, Sheng et al. (2012) showed an active zone contains a wide range (5-218) of VGCCs, and that synaptic strength was correlated with VGCC number. Similar to the calyx of Held, γ-aminobutyric acid (GABA) release from cerebellar MLIs involves the opening of 100-200 VGCCs (Rusakov et al., 2005). However, not all synapses open large number of VGCCs in response to action potentials. Data from the hair-cell ribbon cells (Brandt et al., 2005) and the squid giant synapse (Augustine et al., 1991), suggest action potentials can trigger release through a very small number of VGCCs. In

the case of the the chick ciliary ganglion calyceal synapse, an individual VGCC may evoke transmitter release (Stanley, 1993).

Downstream of VGCC mediated Ca^{2+} influx, the mechanics of vesicle fusion are mediated by SNARE protein complexes. Two major components of the SNARE complex are synaptobrevin-2, which is localised on synaptic vesicle membrane (Trimble et al., 1988; Baumert et al., 1989), as well as syntaxin and SNAP25 positioned on the cell target membrane (Bennett et al., 1992; Oyler et al., 1989). The vesicular and target SNAREs physically join as a four-helix bundle (Sutton et al., 1998), in which two helices contributed by SNAP-25 and one helix from each synaptobrevin-2 and syntaxin-1 proteins act as a 'zip', pulling the vesicle closer to the cell membrane within three sequential binary stages (Gao et al., 2012). For synaptic vesicles involved in action potential-driven synchronous release, this process is thought to occur prior to the incoming action potential in a process termed 'priming'. A protein called complexin binds to the 'zipped' SNARE complex, restricting membrane fusion to provide a mechanism for super fast Ca^{2+} triggered membrane fusion (Yoon et al., 2008; Maximov et al., 2009).

Once membrane depolarisation has occurred the local increase in Ca^{2+} is subsequently recognised by the fast Ca^{2+} sensor, synaptotagmin (Geppert et al., 1994). Synaptotagmins exist in three isoforms -1, -2 and -9 with differential expression patterns in the brain as well as varying kinetics in synaptic vesicle fusion; synaptotagmin-2 being the most rapid followed by -1 and then -9 (Xu et al., 2007). Ca^{2+} binding at each of the two C2 synaptotagmin domains promotes its interaction with both the vesicular and cellular membrane, and also to the SNARE protein complexes, where it displaces complexin and initiates fusion of the two membranes (Maximov et al., 2009).

During physiological cell firing, neurotransmitter is initially released from the readily releasable pool. At a single active zone in the calyx of Held, between 1-10 readily releasable vesicles are docked at the membrane (Sheng et al., 2012). Once depleted, additional vesicles for release are supplied by a recycling pool, located outside the active zone (Südhof, 2012). From the total synaptic vesicle population, only 15-20% are labelled with FM vesicle dyes (Richards et al., 2000, 2003; Rizzoli and Betz, 2004). It is thought that the remaining vesicles reside within a reserve pool maintained relatively immobile

by the protein synapsin and are only recruited during intense firing frequencies (Rosahl et al., 1995). At large presynaptic varicosities, such as the retinal bipolar ribbon synapse (Paillart et al., 2003), the Drosophila NMJ (Denker et al., 2009) and the calyx of Held (de Lange et al., 2003), the recycling vesicles are not spatially segregated from the reserve pool. In comparison, at small neuron terminals in the hippocampus, recycling vesicles are stabilised by actin filaments closer to the active zone than the reserve vesicles (Marra et al., 2012), suggesting their sub-terminal position is important for their function.

1.4.3 | Asynchronous neurotransmitter release occurs >2ms after an action potential

2-6 ms following an action potential, Ca^{2+} levels local to the VGCCs decay to equilibrium through binding of fast Ca^{2+} buffers such as calbindin and diffusion from the active zone (Kochubey et al., 2011). After this rapid decay in the local Ca^{2+} domain a residual <0.5 mM Ca^{2+} concentration is present in the active zone (Helmchen et al., 1997). This residual Ca^{2+} is cleared at a slower rate ($\leqslant$100ms) by alternative extrusion mechanisms including K^+-dependent Na^+/Ca^{2+} exchangers and Ca^{2+}-ATPases within the cell membrane, as well as smooth ER Ca^{2+}-ATPases (Kim et al., 2005), and slow mobile Ca^{2+} buffers such as parvalbumin (Collin et al., 2005a). In contrast to the synchronous action potential driven release, the relatively lengthy equilibrium phase of resting Ca^{2+} levels provide conditions for asynchronous release, defined loosely by its variable delay following an action potential (Atluri and Regehr, 1998; Goda and Stevens, 1994).

The aforementioned fast rise and slow decay of Ca^{2+} provides a temporal separation of synchronous and asynchronous release. Such processes may also be separated in their mechanism of vesicle fusion. Studies of hippocampal neurons (Liu et al., 2009) and the calyx of Held (Nikishi and Augustine, 2004) suggest asynchronous release does not require the Ca^{2+} sensor synaptotagmin-1 or -2. Rather, the SNARE Doc2 may respond to the relatively lower Ca^{2+} levels to initiate the vesicle fusion cascade (Yao et al., 2011). The possibility that the mechanism which mediates asynchronous release differs from that of synchronous release is intriguing given that Ca^{2+} entry through transient receptor potential vanilloid receptor 1 (TRPV1) increases the rate of asynchronous release without

modulating synchronous release (Smith et al., 2012).

1.4.4 | A distinct form of neurotransmitter release occurs 'spontaneously'

In addition to the synchronous or asynchronous vesicle fusion resulting from action potential depolarisation, neurotransmitter release can occur spontaneously with a relatively low probability (Murthy and Stevens, 1999). This was first demonstrated at the frog NMJ using the then recently developed technique of intracellular microelectrode recording. Fatt and Katz (1952) showed that in the absence of motor neuron firing, release of the neurotransmitter ACh could occur spontaneously (Fatt and Katz, 1952). Later work by Katz and Miledi (1969) found that it was possible to block action potential-dependent release through the selective block of voltage-gated Na^+ channels by tetrodotoxin (TTX) (<30 nM for most Na^+ channels besides Nav1.5, 1.8 and 1.9 which are blocked at >1 μM (Hille, 1992)). This allowed for the exclusive study of spontaneous release. Alternatively, the replacement of external Ca^{2+} with Mn^{2+} or Mg^{2+} in central neurons provided further means of isolating spontaneous events (Brown et al., 1979; Kojima and Takahashi, 1985; Shapovalov et al., 1979).

By definition, spontaneous release should involve the random fusion of vesicles with the plasma membrane with no regulatable mechanism. However, from early studies at the NMJ (Hubbard et al., 1968) it was clear the frequency of miniature postsynaptic currents (i.e. in the presence of TTX) could be dependent on external Ca^{2+} levels. Thus, my preconception of the stochastic nature of spontaneous release now appears naive given the present literature describing a huge diversity in Ca^{2+}-dependent and -independent mechanisms across different synapses (Glitsch, 2008b). For example, spontaneous release at hippocampal and cortical interneuron terminals is mediated by high-threshold VGCCs (Goswami et al., 2012; Williams et al., 2012). By comparison, spontaneous release from cortical and hippocampal pyramidal cells, as well as glutamatergic inputs onto cerebellar Purkinje cells, is dependent on Ca^{2+}, but not affected by Ca^{2+} influx through VGCCs (Scanziani et al., 1995; Vyleta and Smith, 2011; Yamasaki et al., 2006). At cortical glutamatergic terminals, a Ca^{2+}-sensing G-protein-coupled receptor has been shown to

elicit spontaneous release (Vyleta and Smith, 2011). A similar scenario exists for cerebellar MLI terminals which contact Purkinje cells, where there is no contribution of VGCCs (Glitsch, 2006), but large amplitude events specifically arise from intracellular ryanodine-sensitive Ca^{2+} stores (Llano et al., 2000; Conti et al., 2004; Collin et al., 2005b).

In contrast to the high cooperativity between Ca^{2+} resulting from action potential invasion and synchronous neurotransmitter release (Dodge and Rahamimoff, 1967), the dose-response curve relating Ca^{2+} concentration to spontaneous release is relatively linear (Lou et al., 2005; Sun et al., 2007). One explanation may be the relative efficiency of Ca^{2+} sensors at partial saturation (Goswami et al., 2012). At synapses where spontaneous release is independent of Ca^{2+} inflow and extracellular or intracellular Ca^{2+} (Scanziani et al., 1992; Llano and Gerschenfeld, 1993) spontaneous release could reflect random vesicular fusion without binding of Ca^{2+} (Lou et al., 2005; Sun et al., 2007).

Downstream of the Ca^{2+} sensor, both Ca^{2+}-dependent and -independent forms of spontaneous release may act through a common SNARE complex mechanism, separate from that which mediates evoked release. Ablation studies show that unlike action potential driven release, a residual low level of spontaneous release can occur without synaptobrevin-2 or SNAP-25 (Bronk et al., 2007; Schoch et al., 2001; Washbourne et al., 2002). Moreover, the specific motifs of SNAP-25 which stabilise the SNARE complex appear to differ between the two forms of release (Weber et al., 2010).

Further divergence from evoked release may arise from the source of spontaneously released vesicles, which has been proposed to differ from the readily-releasable pool (Chung et al., 2010; Koenig and Ikeda, 1999; Sara et al., 2005). Though others have reported that there is no distinction between vesicle pools which contribute to the two forms of release (Groemer and Klingauf, 2007; Hua et al., 2010; Wilhelm et al., 2010). In one study which imaged a biotinylated version of synaptobrevin-2, spontaneously released vesicles were reported to originate from the refractory resting pool (Fredj and Burrone, 2009). A more recent paper identified the non-canonical SNARE protein, Vps10p-tail-interactor-1a to be selectively present at spontaneously released vesicles, rather than synaptobrevin-2, which mediates action potential driven vesicle fusion (Ramirez et al., 2012).

An analogy has been made to the internet and telephone signals transmitted across a

common communication medium. For this analogy to be appropriate, the distinct forms of information must also be separated at the other end. Indeed, separate postsynaptic receptor populations may be tuned to differentiate between spontaneous release and evoked release. Evidence comes from the activation of distinct populations of postsynaptic NMDA (Atasoy et al., 2008) and AMPA receptors (Sara et al., 2011) revealed by use-dependent blockers. How they are able to do this may depend on differential spatial fields of neurotransmitter release in the synapse. A striking example is provided by the retinal bipolar cell ribbon synapse, where spontaneous release occurs ectopically, spatially separate from the active zone (Zenisek, 2008).

Since its discovery, evidence has accumulated to suggest spontaneous quantal release provides the presynaptic neuron with a number of ways to regulate postsynaptic contacts, distinct from the information transferred by cell spiking. Spontaneous release is thought to contribute to the synaptic noise experienced by a neuron. The random fluctuations in membrane voltage have been found to have a number of effects on neuronal excitability. For an average resting membrane potential, increasing the amplitude of membrane voltage fluctuations will increase the chance of action potential initiation (Silver, 2010). In addition, synaptic noise has been shown to have either divisive or multiplicative effects on firing rate following synaptic input (Mitchell and Silver, 2003; Sceniak and Sabo, 2010). Besides contributing to neuronal noise, spontaneous release has been shown to influence cell firing (Carter and Regehr, 2002), stabilise developing synapses and maintain established synapses (McKinney et al., 1999; Verhage et al., 2000), modulate processes involved in local dendritic protein synthesis (Jakawich et al., 2010; Sutton et al., 2004) and regulate the propensity of postsynaptic sites to undergo plasticity (Kombian et al., 2000; Lee et al., 2010a).

1.5 | Probability of neurotransmitter release

Neurotransmitter release is inherently unreliable. The probability of release determines if an action potential successfully induces the fusion of synaptic vesicles. From classical electrophysiological quantal analysis of synaptic transmission, the parameter p has exhibited a characteristically large variability between release sites at different neurons (Branco

and Staras, 2009; del Castillo and Katz, 1954; Murthy et al., 1997; Silver et al., 1998). Heterogeneity further exists between the basal release probability of axonal varicosities upon the same axon (Atwood and Bittner, 1971; Bittner and Baxter, 1991), and even within the same axonal branch (Ariel et al., 2012).

The parameter p is thought to represent a combination of the number of vesicles primed at the plasma membrane (Dobrunz and Stevens, 1997; Schikorski and Stevens, 2001) and the average probability that a readily-releasable vesicle will fuse with the membrane (Rozov et al., 2001). Both the number of releasable vesicles and probability of vesicle fusion can vary across individual release sites (Dobrunz and Stevens, 1997; Ermolyuk et al., 2012). Whilst the variation in readily release vesicle number is correlated to the active zone size and varicosity volume (Holderith et al., 2012; Kay et al., 2011), the probability of vesicle fusion is not, but instead varies according to Ca^{2+} entry following action potential invasion (Ermolyuk et al., 2012). The later occurs with no apparent dependence on the specific subtypes of VGCCs (P/Q or N) involved (Ariel et al., 2012).

1.5.1 | Modulation of release probability

Release probability can be dynamically modulated by a neuron's intrinsic firing properties or processes extrinsic to the nerve terminal. The frequency of presynaptic firing can facilitate synaptic transmission, particularly at boutons with an initially low release probability (Zucker and Regehr, 2002). Repetitive action potential invasion of nerve boutons can result in a build up of residual Ca^{2+}, to increase release probability (Katz and Miledi, 1968). It could be argued that such an incremental increase in Ca^{2+} would be irrelevant considering the large concentrations reached following action potential invasion. One possible explanation could involve the saturation of Ca^{2+} buffers which would allow for the nonlinear summation necessary for facilitation (Neher, 1998; Blatow et al., 2003). Alternatively, the facilitatory effects of residual Ca^{2+} have been proposed to result from a second Ca^{2+} sensor, distinct from the low affinity synaptotagmins which initiate synchronous action potential driven exocytosis (Atluri and Regehr, 1996). A relatively high affinity Ca^{2+} binding protein would be more suited to respond to small increases in Ca^{2+}

concentration. Finally, residual Ca^{2+} may facilitate synaptic transmission through a use-dependent increase in VGCC function (Ishikawa et al., 2005). Ca^{2+} binding proteins such as calmodulin have been proposed to bidirectionally modulate VGCC function (Mochida et al., 2008).

At some synapses, despite the increase in basal Ca^{2+}, repetitive firing can concomitantly produce a depression in neurotransmitter release (Zucker and Regehr, 2002). This may result from either a use-dependent depletion of readily-releasible vesicles at synapses with a high release probability (Schneggenburger et al., 2002), a reduction in available release sites due to high frequency of exocytosis events (Neher and Sakaba, 2008), or through the down-regulation of VGCCs (Forsythe et al., 1998; Xu and Wu, 2005). Together, models incorporating initial release probabilities, vesicle depletion and residual Ca^{2+} levels have accurately predicted the balance between frequency dependent short-term facilitation and depression at particular synapses (Dittman et al., 2000; Varela et al., 1997).

In addition to frequency, differences in the action potential waveform can markedly influence the activity of VGCCs in the terminal, and thus influence neurotransmitter release (Bean, 2007). For example, at the calyx of Held, increasing the axonal Na^{+} conductance resulted in an acceleration of spike depolarisation and a subsequent reduction in the number of activated VGCCs at sites of release (Yang and Wang, 2006). At hippocampal MF boutons, the width of the action potential exhibits a positive relationship with presynaptic Ca^{2+} influx (Geiger and Jonas, 2000). As the action potential width increased with high-frequency stimulation (Geiger and Jonas, 2000), it appears that shape and frequency of action potentials do not act in isolation, but a combination of the two parameters provides presynaptic cells with a dynamic tool to modulate release probability.

A number of factors exogenous to the presynaptic varicosity can also influence neurotransmitter release and thus modulate p. Clues for this are provided by studies demonstrating that p and short-term plasticity can vary depending on the postsynaptic neuron identity (Koester and Johnston, 2005; Markram et al., 1998; Reyes et al., 1998; Sylwestrak and Ghosh, 2012). In hippocampal cultures, such postsynaptic regulation of p was shown to depend on the specific location within the dendrite, with terminals closest to the soma

exhibiting stronger release probabilities than those located more distally (Branco et al., 2010; de Jong et al., 2012). Explaining such phenomena has often involved a feedback system originating from the PSD to control release probability of specific terminals.

Activation of ionotropic and/or metabotropic receptors provide the most common mechanism for the local environment, or network activity, to dynamically shift the p from rest. Dixon (1924) provided the first evidence for presynaptic ionotropic control over release by demonstrating nicotine initially inhibited and subsequently excited the rabbit heart. Though it wasn't until Riker et al. (1957) demonstrated the effect of ammonium compounds on the cat NMJ that the phrase 'presynaptic receptor' was used. Subsequently, γ-aminobutyric acid A receptors ($GABA_ARs$) were shown to modulate release at primary afferent terminals in the spinal cord (Frank and Fuortes, 1957), and the effects of morphine on cat preganglionic nerves provided the first evidence for presynaptic metabotropic receptors (Trendelenburg, 1957).

By the early 1970s, studies were showing that presynaptic receptors could be activated either in a self-autonomous manner by responding to neurotransmitter released from the bouton where they are located (Langer, 1974; Vizi, 1979), or, following transmitter release from a neighbouring neuron (Knoll and Vizi, 1970, 1971). More recent reports describe other routes of activation including neurotransmitter release from glial cells (Jourdain et al., 2007; Mathew and Hablitz, 2011; Sasaki et al., 2011), and also neurotransmitter and diffusable messengers that are released retrogradely from the postsynaptic neuron (Duguid and Smart, 2004; Ohno-Shosaku et al., 2001; Wilson et al., 2001).

Presently, a greater number of studies have profiled presynaptic metabotropic receptors over their ionotropic counterparts. This may reflect their relative predominance at presynaptic sites however, as their effects occur over seconds or even minutes, rather than the millisecond range of ionotropic receptors, their effects may not necessarily overlap. Metabotropic receptors generally produce inhibition through negative coupling with adenyl cyclase or direct inhibition of VGCCs through the Go $\beta\gamma$ or Gq α subunits (Beech et al., 1992; Glaum and Miller, 1995; Takahashi et al., 1996; Tedford and Zamponi, 2006). Alternatively, Gq coupled metabotropic receptors can in some cases enhance Ca^{2+} influx in the terminal through the formation of diacylglycerol and activation of PKC

(Bannister et al., 2004) (Figure 1.1).

Many ionotropic receptors including $GABA_A$ (Trigo et al 2007), glycine (Turecek and Trussell, 2001), nicotinic (Garduño et al., 2012), 5-hydroxytryptamine receptor 3 (Koyama et al., 2000), TRPV1 (Gibson et al., 2008) and P2X receptors (Gu and Macdermott, 1997) have been found to influence presynaptic membrane excitability and thus regulate release properties and synaptic strength. I will next focus on how presynaptic iGluRs modulate release.

1.5.2 | Presynaptic iGluRs modulate release probability

Although predominantly thought to be located post-synaptically to mediate neurotransmission, iGluRs are also widespread at presynaptic sites, typically within axon terminals or en passant swellings where neurotransmitter is released. Presynaptic iGluRs have been implicated within a wide range of neuronal functions, including the motility of filopodia to direct growth cones for correct synaptogenesis (Chang and Camilli, 2001; Tashiro et al., 2003; Wang et al., 2011), the redistribution of synaptic vesicles (Gelsomino et al., 2012; Schenk et al., 2003, 2005), and when positioned in the axon, are capable of modulating the action potential waveform (Sasaki et al., 2011; Semyanov and Kullmann, 2001) (Table 1.1, 1.3). In line with early evidence of their presence at the NMJ and spinal primary afferent terminals (Dixon, 1924; Dudel and Kuffler, 1961; Eccles and Willis, 1963; Frank and Fuortes, 1957; Riker et al., 1957), presynaptic iGluRs have predominantly been investigated for their effects on neurotransmitter release probability (Engelman and Macdermott, 2004; Pinheiro and Mulle, 2008) (Table 1.1 - 1.3). In addition to altering the p from its typical state, presynaptic receptors may contribute to the basal p when tonically activated by ambient neurotransmitter in the extracellular space (Glitsch and Marty, 1999; Lauri et al., 2005; Sallert et al., 2009). Depending on the context, presynaptic iGluRs can either enhance or depress neurotransmitter release. The plethora of electrophysiological studies reporting influences of AMPA, NMDA and kainate receptors on both evoked and spontaneous neurotransmitter release are complied in tables 1.1, 1.2 and 1.3, respectively.

Several sources of glutamate have been proposed to activate presynaptic iGluRs (Tables

1.1 - 1.3). The main source of activation for presynaptic NMDA and kainate receptors appears to be the self-autonomous activation following synaptic release (Berretta and Jones, 1996; Contractor et al., 2001; Schmitz et al., 2001). For AMPARs this appears less common, instead glutamate spillover from neighbouring excitatory synapses (Satake et al., 2006) and release from glial cells appear to be more important (Sasaki et al., 2011). At certain synapses, both phenomena may also contribute to presynaptic NMDA (Huang and Bordey, 2004; Jourdain et al., 2007) and kainate receptor activation (Lourenço et al., 2010). Aside from these main mechanisms there are some rare examples of axo-axonic glutamatergic contacts (Cochilla and Alford, 1999), and retrograde release of glutamate from postsynaptic sites (Duguid and Smart, 2004).

1.5.3 | Presynaptic iGluRs modulate release probability through various mechanisms

The mechanisms by which presynaptic iGluRs modulate release can vary dramatically depending on the receptor involved, the form of release, and the features of a particular synapse. As a general rule, spontaneous release is enhanced following presynaptic AMPA, kainate or NMDA receptor activation (Tables 1.1-1.3). A simple explanation for this involves cation influx that depolarises the presynaptic membrane, and thus increases the propensity of VGCCs to open (Pinheiro and Mulle, 2008). If the iGluR is permeable to Ca^{2+}, then direct Ca^{2+} inflow may trigger release independently of VGCCs (Glitsch, 2008a). Alternatively, such Ca^{2+} influx may modulate spontaneous release by promoting Ca^{2+} release from from internal stores (Duguid and Smart, 2004; Rossi et al., 2008). One exception to this rule comes from the spinal cord, where activation of presynaptic NMDA and kainate receptors on primary afferents reduces miniature excitatory postsynaptic current (mEPSC) frequency (Bardoni et al., 2004; Kerchner et al., 2001).

At synapses where iGluR activation enhances spontaneous release, evoked release is often reduced (Table 1.1 and 1.2). Two theories that have attempted to explain this paradox originated from studies of presynaptic $GABA_A$Rs and AMPARs at sensory afferent terminals in the dorsal horn of the spinal cord and the crayfish NMJ (Segev, 1990; Stuart and Redman, 1992; Cattaert et al., 1992; Cattaert and Manira, 1999).

CNS region	Synapse	Trans-mitter	Source of activation	Subunit	Spontaneous release	Evoked release	Age	References
Visual cortex (V1)	Interneuron - L2/3 pyramidals	GABA	Axo-axonic pyr contacts	n/a	+	n/a	P20 - 30 tested	Ren et al 2007 (though see Hull et al 2009)
Hippocampus	CA3 pyramidals - CA3 pyramidals	Glu	Periaxonal astrocytes	n/a	n/a	+	P7 - 12 tested	Sasaki et al 2011
Cerebellum	MLI - Purkinje cell	GABA	Spillover from climbing fibre	GluA2/3	+	-	Lost at P15	Satake et al 2000, 2004, 2006, 2010, Rusakov et al 2005
	MLI - MLI	GABA	Spillover from parallel fibre	GluA2 lacking	+	-	Lost at P15	Liu 2007, Bureau & Mulle 2000, Rossi et al 2008.
Calyx of Held	Globular bushy cells - MNTB	Glu	n/a	n/a	n/a	-	P7-8 tested	Takago et al 2005
Spinal cord	Non - & nociceptive primary afferent - lamina I & II neurons	Glu	n/a	GluA1 & 2/3 labelled	n/a	-	P6 - 10 tested	Lee et al 2002 Gangadharen et al 2011
	Dorsal horn interneurons - lamina II neurons & NK1R lamina I neurons	GABA/ glycine	Possible glial or neuronal spillover	Indirect evidence for GluA2 lacking	+	-	Persists in 4-5 week old rats	Engelman et al 2006
Zebra fish endplate	1° & 2° motorneurons - axial white fibres	ACh	Likely glial Glu release	n/a	+	n/a	P4 - 6	Todd et al 2004

Table 1.1: Collated functional studies reporting presynaptic AMPAR-mediated modulation of release probability

+ signs indicate release is enhanced, whereas - corresponds to a reduction in neurotransmitter release. Abbreviations: Glu, glutamate; n/a, data not available; L, layer; MNTB, Medial Nucleus of the Trapezoid Body; NK1R, Neurokinin-1 receptor.

CNS Region	Synaptic Projection	Trans-mitter	Source of activation	Subunit	Spontaneous release	Evoked release	Age	References
Visual cortex (V1)	L4 pyr to L2/3 pyramidals	Glu	Autoreceptor / ambient (glia)	GluN1, 2B & 3A	+	+	P7-20 Lost at P23	Corlew et al 2007, Li et al 2008, Larsen et al 2011
	Glutamatergic inputs to L4 pyramidals	Glu	Autoreceptor / ambient (glia)	n/a	+	n/a	P7-20 Lost at P23	Corlew et al 2007
	L5 pyramidals to L5 pyramidals	Glu	n/a	GluN2B containing	+	+	P7-21 Lost at P23	Sjostrom et al 2003 Buchanan et al 2012
Somatosensory cortex (S1) (L4 barrel cortex)	L4 pyramidals to L2/3 pyramidals	Glu	Autoreceptor / Ambient / Spillover	GluN2B containing	+	+	P13-21 tested	Brasier & Feldman 2008, Bender et al 2006 Rodriguez-Moreno & Paulsen 2008
Entorhinal cortex	Glutamatergic inputs to L2 pyramidals	Glu	Autoreceptor / Ambient	GluN2B containing	+	n/a	n/a	Berretta and Jones 1996 Woodhall et al 2001
	Glutamatergic inputs to L5 pyramidals	Glu	Autoreceptor / Ambient	GluN2B containing	+	+	Lost by 5 months	Woodhall et al 2001 Yang et al 2006
Frontal cortex	Interneurons - L2/3 pyramidals	GABA	Ambient (glial)	GluN2B containing	+	+	Lost by P20	Mathew & Habliz 2011
Xenopus retinotectum	GABA inputs to Tectal neurons	GABA	Potential spillover	n/a	+	-	Tadpoles tested	Lien et al 2006
Hippocampus	CA3 pyramidals to CA1 pyramidals	GABA	Retrograde pregnenolone / Autoreceptor	GluN2D / GluN2B	+	+	GluN2D lost at P5	Mameli and others 2005, Suarez and others 2005, Suarez and Solis 2006 McGuinness et al 2010
	Glu inputs – dentate granule cells	Glu	Astrocytic release.	GluN2B immuno	+	+	P10-22	Jourdain and others 2007
Lateral Amygdala	Glu cortical inputs	Glu	n/a	n/a	n/a	n/a	P21-28	Humeau et al 2003
Nucelus Accumbens	VTA - NAc, PFC - NAc, amygdala - NAc		n/a	GluN1 & 3 independent	+	+	3-5 week old animals tested	Huang et al 2011
Cerebellum	Parallel fibre - Purkinje cell		n/a	GluN1, 2A & 2B	n/a	-	P18-26 tested	Casado et al 2000, Casado et al 2002, Bidoret et al 2009
	MLI - Purkinje cell	GABA	Purkinje retro-grade release / CF spillover	n/a	+	+	P11-14 tested	Duguid & Smart 2004, Duguid et al 2007, Glitsch 2008, Glitsch & Marty 1999 Huang & Bordey 2004, Fiszman et al 2005.
	MLI - MLI	GABA	Likely parallel fibre spillover	GluN2A & 2B	+	-	P11-14 tested	Glitsch & Marty 1999, Rossi et al 2012, Liu & Lachamp 2006,
Spinal Cord	Dorsal horn glutamatergic afferents	Glu	Autoreceptor	n/a	-	-	P6-12 tested	Bardoni et al 2004
Zebra fish endplate	1° & 2° motorneurons - axial white fibres	ACh	Likely glial Glu release	GluN2A	+	n/a	4-6 day old zebrafish	Todd et al 2004

Table 1.2: Collated functional studies reporting presynaptic NMDAR-mediated modulation of release probability

+ signs indicate release is enhanced, whereas - corresponds to a reduction in neurotransmitter release. Abbreviations: Glu, glutamate; n/a, data not available; L, layer; VTA, ventral segmental area; NAc, nucleus accumbens; PFC, prefrontal cortex.

CNS Region	Synaptic Projection	Trans-mitter	Source of activation	Subunit	Spontaneous release	Evoked release	Age	References
Prefrontal cortex L2/3	Glutamatergic inputs - L2/3 pyramidals	Glu	n/a	GluK1 containing	+ ([low] kainate)	+ ([low] kainate) - ([high] kainate)	P17-24 tested	Campbell et al 2007
Barrel cortex L4	Glutamatergic thalamocortical inputs - barrel cortex	Glu	Autoreceptor	GluK2/3	n/a	- (10uM kainate) + (3uM kainate)	Lost at P9	Jouhanneau et al., 2011 Kidd et al 2002
Entorhinal cortex L3	Glutamatergic inputs - L3 pyramindal cells	Glu	Autoreceptor	GluK1 containing	+	+	P28-40 tested	Chamberlain et al 2012
	GABAergic inputs - L3 pyramindal cells	GABA	n/a	GluK2 containing	+	+	P28-40 tested	Chamberlain et a l 2012
Hippocampus	CA3 pyramidal cells - CA1 pyramidal cells	Glu	Autoreceptor	GluK1 containing	- In neonate (Sallert '06)	-	Lost in juvenile	Kamiya & Ozawa, 1998 Frerking et al 2001 Sallert et al 2007 Lauri et al 2005 , 2006
	CA3 pyr - CA1 somatostatin interneurons	Glu	Autoreceptor	GluK2/3 heteromers	+	+	P10-15 tested	Sun & Dobrunz 2006 Sun et al 200 9
	GABAergic inputs - CA1 pyramidal cells	GABA	Spillover from Schaffer afferents	GluK1/2 heteromers	- (Maingret, '05) + (Mulle, '00)	- High [Glu] + Low [Glu]	Mixed ages P5-P23	Clarke et al 1997 Rodriguez-Morena et al 1997 Frerking et al 1999 Mulle et al 2000 Jiang et al 2001 Maingret et al 2005 Lourenco et al 2010
	GABAergic inputs - CA1 interneurons	GABA	n/a	GluK2	+ (Rat) No change (Mouse)	+	Mixed ages P5-P45	Cossart et al 2001 Mulle et al 2000 Semyanov & Kullmann 2001
	Granule cell mossy fibre - CA3 pyr	Glu	Autoreceptor	GluK2 & 3 GluK1 in some but not all studies	n/a	+	Mixed ages P14-P26	Lauri et al 2001, 2003 Pinheiro et al 2007 Schmitz et al 2001, 2003 Scott et al 2008
	Granule cell mossy fibre - CA3 pyrs	GABA	n/a	GluK1 containing	n/a	-	P2-5 tested	Caiati et al 2010
	CCK containing interneurons - pyramidal cells	GABA	n/a	GluK1 containing	n/a	-	P12-22 tested	Daw et al 2010
	CA3 - CA3 pairs organotypic slice	Glu	n/a	GluK1c GluK4 heteromers	n/a	-	P7-8 tested	Vesikansa et al 2012
Globus Pallidus	GABAergic inputs from striatum	GABA	n/a	GluK2/3	-	-	P13-17 tested	Jin & Smith 2007
Basolateral Amygdala	Glutamatergic inputs - pyramidal cells	Glu	Autoreceptor / ambient	GluK1 containing	+	+	P35-50 tested	Aroniadou-Anderjaska et al 2012
	Interneurons - pyramidal cells	GABA	n/a	GluK1 containing	+ Low [Glu] - High [Glu]	+ low [Glu] - high [Glu]	P15-22 tested	Braga et al 2003
Supraoptic nucleus of the Hypothalamus	GABAergic inputs - MCNs	GABA	Ambient	GluK1 containing	+ pre lactation - Oxytocin MCNs post lactation	+ pre lactation - Oxytocin MCNs post lactation	2-4 month tested	Bonfardin et al 2010
	Glutamatergic inputs - MCNs	Glu	Ambient	GluK1 containing	+	n/a	2-4 month tested	Bonfardin et al 2012
Cerebellum	Parallel fibre - Purkinje cell	Glu	Ambient / retrograde Glu from Purkinje	GluK2 containing	n/a	+	P13 - 4 month	Crepel 2007, 2009 Delaney & J ahr 2002
	Parallel fibre - Molecular layer interneuron	Glu	n/a	n/a	n/a	+ Low freq PF firing - High freq PF firing	P13-17	Delaney & Jahr 2002
Spinal cord	Non - & nociceptive Primary afferent - lamina I & II neurons	Glu	Autoreceptor	GluK1 containing	-	-	Cultures	Kerchner et al 2001a Kerchner et al 2002
	Dorsal horn interneurons - lamina I & II neurons	GABA & glycine	Spillover from glutamatetic afferents	Not GluK1 containing	+	No change [low] kainate - [high] kainate	Adult	Kerchner et al 2001b Xu et al 2006

Table 1.3: Collated studies of presynaptic kainate receptor function

Table 1.3 continued: + signs indicate release is enhanced, whereas - corresponds to a reduction in neurotransmitter release. Abbreviations: Glu, glutamate; n/a, data not available; L, layer; PF, parallel fibre; MCN, Magnocellular neurons; pry, pyramidal.

During the gating of ionotropic receptors, the increased conductance could create a local environment with reduced input resistance. According to Ohm's law, the amplitude of the action potential will be reduced, or shunted (Segev, 1990; Stuart and Redman, 1992; Cattaert et al., 1992; Cattaert and Manira, 1999; Lee et al., 2002; Engelman et al., 2006). Alternatively, ionotropic receptor-mediated membrane depolarisation may inactivate Na^+ channels to reduce their availability for the propagation of action potentials into the presynaptic varicosity (Graham and Redman, 1994; Cattaert and Manira, 1999; Dudel and Kuffler, 1961). These mechanisms are not necessarily mutually exclusive (Cattaert and Manira, 1999). In either scenario, there would be reduced activation of the voltage-gated Ca^{2+} and Na^+ channels involved in neurotransmitter release (Clements et al., 1987). In the context of these models, the depolarisation resulting from cation influx through AMPA, NMDA or kainate receptors would conceivably enhance neurotransmitter release in the absence of cell firing, yet act to attenuate action potential-driven release.

Though not confirmed, the depression of synaptic transmission at a number of synapses following activity of presynaptic NMDARs is consistent with the shunting and/or Na^+ channel inactivation hypothesis (Bardoni et al., 2004; Bidoret et al., 2009; Casado et al., 2000; Glitsch and Marty, 1999; Lien et al., 2006). However, at other synapses, presynaptic NMDAR activity underlies an enhancement in release probability (Table 1.2). A compatible theory posits a relatively weak depolarisation experienced by release sites may facilitate action potential-driven neurotransmitter release, whereas a greater depolarisation will act to shunt the action potential or inactivate Na^+ channels (Kamiya et al., 2002). The mechanism for the facilitation by NMDARs remains largely unresolved, though Duguid and Smart (2004) propose that instead of activating VGCCs, presynaptic NMDARs at cerebellar MLI – Purkinje cell synapses elicit Ca^{2+}-induced Ca^{2+} release (CICR) from ryanodine-sensitive stores to augment GABA release. The facilitatory effects of kainate receptors on action potential driven release at MF boutons onto CA3 pyramidal cells may also involve CICR (Lauri et al., 2003; Scott et al., 2008) (Table 1.3, Figure 1.7). Furthermore, a direct Ca^{2+} influx through the GluK2/3 channel has also been proposed at this synapse (Pinheiro et al., 2007). Similar to their effects on spontaneous release, kainate receptors may facilitate evoked release through increasing the activation of VGCCs

to increase release probability (Kamiya et al., 2002).

In a surprising revelation, it was found that presynaptic kainate receptors can interact with G-proteins to inhibit release (Rodríguez-Moreno and Lerma, 1998). Such inhibition occurs both through the pertussis sensitive, membrane delimited control of VGCCs (Lauri et al., 2005), and via the second messengers PLC and PKC (Bonfardin et al., 2010; Jin and Smith, 2007; Lauri et al., 2005; Rozas et al., 2003). The metabotropic effects of kainate receptor activation have been proposed to mediate the inhibition observed at the CA3 schaffer collateral synapse onto CA1 pyramidal neurons (Lauri et al., 2005), developing MF terminals which release GABA onto CA3 pyramidal cells (Caiati et al., 2010), GABAergic terminals upon CA1 pramidal cell neurons (Jiang et al., 2001), straital GABAergic boutons upon globus pallidus neurons (Jin and Smith, 2007) and GABAergic inputs to oxytocin containing magnocellular neurons (Bonfardin et al., 2010).

Similarly, the AMPAR-mediated reduction of evoked release has also been proposed to involve an interaction with G-proteins at certain synapses (Takago et al., 2005; Satake et al., 2004). At cerebellar MLI terminals the AMPAR-mediated activation of the $G_{i/o}$-protein was proposed to inhibit VGCC activity, prevent Ca^{2+} entry, and reduce release probability. The evidence for this is mechanism not strong, and whilst it could explain the reduction in evoked GABA release, it is not compatible with the potentiation in miniature inhibitory postsynaptic current (mIPSC) frequency (Bureau and Mulle, 1998; Rossi et al., 2008). This is unless a dichotomic regulation of the two forms of neurotransmitter release exists (subsection 1.4.4).

At some synapses, kainate receptors appear to show bidirectional regulation of release depending on the concentration of glutamate. An example was recently demonstrated in the supraoptic nucleus (SON) of the hypothalamus, where the spatial arrangement of glial-mediated neurotransmitter uptake can both alter presynaptic kainate receptor tonic activity and reverse the sign of their effect on release probability (Bonfardin et al., 2010). At axon terminals of Magnocellular neurons in the SON, presynaptic GluK1-containing kainate receptors responded to ambient glutamate to facilitate GABA release onto vasopressin neurons through a Ca^{2+} permeable ionotropic mechanism (Bonfardin et al., 2010). GluK1-containing kainate receptors, upon Magnocellular neuronal projections that

synapse onto oxytocin-containing neurons in the SON, reduced GABA release through a metabotropic pathway. This heterogeneity was only evident following lactation, which preceded a reduced astrocyte coverage around oxytocin but not vasopressin neurons. The reduced glial uptake produced an enhanced ambient glutamate concentration to switch the kainate receptor-modulation of GABA release from facilitation to inhibition. It will be interesting to examine if such consequences of neurotransmitter concentrations may also extend to bidirectional modulation of transmitter release by kainate receptors previously described in the hippocampus (Jiang et al., 2001; Schmitz et al., 2001), cerebellum (Delaney and Jahr, 2002), amygdala (Braga et al., 2003), spinal cord (Kerchner et al., 2001; Youn and Randic, 2004), and barrel cortex (Jouhanneau et al., 2011) (Table 1.3).

1.5.4 | Heterogeneous distribution of presynaptic iGluRs provides target-selective control of *p*.

Similar to the differential expression of presynaptic metabotropic receptors (Pelkey et al., 2006; Pelkey and McBain, 2007), when ionotropic receptor expression follows target-neuron selective patterns, the activity of such receptors endows the presynaptic cell with a mechanism to differentially excite, or inhibit, separate populations of postsynaptic neurons. In the cortex, presynaptic NMDARs consistently enhance action potential-driven and spontaneous neurotransmitter release (Brasier and Feldman, 2008; Buchanan et al., 2012; Corlew et al., 2007; Larsen et al., 2011; Mathew and Hablitz, 2011; Rodríguez-Moreno and Paulsen, 2008; Yang et al., 2006). An example of their heterogenous expression is provided in the visual cortex; Buchanan et al. (2012) recently demonstrate that during cell firing, localised photolysis of caged NMDA produced super-linear Ca^{2+} responses within layer 5 pyramidal axonal boutons. The presence of NMDARs was demonstrated to vary from one bouton to the next. In fact, this heterogeneity was target neuron-selective, as the subset of boutons which contained NMDARs appeared to synapse onto other layer 5 pyramidal cells and Martinotti interneurons, but not onto basket cells (Buchanan et al., 2012). The differential inter-bouton expression of NMDARs appears a robust characteristic of pyramidal cell axons between cortices and across cortex layers. Electrophysiological data demonstrates NR2B-containing presynaptic NMDARs

selectively modulate synaptic transmission between layer 4 and layer 2/3 pyramidal synapses, but not synapses between connected layer 4 pyramidal cells, or cross-columnar synapses onto other layer 2/3 pyramidal cells (Brasier and Feldman, 2008).

The ability of presynaptic ionotropic receptors to preferentially direct synaptic transmission to specific target neurons is supported by evidence in the hippocampus (Figure 1.7). In particular, differences in short-term plasticity between different types of synaptic connections have been shown to correspond with the presence of presynaptic kainate receptors. For example, glutamate release at MF – CA3 pyramidal cells exhibits greater use-dependent facilitation following subsequent action potentials compared to MF – interneruon and MF – hilar mossy cell synapses (Toth et al., 2000; Contractor et al., 2001; Lysetskiy et al., 2005). Recently, Scott et al. (2008) demonstrated that presynaptic kainate autoreceptors in MFs are located exclusively at synapses upon CA3 pyramidal cells, and not at boutons synapsing at stratum lucidium interneurons or hilar mossy cells (Figure 1.7). As MF glutamate acts on the kainate autoreceptors to facilitate subsequent glutamate release through activation of inositol trisphosphate (IP_3)-sensitive Ca^{2+} stores, Scott et al. (2008) rationalise that the relatively strong synaptic facilitation may partly result from the selective presence of kainate autorecpetors at these boutons.

Rather than enhancing excitation onto principal cells within a local network, the target-specific expression of presynaptic kainate receptors within glutamatergic axons may alternatively potentiate feed-forward inhibition. Presynaptic kainate receptors mediated target cell-specific short-term enhancement of glutamate release from CA3 Schaffer collaterals onto somatostatin-containing interneurons (Sun and Dobrunz, 2006) (Figure 1.7). Such potentiation reached up to 11-fold following physiological firing frequencies of the Schaffer collateral and differed from the typical low or absent short-term facilitation observed at synapses made with the majority of interneurons in the stratum radiatum, which do not contain somatostatin (Sun et al., 2009). As these two populations of interneurons are thought to have divergent axonal arborisations onto CA1 pyramidal cells (Freund and Buzsáki, 1996; Oliva et al., 2000), target cell-specific expression of presynaptic kainate receptors provides a mechanism to modulate the spatial inhibition of principal cells. In the local hippocampal network, high frequency firing of the CA3 Schaffer collateral would

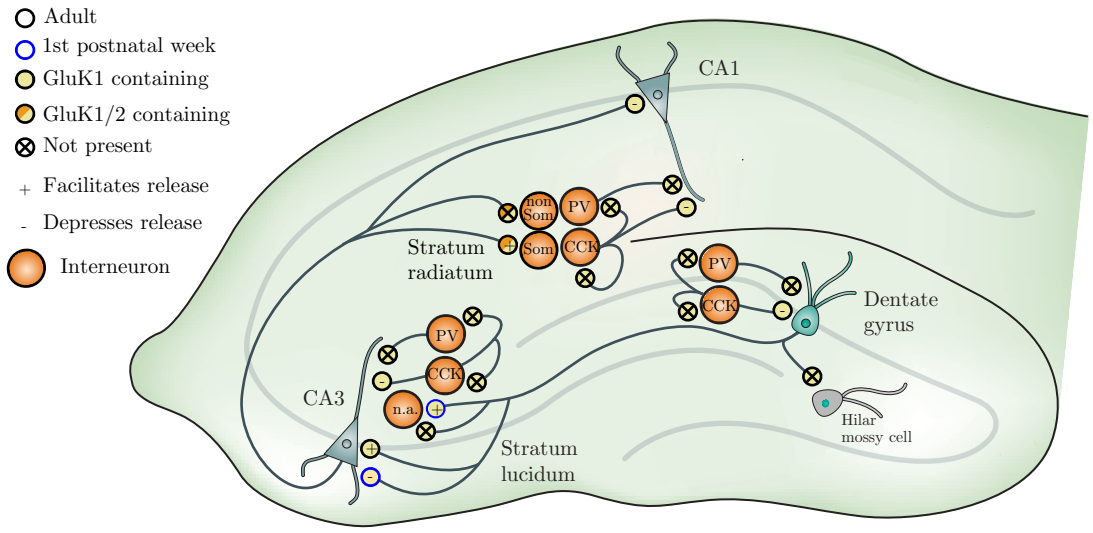

Figure 1.7: Schematic representation of presynaptic ionotropic receptor heterogeneity in the hippocampus

Illustration provides a diagrammatic portrayal of studies in the text that have demonstrated target-neuron specific differences in presynaptic ionotropic receptor expression. The small circles refer to boutons, the presence of a particular receptor is represented by the colour, as shown in the key. A circle with a cross through indicates the boutons where the receptor is not present. Where presynaptic ionotropic receptors are present a + or - sign shows whether they facilitate or depress neurotransmitter release, respectively. Interneurons are positioned around the 3 different types of pyramidal cells in the dentate gyrus, CA3 region and CA1 region. The text within the interneuron refers to their biochemical maker (Som: somatostatin-containing, PV: parvalbumin-containing, CCK: cholecystokinin- containing, n.a.: data not available).

relatively enhance the activity of somatostatin-containing interneurons. The enhanced inhibition would be concentrated upon distal CA1 dendrites in the stratum lacunosum-moleculare and result in preferential filtering of excitatory information from the entorhinal cortex (Sun et al., 2009).

In the hippocampus there are at least 21 different types of interneurons, differentiated by their firing patterns, morphologies, and biochemical markers (Klausberger and Somogyi, 2008). Such diversity provides a challenge to electrophysiological measures of presynaptic neurotransmitter release which are often taken indirectly from the postsynaptic neuron. This is particularly the case if release is evoked by extracellular stimulation, where a potentially mixed population of interneurons would be recruited, and differences between interneuron subtypes might be lost in the net effect. By using paired recordings or cell-specific channel rhodopsin driven expression in mouse lines, the ambiguity associated with extracellular stimulation can be reduced. Indeed, another study profiling synaptic transmission of a specific subset of hippocampal interneurons has further highlighted target- and input-specific differences in the presynaptic receptor control of p. Daw et al. (2010) showed that the release of GABA from cholecystokinin- but not parvalbumin-containing interneurons was strongly depressed by presynaptic GluK1-containing kainate receptors. In addition to this input-specific heterogeneity, the inhibition was shown to be target neuron-selective, as the presynaptic kainate receptor-mediated depression was evident at axon boutons which synapse upon pyramidal cells, but not surrounding interneurons (Figure 1.7).

The target-specific, inter-bouton, heterogeneity of presynaptic ionotropic receptors does not exclusively manifest as differences in expression, but has been shown to extend to the mechanism by which the receptors modulate release (Figure 1.7). For example, during the first postnatal week, presynaptic kainate receptors at MF – CA3 pyramidal cell synapses inhibit glutamate release, potentially via a G-protein and PKC-dependent mechanism (Lauri et al., 2005). In contrast, at MF terminals onto CA3 interneurons in the stratum lucidum, presynaptic kainate receptors facilitate release via a G-protein-independent mechanism (Lauri et al., 2005). A similar orientation of inhibition and excitation to principal and interneuron cells, respectively, also occurs at the Schaffer

collateral terminals. In addition to their presence at boutons which contact interneurons, presynaptic kainate receptors are also present at varicosities that synapse directly onto CA1 pyramidal cells. However, they do not mediate the same short-term facilitation seen at somatostatin-containing interneuron synapses. In fact, at CA3 – CA1 boutons, kainate receptors inhibit glutamate release (Kamiya and Ozawa, 1998; Frerking et al., 2001; Lauri et al., 2006; Partovi and Frerking, 2006). The reason for the difference is not clear but may reflect receptor subunit compositions. Sun et al. (2009) suggested the enhanced p at synapses onto somatostatin-containing interneurons results from Ca^{2+} entry through GluK1/2 heteromeric kainate receptors, whereas at the C3 – CA1 synapse, whilst GluK1 is present (Lauri et al., 2006; Partovi and Frerking, 2006), the inhibition could result from heteromeric assembly with subunits other than GluK2, or even homomeric assembly of GluK1.

Heterogeneity in subunit composition of presynaptic ionotropic receptors with target neuron selectivity is not without precedent. In the cerebellar molecular layer for example, presynaptic AMPARs are present upon axonal boutons of MLIs. Boutons which contact other MLIs predominantly lack the GluA2 subunit and thus are Ca^{2+} permeable, whereas AMPARs at presynaptic sites which contact Purkinje cells contain the edited GluA2 subunit and are thus Ca^{2+} impermeable (Rossi et al., 2008) (Table 1.1).

1.5.5 | Metabotropic receptors can exert substantial control over iGluR activity

Presynaptic iGluR control of neurotransmitter release does not occur in isolation. In the majority of presynaptic axonal varicosities studied there are multiple combinations of ionotropic and metabotropic receptors present. A number of reports have described how metabotropic receptors can influence presynaptic iGluR activity, even changing the direction in which iGluRs modulate release. In the hypothalamus, glutamatergic projections from the SON contain presynaptic, GluK1-containing, kainate autoreceptors that facilitate and inhibit transmission onto oxytocin and vasopressin containing neurons, respectively (Bonfardin et al., 2012). The inter-bouton, target neuron-specific, heterogeneity was not due to differences in presynaptic kainate receptor properties but due to

selective functional coupling with presynaptic κ-opioid receptors. Following glutamate release, postsynaptic kainate receptors were also activated on oxytocin and vasopressin containing neurons, however as only vasopressin neurons express GluK1-containing kainate receptors, a Ca^{2+}-mediated mobilisation of dynorphin occurred within vasopressin but not oxytocin neurons (Bonfardin et al., 2012). The retrograde release of dynorphin activated κ-opioid receptors on axonal boutons synapsing upon vasopressin neurons, and through a metabotropic mechanism, occluded the presynaptic kainate receptor-mediated augmented release (Bonfardin et al., 2012). Thus, presynaptic iGluR control over p is subject to the variable activity of other receptors.

Heterogeneity in the regulation of presynaptic iGluR activity by neighbouring metabotropic receptors offers further dynanism in the control of CA1 pyramidal cell firing. Glutamate released from Schaffer collaterals activates presynaptic GluK1-containing kainate receptors at terminals of stratum radiatum interneurons. Strangely, such activation has reported to both enhance (Jiang et al., 2001), and inhibit GABA release onto CA1 pyramidal cells (Min et al., 1999). Lourenço et al. (2010) recently provide evidence that the discrepancy in feedforward inhibition or facilitation mediated by presynaptic kainate receptors depends on the presence of the presynaptic metabotropic endocannabinoid 1 receptor (CB1R). In addition to activating presynaptic kainate receptors, glutamate released onto CA1 pyramidal dendrites concomitantly activated postsynaptic mGluRs-1 and -5 to induce retrograde release of the endocannabinoid 2-arachidonoylglycerol. At a subpopulation of CA1 interneurons which did not express CB1Rs at their terminals, presynaptic kainate receptors functioned to depolarise the axon terminal and facilitate inhibitory transmission onto CA1 pyramidal cells. Alternatively, at the axon terminals of the cholecystokinin-containing family of basket cells which co-express CB1 and kainate receptors, CB1R activation overrode the kainate receptor-mediated facilitation to inhibit GABA release (Lourenço et al., 2010). However, contrary to these findings, another study found that application of CB1R antagonists did not affect the presynaptic kainate-mediated inhibition of release from cholecystokinin-containing interneurons (Daw et al., 2010). Further validation of the CB1R influence over presynaptic kainate receptors at these synapses may be required.

Functional coupling between presynaptic CB1 and NMDA receptors has also been demonstrated within the cortex, where the coincident activity of presynaptic CB1R and NMDA auto-receptors on layer 5 pyramidal cell terminals resulted in a long term reduction of glutamate release (Sjöström et al., 2003). In consideration of the recent paper reporting heterogenous expression of presynaptic NMDA receptors at layer 5 pyramidal axonal boutons (Buchanan et al., 2012), the functional coupling between CB1 and NMDA receptors necessary for long term depression could be rationally assumed to occur with a similar target neuron specificity. However, this interpretation may be rather simplistic as the distribution of presynaptic CB1Rs may also differ between axonal boutons, independently of presynaptic NMDARs.

1.6 | The cerebellum

The thesis specifically concerns presynaptic AMPARs which occur at the terminals of MLIs in the cerebellum. This structure, whose name originated as a diminutive form of the word 'cerebrum', sits at the base of the brain, and is evolutionary conserved in all vertebrates (Bell, 2002) - though there is debate about its presence in the pacific hagfish and it has a very limited size in lamprey (Bell, 2002). The cerebellum is believed to coordinate movement and balance through the timing of its signals to other areas of the CNS (Dean et al., 2009).

The external anatomy of the cerebellum varies between vertebrates but in birds and mammals it is extensively foliated (Voogd and Glickstein, 1998). In mammals the cerebellum is symmetrical about the midline, with two hemispheres either side of the central longitudinal vermis (Larsell, 1952). The cerebellum can be divided rostrocaudally into zones, distinguished by fissures which mark where the cerebellar cortex folds into lobes (Larsell, 1952) (Figure 1.8 *A*). Lobes I-V form the anterior zone, lobe VI corresponds to the central zone anterior (VI), central zone posterior refers to lobe VII, posterior zone consists of lobes VIII-IX, and the nodular zone is also known as lobe X. Along with the flocculus lobe, the nodular zone is more closely associated with the vestibular system compared with the rest of the cerebellum (Voogd et al., 1996).

The lobes arise from a folded homogenous layer structure which is comprised of the white matter layer, the granule cell layer, the Purkinje cell layer and the molecular layer (Figure 1.8 *B* and *C*). The layers are distinguished by cell type and are connected by a well characterised neuronal circuit that is repeated in an adjacent fashion (Eccles, 1967). For mammals, the different types and morphologies of neurons were revealed in detail by Ramón y Cajal, who used the sparse Golgi stain to identify individual cells (Carlos and Borrell, 2007). This repeating microcircuit is described in Figure 1.8 *C* and involves input from specific regions of the brainstem to the cerebellar cortex. Two forms of excitatory input converge on Purkinje cells, the principal cell type in the cerebellum; direct climbing fibre synaptic connections, and mossy fibre input relayed through granule cells. The GABAergic Purkinje cells provide the only output of the cerebellar cortex by sending axonal projections to the deep cerebellar nuclei. The response of Purkinje cells to excitatory input is modulated by inhibitory interneurons.

1.6.1 | A climbing fibre powerfully innervates a single Purkinje cell

The cerebellum receives two myelinated afferents, the climbing and mossy fibre. The climbing fibre originates from the inferior olivary nucleus, which lies in the lower half of the brainstem within the medulla oblongata and receives input from the spinal cord, the brainstem and the motor cortex, amongst other areas (De-Zeeuw et al., 1998). Olivocerebellar fibres project from cells within this nucleus and generally ascend contralaterally through the hilum to the cerebellum predominately via the inferior peduncle (Sotelo, 2004), though a small component of fibres can alternatively innervate the cerebellum ipsilaterally (Sugihara et al., 1999). In the cerebellum, olivocerebellar fibres extend to the vermis and hemispheres (Figure 1.8 *A*) where they are termed climbing fibres (De-Zeeuw et al., 1998). A single climbing fibre initially branches approximately ∼10 times in a narrow rostocaudal plane of the cerebellum (Sugihara et al., 2001). An individual branch either forms direct synapses with the neurons in the cerebellar nuclei, or more frequently, climbs to innervate a Purkinje cell (Sugihara et al., 2001).

The climbing fibre is perhaps the defining feature of the cerebellum, which differentiates

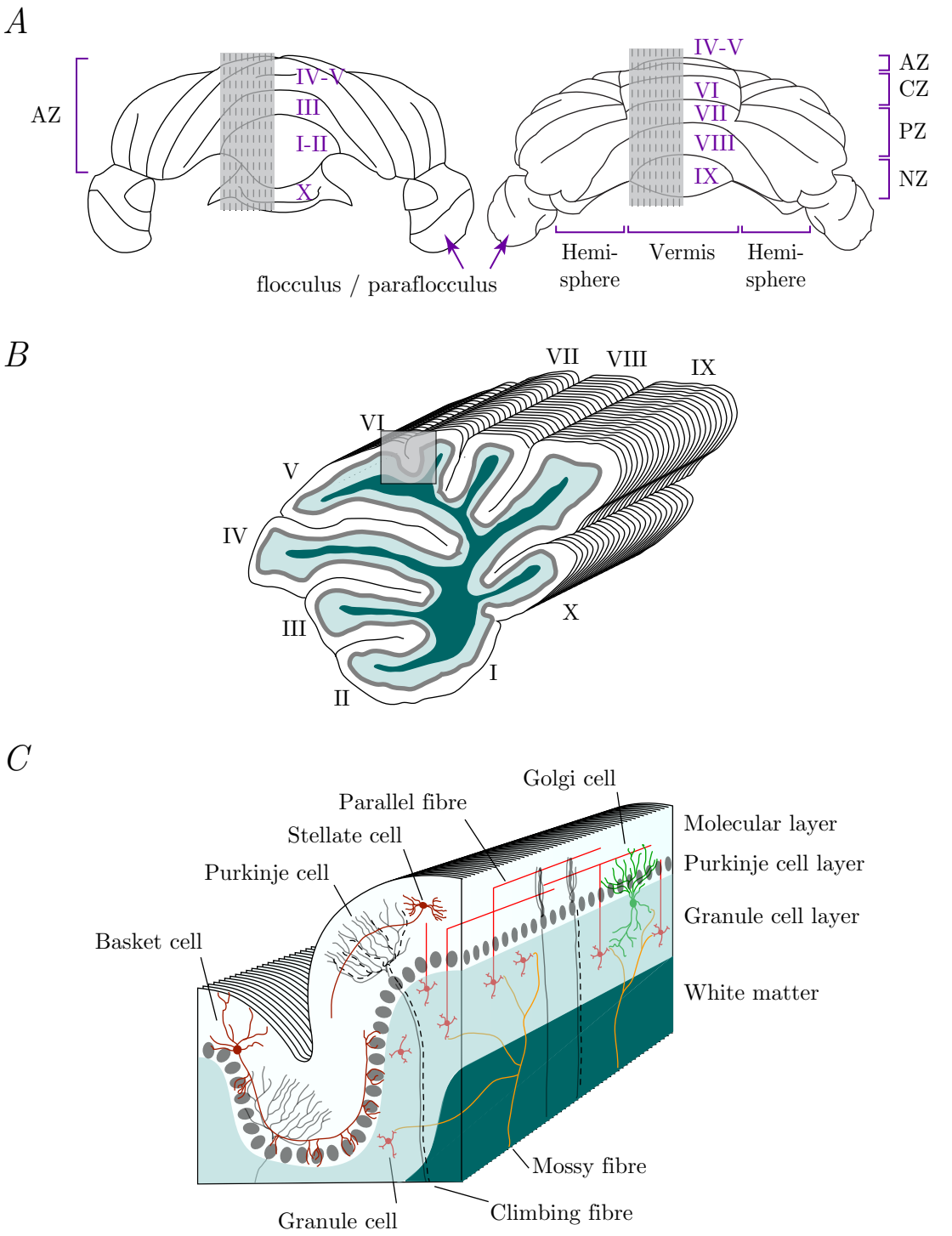

Figure 1.8: An overview of gross rodent cerebellar structure and the cerebellar microcircuit

(*A*) Anterior (left) and posterior (right) views of the whole rodent cerebellum reveals the structurally segregated vermis, hemispheres, flocculus and paraflocculus. Cerebellar lobules are indicated with Roman numerals I-X. The estimated transverse zones of the vermis AZ, CZ, PZ and NZ correspond to the anterior zone, central zone, posterior zone, and nodular zone, respectively.

Figure 1.8 continued: (*B*) Sagittal section of the cerebellar vermis demonstrating the arrangement of lobules, Roman numerals correspond to *A*. (*C*) A zoomed in window of the sagittal section in *B* schematically represents the cellular microcircuit of the cerebellar cortex. The afferent climbing and mossy fibres inputs, Purkinje cells and interneurons. Both sagittal and transverse sections are shown. Colours correspond to the layers in *B*. Figure adapted from a version provided by Mark Farrant

it from other cerebellar-like structures such as the dorsal cochlear nucleus in mammals (Bell, 2002). In the adult, one climbing fibre innervates a single Purkinje cell (Eccles et al., 1966b). The one to one specificity is determined during the first three postnatal weeks where many climbing fibres compete to form strong synaptic connections (Hashimoto and Kano, 2003). The remaining climbing fibre extends from the perisomatic domain to form around 300 strong connections on the aspiny, proximal dendrites (Crepel et al., 1976; Hashimoto and Kano, 2003, 2005).

When stimulated, the multiple climbing fibre contacts evoke a multi-peaked action potential in the Purkinje cell that lasts between 2-5 ms occurring, on average, once every 1-5 s (Eccles et al., 1966b). The initial phase of the complex spike results from the integration of large excitatory postsynaptic conductances, predominantly mediated by AMPARs, though NMDARs contribute in the adult (Piochon et al., 2007; Renzi et al., 2007). The depolarisation spreads through the proximal dendrite and is integrated at the axon initial segment to generate a spike (Stuart and Häusser, 1994). The action potential not only propagates down the axon but weakly back propagates into the dendrites (Llinás and Sugimori, 1980; Stuart and Häusser, 1994; Tank et al., 1988). It was initially thought that the high frequency spikelets which follow the initial depolarisation reflected back propagating action potentials that activated VGCCs within the dendrites to produce Ca^{2+} spikes (Eccles et al., 1966b; Llinás et al., 1968; Llinás and Nicholson, 1971). However, recent studies suggest that the trademark spikelets indicative of the complex spike originate in the axon (Davie et al., 2008; Schmolesky et al., 2002).

Each individual climbing fibre – Purkinje synapse is, on average, 94 % enclosed by a glial sheath formed from radial Bergmann fibres (Xu-Friedman et al., 2001). The glial cell glutamate transporter; excitatory amino-acid transporter (EAAT) 1 and the neuronal glutamate transporter; EAAT4 are highly expressed in Bergmann glial processes and extrasynaptic regions surrounding Purkinje neuron dendritic spines, respectively (Dehnes et al., 1998; Lehre and Danbolt, 1998; Yamada et al., 2000). Following climbing fibre synaptic transmission, EAAT1 initially predominates to limit glutamate overflow from the synaptic cleft. During the later stages of transmission, EAAT4 is expected to remove relatively low concentrations of glutamate escaping from EAAT1-mediated uptake

(Takayasu et al., 2005, 2006). Despite the high levels of glutamate transporters, multivesicular glutamate release from the climbing fibre (Wadiche and Jahr, 2001), even at low firing frequencies, can saturate transporters resulting in a high occupancy of postsynaptic AMPARs and a relatively low clearance rate (Dittman and Regehr, 1998; Silver et al., 1998). Such phenomena are thought to contribute to the characteristic slow EPSC decay (Barbour et al., 1994; Harrison and Jahr, 2003; Wadiche and Jahr, 2001). One implication of the high saturation and low clearance rate of climbing fibre – Purkinje cell synapses, is that glutamate can spillover and activate non-synaptic receptors. This has been shown for metabotropic glutamate receptors at perisynaptic Purkinje cell locations within regions where the density of EAAT4 is low (Dzubay and Otis, 2002; Zhao et al., 1997).

1.6.2 | Cerebellar mossy fibre afferents

In the cerebellum there are between 1 and 4 mossy fibre afferents per Purkinje cell, which contrasts to the 1:10 ratio for climbing fibres (before branching to innervate single climbing fibre) (Palkovits et al., 1972). Mossy fibres have multiple origins including the vestibular nuclei (Kotchabhakdi and Walberg, 1978) and reticular formation (Sugihara et al., 1999) in the brainstem, as well as the spinal cord (Ji and Hawkes, 1994) and the pons (Pijpers and Ruigrok, 2006), amongst other areas. The fibres enter the cerebellum through either one of the inferior, middle or superior peduncles to innervate both the deep cerebellar nuclei and granule cells (Shinoda et al., 1992) (Figure 1.8 *C*). An individual mossy fibre repetitively branches so to provide glutamatergic innervation to ∼400 granule cells (Eccles et al., 1967). Transmission occurs from large rosette-shaped terminals that occur at intervals of 20-80 μm along the mossy fibre (Palay and Chan-Palay, 1974). Each terminal forms up to fifty synaptic connections (Hámori and Somogyi, 1983) within a glial enclosed glomerulus. Many granule cells contribute one of their four claw-like dendrites to a mossy fibre terminal, responding to glutamate from between 1-10 release sites (Jakab and Hámori, 1988). The close proximity of active zones allows for spillover between adjacent release sites (DiGregorio et al., 2002). From quantal analysis, a single active zone within the mossy fibre bouton contains just 1 or 2 vesicles available for release with a probability of approximately 0.5 (Delvendahl et al., 2013). It is thought that the reason

why mossy fibre boutons can reliably respond to high frequencies of stimulation (Rancz et al., 2007) is due to the large number of reserve vesicles ($\sim$ 300 per release site) which are rapidly docked at the active zone (Saviane and Silver, 2006). The release of glutamate from just a few mossy fibre inputs is able to induce a burst of spikes in the granule cells (Chadderton et al., 2004; Rancz et al., 2007).

The activity of granule cells is not only controlled by mossy fibre input, but is regulated by the GABAergic Golgi cells (Eccles et al., 1964). These interneurons reside in the granule cell layer where they receive input from mossy fibre boutons within the glomerulus, in addition to parallel fibre input at their ascending dendrites in the molecular layer (Eccles et al., 1966a). Though sparsely distributed in the granule cell layer, they can individually inhibit $\sim$100,000 granule cells either through direct synaptic connections on granule cell dendrites (Bisti et al., 1971; Kaneda et al., 1995), via spillover of GABA (Rossi and Hamann, 1998), or through the tonic activation of α6 subunit-containing $GABA_ARs$ present in granule cells (Brickley et al., 1996; Wall and Usowicz, 1997).

The ascending axons of granule cells project into the molecular layer to form synapses at Purkinje cell dendritic spines. The parallel fibre bifurcates in the molecular layer and extends coronally for approximately 5 mm (Figure 1.8 *C*). It is thought that $\sim$20% of synapses onto Purkinje cells are formed by the ascending parallel fibre (Gundappa-Sulur et al., 1999), and the remaining synapses are made by the bifurcated axons which run perpendicular to the sagittally orientated planar Purkinje cell dendrites (Harvey and Napper, 1991).

Each parallel fibre is thought to make 1, and sometimes 2, connections with every second or third Purkinje cell dendrite it passes (Napper and Harvey, 1988), though 85% of such synapses are thought to be silent, i.e. with no functional AMPARs (Isope and Barbour, 2002). The combined population of parallel fibres that bisect a single Purkinje cell can form in the region of 170,000 excitatory synapses (Harvey and Napper, 1991).

At those synapses which are not silent, the fast excitatory responses at Purkinje cell spines are soley mediated by AMPARs, without any contribution of NMDARs (Llano et al., 1991; Perkel et al., 1990). In addition to AMPARs, repetitive stimulation of parallel fibres can also activate mGluRs (Batchelor et al., 1994; Takechi et al., 1998),

Due to the AMPAR-mediated currents ($\sim$ 2-60 pA) produced at individual synapses, the activity of approximately 50 parallel fibres is required to initiate a single 'simple' spike in the Purkinje cell (Barbour, 1993).

1.6.3 | Purkinje cells provide the sole output from the cerebellum

The GABAergic Purkinje cells integrate excitation from parallel and climbing fibres to produce a firing rate code which represents the entire output of the cerebellar cortex. Purkinje cells have a large cell soma (20-40 μm) with a single proximal dendrite that repeatedly branches in a planar manner (Fujishima et al., 2012). Much like the aerial plan of a tree is optimised to collect the most sunlight, the extensive arborisations of the dendritic tree do not overlap within the sagittal axis, in respect to the perpendicular flow of parallel fibres (Napper and Harvey, 1988). Purkinje cell dendrites integrate information from both parallel and climbing fibre inputs, which are regulated by the active generation of Ca^{2+}-mediated action potentials in the dendrites (Llinás and Sugimori, 1980). Recently, it was found that dendritic spikes have a bipolar effect on parallel fibre input, enhancing somatic firing following brief parallel fibre firing, yet reducing the synaptic gain for prolonged bursts (Rancz and Häusser, 2010).

Purkinje cells sit shoulder to shoulder and each send a single axon from the base of their soma down through the granule cell layer. The long axonal projections form the sole output of the cerebellar cortex, inhibiting target neurons within the deep cerebellar nuclei (Ito et al., 1964). The precise location of the efferents correspond topographically to the sagittal position of the Purkinje cell in the cerebellar cortex. Pukinje cells located in the vermis, paravermis and hemispheres predominately project to the medial fastigial, interpositus (combination of emboliform and globose nuclei) and lateral dentate nuclei, respectively (Larsell, 1952). The Purkinje cell axons not only project to the deep cerebellar nuclei but also branch to form recurrent collaterals onto neighbouring Purkinje, basket and Golgi cells upto 300 μm away (Larramendi and Lemkey-Johnston, 1970) where they form ganglionic plexuses above and below the Purkinje cell layer.

As described above, Purkinje cell spiking occurs in two forms, parallel fibre activity evokes

a Na^+-mediated 'simple spike', whereas climbing fibre stimulation produces widespread Ca^{2+} entry in the dendrites to trigger the multi-peaked complex spike (Llinás and Sugimori, 1980). In awake and anaesthetised animals Purkinje cells oscillate between hyperpolarised potentials where cells are silent, and a depolarised state of regular action potential firing (Llinás and Sugimori, 1980; Loewenstein et al., 2005).

Purkinje cells regularly fire spontaneous action potentials, and, unusually for a principle cell in the mammalian CNS, exhibit high firing frequencies (Bell and Grimm, 1969; Thach, 1968). This is believed to be possible due to the rapid repolarisation properties of Kv3 channels expressed in the axon, which narrow the action potential width (Ishikawa et al., 2003; McKay and Turner, 2004; Southan and Robertson, 2000), and also a resurgent Na^+ channel current (Raman and Bean, 1997), which speeds recovery from inactivation (Khaliq et al., 2003). A Purkinje cell typically has an intrinsic simple spike rate of ∼50 Hz. Action potentials resulting from both complex and simple spikes initiate in the distal region of the axon initial segment (Foust et al., 2010; Palmer et al., 2010). Simple spikes can occur between the large range of 0 - 400 Hz (Monsivais et al., 2005), albeit with marked irregularity *in vivo* (Goossens et al., 2004) compared with *in vitro* (Häusser and Clark, 1997). Simple spikes propagate with very few failures up to a frequency of 250 Hz (Foust et al., 2010), in comparison the individual spikelets within the complex spike can reach up to ∼500 Hz (Maruta et al., 2007) and can be often lost at axonal branch points (Foust et al., 2010). The firing of Purkinje cells is subject to inhibition from synaptically connected molecular layer interneurons.

1.6.4 | Molecular layer interneurons

In the cerebellar cortex, MLIs receive excitation from both afferent cerebellar fibres to provide spatiotemporal inhibition of Purkinje cells. MLIs have been classified as either stellate or basket cells depending on their location in the molecular layer, their characteristic axonal morphologies and the subcellular Purkinje neuron compartment they synapse upon (Chan-Palay and Palay, 1970, 1972). Stellate cells are found in the outer two thirds of the molecular layer, and are thought to selectively innervate Purkinje cell dendrites with ascending and descending axonal collaterals orientated according to

Bergmann glia scaffolds (Ango et al., 2008). Basket cells are traditionally thought to reside in the lower third of the molecular layer, close to the Purkinje cell bodies. They are distinguished from stellate cells by their characteristic axon arborization which surrounds the base of the Purkinje cell body and forms the characteristic pinceau synapse on the soma and axon initial segment (Eccles et al., 1966a; Huang et al., 2007). However, findings that MLIs located in the upper two thirds of the molecular layer can also form basket-like synapses onto Purkinje cell bodies (Sultan and Bower, 1998), and, a paucity of studies describing functional differences between the two cells, suggest stellate and basket cells are perhaps more appropriately thought of as a continuum of the same cell (Rakic, 1972; Schilling et al., 2008; Sultan and Bower, 1998). Rather than the proximity to the Purkinje cell layer, the probability of finding a somatic basket synapse seems to be positively related to the depth in the cerebellar slice (Sultan and Bower, 1998).

The separation of basket and stellate cells according to their axonal arborisation occurs early in their development ∼P3-10 (Carletti and Rossi, 2008). MLIs move from the white matter into the molecular layer, where they synapse with ∼40 Purkinje cells. Over the first 3 weeks, cerebellar development occurs predominantly in the rostocaudal plane to sagittally spread the Purkinje cells. As described in Figure 1.9, those MLIs which arrive in the molecular layer early have a greater spread of axonal contacts (i.e. basket cells) than those which arrive much later during development (stellate cells) (Consalez and Hawkes, 2012).

1.6.5 | MLIs are excited by parallel and climbing fibre activity

Due to their high input resistance, MLIs can respond to high frequency granule cell firing patterns with millisecond precision (Suter and Jaeger, 2004). Initial studies found parallel fibre stimulation was only capable of eliciting fast, exclusively AMPAR-mediated currents, whilst NMDARs contributed to the EPSC only when either the frequency or intensity of stimulation was increased (Carter and Regehr, 2000). The segregation of different glutamate receptor types into cellular compartments was later found to explain this observation. Clark and Cull-Candy (2002) demonstrated that glutamatergic transmission at MLI synapses was solely mediated by AMPARs, whereas NMDARs were likely located

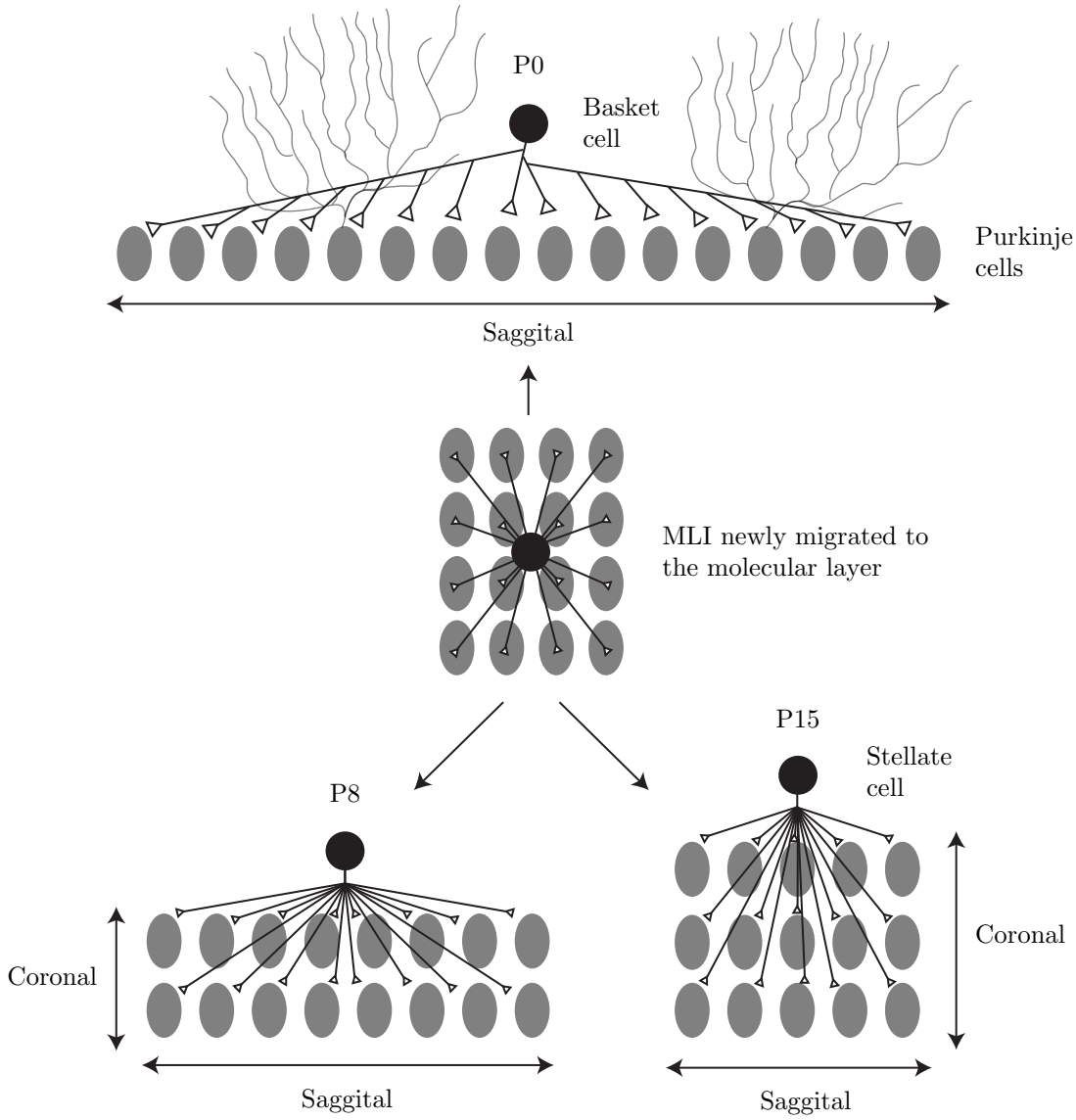

Figure 1.9: Timing of MLI migration determines axon morphology

Following MLI migration from the white matter layer into the molecular layer, MLIs (black circles) form synapses with ∼40 Purkinje cells (grey ovals) in relatively close proximity (centre). From P0 the cerebellum grows in the rostrocaudal axis. Those MLIs cells which migrate early, around P0, have axonal arbors which extend as the Purkinje cells separate during cerebellar expansion. Such cells have morphologies typical of basket cells. By comparison the axonal arbours of MLIs that migrate at later stages of development (P15 for example), exhibit less sagittal extension as the rate of cerebellar growth slows. Image based on a figure from Consalez and Hawkes (2012).

at extrasynaptic locations, as they were only activated when a large enough quantity of glutamate spilled from the synapse. Similarly, mGluR1 was only activated following such high-intensity glutamate release (Karakossian and Otis, 2004).

Excitatory synapses made by parallel fibre onto MLIs typically exhibit a high number of failures and generally facilitate following subsequent stimulations (Rancillac and Barbara, 2005). The reliability of glutamatergic transmission is increased with higher frequency stimulations as generated by granule cells *in vivo* (Chadderton et al., 2004; Rancillac and Barbara, 2005).

The synaptic AMPAR subunit composition varies with frequency of parallel fibre stimulation. In juvenile animals, glutamate-evoked synaptic currents are typically mediated by AMPARs which lack the GluA2 subunit (Clark and Cull-Candy, 2002; Liu and Cull-Candy, 2000). Repetitive activation of synaptic CP-AMPARs can induce a switch in the subunit composition of synaptic AMPARs from GluA2-lacking to GluA2-containing receptors (Liu and Cull-Candy, 2000). Induction of the plasticity either involves the concomitant activation of mGluR and CP-AMPARs (Kelly et al., 2009) or coincident activation of extrasynaptic NMDAR and CP-AMPARs (Sun and Liu, 2007). The removal of CP-AMPARs from the PSD is mediated through disruption of the interaction between the AMPAR and GRIP1, following PKC phosphorylation of GluA3 (Liu and Cull-Candy, 2005). Meanwhile, the delivery of extrasynaptic CI-AMPARs to the PSD is dependent on PICK1 and NSF (Gardner et al., 2005).

Climbing fibres come within close apposition with MLI somata (Brown et al., 2012; Lemkey-Johnston and Larramendi, 1968; Kollo et al., 2006; Sugihara et al., 1999), but gold labelling of active zones and the PSD, indicative of synaptic connections, has not been observed (Brown et al., 2012; Kollo et al., 2006). Instead, electrophysiological experiments suggest climbing fibre – MLI transmission occurs exclusively through glutamate spillover from the climbing fibre – Purkinje cell synapse (Coddington et al., 2013; Mathews et al., 2012; Szapiro and Barbour, 2007). Such evidence is consistent with the early observation that the climbing fibre – MLI transmission elicited weaker responses compared to glutamate release from parallel fibre synapses (Eccles et al., 1966a). The MLI response to climbing fibre spillover glutamate is mediated through both NMDA and AMPA receptors

(Coddington et al., 2013).

MLIs may alternatively be excited through non-synaptic means. At MLI somata and dendrites, the low voltage-activated A-type K^+ channels, Kv4, form a complex with T-type VGCCs and K^+ channel-interacting proteins that bind Ca^{2+} (Anderson et al., 2010). Kv4 channels mediate the repolarisation phase of the action potential, and through binding of Ca^{2+} are activated at relatively hyperpolarised membrane potentials. Correspondingly, Kv4 channels inactivate at low extracellular Ca^{2+} concentrations (Anderson et al., 2010). As extracellular Ca^{2+} concentration drops dramatically following repetitive parallel (Nicholson et al., 1978) and climbing fibre (Stöckle and ten Bruggencate, 1980) stimulation, it has been proposed that afferent activity can reduce Kv4 activity to further enhance MLI excitability (Barmack and Yakhnitsa, 2011).

1.6.6 | Structural and electrophysiological features of MLIs

The mechanism by which MLIs temporally and spatially integrate excitation requires knowledge of their properties. The standard dimensions of MLIs include a soma diameter of 7-10 μm in mice (Barmack and Yakhnitsa, 2008; Llano and Gerschenfeld, 1993), whereas in rats the sizes are slightly larger; 10-15 μm and 8-12 μm for basket and stellate cells, respectively (Ruigrok et al., 2011). Both forms of MLIs project a relatively short dendritic field of $\sim$200 μm (Barmack and Yakhnitsa, 2008). Such dendrites are apsiny, and exhibit few branches that extend with little deviation in the sagittal plane (Barmack and Yakhnitsa, 2008; Sultan and Bower, 1998). The relatively compact somatodendritic compartment suggests MLIs have a high input resistance, which would favour the propensity of individual glutamate (and GABA) quanta to modulate their firing (Carter and Regehr, 2002). Indeed, an individual granule cell has been shown to evoke MLI firing (Barbour, 1993). Despite their short length, not all conductances in the dendrites are represented equally at the soma. The thin diameter of MLI dendrites (0.4 μm) (Sultan and Bower, 1998) confers passive cable properties, suitable for sublinear synaptic integration (Rall et al., 1967; Rinzel and Rall, 1974). Recently, Abrahamsson et al. (2012) demonstrated a greater filtering of the amplitude and speed of conductances originating further away from the MLI soma, relative to those generated more proximally.

Studies reporting the number of MLIs relative to Purkinje cells have ranged from 10:1 (Korbo et al., 1993) to 22.9 ± 1.5 per Purkinje cell (Barmack and Yakhnitsa, 2008). With a single stellate cell forming an average of 149 synapses (Sultan and Bower, 1998) onto ∼ 40 Purkinje cells (Consalez and Hawkes, 2012). Each Purkinje cell has previously been estimated to receive a total of 1500 inhibitory inputs (Jaeger et al., 1997), though this figure has been more recently raised to 7920 GABAergic synapses (Briatore et al., 2010).

MLIs spike spontaneously at 0.6-35.5 Hz, with broadly distributed intervals between spikes (Ruigrok et al., 2011). MLI spiking occurs either at regular intervals (Häusser and Clark, 1997; Midtgaard, 1992) or, following synaptic input, can occur as jittery bursts (Mann-Metzer and Yarom, 2002a). Compared with aforementioned recordings from acute slices, the spiking patterns recorded *in vivo* show greater irregularity (Jörntell and Ekerot, 2003). The generation and propagation of action potentials is subject to a number of conductances in the MLI axon, including a non-inactivating Na^+ current which modulates action potential width (Mann-Metzer and Yarom, 2002b), and a mixed inward Na^+/K^+ hyperpolarisation-activated I_h current that may modulate release probability (Southan et al., 2000).

1.6.7 | MLIs shape Purkinje cell firing

Stimulation of a single MLI has been shown to elicit a brief pause in spontaneous Purkinje cell firing (Häusser and Clark, 1997). In comparison to a single MLI, the effects of multiple MLI activity following parallel fibre burst stimulation is more complex. When Purkinje cells are within a depolarised 'up state', MLI population activity acts to reduce Purkinje cell firing. However, during a hyperpolarised 'down state' multiple inhibitory inputs increase Purkinje cell firing (Oldfield et al., 2010).

The precise form of Purkinje cell inhibition depends on the position and morphology of MLIs. Those traditionally known as stellate cells predominantly modulate parallel fibre excitation in local domains of the Purkinje cell dendrites. With very few projections onto the Purkinje cell soma, stellate cells have very little direct impact on spike output (Vincent and Marty, 1996). At the dendritic regions that undergo concomitant parallel fibre

excitation, it has been proposed that inhibition from stellate cells does not result from the sum of excitatory and inhibitory currents integrated at the soma, but rather the relative contribution of excitation and inhibition clamps the local dendritic membrane voltage (Jaeger et al., 1997; Jaeger and Bower, 1999). This clamp modulates the active voltage-gated Ca^{2+} and K^{+} conductances present in Purkinje cell dendrites. MLI inhibition would increase the propensity for K^{+} channel openings and thus reduce Ca^{2+} dependent spikes resulting from parallel fibre synaptic transmission. An alternative explanation for stellate mediated inhibition involves a $GABA_AR$-mediated shunting conductance which blocks the active Ca^{2+} conductance (Callaway et al., 1995). More often than not the membrane shunt was observed throughout an extended region of the Purkinje cell dendrite tree, rather than localised regions (Callaway et al., 1995). This may have reflected excitation of multiple MLIs, or alternatively, could have involved a more global dendritic membrane shunt. Recent work found that localised synaptic shunting from multiple Martinotti cell contacts upon cortical pyramidal cells, produced a spatially protracted membrane shunt far beyond the synaptic domains (Gidon and Segev, 2012). In comparison to the dendritic influence of stellate-like MLIs, parallel fibre activation of basket cells produce strong, rapid and direct modulation of spike output from Purkinje cells at the level of the cell body and axon initial segment (Donato et al., 2008; Rokni et al., 2007; Sakaba, 2008; Vincent and Marty, 1996).

MLI activity inhibits Purkinje cells by two distinct circuits. 'Feed-forward' inhibition refers to a local region in a Purkinje cell that is both excited by parallel fibres and inhibited by MLIs, which experience excitation by the same set of parallel fibres (Brunel et al., 2004; Eccles et al., 1966). Depending on the timing and spatial organisation of synapses, as well as the relative strength of MLI – Purkinje cell synaptic transmission, MLIs will reduce the amplitude and duration of parallel fibre excitation (Mittmann et al., 2005).

Climbing fibres also promote MLI feed-forward inhibition of Purkinje cells (Callaway et al., 1995). The climbing fibre-evoked increase in MLI activity produces a pause in spontaneous firing of Purkinje cells that do not receive the same climbing fibre input, whereas the increased MLI activity prolongs the pause in complex spike activity in

Purkinje cells with a common climbing fibre input (Mathews et al., 2012).

In addition to the feed-forward inhibition of Purkinje cells, MLIs can provide lateral inhibition to Purkinje cells positioned several hundred μms away in the sagittal axis (Dizon and Khodakhah, 2011). Both stellate and basket cell axons run in the parasagittal plane, consistent with the rostalcaudal expansion of the cerebellum during development (Figure 1.9). Due to their differences in axonal arborisation, basket cell terminals are distributed over a larger sagittal field than stellate cells (Rakic, 1972). Thus, basket cell mediated lateral inhibition is expected to be distributed over a large longitudinal range than stellate cells (Dizon and Khodakhah, 2011).

1.6.8 | Presynaptic iGluRs further modulate Purkinje cell activity

Besides the integration of excitatory inputs from the activation of somatodendritic iGluRs, MLIs which synapse onto Purkinje cells contain both presynaptic AMPA and NMDA heteroreceptors (Duguid and Smart, 2004; Duguid et al., 2007; Huang and Bordey, 2004; Rusakov et al., 2005; Satake et al., 2000, 2006, 2010). Presynaptic AMPARs upon basket cell boutons function to inhibit GABA release onto Purkinje cells (Satake et al., 2000). Such inhibition depends on a low concentration of glutamate diffusing from climbing fibres following saturation of glial and neuronal glutamate transporters, demonstrated by the competitive low-affinity GluR antagonist, γ-DGG and the non specific glutamate transporter blocker, TBOA, respectively (Satake et al., 2006). By analysing the distribution of glutamate transporters across cerebellar lobes, Satake et al. (2010) suggested that glutamate spillover from climbing fibres occurs predominantly in the vicinity of Purkinje cells where EAAT4 is expressed at relatively low levels. This is despite EAAT4 levels positively correlating with climbing fibre synaptic vesicle number and propensity for multivesicular release, which suggests glutamate would always spillover, independent of transporter levels (Paukert et al., 2010). The reduced expression of EAAT4 at the Purkinje cell soma compared to the dendrites is suggested to explain why basket cell, but not stellate cell, subtypes of MLIs respond to climbing fibre spillover glutamate (Liu, 2007; Satake et al., 2010).

In contrast, the facilitatory effects of presynaptic NMDARs on both action potential driven and spontaneous GABA release at the MLI – Purkinje cell synapse, appear not to be rely on spillover climbing fibre glutamate (Duguid and Smart, 2004). Instead, climbing fibre-evoked depolarisation of Purkinje cell dendrites was proposed to produce a retrograde release of glutamate onto MLI boutons (Duguid and Smart, 2004; Duguid et al., 2007). However, another group found that climbing fibre glutamate could spill out of the Purkinje cell synapse and directly activate presynaptic NMDARs following the saturation of glutamate transporters present within Bergmann glia (Huang and Bordey, 2004), though the effects of blocking glutamate uptake could not be replicated in a later study (Duguid et al., 2007). Rather than facilitating evoked release, as reported following retrograde release of glutamate, the activation of presynaptic NMDARs by climbing fibre spillover glutamate was reported to reduce GABA release onto Purkinje cells (Huang and Bordey, 2004).

1.6.9 | MLIs form connections with other MLIs

In addition to regulating Purkinje cell output, ∼30-40% of MLI axonal contacts are made onto other MLIs (Briatore et al., 2010), as well as autaptic connections, which increase in prevalence from 5% at P12-15 to 26% at P26-49 (Pouzat and Marty, 1998). Though it was previously suggested that MLIs also synapse onto Golgi interneurons (Dumoulin et al., 2001), recent evidence suggests this is not the case (Hull and Regehr, 2012).

Each MLI receives synaptic connections from 4.25 MLIs, with a ∼15% probability that one MLI contacts another. A successful synaptic connection comprises of between 1-4 release sites (Kondo and Marty, 1998) and exhibits a release probability within the range of 0.1-0.54 (Auger et al., 1998). Consistent with the rostrocaudal development of their axonal Purkinje cell contacts, it is thought that MLIs only contact other MLIs specifically from the same sagittally arranged cerebellar microzone they reside in. Indeed in vivo recordings show inhibitory potentials are only evoked by peripheral input corresponding to where the mossy fibre originated (Jörntell and Ekerot, 2003). Such contacts are not necessarily inhibitory, like many other interneurons the reversal potential of GABA in these cells is relatively depolarised (-58 mV) and lies very close to the resting membrane

potential (-56.5 mV) (Chavas and Marty, 2003). As a result, in the adult as well as in the juvenile animals, inhibition from surrounding MLIs produces an almost equal mix of synapses which confer inhibition, excitation, or synapses with mixed excitatory and inhibitory actions (Chavas and Marty, 2003).

In addition to chemical transmission, 40% of MLIs form weak electrical connections via gap junctions (Sotelo and Llinás, 1972); on average to nine other MLIs. The spikelets which can be recorded in electrically connected MLIs have been proposed to contribute to their synchronous firing (Mann-Metzer and Yarom, 1999). Such electrical connections could act to speed or further distribute MLI and Purkinje cell inhibition. Synaptic connections between MLIs may also act to extend the influence from a single climbing fibre. Recently, Coddington et al. (2013) demonstrated that climbing fibre-evoked excitation of MLIs produced a prolonged feed-forward inhibition onto MLIs beyond the glutamate spillover domain. This inhibition thus promotes enhanced activity of Purkinje cells other than the one initially stimulated.

GABAergic transmission between MLIs is regulated by presynaptic iGluRs, similar to what is seen at MLI – Purkinje synapses (see 1.6.8). The activation of both AMPARs and NMDARs increase the frequency of miniature and spontaneous IPSCs in MLIs (Farrant and Cull-Candy, 1991; Llano et al., 1991; Bureau and Mulle, 1998; Glitsch and Marty, 1999; Liu and Lachamp, 2006; Glitsch, 2008a; Rossi et al., 2008). In addition, NMDAR activation was further shown to reduce the amplitude, and increase the failure rate of action potential evoked IPSCs (Glitsch and Marty, 1999). From Ca^{2+} imaging and inspection of the evoked autoreceptor/autaptic GABAergic current in MLIs, AMPAR activation serves to reduce evoked release; for stellate cells this may occur following spillover from parallel fibres (Liu, 2007; Rossi et al., 2008). Direct recordings from enlarged boutons of cultured cerebellar interneurons not only demonstrated AMPA and NMDA receptor mediated currents, but also suggested the presence of kainate receptors on these boutons, though this remains the only evidence (Fiszman et al., 2005, 2007).

1.7 | Justification and objectives of thesis

Presynaptic AMPARs modulate neurotransmitter release at a number of synapses in the CNS, but little is known about their regulation. To date the only information on presyanptic AMPAR regulation comes from hippocampal/cortical synaptosomal studies, which suggest their trafficking is subject to interacting proteins similar to those observed at the PSD. For example, GRIP1 is expressed in cultured hippocampal neuron axons (Wyszynski et al., 2002), and disrupting interactions between presynaptic GluA2 subunits and GRIP1, ABP, PICK1 or NSF, significantly decreased AMPAR-mediated modulation of synaptosomal noradrenaline release (Pittaluga et al., 2006). Evidence for presynaptic AMPAR regulation implicitly comes from studies which demonstrate their activity can modulate their properties. For example, AMPAR agonist application upregulated the GluA-2/-3 fraction of surface AMPARs in synaptosomes (Feligioni et al., 2006), whereas in hippocampal growth cones GluA-1 and -2 containing AMPARs were actively internalised upon activation and recruited to the surface upon depolarisation (Schenk et al., 2003). Such data suggests that classical postsynaptic AMPAR interacting proteins are expressed at axon terminals, and AMPARs may potentially undergo constitutive recycling processes resembling those at the PSD. Nonetheless a greater concerted effort in more physiological preparations is required to fully characterise the regulation of presynaptic AMPARs.

Transmembrane auxiliary proteins are of great importance for the trafficking and function of somatodendritic iGluRs (subsection 1.3.2), but their role at presynaptic sites is unclear. Recent evidence has suggested that presynaptic kainate receptors may not require the auxiliary subunit NETO1 (Copits and Swanson, 2012; Straub and Tomita, 2012), but nothing is known regarding the role of auxiliary proteins in the regulation of presynaptic AMPARs. In MLIs, the TARPs γ-2 and γ-7 regulate somotodendritic AMPAR-mediated signalling. These interneurons also contain presynaptic AMPARs that modulate the release of GABA onto Purkinje cells and other MLIs (subsections 1.6.8 and 1.6.9). The principal aim of the work described in this thesis was to determine whether TARPs regulate presynaptic AMPARs. To this end, I examined AMPAR-mediated modulation

of GABA release from MLIs in acute cerebellar slices from wild-type and *stg/stg* mice that lack TARP γ-2.

2 | Methods and Materials

2.1 | Animals

Stargazer (*stg/stg*) mice were bred from +/*stg* mice (C57BL/6 background) and identified according to phenotype - smaller size, head tossing, unsteady gait (Noebels et al., 1990). In each case, identification was confirmed post-experiment by genotyping using tail samples from individual mice with primers as illustrated briefly in Figure 2.1 *A*, and described in more detail by Letts et al. (1998). Age-matched C57BL/6 wild-type mice were used as controls. For some experiments where MLIs were imaged, transgenic mice were used with enhanced green fluorescent protein (eGFP) driven by the promoter for the 65-kDa isoform of glutamic acid decarboxylase (GAD65).

2.2 | Slice preparation

Sagittal slices were cut from the cerebellar vermis of P10-14 and P20-23 C57BL/6 mice and P10-14 *stg/stg* mutant mice, in accordance with UK Animals (Scientific Procedures) Act 1986. Following anaesthesia with 5% isoflurane (SurgiVet system Model 100), mice were decapitated, and the brains removed and placed in ice-cold slicing solution. For most experiments, a slicing solution with partial sucrose replacement was used, which contained (in mM): 85 NaCl, 2.5 KCl, 0.5 $CaCl_2$, 4 $MgCl_2$, 1.25 NaH_2PO_4, 25 $NaHCO_3$, 25 glucose, and 64 sucrose (pH 7.4 when bubbled with 95% O_2 and 5% CO_2) (Geiger and Jonas, 2000). Alternatively, in some experiments, a Kgluconate solution was used containing (in mM); 130 Kgluconate, 15 KCl, 0.05 EGTA, 20 HEPES, and 25 glucose, 4 Na-pyruvate with pH adjusted to 7.4 by NaOH. The latter solution was thought to mimic the intracellular solution, and limit the entry of Ca^{2+} and other extracellular ions into cells whose neurites were cut during the slicing procedure (Dugué et al., 2005). 20 μM D-2-amino-5-phosphonopentanoic acid (D-APV) was added to both slicing solutions to limit glutamate-mediated excitotoxicity. Slices were cut with a vibrating microslicer (650 V HM; Micron GmbH) either at 250 μm thick for acute slice experiments, or 400

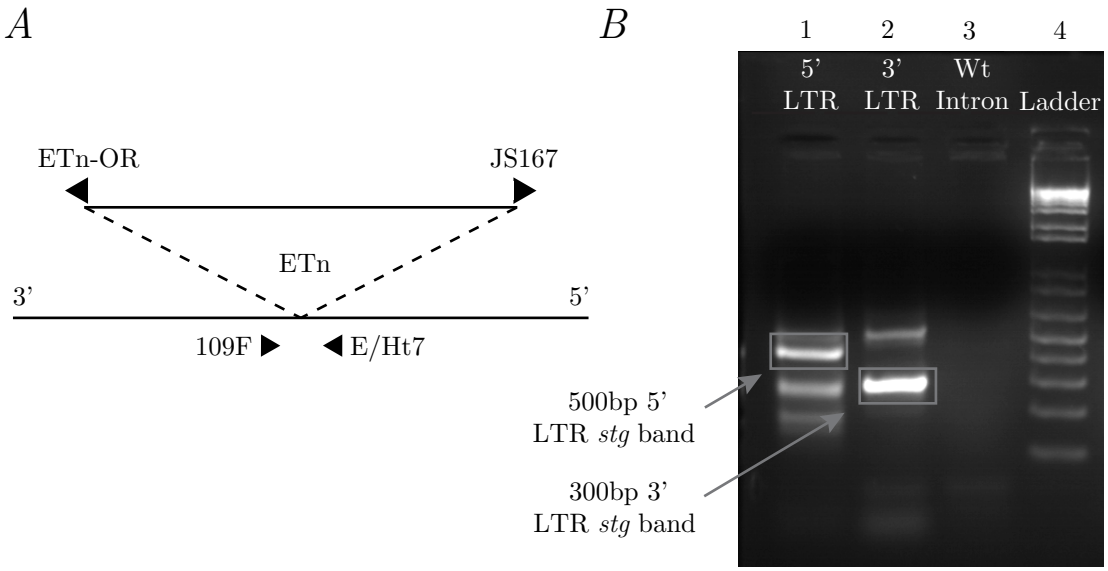

Figure 2.1: Genotyping of *stg*/*stg* animals.

(*A*) Alignment of primers for *stg*/*stg* genotyping polymerase chain reaction. An Early transposon (ETn) retrotransposon insertion is genetically and physically linked with the *stg*/*stg* locus on mouse chromosome 15. When inserted, both the 3′ and 5′ long terminal repeats (LTR) of the retrotransposon are amplified. 109F and ETn-OR are the forward and reverse primers respectively for the the 3′ LTR, whilst the 5′ LTR is amplified using JS167 as a forward primer and E/Ht7 as a reverse primer. In wild-type (Wt) animals, the retrotransposon is not inserted and the wild-type intron is amplified using 109F as a forward primer and E/Ht7 as a reverse primer. (*B*) Detection of the *stg*/*stg* allele using gel electrophoresis of the genotyping PCR product. Lane 1 and 2 show the presence of the 5′ LTR and 3′ LTR bands, respectively. Lane 3 shows the absence of a wild-type intron band and Lane 4 is the ladder. The 3′ and 5′ LTR bands are highlighted with rectangles and labelled.

μm thick for mechanical dissociation experiments (see below). Slices were transferred to a submerged bathing chamber containing extracellular solution (in mM): 125 NaCl, 2.5 KCl, 2 $CaCl_2$, 1 $MgCl_2$, 25 $NaHCO_3$, 1.25 NaH_2PO_4 and 25 glucose (bubbled with 95% O_2 and 5% CO_2), and incubated at 34 °C for 45 minutes prior to recording.

2.3 | Mechanical dissociation of Purkinje cells

Purkinje cells were dissociated from 400 μm sagittal cerebellar slices (prepared as described above) using acute vibrodissociation in the absence of enzyme treatment (Akaike and Moorhouse, 2003; Duguid et al., 2007; Vorobjev, 1991). Slices were placed in a 35 mm culture dish (Nunc) on the stage of a BX51 WI upright microscope (Olympus) and viewed using oblique infrared illumination with a 4X objective. A fire-polished glass pipette was mounted in a holder connected to a speaker cone and placed over the Purkinje cell layer. Horizontal vibration was achieved by driving the speaker with a 4 V, 6 ms square pulse delivered at 90 Hz (S48 stimulator; Grass). The glass pipette was first vibrated in an elliptical pattern at the slice surface before being driven through the slice. The dissociation was performed in a solution containing (in mM): 145 NaCl, 2.5 KCl, 1 $CaCl_2$, 1 $MgCl_2$, 10 glucose and 10 HEPES (pH 7.3 with NaOH). Dissociated cells were allowed to adhere to the bottom of the dish for 10 minutes before the recording commenced.

2.4 | Electrophysiology

During recording, cerebellar slices or dissociated cells were continuously perfused with an extracellular solution containing (in mM): 125 mM NaCl, 2.5 mM KCl, 2 mM $CaCl_2$, 1 mM $MgCl_2$, 25 mM $NaHCO_3$, 1.25 mM NaH_2PO_4 and 25 mM glucose (pH 7.3 when bubbled with 95% O_2 and 5% CO_2). In all experiments, 20 μM D-AP5 and 10 μM (2S)-3-[[(1S)-1-(3,4-dichlorophenyl)ethyl]amino-2-hydro xypropyl](phenylmethyl)phosphinic acid hydrochloride (CGP 55845) were added to block NMDA and $GABA_B$ receptors, respectively. Other drugs used were 1 μM TTX, 20 μM or 40 μM CNQX, 20 μM 2,3-dihydroxy-6-nitro-7-sulfamoyl-benzo[f]quinoxaline-2,3-dione (NBQX), 1 or 2 μM (S)-α-

amino-3-(3-hydroxy-5-methyl-isoxazol-4-yl)propanoic acid (AMPA), 50 μM cyclothiazide, 6 μM (S)-N-[4-[[3-[(3-aminopropyl) amino] propyl] amino] butyl]-4-hydroxy-α-[(1-oxo-butyl)amino] benzenepropanamide tris(trifluoroacetate) salt (philanthotoxin 443, PhTx-433), 20 μM 2-(3-carboxypropyl)-3-amino-6-(4 methoxyphenyl)pyridazinium bromide (SR 95531), 100 μM EGTA-acetoxymethyl ester (EGTA-AM), 100 μM BAPTA-acetoxymethyl ester (BAPTA-AM), 100 μM cadmium chloride ($CdCl_2$), 40 μM 1-(4-aminophenyl)-4-methyl-7,8-methylenedioxy-5H-2,3-benzodiazepine hydrochloride (GYKI 52466) and 1 μM ω-Agatoxin-IVA (Agatoxin). All drugs, except PhTx-433 and GYKI 52466 (Sigma), were purchased from Ascent (now Abcam).

2.4.1 | Cell visualisation

Whole-cell patch-clamp recordings were made from the soma of either MLIs or Purkinje cells. For all recordings, neurons were visually identified with a BX51 WI upright microscope (Olympus) using a 40× water immersion objective and infrared oblique illumination. Images were acquired with an infrared-sensitive charge-coupled device (CCD) camera (TILL Photonics, model VX55), and viewed on a video monitor. For fluorescence, slices were illuminated using a Polychrome II monochromator (TILL Photonics, model Polychrome V) controlled by Poly Con 3.0 software, and images were captured using a Rolera-XR CCD camera and Q Capture Pro 6.0 software (Q-imaging).

2.4.2 | Patch pipettes

For MLIs, patch pipettes were made from thick-walled borosilicate glass (GC-150F; Clark Electromedical) and fire polished to a resistance of 5-10 MΩ. For Purkinje cell recordings, patch pipettes were made from thin-walled borosilicate glass (G150TF-3; Warner Instruments) and fire polished to a resistance of 3.5-6 MΩ. All patch pipettes were coated with Sylgard resin (Dow Corning 184) to reduce pipette capacitance. To clean and smooth the tip of the glass that forms the seal with the cell membrane, patch pipettes were lightly fire polished with a MF-83 microforge (Narishige).

Patch pipettes were filled with 'internal' solution, which was filtered with a Minisart RC4

0.22 μm filter (Sartorius Stedium Biotech) before being applied through a MicroFil 28 gauge micropipette (World Precision Instruments). Pipette glass contained a filament to facilitate capillary flow of solution to the pipette tip. For most voltage-clamp recordings, the internal solution contained (in mM): 128 CsCl, 10 HEPES, 10 EGTA, 10 TEACl, 2 MgATP, 1 $CaCl_2$ and 2 NaCl, (pH 7.4 with CsOH, final osmolarity ∼285 mOsmol/l), and the holding potential was set at –70 mV. For Purkinje cell recordings involving climbing fibre stimulation, the internal solution contained (in mM): 150 Kgluconate, 10 HEPES, 1 EGTA, 4 MgATP, 0.1 $CaCl_2$, 4.6 $MgCl_2$ and 0.4 NaATP (pH 7.4 with KOH, final osmolarity ∼285 mOsmol/l) and the cells were held at –30 mV. The same internal solution was used for current-clamp recordings from MLIs.

Within each electrophysiological recording, the bath and pipette electrodes were placed within solutions of different ionic compositions, thus providing an additional source of potential difference, termed the liquid junction potential. When uncorrected, the junction potential can obscure true measures of membrane voltage. The junction potential depends on the difference in ionic charge between the internal and external solutions as well as the relative size of the individual ions, which influences their mobility. Junction potentials were calculated using the junction potential calculator tool within pClamp 10 software (Molecular Devices). When using the CsCl voltage-clamp internal the junction potential was –2.6 mV, whereas for the Kgluconate current-clamp internal it was much higher at –14.9. Neither values were corrected for in the reported values of membrane voltage.

The patch pipette was secured in a DB-P-1.5G electrode holder (G23 Instruments), which was connected to an Axon Instruments CV-7B current- and voltage-clamp headstage of a Multiclamp 700B patch-clamp amplifier (Molecular Devices). The headstage was mounted on a PatchStar motorised micromanipulator (Scientifica). Recordings were filtered at 3 kHz using a 8-pole low-pass digital Bessel, and digitised at 10 kHz using a Digidata 1440A interface and pClamp 10 software (Molecular Devices). Experiments were performed at room temperature (20-25 °C).

2.4.3 | Seal formation and rupture

The seal formation between the pipette and the cell membrane was judged according to electrode resistance, which was monitored by measuring the current transient elicited by a 10 mV hyperpolarising voltage step applied every 33 ms. Between 20-40 mbar positive pressure was applied to the pipette during transition through the air-water interface. The pipette was lowered to the level of the slice and the positive presure was then released to zero the pipette voltage offset, before being reapplied to aid seal formation. When an expanding dimple in the cell membrane was observed, positive pressure was released and negative pressure applied until a GΩ seal was achieved, the holding potential was slowly bought from 0 mV to –70 mV to aid seal formation. The pipette capacitance was corrected (see below), before a slow ramp of negative pressure was applied to rupture the membrane and provide electrical access to the neruon.

2.4.4 | Recording in the whole-cell voltage-clamp configuration

Continuous single electrode voltage-clamp was used to record current from MLIs and Purkinje cells. The technique relies on a current-following operational amplifier in the headstage that maintains a set potential difference between the pipette and bath electrodes by injecting current proportional, and with a reversed polarity, to fluctuations in the membrane current. Changes in membrane current are measured as the voltage drop across a feedback resistor.

The membrane acts as a capacitor that requires charging. The combination of the pipette resistance and the whole cell capacitance produces a low pass filter effect that if left alone slows the speed of fluctuations in membrane current, as well as current injection from the amplifier, with a time constant equal to the product of the whole-cell capacitance (C_m) and series resistance (R_e):

$$\tau = R_e C_m \tag{2.1}$$

Pipette and whole-cell capacitive transients were cancelled from the recording through

adjusting amplifier circuits which consist of a variable resistor and capacitor in series. In voltage-clamp amplifiers, the arrangement of this circuit in parallel to the operational amplifier provides an alternative path for the capacity current to preferentially charge. As the pipette and whole-cell capacitances are measured prior to each recording, the parallel circuit removes a current equal to the capacitive transients, leaving the current recorded at the inverting node of the amplifier uncontaminated. Pipette capacitance was cancelled prior to patch rupture.

Following the cancellation of the whole-cell capacitance, it was necessary to compensate for series resistance The series resistance of a voltage-clamp recording refers to the resistance at the patch pipette tip when in the whole-cell mode. For MLI and Purkinje cell recordings, the series resistance was typically between 10 and 20 MΩ. The series resistance is usually larger than the pipette resistance, due to intracellular debris that partially occludes the pipette. Voltage errors arise from the pipette resistance being in series with the membrane resistance. The resulting voltage drop across the series and membrane resistance means that command voltages would be insufficiently conveyed to the cell, and currents originating from the cell would be reduced in amplitude at the amplifier. Another consequence of series resistance, is the temporal filtering of current. In equation 2.2, the τ of the capacitive transient is subject to the series resistance. By reducing the series resistance it is possible to increase the accuracy of current kinetics.

I compensated for series resistance by adjusting the 'correction' positive feedback circuit in the headstage. The positive feedback circuit introduces an additional current into the cell. As current and resistance are inversely related according to Ohm's law, the 'correction' effectively reduces the series resistance. The amount of current injected by the amplifier was adjusted as a percentage of the pipette resistance, previously calculated prior to seal formation. To adjust the correction, the R_eC_m cancellation circuit was turned off, so the correction circuit, which reacts to current flowing in the recording circuit is responding to the accurate capacitive current. I applied as much correction as possible before a squaring or overshoot of the capacitive current was observed. Typically, the value was between 50-80%. Recordings were rejected if the series resistance increased above 30 MΩ or altered by >30%.

2.4.5 | Whole cell current-clamp recordings

In some MLI recordings, once electrical access had been achieved, I switched to current-clamp to record the resting membrane potential. Loading of the pipette capacitance by the cell can both slow fluctuations in the recorded membrane potential and can alter cell behaviour. To avoid these unnecessary filtering and loading errors, a positive feedback capacitance neutralisation circuit in the amplifier was tuned to inject additional current required to charge the pipette capacitance.

2.4.6 | Space-clamp issues

Voltage-clamp is spatially limited within non-spherical cells such as neurons. The cable properties of dendrites and axons dramatically filter and distort the kinetics and amplitude of currents from locations distal to the soma, and in addition, limit the volume over which current injection effectively maintains the holding potential. Consistent with modelling studies (Spruston et al., 1993), experimental data from cortical pyramidal cells suggests somatic voltage-clamp is greatly attenuated over distance, to a degree where only the perisomatic domain is sufficiently clamped for faithful measurement of fast synaptic currents (Williams and Mitchell, 2008). By recording at the soma, and injecting a conductance at dendritic locations, Williams and Mitchell (2008) showed that only $\sim 50\%$ of a postsynaptic current amplitude was recorded when the conductance was positioned 60 μm away from the soma. The inadequate space-clamp limits the ability of somatic recording to clamp the voltage of dendrites and axons at the holding potential. Indeed, the escape of voltage rapidly increased with distance, and was almost completely attenuated at locations 200 μm from the soma (Williams and Mitchell, 2008).

The problem of space-clamp applies to the electrophysiological recordings of MLIs and Purkinje cells described in this thesis. MLIs are relatively compact compared to the Purkinje cell, with short dendrites and few branch points. Due to their electronic compactness, they are often thought to be ideally suited for electrophysiological recordings. However, Abrahamsson et al. (2012) recently demonstrated that adult stellate cells exhibit a distance-dependent filtering of postsynaptic currents to reduce amplitude and slow

kinetics. Most MLI recordings in this thesis were conducted in P10-14 MLIs; their smaller size may confer greater space-clamp than the adults used in the Abrahamsson et al. (2012) study. By comparison, even in young animals, Purkinje cells have an extremely large and branched dendritic tree with a high expression of VGCCs. Due to the large distances, branch points and leaky membrane, it is likely that synaptic currents originating at a distance from the soma (i.e. stellate cell synapses) (see subsection 1.6.7) are not accurately measured, or missed entirely (Roth and Häusser, 2001). Relative to stellate cell inputs, the amplitude and kinetics of IPSCs originating from basket cells, which synapse onto Purkinje cell somata, will be more faithfully measured, and thus may contribute a greater proportion of recorded IPSCs. One advantage of the mechanically dissociated Purkinje cell preparation, is that the remaining somatic structure, in the absence of the axon and dendrites, allows for excellent space-clamp (Akaike and Moorhouse, 2003).

2.4.7 | Neuronal stimulation

In slice recordings, IPSCs were evoked using a patch electrode (3-5 MΩ) filled with extracellular solution and placed in the molecular layer, approximately 100-300 μm from the recorded Purkinje cell, and in close proximity to the Purkinje cell layer. Paired pulses of 20 μs duration (10-40 V), separated by 30 ms, were applied at a voltage between 10-40 V. Single IPSCs were evoked in mechanically dissociated Purkinje cells by stimulation of adherent presynaptic boutons using a patch electrode (4-6 MΩ) filled with external solution. 1.3 ms current pulses (50-100 μA) were applied with an iontophoretic amplifier (MVCS-C Iontophoresis system; NPI electronic).

For paired MLI recordings, one cell was recorded in whole-cell voltage-clamp configuration, and from a paired MLI, action potentials were recorded in the cell-attached mode in current-clamp. The cell-attached pipette was moved from MLI to MLI until paired action potentials and IPSCs were observed. Loose cell-attached recordings were achieved with low resistance (3-5 MΩ) thin-walled borosilicate glass patch pipettes containing extracellular recording solution. Prior to attaining a loose (MΩ) seal on the desired cell, a separate cell was patched to 'dirty' the pipette tip and prevent GΩ seals forming on the desired cell. No suction was applied during recording, and the electrode potential was

maintained at bath potential.

2.4.8 | MLI classification

MLIs are sometimes sub-classified as either stellate or basket cells according to their location in the molecular layer. Stellate cells reside in the outer two thirds of the molecular layer, whereas basket cells are generally located within the inner third nearest the Purkinje cell layer. Aside from their different axonal contacts, there appear to be few differences between the cells, and they are thought to be a spectrum of the same cell type (Sultan and Bower, 1998). I noted the position in the molecular layer at which each recorded MLI was located. In different experimental treatments, there was no location-dependent difference in the drug treatment on normalised mIPSC frequency. Throughout the thesis, results from stellate and basket cells were therefore pooled, and collectively referred to as MLIs.

2.5 | Data analysis

2.5.1 | IPSC event detection

All electrophysiological recordings were analysed using Igor Pro 6.10 (Wavemetrics Inc.). Miniature inhibitory postsynaptic currents (mIPSCs) were detected using a scaled template algorithm (Clements and Bekkers, 1997), within Neuromatic 2.6 (http://www.neuromatic.thinkrandom.com/). The template was based on rising and decaying exponentials with time constants that were typically set at 1 and 3 ms, respectively. A 4:1 ratio between the amplitude of the template and the residual sum of squares was used as the detection criterion.

For some cells, the records were reanalysed using threshold-based event detection; events were detected if the peak current crossed the threshold value which was typically set at 3 times the standard deviation of the background noise (calculated using a one-sided gaussian fit to an all-point amplitude histogram of the recorded current). Detected events were then checked by eye. An additional measure of frequency was determined from the

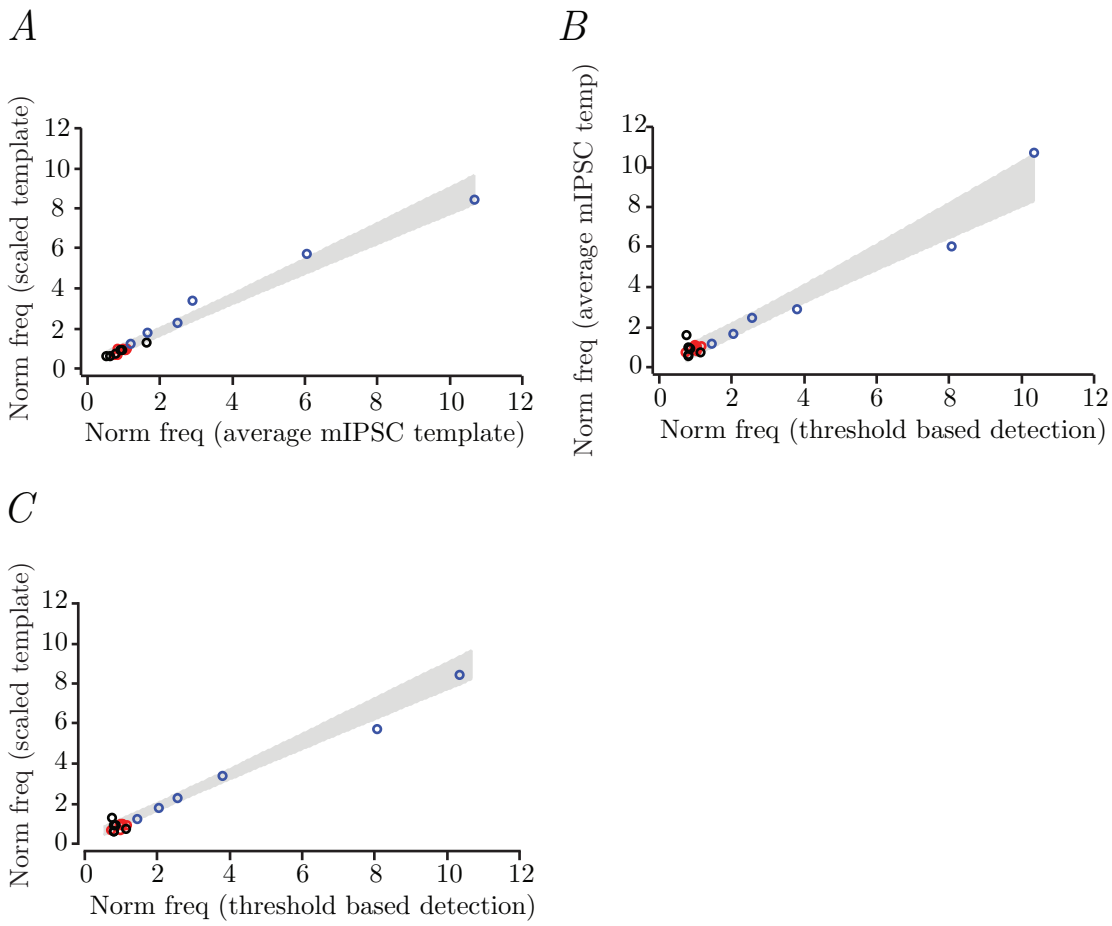

Figure 2.2: Alternative measures of mIPSC frequency provide consistent results. (*A-C*) Each axis on the three scatter plots describes the frequency of mIPSCs recorded from neurons in the presence of AMPAR agonists when normalised to their frequency in control. Recordings from pyramidal cells in V1 layer 2/3 held at a 0 mV holding potential exposed to 1 μM AMPA are shown in black, pyramidal cells in V1 cortical layer 2/3 held at –70 mV holding potential exposed to 1 μM AMPA shown in red and MLIs held at –70 mV and exposed to 20 μM CNQX are illustrated in blue. Scatter plots were constructed to compare the relative changes in frequency when mIPSC events were detected with three different methods. Normalised mIPSC frequency for individual cells calculated using a scaled template algorithm was strongly correlated to the normalised frequency calculated using an average event based template detection system (*A*; $n = 20$, $P < 0.0001$). Strong correlations were also observed between values of normalised mIPSC frequency calculated using the scaled template algorithm and the threshold-based system (*C*; $n = 20$, $P < 0.0005$), as well as between the average event based and threshold-based systems (*B*; $n = 20$, $P = 0.0004$). All data analysed with a Spearman's rank-order correlation; grey shading indicates the 99% confidence limits of a linear fit to the data, the fit was removed for clarity. Norm; normalised, freq; frequency, temp; template

same reanalysed cells, in which the average mIPSC waveform of the threshold detected events was used as a template. For individual recordings taken from MLIs or layer V pyramidal cells in the visual cortex, Figure 2.2 *A*-*C* plots the frequency of detected events in AMPA or CNQX when normalised to their frequency in control values. Normalised changes in events detected by the scaled template algorithm strongly correlated with the corresponding normalised frequency of mIPSCs detected using either the average mIPSC template system (Figure 2.2 *A*; $n = 20$, $P = 0.0004$), or the threshold based detection approach (Figure 2.2 *C*; $n = 20$, $P = 0.0005$). The strong agreement between alternative methods of mIPSC detection provided justification for the use of the scaled template algorithm to measure frequency changes.

2.5.2 | Measurements of phasic charge transfer

The phasic charge transfer during each recording in TTX was calculated using an automated procedure (written in Igor Pro). As demonstrated in Figure 2.3 *A* and *B*, for each 4 s epoch, an all-point amplitude histogram was generated and fit with a single-sided Gaussian of the most-positive current values. The peak of the histogram was taken as the baseline current value. The integral of the section of histogram not fitted by the Gaussian represents the charge carried by the phasic synaptic events. The total phasic charge was divided by the recording time, to give a measure of phasic charge s^{-1}. Unlike measurement of mIPSC frequency, this approach involved no subjective assignment of parameters for the template, or the subjective selection of the synaptic events themselves.

There a few caveats to acknowledge with this method. Firstly, the phasic charge measure does not distinguish between mEPSCs and mIPSCs. However as Figure 2.4 illustrates, mEPSCs were relatively infrequent and small. For example, from a representative MLI which exhibited a relatively high mEPSC frequency (0.21 Hz), mEPSCs contributed only 1% to the total phasic charge for a ∼3 minute recording (Figure 2.4 *D*). Furthermore, when the relative frequency of mEPSCs and mIPSCs is ignored, the smaller amplitudes and considerably faster decay of mEPSCs compared to mIPSCs (Figure 2.4 *C*) results in a substantially smaller magnitude of phasic charge for individual events. For example, Figure 2.4 *E* demonstrates that when the phasic charge for mIPSCs and mEPSCs is

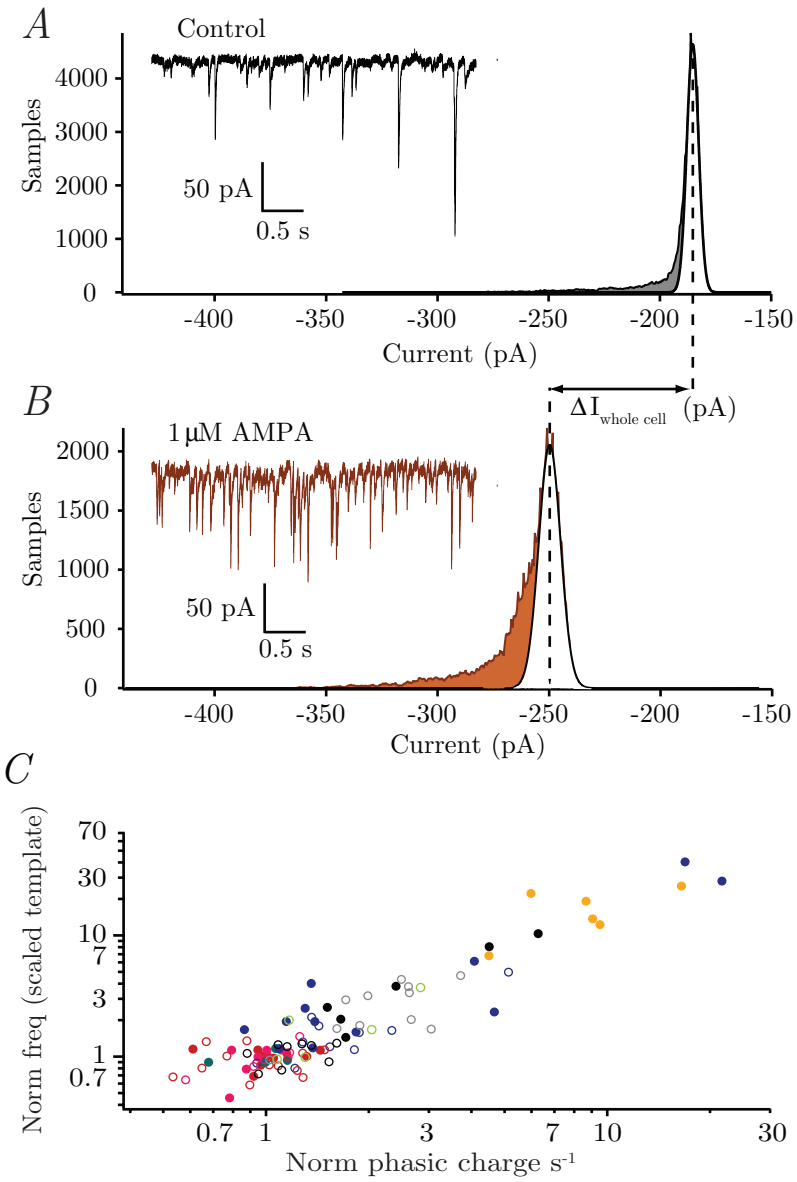

Figure 2.3: Automated calculation of phasic charge transfer provides an alternative measure to mIPSC frequency.

(*A*) All-point amplitude histogram (thick black line) of the current recorded over a 4 s period from a P12 Purkinje cell (inset black trace). A single-sided Gaussian fit of the right-hand peak of the histogram (most-positive current values, white) provides an estimate of the baseline current noise. The peak of the histogram is taken as the zero current value to give the average baseline

Figure 2.3 continued: (dotted line). The integral (grey) of the histogram not fitted by the Gaussian represents the current produced by synaptic events. (*B*) All-point histogram from the same cell as *A*, recorded in the presence of 1 μM AMPA. A clearly observable increase in frequency of synaptic events (inset brown trace) is reflected by the larger area of the histogram (orange) not fitted by the single sided Guassian. The baseline, calculated from the peak position of the Gaussian fit was shifted to a more negative value compared to control ($\Delta I_{\text{whole cell}}$ = -64.5 pA). (*C*) Normalised phasic charge s^{-1} correlates strongly with normalised frequency, calculated using the scaled template algorithm ($n = 92$, $P < 0.0001$, Spearman's rank-order correlation; fit removed for clarity). The key shows from which experimental group cells were taken from. Norm; normalised, freq; frequency.

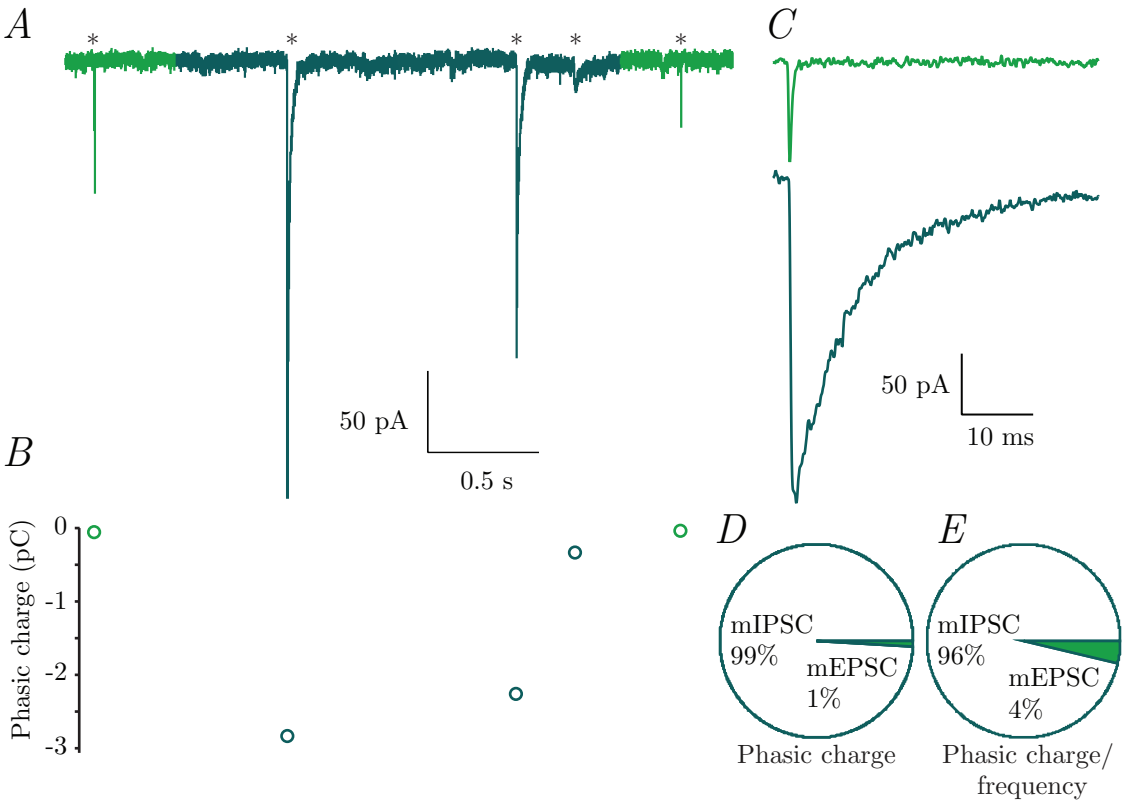

Figure 2.4: Relative contributions of mIPSCs and mEPSCs to total phasic charge. (*A*) Representative current record from a MLI in a slice from a P13 mouse (holding potential –70 mV). The transient inward currents reflect mIPSCs (turquoise) and mEPSCs (green). (*B*) Corresponding phasic charge of each event in *A* indicated with an asterisk. (*C*) Expanded sections of the first two currents asterisked in *A*. mEPSCs are typically much smaller in amplitude and have a considerably faster decay. (*D*) Pie chart demonstrates the relative contribution of mEPSCs and mIPSCs to phasic charge within a representative ∼3 min recording. From the same recording, *E* shows the contribution of mEPSCs and mIPSCs to phasic charge when normalised to the frequency at which they occurred.

normalised to their respective frequency, mEPSCs still only contributed 4% to the total phasic charge. Secondly, this measure does not take into consideration any potential differences over time in the amplitude of synaptic events. Lastly, when the baseline was not sufficiently stable, due to an extremely high frequency of events or an unstable seal between the patch pipette and cell membrane, it was difficult to fit the histogram accurately. Using shorter or longer epochs for analysis sometimes circumvented this issue. However, in some acute slice experiments, the frequency of mIPSCs following the application of 1 μM AMPA was too high to allow the baseline current to be identified. Nevertheless, the phasic charge measure was successfully used for the majority of recordings, and the normalised phasic charge s^{-1} correlated strongly with normalised frequency (determined with a scaled template algorithm) (Figure 2.3 *D*; $n = 92$, $p < 0.0001$), to provide a useful alternative measure to mIPSC frequency.

2.5.3 | Parameters of evoked neurotransmitter release

In acute slice experiments where evoked IPSCs were recorded, the paired-pulse ratio (PPR) was determined by dividing the amplitude of the second evoked IPSC by the amplitude of the first.

$$PPR = \frac{amplitude(IPSC)^{\text{2nd}}}{amplitude(IPSC)^{\text{1st}}} \tag{2.2}$$

Amplitudes were taken and the PPR calculated from individual sweeps before averaged. The noise-free coefficient of variation (CV) of first evoked IPSCs was calculated according to the protocol described by Clements (1990), as:

$$CV = \frac{\sigma^2(IPSC) - \sigma^2(noise)}{MeanAmplitude(IPSC)} \tag{2.3}$$

where σ^2(IPSC) and σ^2(noise) are the variance of the IPSC and baseline noise, respectively. For this analysis, IPSC amplitudes were taken by subtracting the average current over a 1 ms period before the IPSC, from the average current over a 1 ms period that straddled the IPSC peak. The noise was calculated by subtracting the average current from 1 ms periods separated by the same time as that used to calculate the peak

amplitude. To increase accuracy noise measurements were made at ten positions along each baseline record.

2.6 | Statistics

All data are expressed as the mean ± the standard error of the mean (SEM). Data were not assumed to be normally distributed. For comparisons between two paired data sets, a Wilcoxon matched-pairs test was used to test for a significance. When normalised, data was compared to 0 or 1 using a Wilcoxon signed-rank test. Differences between non-paired data were tested using a Mann-Whitney U-test. Where appropriate, group comparisons of more than 2 groups were performed using a non-parametric Kruskal-Wallis rank-sum test followed by selected Mann-Whitney U-tests with Holm's sequential Bonferroni correction. Results were considered significant at $P < 0.05$.

Although often presented as pairwise comparisons in the figures and text, the multiple groups compared with a Kruskal-Wallis test were spread across different experimental chapters. Group comparisons were performed only on measures of normalised mIPSC frequency. For clarity, Table 2.1 describes the individual groups within the different multiple group comparisons.

Correlations were tested using Spearman's rank order correlation. Hierarchical cluster analysis was performed using the DIvisive ANAlysis clustering algorithm ('Diana') in the R package 'cluster', and grouping was identified using 'cutree'. All statistical tests were carried out using R 2.15.1 (the R Foundation for Statistical Computing; http://www.r-project.org/) and RStudio IDE 0.96.331 (RStudio, Inc.).

Normalised mIPSC frequency								
CNQX						AMPA		
MLI acute slice			Purkinje cell acute slice			Mechanically dissociated Purkinje cell		
Age & mouse	Drug	Figure	Age & mouse	Drug	Figure	Age & mouse	Drug	Figure
P10-14 wild-type		3.3	P10-14 wild-type		3.5	P10-14 wild-type		3.11
P10-14 wild-type	+ $CdCl_2$	5.1	P10-14 wild-type	+ CTZ	3.5	P10-14 wild-type	GYKI	3.13
P10-14 wild-type	+ PhTx	5.5	P10-14 wild-type	+ CTZ + $CdCl_2$	5.1	P10-14 wild-type	Agatoxin	5.2
P20-23 wild-type		3.3	P10-14 wild-type	+ CTZ + PhTx	5.5	P10-14 wild-type	BAPTA-AM	5.3
P10-14 *stg/stg*		3.3				P10-14 wild-type	EGTA-AM	5.3
			P20-23 wild-type	+ CTZ	3.5	P10-14 *stg/stg*		3.12
			P10-14 *stg/stg*	+ CTZ	3.5			

Table 2.1: Data populations tested for the same continuous distribution using the Kruskal-Wallis one-way analysis of variance.

3 different analyses of variance on measures of normalised mIPSC frequency were performed in this thesis. One for different CNQX treatments in MLI recordings, another for the various experiments involving CNQX treatments in Purkinje cell recordings, and a third for the multiple experiments that involved AMPA treatment in recordings from mechanically dissociated Purkinje cells. Within each group, individual rows provide details of the individual conditions and where in the thesis the data set is referred to.

3 | TARP γ-2 is required for presynaptic AMPAR modulation of spontaneous GABA release

3.1 | Summary

I examined AMPAR-mediated modulation of spontaneous GABA release from cerebellar MLIs in acute slices from wild-type mice and *stg/stg* mice, which lack the prototypical TARP γ-2.

CNQX, which acts as a partial agonist only at TARP-associated AMPARs, increased the frequency of mIPSCs. This effect was abolished in both *stg/stg* mice, and in older mice which are thought to lack presynaptic AMPARs.

In both MLIs and Purkinje cells, application of AMPA increased the frequency of all mIPSCs, as well as the slow rising, small amplitude 'pre-mIPSC' subset of mIPSCs in MLI recordings. In *stg/stg* mice, the AMPA-induced increase in mIPSC frequency was greatly attenuated, but not abolished, whereas no increase in pre-mIPSC frequency was observed.

Findings in wild-type Purkinje cells were replicated in mechanically dissociated Purkinje cells with functionally adherent synaptic boutons, demonstrating the presynaptic locus of modulation. The residual effect of AMPA on mIPSC frequency in *stg/stg* Purkinje cells from acute slices was absent in recordings from acutely dissociated *stg/stg* Purkinje cells.

The data establish that γ-2 associates with presynaptic AMPARs and is required for AMPAR-mediated modulation of spontaneous GABA release from MLIs.

3.2 | Introduction

The analysis of spontaneous synaptic currents (subsection 1.4.4) has been regularly used as a tool to decipher properties of transmitter release. Traditionally, the frequency of individual quanta, commonly referred to as miniature postsynaptic currents (mPSCs), reflects changes in the condition of the presynaptic membrane, whereas changes in their amplitude reflect properties of the postsynaptic element. At the NMJ, del Castillo and Katz (1954) originally described the number of released quanta (m) that dictated the size of the EPP was the product of the number of quanta available for release (N) and the probability of release (p):

$$m = Np \tag{3.1}$$

Supposing that spontaneous neurotransmitter release is random, and the probability of release is low, then the probability (P) of observing x number of quantal events over a given time (i.e. the frequency) can be approximated by Poissonian statistics (del Castillo and Katz, 1954):

$$P(x) = exp(-m)\frac{m^x}{x!} \tag{3.2}$$

Thus, the frequency of spontaneous events can be explained by m alone, and since it is likely that most spontaneous events reflect the release of a single quantum ($n = 1$), then the probability of observing a mPSC will be solely due to the probability of release. By recording the frequency of spontaneously occurring events in the absence of action potential firing, it is possible to indirectly monitor changes in release probability under different conditions.

The application of pharmacological ligands has revealed a large repertoire of ionotropic and metabotropic receptors present at presynaptic sites capable of altering the frequency of mPSCs (Engelman and Macdermott, 2004; Hori et al., 1992; Schicker et al., 2008). Notably, the increase in mIPSC frequency recorded from Purkinje cells and MLIs following application of AMPAR agonists, was taken to suggest the presence of presynaptic

AMPARs at MLI axonal boutons (Bureau and Mulle, 1998; Rossi et al., 2008). Thus, the spontaneous release of GABA from MLIs provides an opportunity to investigate the role of auxiliary subunits on presynaptic AMPAR function.

Following the quantal release of GABA, mIPSCs recorded from both MLIs and Purkinje cells reflect an increase in Cl^- (and HCO_3^-) conductance mediated by $GABA_A$Rs (Farrant and Kaila, 2007). In general, these pentameric structures can form from two α subunits (α1-6), two β subunits (β1-3) and either one of the γ1-3, δ, ρ1-3, π, ϵ, or θ subunits. Alternatively, $GABA_A$Rs can consist exclusively of α and β subunits (Mortensen and Smart, 2006). Each subunit comprises of four TMDs and extracellular N- and C-terminal domains.

The nineteen subunits in theory allow for a large number of distinct $GABA_A$R subtypes, with additional diversity coming from alternate splicing, particularly of the genes coding for α5, β2, β3 and γ2 subunits. In reality, neurons predominantly contain the $\alpha\beta\gamma$ or $\alpha\beta\delta$ permutations, with α1 and γ2 exhibiting a widespread expression in the CNS (Farrant and Kaila, 2007). In MLIs, a constrained $GABA_A$R subunit expression (Persohn et al., 1992; Somogyi et al., 1996), and preferential subunit co-assembly (Angelotti and Macdonald, 1993; Tretter et al., 1997), dictate that they exclusively contain the $\alpha1\beta2\gamma2$ form of the $GABA_A$R. Similarly, $GABA_A$Rs in Purkinje cells are thought to be limited to the $\alpha1\beta2\gamma2$ and/or $\alpha1\beta3\gamma2$ subtypes (Wisden and Seeburg, 1993). Upon binding of GABA at binding sites situated at the interface between α and β subunits, the $\alpha\beta\gamma$ receptor opens with a single-channel conductance of $\sim$ 25-28 pS (Angelotti and Macdonald, 1993), $GABA_A$Rs at MLI and Purkinje cell synapses typically have sub-millisecond 20-80% rise times, and a much slower decay largely dependent on the receptor closing rate and entry and exit from desensitised states (Farrant and Kaila, 2007),

Cerebellar MLIs have many features that make them a suitable model in which to study the effects of presynaptic AMPARs on mIPSC frequency. Due to their high input resistance and short dendrites, MLIs are thought of as 'electrically compact'. In addition, MLIs can produce large amplitude inhibitory currents (Llano et al., 2000; Nusser et al., 1997). Such features confer a favourable signal to noise ratio, reducing the likelihood that small amplitude currents are omitted from frequency measurements. Indeed, the

discovery of a relatively novel subclass of mIPSCs was likely aided by such low recording noise. Thus, Trigo et al. (2010) found that mIPSCs with a characteristic small amplitude and slow rise time originated from $GABA_A$Rs present at axonal sites, which were recorded somatically following significant passive filtering along the axon cable.

In addition to frequency measurements, mIPSC decay kinetics may provide information about spontaneous GABA release from MLIs. A subset of MLI – MLI synapses contain relatively few $GABA_A$Rs (Nusser et al., 1997). At such individual release sites, quantal transmission will likely saturate the postsynaptic response leading to small amplitude mIPSCs with little variation in their amplitude (Nusser et al., 2001). The single-channel conductance of $GABA_A$Rs at these synapses, revealed by peak-scaled non-stationary fluctuation analysis, was unusually high; the overestimation was suggested to arise from sources of variability in mIPSC decay other than the stochastic gating of the $GABA_A$R channels. Simulations suggested that changes in GABA release were able to account for the additional variability in mIPSC decay at small MLI – MLI synapses (Nusser et al., 2001). Thus, assuming that some small MLI synapses contribute to the mIPSCs observed in a given recording, an increase in release probability will be expected to prolong the spatiotemporal profile of GABA concentration and slow the rate of mIPSC decay.

To determine the dependence of TARP-association for presynaptic AMPAR function, I recorded mIPSCs from MLIs and Purkinje cells. The effects of CNQX, a TARP-selective partial agonist (Menuz et al., 2007), and those of the full agonist AMPA were tested in both wild-type mice and *stg*/*stg* mice, which lack γ-2. I further considered differences between the effect of AMPAR activation on spontaneous release at MLI – MLI and MLI – Purkinje cell synapses, the influence of AMPAR activation on the distinct mIPSC population described by Trigo et al. (2010), and if the effects on spontaneous GABA release represent AMPAR activation at presynaptic MLI sites or passive spread of depolarisation following activation of somatodendritic AMPARs.

3.3 | Results

3.3.1 | mIPSCs in MLIs

Electrophysiological recordings were taken from MLIs, visually identified based on their size (8-9 μm), the translucent 'flattened disc' appearance of their somata, and their localisation in the molecular layer (Figure 3.1 *A*; arrow). Their molecular layer location can be more clearly observed in Figure 3.1 *B*, which is an image of a cerebellar lobule from a transgenic mouse that expressed eGFP driven by the GAD65 promoter, which selectively, but sparsely, labels interneurons (Brager et al., 2003; Fiszman et al., 2005; Galarreta et al., 2004). eGFP-GAD65 expression was limited to the molecular layer, where the somata of basket and stellate cell interneurons are thought to be located. Golgi and Purkinje cells were typically not strongly labelled in these mice. During seal formation, spontaneous cell firing was regularly observed (Häusser and Clark, 1997), and upon gaining electrical access, MLIs exhibited a relatively high input resistance (1-5 GΩ) and whole-cell capacitance within the range of 10-20 pF. Such characteristic features were always employed to distinguish MLIs from other potential cells in the molecular layer, namely Bergmann glial cells and granule cells migrating from the germinal layer. On occasion where it was possible to fill the MLI with Alexa-594 dye and image with a multi-photon microscope, the morphology of MLIs could be clearly observed. MLIs exhibited a short dendritic tree and a pronounced axon, preferentially distributed one side of the MLI soma that extended for hundreds of μms parallel to the Purkinje cell layer, as originally described by Chan-Palay and Palay (1972) (Figure 4.1 *C*). For the most part, basket and stellate cells were differentiated based on which third of the molecular layer they resided in (subsection 2.4.8). Intracellularly filled MLIs allowed for unambiguous distinction between the two types of MLIs. In comparison to the stellate cell in Figure 3.1 *C*, which corresponded to the second type of stellate cell described by Chan-Palay and Palay (1972), the basket cell in Figure 3.1 *D* is identified by the horizontally directed axon which gives rise to the characteristic descending axonal specialisations that form the complex endings around the axon hillocks and somata of Purkinje cells, referred to as the pinceau (Bishop, 1993) (Figure 3.1 *D*; arrow).

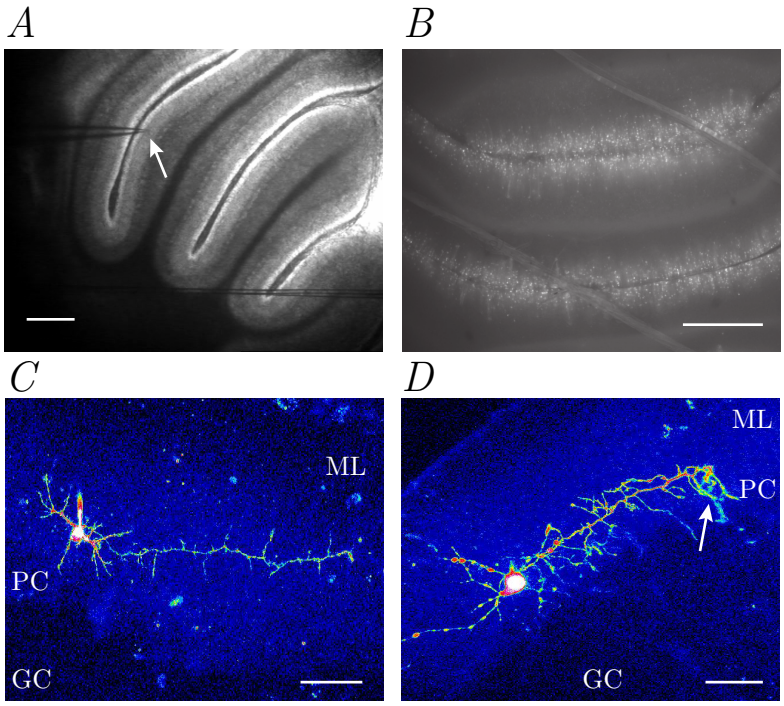

Figure 3.1: Localisation and morphology are distinguishing features of MLIs

(*A*) Bright field image of a cerebellum with 4X magnification. In the molecular layer, the pipette tip (arrowed) shows the position of the recorded MLI. Scale bar: 1 mm. (*B*) 10X magnification image of a different acutely sliced cerebellar slice from an adult eGFP-GAD65 mouse that illustrates the eGFP-positive neurons are located in the molecular layer but not in the granule cell layer. Scale bar: 1 mm. (*C*) Z-stack image of a stellate cell filled with Alexa-594 dye. Many short dendrites extend from the soma in a radiating and twisted fashion. The axon runs for $>$ 100 μM and produces ascending and descending varicose collaterals, that are short relative to that of the basket cell. The molecular and granule cell layers can be differentiated by their different shade off blue, for clarity they are labelled. ML; molecular layer, PC; Purkinje cell layer, GC; granule cell layer. Scale bar, 30 μm. (*D*) Basket cells could be differentiated from stellate cells based on fluorescence imaging after loading with Alexa–594 during somatic whole cell recording. The z-projected image shows a soma, the dendritic tree extending predominantly to the left, and the axon, which from the soma, extends parallel to the Purkinje cell layer, and produces descending branches that wrap around Purkinje cell bodies contributing to the pericellular basket and pinceau structures. Scale bar, 20 μm. Labels as in *C*. Images in *C* and *D* were taken with the help of Dr Emmanuelle Chaigneau.

To examine spontaneous quantal release, TTX was included in the recording solution to block voltage gated Na^+ channels and thus prevent cell firing. It is unlikely that any TTX resistant Na^+ channels are present in MLIs, as previous studies have reported a fast-inactivating current, which activated around –55mV, and was completely blocked by TTX (Llano and Gerschenfeld, 1993; Southan and Robertson, 1998).

Spontaneous inward currents were observed in the presence of 1 μM TTX, 20 μM D-APV and 10 μM CGP55845 to block Na^+ channels, NMDA and $GABA_B$ receptors, respectively (Figure 3.2 *A*). Such currents were overwhelming GABAegic mIPSCs as they displayed relatively slow decay kinetics and large amplitudes (Llano and Gerschenfeld, 1993; Nusser et al., 1997). These characteristic features allowed them to be easily distinguished from the relatively faster, smaller, and less frequent mEPSCs (Figure 3.2 *A*, see also Figure 2.4 for quantification in an individual MLI). Such mEPSCs were most likely mediated by AMPARs as their frequency dramatically reduced following application of CNQX. The histogram of inter-mIPSC intervals in Figure 3.2*B* is well described by an exponential function (smooth purple curve), with a time constant close to the mean inter-event interval, indicating the random occurrence of mIPSCs and the probabilistic nature of quantal transmission. It might be interesting to note that mIPSCs recorded from MLIs are likely to result from a Ca^{2+}-independent random fusion of individual vesicles (Llano and Gerschenfeld, 1993; Glitsch, 2008b).

A large range of mIPSC amplitudes was observed (Figure 3.2 *C*), which typically exhibited a non-symmetrical gaussian distribution skewed towards larger events (Figure 3.2 *D*) (Nusser et al., 1997). As MLIs are likely to just contain the $\alpha1\beta2\gamma2$ type of $GABA_AR$ (Angelotti and Macdonald, 1993; Nusser et al., 1997; Tretter et al., 1997), the variability in amplitude is thought to be a function of synaptic area and thus number of postsynaptic $GABA_A$ receptors (Nusser et al., 1997). However, recent data also suggests the amplitude can depend on the proximity of the synaptic contact to the recording site, as although short, MLI dendrites are relatively thin and thus passively filter synaptic currents (Abrahamsson et al., 2012).

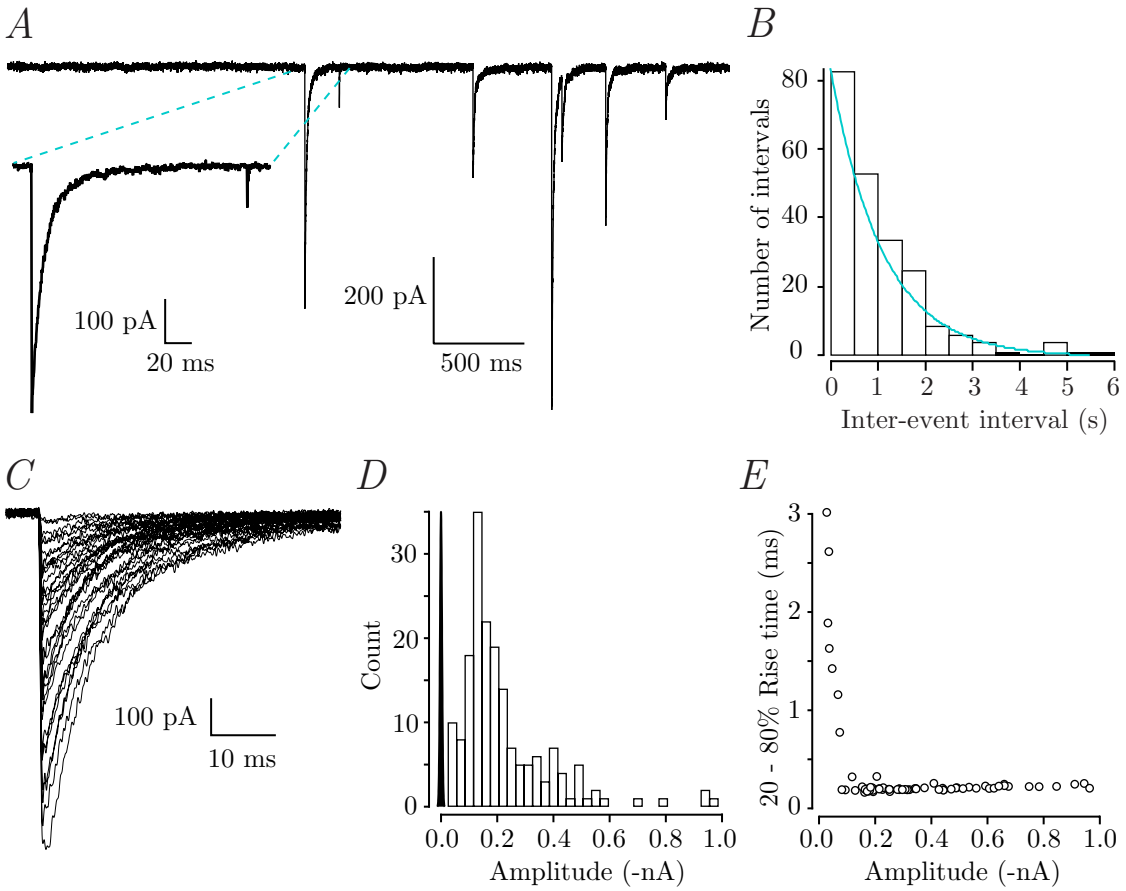

Figure 3.2: mIPSCs occur randomly and exhibit a wide range of amplitudes

(*A*) Continuous whole-cell voltage-clamp record from a MLI (P14) held at –70 mV, showing spontaneous inward currents (predominantly mIPSCs and 1 mEPSC). The inset shows the typically dramatic difference between mIPSC (left) and mEPSC (right) kinetics and amplitudes (see Figure 2.4 for quantification). (*B*) Histogram of inter-mIPSC intervals recorded from another cell (P18). The data are well described by an exponential function (smooth curve) with a time constant close to the mean frequency. (*C*) 33 mIPSCs superimposed show rapid rise and a large range of amplitudes (–27.3 to –783.8 pA). (*D*) Amplitude histogram of mIPSCs recorded from the cell shown in *C*. The distribution is not Gaussian but is skewed toward larger values. The events can be distinguished from the baseline noise, illustrated by the black histogram. (*E*) Scatter plot of rise time versus peak amplitude show a L-shaped distribution (same cell as in *A*).

3.3.2 | CNQX enhances mIPSC frequency in MLIs

The frequency of MLI mIPSCs is known to increase following application of either the partial AMPAR agonist domoate (Bureau and Mulle, 1998), or the full agonist AMPA (Rossi et al., 2008). As either effect was blocked by application of the AMPAR selective antagonist GYKI 53655, both studies suggested effects were due to the activation of presynaptic AMPARs and not kainate receptors, which also respond to both agonists. In slices from P10-14 wild-type mice, mIPSCs recorded from MLIs increased in frequency following application of 20 μM CNQX (Figure 3.3 *A*) from 0.54 ± 0.15 Hz to 2.66 ± 0.73 Hz (n = 11; P = 0.00098 Wilcoxon matched-pairs test). Correspondingly, the phasic charge transfer (see section 2.5.2) was greatly increased by CNQX (Figure 3.3 *B*; from 2.27 ± 0.42 pC to 7.24 ± 1.46 pC; P = 0.00098, Wilcoxon matched-pairs test). This latter measure reflected a change in mIPSCs rather than mEPSCs, as the recorded currents were overwhelmingly GABAergic and the individual charge conferred by mEPSCs was relatively insignificant compared to the charge transfer carried by a typical mIPSC (Figure 2.5). The changes in mIPSC frequency and charge were fully reversible on washout of CNQX (Figure 3.3 *A* & *B*), and occurred without a significant alteration in amplitude (198.80 ± 25.98 pA and 175.04 ± 20.20 pA; P = 0.58, Wilcoxon matched-pairs test). Upon treatment with CNQX, the 37% decay time of mIPSCs (re-selected based on uncontaminated rise and decay kinetics) was significantly increased from 9.25 ± 0.86 ms to 10.50 ± 1.00 ms (Figure 3.3 *D*; n = 11, P = 0.0049, Wilcoxon matched-pairs test). As the decay of mIPSCs at MLI – MLI synapses is likely to partly reflect GABA release (Nusser et al., 2001), an increased decay time in the presence of CNQX is consistent with a greater release of GABA from MLI boutons. Thus, both the increase in mIPSC frequency, and the slowed rate of mIPSC decay following CNQX treatment suggest TARP-associated AMPARs increased release probability and prolonged increased GABA concentrations at MLI – MLI synapses.

Consistent with a role for γ-2-associated AMPARs, CNQX had no effect on mIPSC frequency or phasic charge recorded from *stg/stg* MLIs (Figure 3.3 *D*; normalised frequency, 0.96 ± 0.10, n = 7, P = 0.68; normalised charge 0.95 ± 0.06, P = 0.68). From the age of P15 it is believed that there is a developmental switch leading to the disappearance

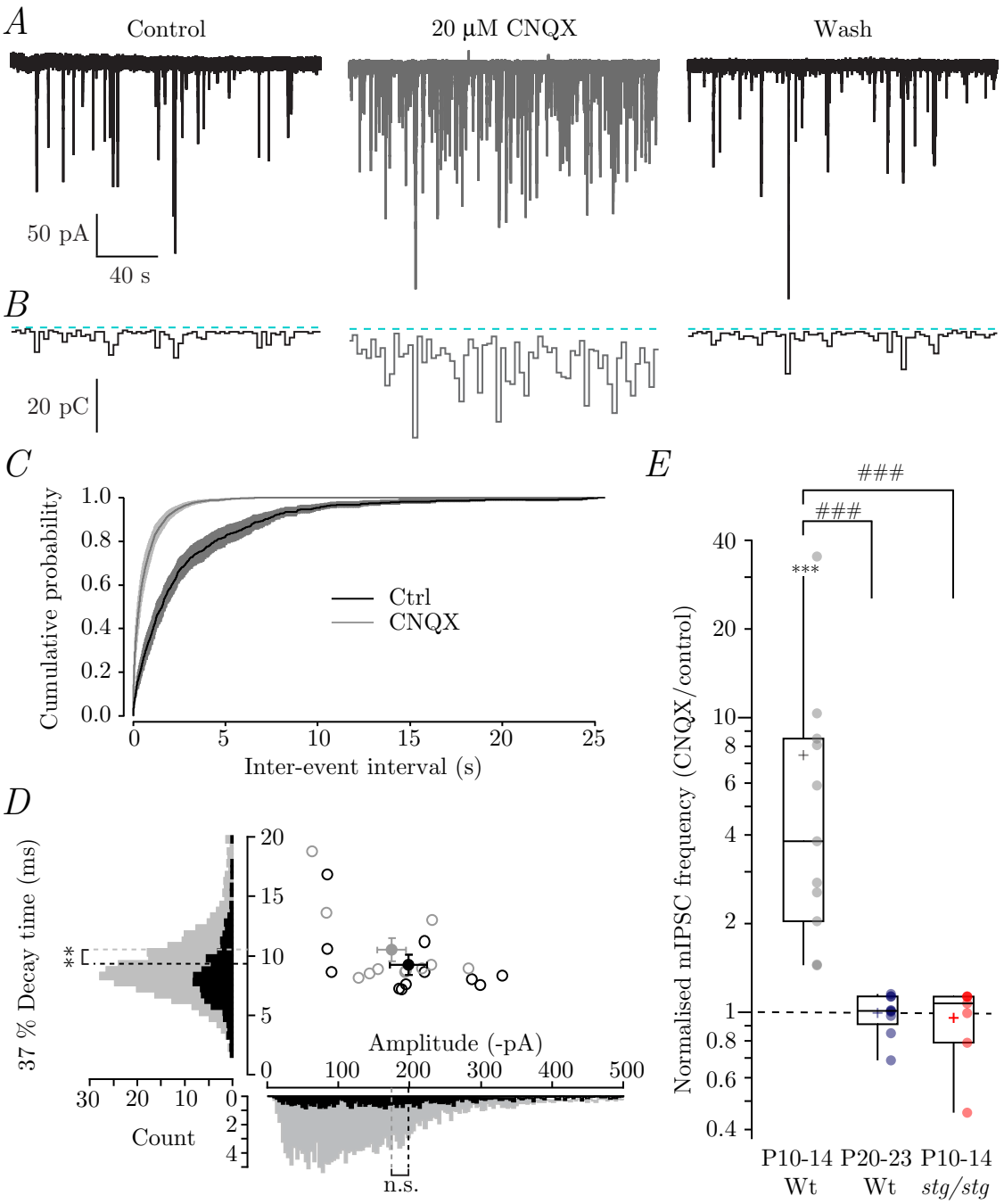

Figure 3.3: CNQX increases mIPSC frequency in wild-type P10-14 MLIs.

(*A* & *B*) Representative current records and phasic charge transfer measurements from a MLI in a slice from a P10 wild-type mouse obtained before, during (grey), and following application of 20 μM CNQX (dashed lines in *B* indicate zero charge). (*C*) Averaged cumulative probability histograms from eleven cells; lines and shaded regions represent the averages and SEMs, respectively. *D* Plot of 37% decay time against amplitude of P10-14 wild-type cells, before (black) and after (grey) CNQX application (open circles). Solid circles and error bars illustrate the average ± SEM from 11 cells. At the bottom and left of each axis is the corresponding average

Figure 3.3 continued: histogram for each measure in control (black) and CNQX (grey), dotted lines represent the average values. (*E*) Pooled data showing the effects of CNQX on mIPSC frequency in P10-14 wild-type (Wt) (grey), P20-23 wild-type (blue) and P10-14 *stg/stg* (red) MLIs. Box-and-whisker plots indicate the median (line), the 25-75$^{\text{th}}$ percentiles (box) and the 10-90$^{\text{th}}$ percentiles (whiskers); filled circles and crosses represent individual and mean values, respectively. *** P <0.001 (Wilcoxon signed-rank test versus one). ### P <0.001, (Mann-Whitney U-test versus CNQX in P10-14 cells, following a Kruskal-Wallis tests that revealed a significant effect of the group described in Table 2.1; $\chi^2(4) = 26.9$, $P = 0.000021$).

of presynaptic AMPARs. Both the increase in mIPSC frequency (Bureau and Mulle, 1998) and Ca^{2+} transients (Rossi et al., 2008) following AMPAR agonist treatment were shown to be absent in P19-25 animals. A similar developmental loss of $GABA_A$Rs was also reported to occur in MLI axons (Mejia-Gervacio and Marty, 2006; Trigo et al., 2007, 2010). In agreement with this age-dependence, my recordings from older wild-type MLIs (P20-23) showed no significant effect of CNQX on mIPSC frequency or phasic charge s^{-1} (normalised frequency and charge, 1.00 ± 0.05 and 1.03 ± 0.08, $n = 9$; $P = 0.22$ and 0.71, respectively). The normalised mIPSC frequency ratio in both *stg*/*stg* and P20-23 wild-type mice was significantly different to that observed for P10-14 wild-type mice (Figure 3.3 *E*; $P = 0.0002$ and 0.00005, respectively, Mann-Whitney *U*-test). Unlike CNQX, the related quinoxaline derivative, NBQX (20 μM), which does not act as an AMPAR partial agonist (Lee et al., 2010b; Menuz et al., 2007), failed to increase mIPSC frequency or phasic charge s^{-1} (Figure 3.4 *A*-*C*; normalised values 1.08 ± 0.11 and 0.92 ± 0.11, respectively; $n = 4$; both P values = 0.63, Wilcoxon signed-rank test).

3.3.3 | The AMPAR potentiator-dependent effects of CNQX in Purkinje cells

MLI axons form synaptic contacts not only with other MLIs, but also with Purkinje cells. I next tested if the TARP regulation of AMPAR-mediated effects on spontaneous release at MLI – MLI synapses could also be observed at MLI boutons which contact Purkinje cells. I performed whole-cell voltage-clamp recordings from P10-14 Purkinje cells under the same conditions used for MLIs (room temperature; addition of 1 μM TTX, 20 μM D-APV and 10 μM CGP 55845). In contrast to MLI recordings, CNQX (40 μM) failed to produce a significant change in the frequency of mIPSCs (Figure 3.5 *A* upper panels, *C* & *D*; normalised to the control, 1.01 ± 0.05, $n = 10$, $P = 1$, Mann-Whitney *U*-test) but did increase the phasic charge s^{-1} (Figure 3.5 *A* lower panels; ratio to control not shown, 1.19 ± 0.08, $n = 10$, $P = 0.048$). The difference in effect between these two measures could have resulted from the relatively large whole-cell current in response to AMPA. As the all point histogram used to calculate the phasic charge relies on a stable baseline to determine the integral of synaptic currents (subsection 2.5.2), this could have caused

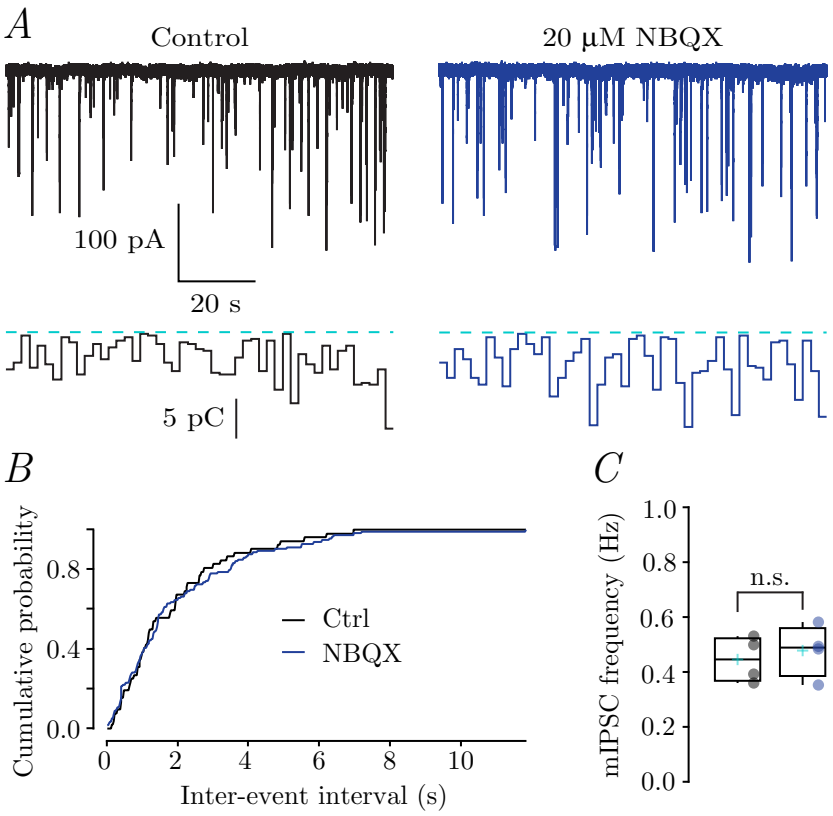

Figure 3.4: NBQX does not alter mIPSC frequency in wild-type P10-14 MLIs.
(*A*) Representative current records from a P13 wild-type MLI and the corresponding phasic charge transfer, calculated every 2 seconds over the same time period (bottom panels, dashed line refers to 0 pC). (*B*) Cumulative event frequency histograms of the cell in *A* (black traces; control, blue trace; 20 μM NBQX). (*C*) Pooled data showing the effects of NBQX on mIPSC frequency in P10-14 wild-type MLIs. Box-and-whisker plots indicate the median (line), the 25-75$^{\text{th}}$ percentiles (box) and the 10-90$^{\text{th}}$ percentiles (whiskers); filled circles and crosses represent individual and mean values, respectively.

overestimation. When the slices were pre-incubated in the positive AMPAR modulator cyclothiazide (50 μM), both mIPSC frequency and phasic charge were significantly and reversibly increased in the presence of CNQX (Figure 3.5 *B-D*; normalised to control; 2.48 ± 0.07 and 2.31 ± 0.07, respectively, $n = 11$, $P = 0.001$ for both measures). Thus, a CNQX-induced increase in mIPSC frequency was observed in both MLIs and Purkinje cells, however the effects of CNQX, in the absence of cyclothiazide, exhibited an inter-axonal bouton specificity. Consistent with recordings from MLIs, the effect of CNQX was absent from Purkinje cells in both *stg/stg* mice (0.98 ± 0.09 relative to control, $n = 5$, $P = 0.81$), and P20-23 wild-type mice (0.91 ± 0.04 relative to control, $n = 13$, $P = 0.094$). The absence of effect in both *stg/stg* and P20-23 wild-type mice was significantly different from the CNQX-induced increase in mIPSC frequency observed in P10-14 wild-type mice ($P = 0.0018$ and 0.0000040, respectively).

3.3.4 | AMPA-induced changes in mIPSC frequency are reduced in *stg/stg*

The abolition of CNQX-evoked potentiation of mIPSC frequency in slices from *stg/stg* mice is consistent with the view that presynaptic AMPARs require γ-2 for their normal trafficking and/or function. Alternatively, the lack of response to CNQX could suggest that presynaptic AMPARs in *stg/stg* mice are present, but are either TARPless or associated with γ-7 (Fukaya et al., 2005; Yamazaki et al., 2010), which does not confer sensitivity to CNQX (Bats et al., 2012). I therefore examined the effect of the full agonist AMPA, which would be expected to activate AMPARs irrespective of TARP-association. Application of 1 μM AMPA increased mIPSC frequency in both wild-type and *stg/stg* MLIs (Figure 3.6 *A-D*; normalised frequency 16.8 ± 2.7, $n = 9$, $P = 0.004$ in wild-type and 2.0 ± 0.4, $n = 14$, $P = 0.0040$ in *stg/stg*) but the effect was significantly reduced in the latter ($P = 0.0000025$) (Figure 3.6 *D*). A similar differential effect was observed in Purkinje cell recordings, where mIPSC frequency was increased by ∼10-fold in wild-type mice but only doubled in *stg/stg* mice (Figure 3.6 *D*; normalised frequency 10.8 ± 2.6 and 1.8 ± 0.2, respectively; $n = 10$ and $P = 0.0020$ for both). The effect of AMPA was significantly reduced in *stg/stg* Purkinje cells compared to wild-type ($P = 0.000022$)

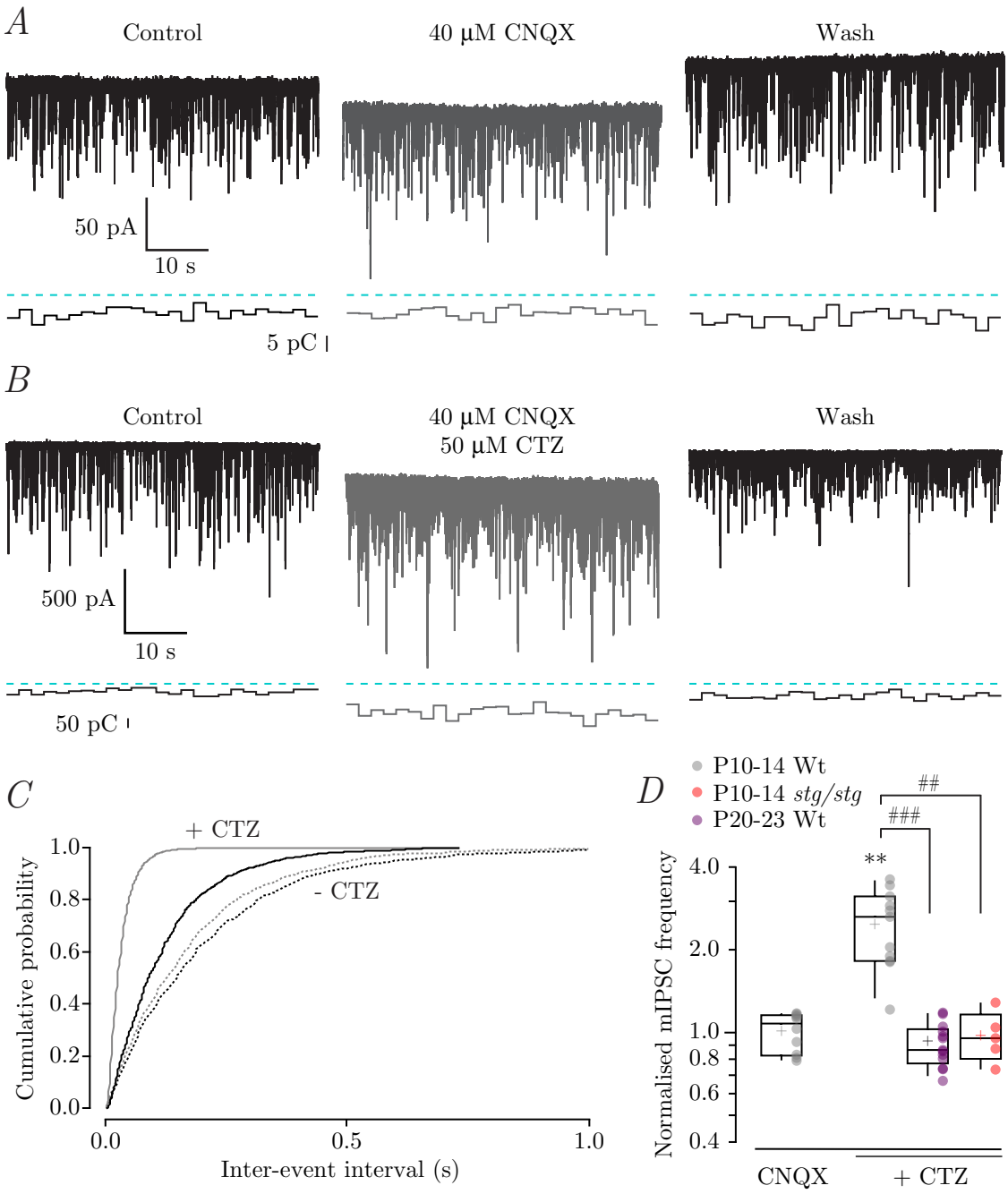

Figure 3.5: CNQX increases mIPSC frequency in Purkinje cells only in the presence of cyclothiazide.

(*A* & *B*) Representative current records from a P13 and P12 wild-type Purkinje cell, respectively (top panels). Below each current record is the corresponding record of phasic charge transfer, calculated every 2 seconds (dotted lines represent 0 pC). (*C*) Cumulative inter-event interval histograms for the cells shown in *A* (dotted lines; right) and *B* (solid lines; left), black traces; control, grey traces; 40 μM CNQX. (*D*) Pooled data showing the effect of 40 μM CNQX on mIPSC frequency normalised to control values. Box-and-whisker plots indicate the median (line), the 25-

Figure 3.5 continued: 75^{th} percentiles (box) and the 10-90^{th} percentiles (whiskers); circles and crosses represent individual and mean values, respectively. ** P <0.01 (Wilcoxon signed-rank test versus zero). ## and ### indicate P <0.01 and 0.001, respectively (Mann-Whitney U-test versus CNQX in P10-14 Purkinje cells, following a Kruskal-Wallis test that revealed a significant effect of group shown in table 2.1; $\chi^2(5) = 38.6$, $P = 0.00000029$).

(Figure 3.6 *D*). The significant reduction in (but not abolition of) the effects of AMPA in cells from *stg/stg* mice suggests that while a substantial fraction of presynaptic AMPARs in wild-type MLIs are associated with γ-2, in its absence, presynaptic AMPARs (either associated with γ-7 or TARPless) remain functional, albeit with a markedly diminished effect on release.

3.3.5 | AMPA and CNQX increase the frequency of slow rising, small amplitude mIPSCs in MLIs

To further test the presence of TARP-associated presynaptic AMPARs at MLI axonal boutons I next measured the frequency of a recently identified class of mIPSCs termed 'preminis' (referred to here as 'pre-mIPSCs') (Trigo et al., 2010). Within the large range of mIPSC amplitudes observed in MLIs (Figure 3.2 *C* & *D*), the smaller amplitude mIPSCs often exhibit a varied distribution in rise kinetics (Figure 3.2 *E*) (Trigo et al., 2010). It is suggested that these currents originate from $GABA_A$Rs in the MLI axon and their small amplitude and slow rise time result from the passive filtering along the axon (Mejia-Gervacio et al., 2007; Pouzat and Marty, 1999). Correspondingly, the $GABA_A$R mediated autoreceptor current, previously identified in these cells, also exhibits a delayed rise time (Pouzat and Marty, 1999). Positive confirmation of the axonal origin of the small currents was revealed following photo-release of caged-GABA at axonal sites, which artificially reproduced currents with similar properties. Moreover, as their frequency was markedly reduced in axotomised MLIs, it seems likely that the slow rising, small amplitude mIPSCs in MLIs originate from axonal $GABA_A$Rs (Trigo et al., 2010).

A representative experiment from a P14 wild-type MLI is illustrated in Figure 3.7, where mIPSCs (recorded in the presence of TTX, CGP55845 and D-APV) could be separated by eye into 2 populations; fast rising, large amplitude currents and slow rising, small amplitude transients (black and light blue currents respectively; Figure 3.7 *A* & *B*). The peak amplitude histogram from a P11 *stg/stg* MLI shows 2 distinct peaks, the smaller of which is likely to correspond to pre-mIPSCs (Figure 4.7 *C*). When the peak amplitudes of mIPSCs from the same cell as in *C* are plotted against their 20-80% rise times, 2 distinct populations are clearly observed (Figure 3.7 *D*). Previous studies have separated these

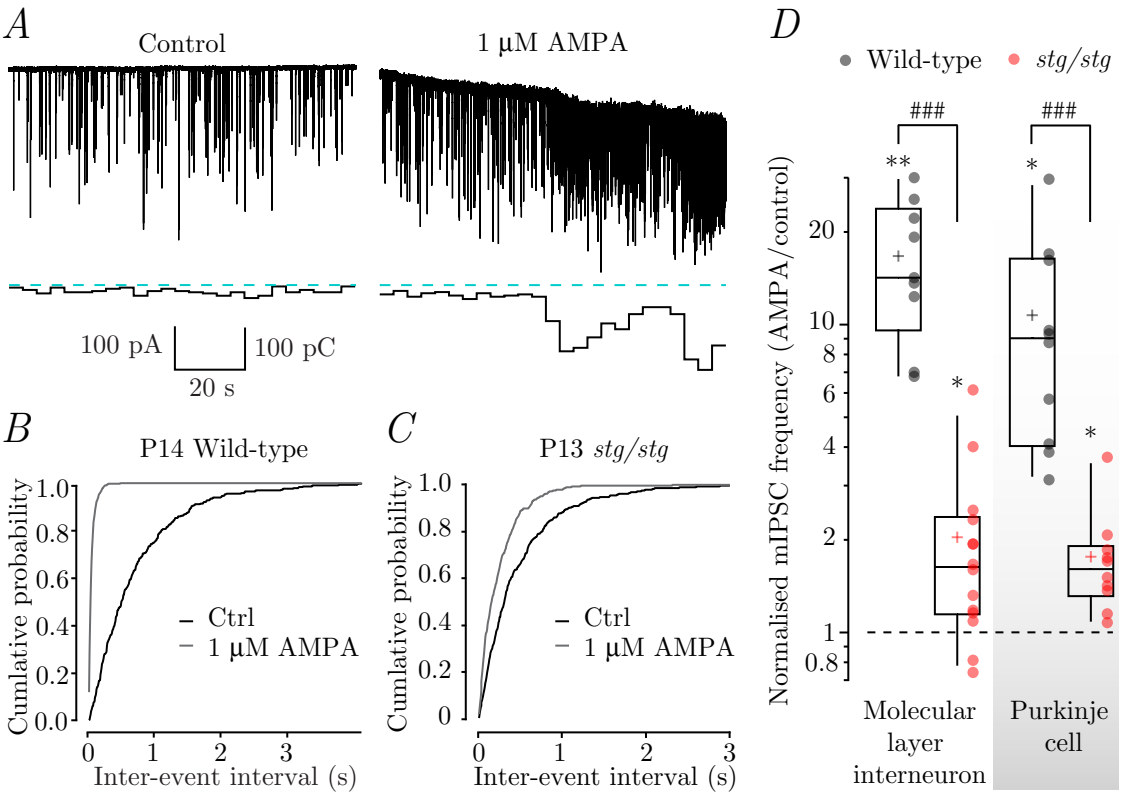

Figure 3.6: AMPA induced-increase in mIPSC frequency is reduced but not abolished in *stg/stg*.

(*A*) Representative current records from a P14 wild-type MLI (left) and below the corresponding record of phasic charge transfer, calculated every 4 s. (*B* & *C*) Cumulative inter-event interval histograms of the individual wild-type MLI in *A* and an example *stg/stg* MLI, respectively (black traces; control, grey traces; 1 μM AMPA). Though the effect was much larger in the wild-type cell, there was an increase in mIPSC frequency in both examples. (*D*) Pooled data showing the increase in mIPSC frequency during application of AMPA in both P10-14 wild-type (grey) and P10-14 *stg/stg* (red) MLIs (left) and Purkinje cells (right). Box-and-whisker plots indicate the median (line), the 25-75$^{\text{th}}$ percentiles (box) and the 10-90$^{\text{th}}$ percentiles (whiskers); filled circles and crosses represent individual and mean values, respectively. * P <0.05, ** P <0.01 (Wilcoxon signed-rank test versus zero). ### P <0.001 P10-14 wild-type versus P10-14 *stg/stg* (Mann-Whitney U-test).

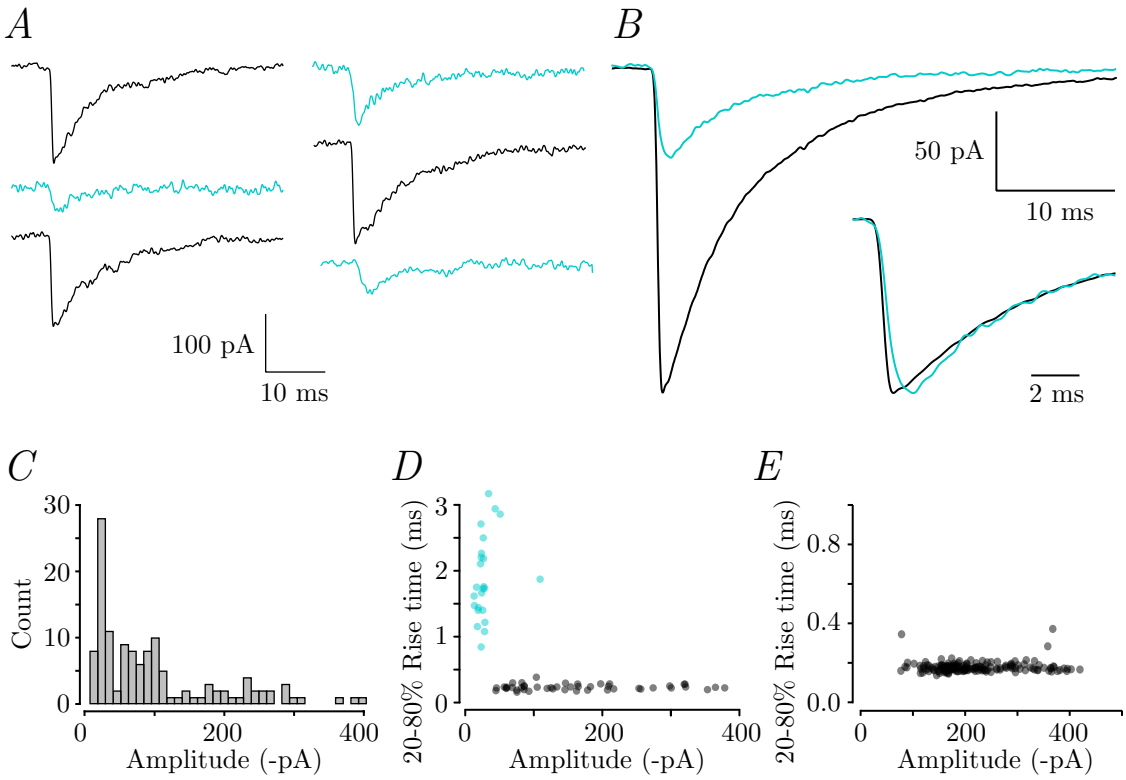

Figure 3.7: Identification of slow rising, small amplitude mIPSCs.

(*A*) Individual representative mIPSCs recorded from a single P12 wild-type MLI, show a mixture of large, fast rising, events (black) and low amplitude, slow rising,events (blue). (*B*) Averages of the two classes of events recorded from the MLI in *A* reveals a clear difference in amplitudes, and within the inset, when normalised to their peak amplitude a relatively slower rise kinetics of the smaller events. (*C*) Peak amplitude histogram showing two components from a P11 *stg*/*stg* mouse. Two populations are apparent. (*D*) A plot of the 20%-80% rise time of individual events as a function of peak amplitude from the same MLI as in (*C*) shows that small events have a longer rise time than large events. By comparison, an equivalent rise time versus amplitude plot of mIPSCs from a P22 wild-type mouse (*E*) shows a relatively tight distribution of rise times.

mIPSCs based on their amplitude, i.e. currents with a peak amplitude of <30 pA have been considered to be pre-mIPSCs (Trigo et al., 2010; Rossi et al., 2008). I found that the success of this criterion in identifying slow rising, small amplitude mIPSCs was dependent on the recording; for example, the quality of the electrical access, and the baseline noise could shift the amplitude range and thus dictate the appropriateness of this 30 pA point. Rather, I found cluster analysis to be a more robust method of separation. Although the user has to stipulate the number of clusters, this method provided greater objectivity than that of an amplitude cut off. A number of cluster analysis methods were compared, of which Divisive analysis (DIANA) consistently appeared to be the most appropriate. The validity of this method is supported by the lack of a pre-mIPSC cluster shown in a P22 wild-type MLI (Figure 3.7 *E*). This is to be expected, as the presence of $GABA_A$Rs in MLI axons are thought to disappear following P15 (Mejia-Gervacio and Marty, 2006; Trigo et al., 2007, 2010), and in addition, provides further support for the axonal origin of pre-mIPSCs (Trigo et al., 2010).

As demonstrated in Figure 3.8, the frequency of pre-mIPSCs recorded in control conditions from P10-14 MLIs was increased following application of 20 μM CNQX (*A*; far left peak of histogram and *B*; blue filled circles) and 1 μM AMPA (*C*; blue filled circles). The distribution of amplitudes and rise times shown in Figure 4.8 *C* provides a good example of mIPSCs which are not easily separated into 'normal mIPSC' and pre-mIPSC populations due to the high frequency of small amplitude events. Again, in these cases objective cluster analysis seemed more appropriate than an amplitude cut off point. Pooled data from 11 cells demonstrated CNQX approximately tripled the frequency of pre-mIPSCs from 0.05 ± 0.01 Hz to 0.17 ± 0.06 (P = 0.019; Wilcoxon matched-pairs test), and AMPA increased pre-mIPSC frequency from 0.03 ± 0.01 to 0.65 ± 0.14 (n = 9, P = 0.012; Wilcoxon matched-pairs test). Under these experimental conditions, it is likely that the somatodendritic compartment is voltage-clamped, but due to the spatial constraints of somatic voltage-clamp (Williams and Mitchell, 2008), the axonal domain is not (Trigo et al., 2010). Thus, any depolarisation resulting from the activation of somatodendritic AMPARs would be prevented from reaching the axonal boutons. By contrast, presynaptic AMPAR activation would depolarise the axonal compartment

through the activation of VGCCs, the resulting increase in GABA release would activate axonal $GABA_A$ autoreceptors to a greater extent and explain the greater frequency of pre-mIPSCs. In a separate study of MLIs, the finding that NMDA application also increased pre-mIPSC frequency was similarly argued to exclusively result from axonal bouton depolarisation, in this case presynaptic NMDA receptors were proposed to elicit the depolarisation (Rossi et al., 2012).

In slices from P10-14 *stg/stg* mice, pre-mIPSC frequency did not change following application of either 20 μM CNQX (Figure 3.9 *A*, *B* & *D*; from 0.07 ± 0.02 to 0.07 ± 0.02, $n = 11$, $P = 0.019$), or 1μM AMPA (Figure 3.9 *A*, *B* & *D*; from 0.05 ± 0.01 to 0.08 ± 0.05, $n = 11$, $P = 0.019$). The absence of effect in response to AMPA differs significantly from the increase in pre-mIPSC frequency in wild-type MLIs observed in Figure 3.6 ($P = 0.0044$, Mann-Whitney *U*-test). Unlike the change in total mIPSC frequency shown in Figure 3.3, I did not observe a significant effect of AMPA on pre-mIPSC frequency in *stg/stg* mice. Thus, the suggestion that a population of AMPARs can function to modulate GABA release from MLIs without γ-2 does not hold in this experiment, which instead indicates that presynaptic AMPARs at MLI axonal boutons are completely reliant on γ-2 for their influence on spontaneous GABA release.

3.3.6 | CNQX-induced depolarisation in MLIs

Thus far my data are consistent with the existence of axonal AMPARs in MLIs that are associated with γ-2. However, the passive spread of somatodendritic depolarisation into axonal compartments (Christie et al., 2011; Glitsch and Marty, 1999) is an alternative mechanism by which AMPAR activation could increase total mIPSC frequency without requiring the receptors to be presynaptic. Indeed, in current-clamp recordings from P10-14 wild-type MLIs I found that 20 μM CNQX produced a small somatic depolarisation (Figure 3.10 *A*-*C*; 4.9 ± 0.1 mV; $n = 15$). Although of relatively long duration, this is less that the 20 mV depolarisation identified as being necessary to influence asynchronous IPSC frequency in paired MLI recordings (Christie et al., 2011). Moreover, I observed a CNQX-induced depolarisation of 4.8 ± 0.4 mV (Figure 3.10 *C*; $n = 7$) in MLIs from older mice (P20-23), in which there was no effect of CNQX on mIPSC frequency or phasic

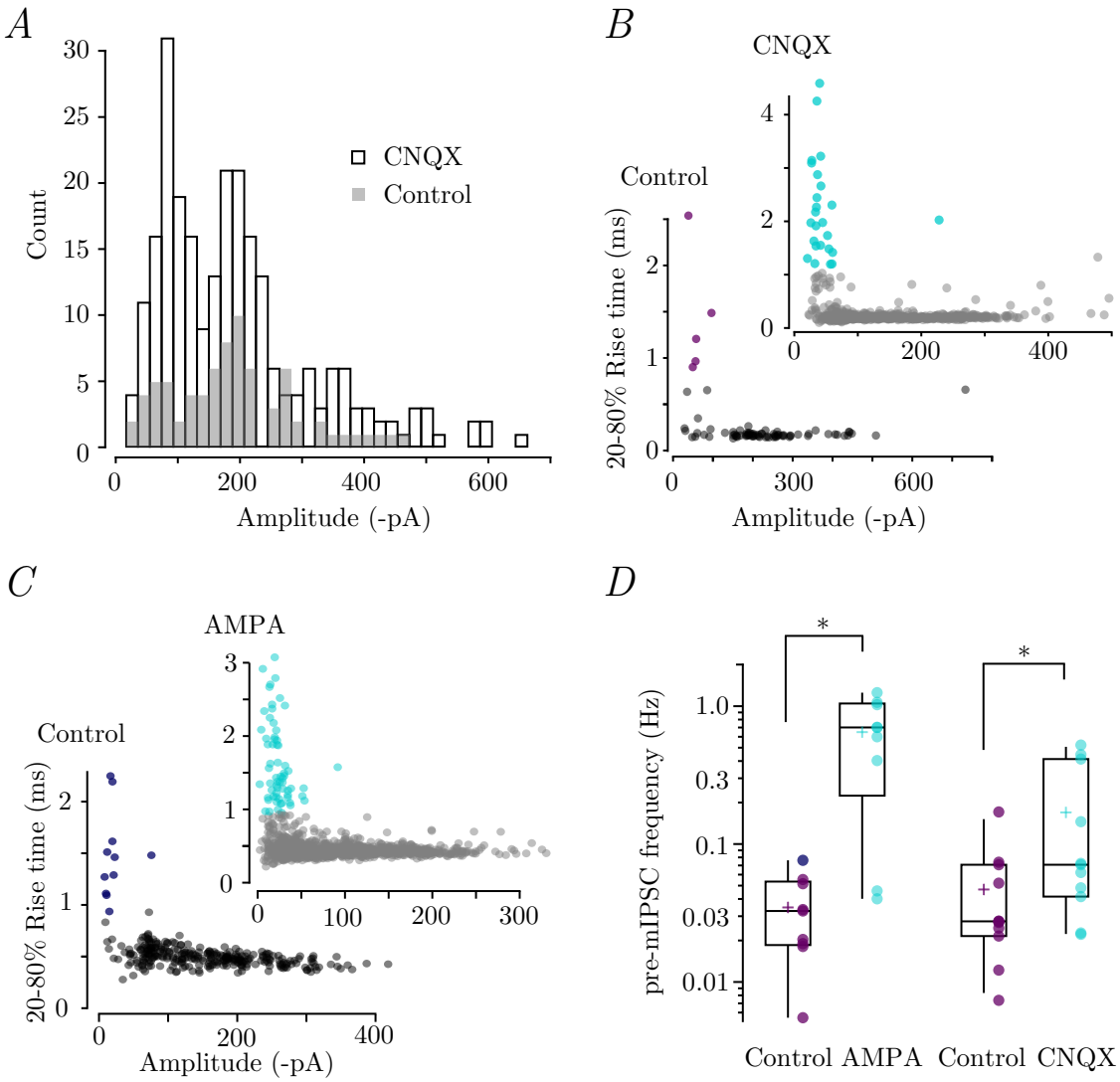

Figure 3.8: AMPAR activation increases the frequency of slow rising, small amplitude mIPSCs.

(*A*) Peak amplitude histogram from a P10 wild-type MLI in control and CNQX conditions. In both histograms 2 peaks are clearly resolvable, of which, the smaller amplitude peak is likely to represent a significant population of pre-mIPSCs. In this MLI, CNQX clearly increased both the total number of mIPSCs, and the number of pre-mIPSCs. (*B* & *C*) Plots of 20-80% rise time of individual mIPSCs as a function of peak amplitude before (left) and after (right) application of 20 μM CNQX or 1 μM AMPA in P10-14 MLIs. (*D*) Pooled data show the frequency of slow rising, small amplitude mIPSCs is increased following treatment with CNQX or AMPA. Box-and-whisker plots indicate the median (line), the 25-75$^{\text{th}}$ percentiles (box) and the 10-90$^{\text{th}}$ percentiles (whiskers); circles and crosses represent individual and mean values, respectively. * $P < 0.05$ (Wilcoxon signed-rank test).

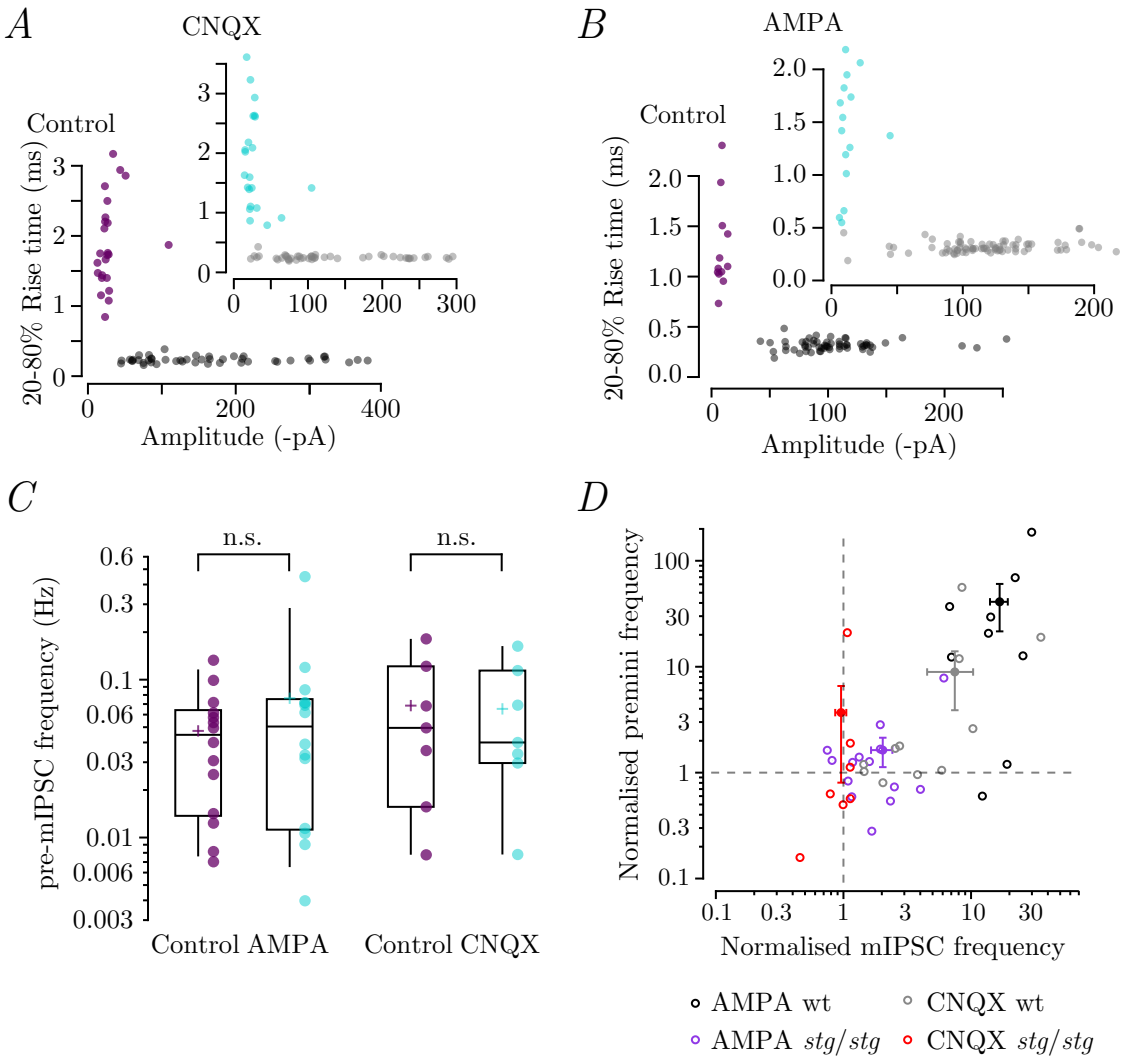

Figure 3.9: CNQX and AMPA induced increase in pre-mIPSC frequency was absent in *stg/stg*.

(*A* & *B*) Plots of 20-80% rise time of individual events as a function of peak amplitude from P11 and P10 *stg/stg* MLIs exposed to CNQX (*A*) and AMPA (*B*), respectively. (*C*) Pooled data shows that neither AMPA (2 μM) nor CNQX (20 μM) altered mIPSC frequency. Box-and-whisker plots indicate the median (line), the 25-75$^{\text{th}}$ percentiles (box) and the 10-90$^{\text{th}}$ percentiles (whiskers); circles and crosses represent individual and mean values, respectively. n.s.; non-significant ($P > 0.05$, Wilcoxon signed-rank test). (*D*) A plot of normalised pre-mIPSC frequency (treatment/control) versus normalised total mIPSC frequency (treatment/control), both measures plotted on a log scale. Open circles represent individual cells, closed circles and error bars indicate the average and SEM, respectively. Recordings from wild-type (wt) MLIs show AMPA treatment induced a relatively greater increase in both pre-mIPSC and mIPSC frequency than did CNQX (black and grey respectively). Though AMPA induced an increase in total mIPSC frequency in *stg/stg* (blue), there was no significant increase in pre-mIPSC frequency. CNQX had no effect on either measure in *stg/stg* MLIs (red).

charge. While the absence of an obligate link between somatodendritic depolarisation and altered mIPSC frequency could be taken to support a presynaptic locus of AMPARs in juvenile mice, these data do not address the possibility that this simply reflects age-dependent changes in the axonal spread of depolarisation. Thus, I next examined the effects of AMPAR activation in the absence of presynaptic cells, using a 'nerve-adherent-bouton' preparation (Akaike and Moorhouse, 2003).

3.3.7 | AMPA and CNQX increase mIPSC frequency in dissociated Purkinje cells

Purkinje cells were mechanically dissociated from acute cerebellar slices using a fire polished pipette attached to a loudspeaker cone that was vibrated at a frequency where the pipette tip resonated in an elliptical pattern (section 2.3). This enzyme-free mechanical dissociation isolates and maintains viable cell somata which lack the majority of their dendritic and axonal process, but still posses functional adherent synaptic boutons (Figure 3.11 *A*), which spontaneously release GABA (Figure 3.11 *B*). The preparation avoids complications arising from synaptically connected cells and from possible changes in protein distribution and/or function as a result of enzyme treatment or *in vitro* culture. Although only used by a few laboratories, by eliminating the influence of presynaptic cell somatodendritic compartments on release probability, the method allows for greater accuracy when investigating how processes at presynaptic sites modulate synaptic transmission (Akaike and Moorhouse, 2003).

Purkinje cells were mechanically dissociated from P10-14 wild-type acute cerebellar slices and identified by their large soma and characteristic remains of the apical dendrite (Figure 3.11 *A*). In the presence of TTX, all cells displayed mIPSCs, with a mean peak amplitude (at –70 mV) of –262 ± 28 pA and 37% decay time of 6.6 ± 0.7 ms (Figure 3.11 *B*; n = 16). Consistent with the absence of the dendritic tree, the mean mIPSC frequency (0.6 ± 0.1 Hz) was less than that seen in Purkinje cells in acute slices (3.6 ± 2.4 Hz, n = 73). Application of AMPA (2 μM) or CNQX (40 μM plus 50 μM cyclothiazide) significantly increased mIPSC frequency (Figure 3.11 *C*-*E*; normalised frequency 2.50 ± 0.39 and 1.57 ± 0.11, respectively; n = 9 and 7; P = 0.004 and 0.016). In the absence of MLI somata,

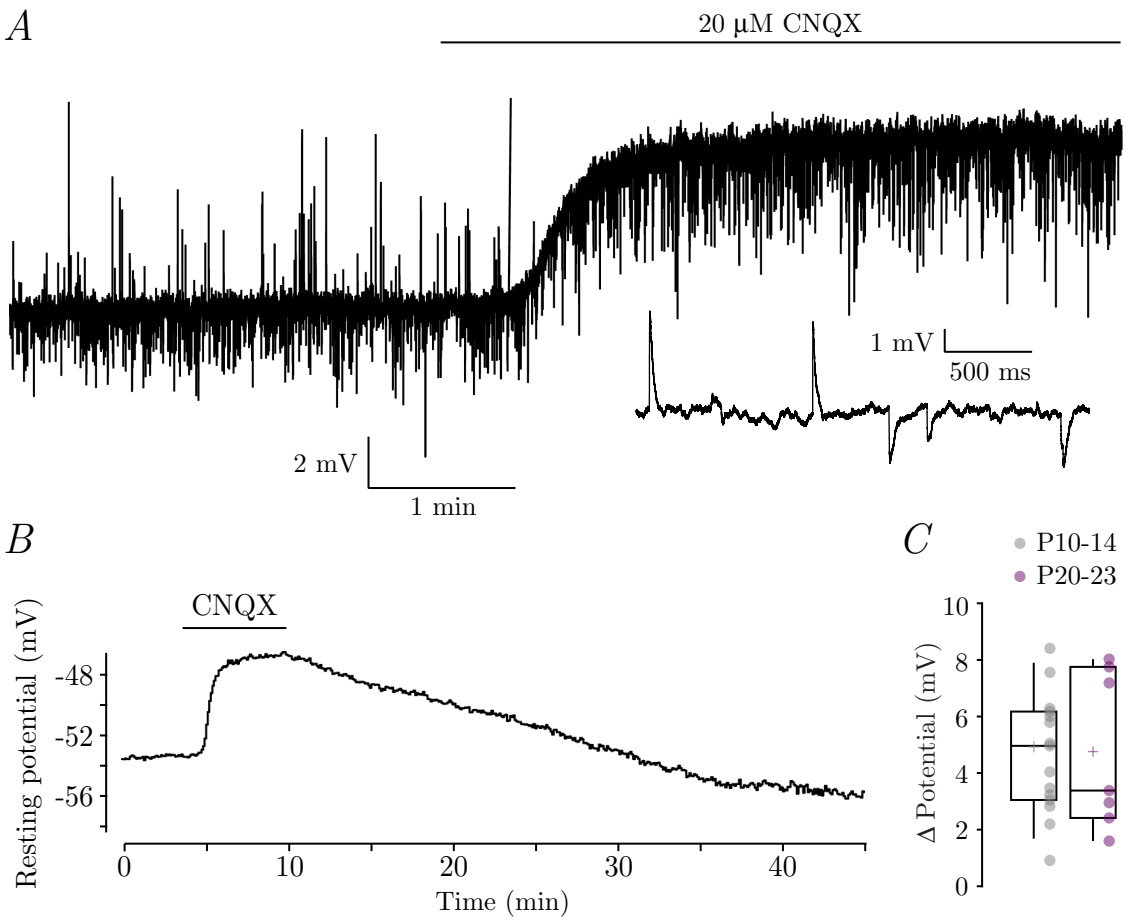

Figure 3.10: CNQX causes equivalent somatic depolarisation in P10-14 and P20-23 MLIs.

(*A*) Representative record of membrane voltage from a P14 wild-type MLI, downward deflections are inhibitory postsynaptic potentials, and upward deflections are excitatory postsynaptic potentials (revealed more clearly in the inset). Upon application of CNQX, a depolarisation and suppression of excitatory postsynaptic currents was observed. (*B*) Plot of resting membrane potential (from *A*) calculated using an all point histogram for each 4 s division of the voltage record. CNQX produced a 6.3 mV depolarisation that reversed upon washout. (*C*) Pooled data from P10-14 and P20-23 wild-type animals. Box-and-whisker plots indicate the median (line), the 25-75$^{\text{th}}$ percentiles (box) and the 10-90$^{\text{th}}$ percentiles (whiskers); filled circles and crosses represent individual and mean values, respectively.

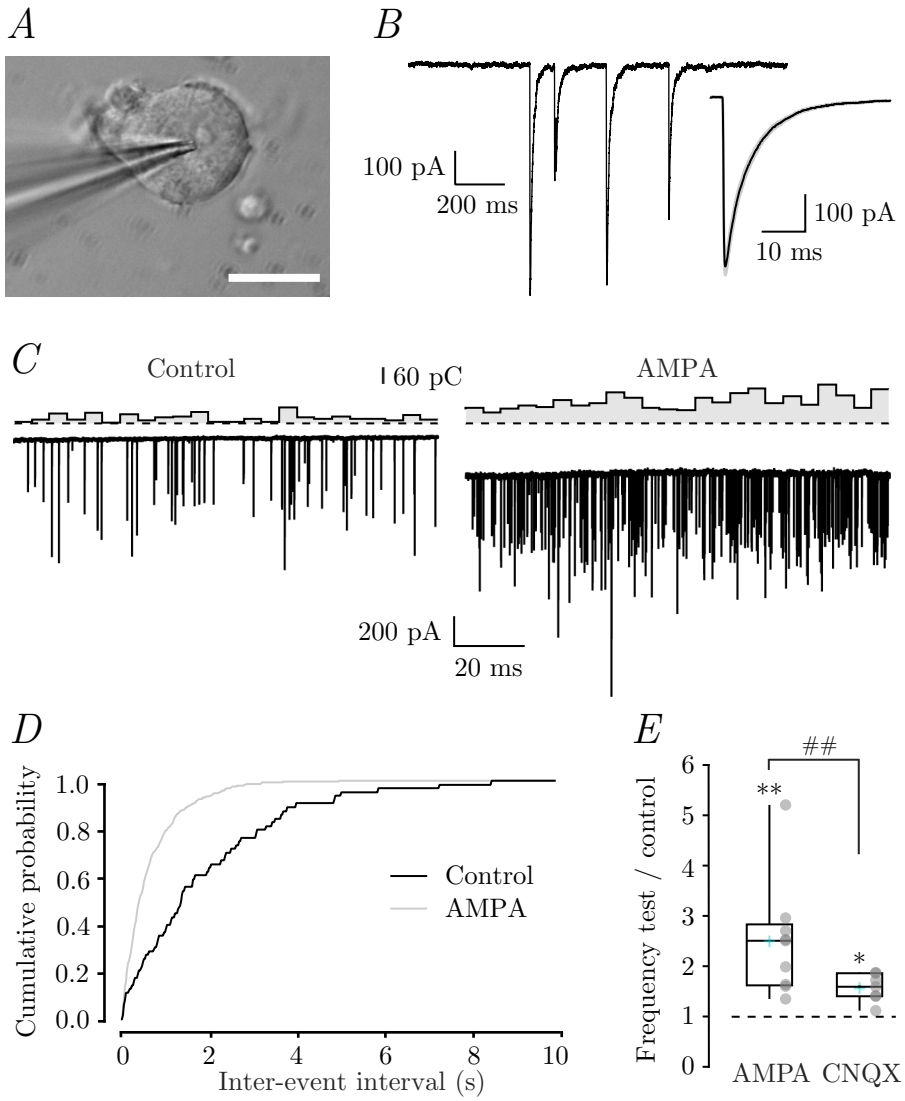

Figure 3.11: Activation of AMPARs increases mIPSC frequency in mechanically dissociated Purkinje cells with adherent nerve boutons.

(*A*) Image of an acutely dissociated cell, illustrating the large soma and truncated proximal dendritic tree. Scale bar 20 μm. (*B*) Representative current record from a Purkinje cell dissociated from a P11 wild-type mouse with typical mIPSCs, inset shows average waveform from 48 mIPSCs recorded under control conditions; shaded areas denote SEM. (*C*) mIPSCs (and corresponding phasic charge measurements) obtained before and during application of 2 μM AMPA (same cell as *B*). (*D*) Cumulative probability histogram shows a clear decrease in the inter-event interval in AMPA (same cell as *B*; $n = 63$ and 466 mIPSCs). (*E*) Pooled data shows that both AMPA (2 μM) and CNQX (40 μM plus 50 μM cyclothiazide) significantly increased mIPSC frequency. * $P < 0.05$, ** $P < 0.01$ (Wilcoxon signed-rank test versus one). ## $P < 0.01$ (Mann- Whitney U-test). Box-and-whisker plots indicate the median (line), the 25-75$^{\text{th}}$ percentiles (box) and the 10-90$^{\text{th}}$ percentiles (whiskers); circles and crosses represent individual and mean values, respectively.

dendrites and most of the axons, the effects of AMPA and CNQX on mIPSC frequency can only result from the activation of presynaptic AMPARs.

In acute cerebellar slices from *stg/stg* mice, application of AMPA increased mIPSC frequency in Purkinje cells and MLIs (Figure 3.6). As discussed, one implication of this result is that a population of presynaptic AMPARs may function without γ-2. However, this is inconsistent with the lack of effect of AMPA on pre-mIPSC frequency in *stg/stg* MLIs. Conceivably, AMPA may have produced a larger somatodendirtic membrane depolarisation than CNQX (Figure 3.10) that could have passively spread to MLI axon terminals to enhance release. To determine whether presynaptic AMPARs can in fact function without γ-2, I examined the effect of AMPA on mIPSC frequency in acutely dissociated Purkinje cells from *stg/stg* mice. 2 μM AMPA had no effect on mIPSC frequency (0.85 ± 0.09 normalised to control, $n = 11$, $P = 0.12$, Wilcoxon matched-pairs test) (Figure 3.12), this was significantly different from the AMPA effect in dissociated Purkinje cells from wild-type animals; $P = 0.000060$, Mann-Whitney U-test following a Kruskal-Wallis test; $\chi^2(5) = 23.39$, $P = 0.00028$ (Table 2.1). Thus, in agreement with pre-mIPSC data, without γ-2-association, presynaptic AMPARs are unable to modulate GABA release from MLIs. The residual effect of AMPA in acute slice recordings from *stg/stg* mice may have resulted from the passive spread of depolarisation following activation of somatodendritic AMPARs.

3.3.8 | Presynaptic kainate receptors do not contribute to AMPA-induced changes in mIPSC frequency

AMPA activates kainate receptors as well as AMPARs. Previous studies have suggested that the effects of domoate or AMPA were exclusively mediated by AMPARs, as the effects were blocked by 50 μM (Bureau and Mulle, 1998) and 40 μM (Rossi et al., 2008) GYKI 53655, respectively. Subsequently, it has been shown that GYKI 53655 also blocks responses from GluK3 homomers with an IC50 of ∼ 60 μM (Perrais et al., 2009). As MLIs express GluK3 (Wisden and Seeburg, 1993), the effects of GYKI 53655 could have revealed a combination of presynaptic AMPA and kainate receptor block, rather than an exclusive AMPAR-mediated effect. To test the contribution of presynaptic kainate

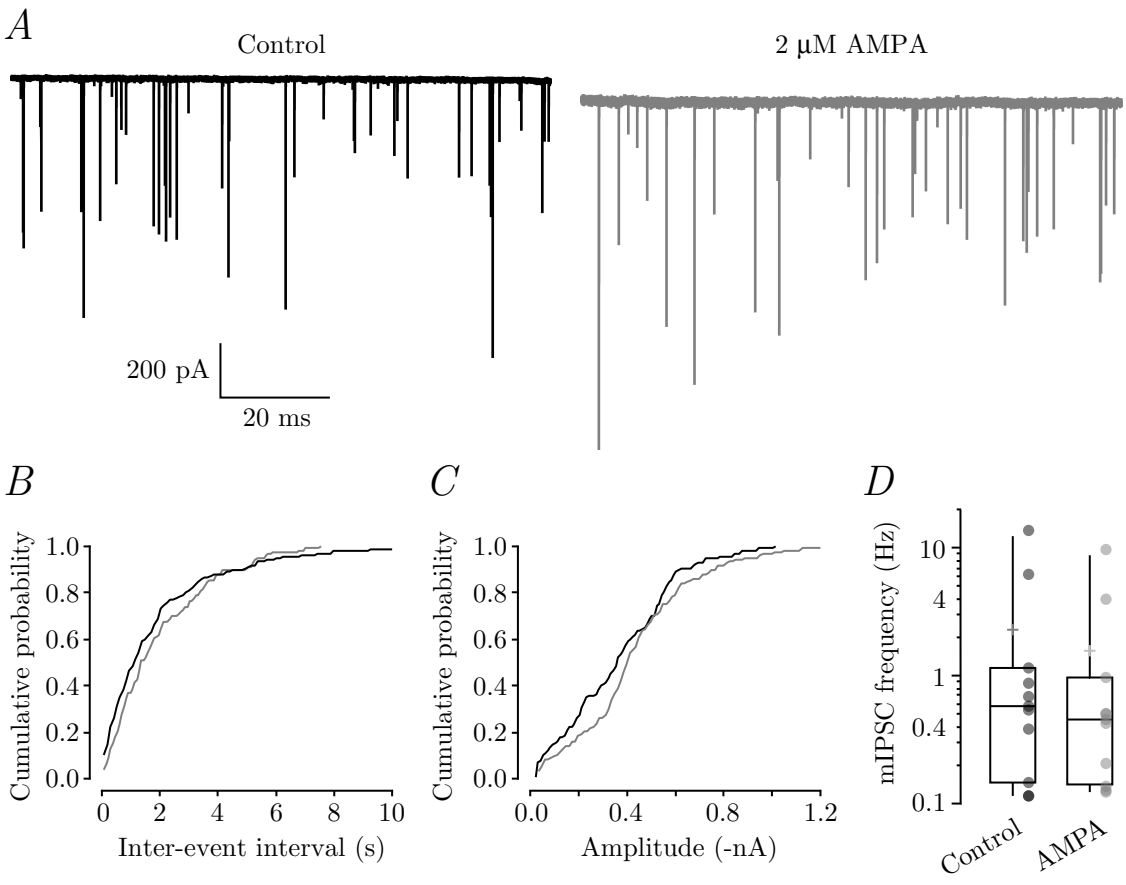

Figure 3.12: AMPA fails to alter mIPSC frequency in dissociated *stg/stg* Purkinje cells.

(*A*) Sample current record from a P12 *stg/stg* mouse in the absence (left, black) and presence (right, grey) of 2μM AMPA. (*B* & *C*) Cumulative probability histograms from a representative P12 dissociated Purkinje cell show no difference in inter-mIPSC interval or mIPSC amplitude following AMPA treatment. (*D*) Pooled data shows that AMPA (2 μM) had no effect on mIPSC frequency in mechanically dissociated *stg/stg* Purkinje cells. Box-and-whisker plots indicate the median (line), the 25-75$^{\text{th}}$ percentiles (box) and the 10-90$^{\text{th}}$ percentiles (whiskers); circles and crosses represent individual and mean values, respectively.

receptors to the AMPA-induced effects on spontaneous release I examined the effect of AMPA on mIPSC frequency from acutely dissociated Purkinje cells from wild-type mice in the presence of GYKI 52466 (40 μM), which has relatively weak effects on kainate receptors at 100 μM concentrations (Bleakman et al., 1996). In these recordings, mIPSC frequency was unaltered following application of 2 μM AMPA (0.89 $\pm$ 0.11, $n = 6$. $P = 0.69$, Wilcoxon matched-pairs test) (Figure 3.13). As mentioned, the difference between groups measuring the effect of AMPA on normalised mIPSC frequency recorded from dissociated Purkinje cells was significant ($\chi^2(5) = 23.39$, $P = 0.00028$; Kruskal-Wallis test) (Table 2.1). A *Post hoc* Mann-Whitney U-test revealed the effect of AMPA in the presence of GYKI 52466 was significant from AMPA treatment alone; $P = 0.0016$.

3.4 | Discussion

This chapter establishes a role for TARP γ-2 in the regulation of presynaptic AMPARs at MLI axonal boutons which contact Purkinje cells and other MLIs. This was apparent from the TARP-dependent actions of CNQX on mIPSC frequency and phasic charge. The requirement of γ-2 for effective AMPAR modulation of GABAergic quantal transmission was confirmed by the markedly attenuated response to AMPA in recordings from *stg/stg* mice. The actions of CNQX and AMPA were reproducible in mechanically dissociated cells, demonstrating that they arose from direct activation of TARPed presynaptic AMPARs.

3.4.1 | The relative influence of axonal and somatodendritic AMPARs

It can be rather challenging to interpret measures of mIPSC frequency, in that changes in release probability do not necessarily reflect causal processes occurring at presynaptic sites. Depolarisation originating in the somatodendritic compartment of MLIs can passively propagate into axonal compartments (Glitsch and Marty, 1999; Shu et al., 2006; Alle and Geiger, 2006; Mejia-Gervacio et al., 2007). Recently, it was found in MLIs that such sub-threshold somatodendritic events are sufficient to activate axonal VGCCs,

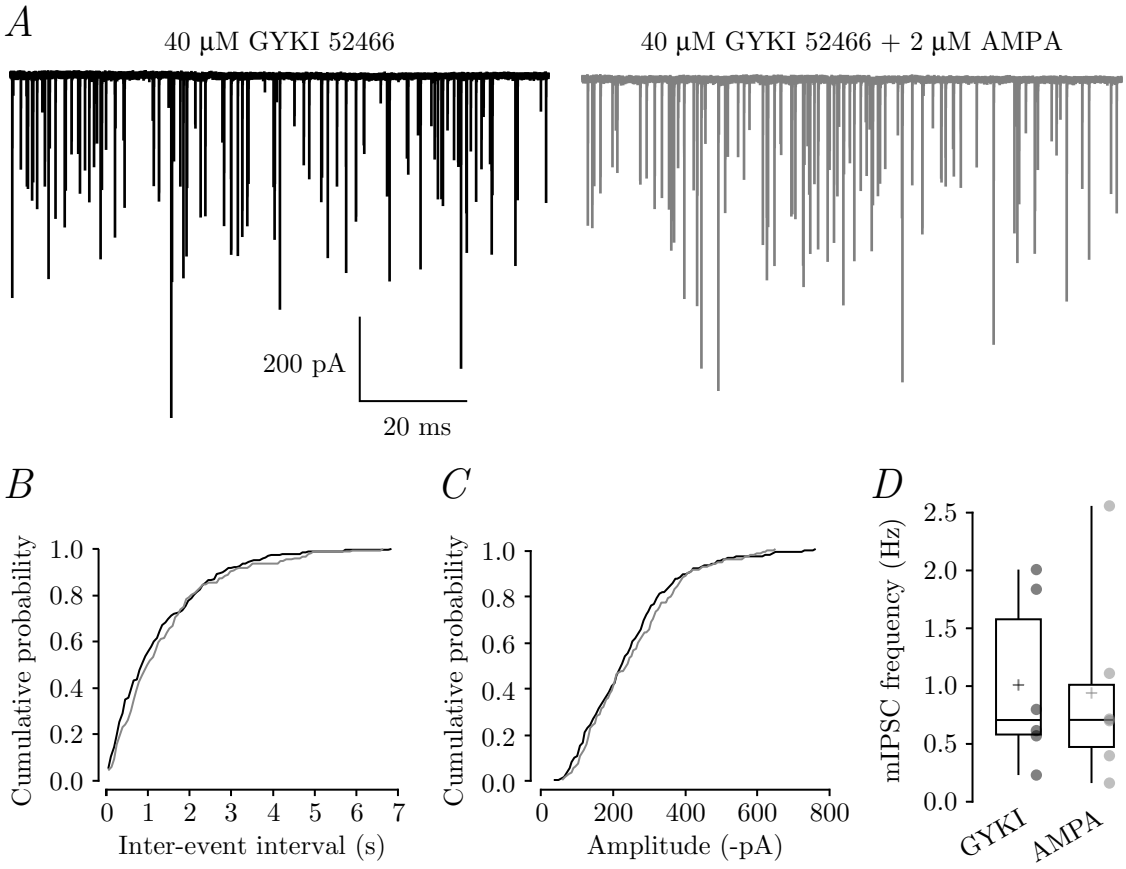

Figure 3.13: GYKI 52466 completely blocks AMPA-induced increase in mIPSC frequency.

(*A*) Recording from a P14 wild-type acutely dissociated Purkinje cell incubated in 40 μM GYKI 52466 before (left, black) and after (right, grey) application of 2 μM AMPA (*B* & *C*) Cumulative probability histograms from the same cell as in *A* show that, in the presence of GYKI 52466, AMPA produced no difference in inter-mIPSC interval or mIPSC amplitude. (*D*) Pooled data shows that both AMPA (2 μM) had no effect on mIPSC frequency from mechanically dissociated Purkinje cells. Box-and-whisker plots indicate the median (line), the 25-75$^{\text{th}}$ percentiles (box) and the 10-90$^{\text{th}}$ percentiles (whiskers); circles and crosses represent individual and mean values, respectively.

	mIPSC Frequency (Hz)											
	Molecular layer interneurons				Purkinje cells *				Dissociated Purkinje cells *			
	n	Control	Treatment (normalised)	*P*	*n*	Control	Treatment (normalised)	*P*	*n*	Control	Treatment (normalised)	*P*
P10-14 Wt												
CNQX	11	0.54 ± 0.15	2.66 ± 0.73 7.46 ± 2.93	0.00097 0.00097	11	5.43 ± 0.90	13.68 ± 2.97 2.48 ± 0.23	0.00098 0.00098	7	0.49 ± 0.17	0.80 ± 0.32 1.57 ± 0.10	0.016 0.016
AMPA	9	0.81 ± 0.18	11.30 ± 1.65 16.76 ± 2.67	0.0039 0.0039	10	3.49 ± 0.45	28.70 ± 3.32 10.77 ± 2.61	0.0020 0.0020	9	0.62 ± 0.09	1.64 ± 0.37 2.50 ± 0.39	0.0039 0.0039
+ GYKI									6	1.01 ± 0.30	0.94 ± 0.35 0.89 ± 0.11	0.69 0.31
NBQX	4	0.45 ± 0.04	0.48 ± 0.05 1.08 ± 0.11	0.63 0.63								
P10-14 stg/stg												
CNQX	7	0.63 ± 0.23	0.64 ± 0.25 0.96 ± 0.10	0.81 1.00	5	2.27 ± 0.69	2.15 ± 0.61 0.98 ± 0.09	0.44 0.81				
AMPA	14	0.51 ± 0.14	1.03 ± 0.32 2.03 ± 0.39	0.00086 0.004	10	3.31 ± 0.59	5.45 ± 0.90 1.76 ± 0.24	0.0020 0.0020	11	2.25 ± 1.28	1.56 ± 0.88 0.85 ± 0.09	0.12 0.12
P20-23 Wt												
CNQX	9	1.24 ± 0.34	1.22 ± 0.31 1.00 ± 0.05	0.73 0.82	13	2.76 ± 0.28	2.54 ± 0.32 0.91 ± 0.04	0.13 0.094				

Table 3.1: Collated measures of mIPSC frequency.

Raw values were compared using a two-sample Wilcoxon matched-pairs test; normalised values (below raw values in treatment) were compared against 1 using a one-sample Wilcoxon signed-rank test. P values < 0.05 are shown in red. * In recordings from Purkinje cells and dissociated Purkinje cells, 50 μM cyclothiazide was applied during experiments where CNQX was added.

causing Ca^{2+} influx that potentiates both action potential-evoked release, and spontaneous transmitter release, recorded in the presence of TTX (Christie et al., 2011). Thus, in the current experiments, the observations involving modulation of release probability could have two conceivable origins; either the activation of AMPARs at presynaptic sites provided local depolarisation to enhance release probability, or AMPARs were activated at somatodendritic locations, and the subsequent depolarisation spread to presynaptic boutons to enhance release. It is also possible that a mixture of the two effects was responsible for the increase in mIPSC frequency. Indeed, dendritic NMDAR-induced depolarisation has been used to discredit the previous finding that presynaptic NMDARs modulate GABA release from MLI boutons (Christie and Jahr, 2008; Glitsch and Marty, 1999), though see Rossi et al. (2012) for evidence of axonal NMDAR-mediated Ca^{2+} transients. Nevertheless, as explained below, a number of observations have led me to the conclusion that the increase in mIPSC frequency was predominantly mediated by γ-2 associated AMPARs located at the axon, close to sites of GABA release.

Firstly, direct evidence for the presence of axonal AMPARs on basket cells was provided by Rusakov et al. (2005) who show that local application of AMPA onto a basket cell axon reduces the Ca^{2+} signal resulting from evoked action potentials. In addition, AMPAR-mediated currents have been recorded from cultured cerebellar GABAergic axonal boutons (Fiszman et al., 2007). It is difficult to imagine that such AMPARs would not modulate spontaneous release in my experiments. Moreover, I found that both AMPA and CNQX elicited an increase in mIPSC frequency from mechanically dissociated Purkinje cells. This reduced system effectively separates functional axon terminals from the rest of the MLI. By abolishing the possibility of active or passive depolarisations originating from the somatodendritic compartment, this preparation provides ideal conditions for investigation of processes that occur at the presynaptic terminal. Thus, this approach confirmed results from acute slices and established that the increase in Purkinje cell mIPSC frequency involves the activation of AMPARs located at MLI axon terminals. It could be argued that AMPA or CNQX could have depolarised the Purkinje cell which in turn may have affected mIPSC frequency via release of some putative retrograde messenger, though this seems unlikely due to the excellent space-clamp achieved in these

Purkinje cells which lack a dendritic tree. Whilst this experiment provided positive confirmation of presynaptic TARP-associated AMPARs at MLI – Purkinje cell synapses, no correspondingly direct evidence was gathered for MLI – MLI synapses. However, if one assumes that in slice recordings pre-mIPSCs arose from presynaptic $GABA_A$Rs present at both MLI – MLI and MLI – Purkinje cell contacts, then the increase in pre-mIPSC frequency following presynaptic AMPAR activation would have similarly occurred without AMPAR-induced somatodendritic depolarisation, given the somatic voltage-clamp in these recordings.

Though I have established a role for γ-2-associated AMPARs at MLI presynaptic sites in modulating spontaneous GABA release, I have not excluded the possibility that in acute slice recordings, activation of somatodendritic AMPARs, following bath application of AMPAR agonists, contributed to the increased release probability through passive depolarisation. According to paired MLI recordings conducted by Christie et al. (2011), a 10 mV depolarisation of the presynaptic cell had no significant effect on mIPSC frequency recorded from the postsynaptic cell. The < 5 mV mean depolarisation I observed in response to 20 μM CNQX in P10-14 mice falls short of the required MLI depolarisation, but a larger depolarisation could have been attained following application of 1 μM AMPA. In experiments where the potential influence of somatodendritic depolarisation was removed, i.e. pre-mIPSC frequency data in acute slices and mIPSC frequency data in dissociated Purkinje cells, the relative increase in mIPSC frequency was less than that observed for total mIPSC frequency in acute slices. One might speculate that the smaller effect on pre-IPSC frequency may have reflected a relative insensitivity of axonal $GABA_A$Rs compared to postsynaptic $GABA_A$Rs, perhaps due to a lower receptor number. For the dissociated Purkinje cell experiment, a reduced number of MLI boutons, or axonal boutons damaged during the dissociation may account for the smaller increase in mIPSC frequency than that observed in acute slices. Alternatively, the relatively small increase in mIPSC frequency in these experiments could have reflected the absence of somatodendritic AMPARs.

Previous studies that have described the effect of CNQX on mIPSC frequency in other neurons provide some indirect insight into the likely contribution of somatodendritic depolarisation on release probability. From cerebellar granule cell recordings, Brickley et al.

(2001) reported that CNQX increased the frequency of spontaneous $GABA_AR$-mediated IPSCs, but did not affect mIPSC frequency. One could hypothesise that the increase in sIPSC frequency was mediated by CNQX activity at somatodenditic TARP-associated AMPARs which increased cell firing. However, following TTX block of Na^+ channels, CNQX was incapable of increasing mIPSC frequency suggesting an absence of presynaptic AMPARs within Golgi cell axons that contact granule cells. Furthermore, the lack of change in mIPSC frequency suggests that the sub-threshold depolarisation resulting from somatodendritic AMPAR activation in Golgi cells was insufficient to modulate release probability (note a lower concentration of CNQX was used in this study to that used here). As MLIs and Golgi cells have similar axonal morphologies (Barmack and Yakhnitsa, 2008) and indistinguishable electrophysiological properties; input resistance, resting membrane potential, spiking threshold and spiking frequency (Midtgaard, 1992), it could be argued that in MLIs, the CNQX-induced somatodendritic sub-threshold depolarisation would similarly produce negligible effects on release probability. Thus, the effect of CNQX on mIPSC frequency in MLIs but not Golgi cells was likely to be exclusively due to a differential expression of presynaptic AMPARs. The absence of presynaptic AMPARs, and the inability of sub-threshold depolarisation to modulate release probability may explain similar observations from CA1 interneurons in the hippocampus (Maccaferri and Dingledine, 2002).

3.4.2 | The role of TARP family members in the regulation of presynaptic AMPARs

On the basis of the recent reclassification of CNQX as an AMPAR partial agonist I was able to provide insight into the role for the TARP γ-2. Only AMPARs associated with γ-2, -3, -4 and -8 are capable of gating in response to CNQX (Menuz et al., 2007; Bats et al., 2012). Since MLIs express TARPs γ-2 and -7 possibly with low levels of γ-3 and -4 (Fukaya et al., 2005; Yamazaki et al., 2010), γ-2 became the most likely candidate. This speculation was confirmed, when the experiments were repeated in *stg/stg* animals, where CNQX effects were absent.

In addition to γ-2, MLIs express the atypical TARP γ-7 (Jackson and Nicoll, 2011a; Bats

et al., 2012). As the AMPA-induced increase in mIPSC frequency was not completely abolished in acute slice recordings, it was possible that a population of presynaptic AMPARs functioned without γ-2. In the *stg/stg* mouse it has previously been shown that extrasynaptic AMPARs can function through association with γ-7 (Jackson and Nicoll, 2011a; Bats et al., 2012) and AMPARs at the PSD can function when TARPless (Bats et al., 2012). At presynaptic sites, neither scenario seems to occur. In contrast to acute slice recordings of total mIPSC frequency, there was no increase in pre-mIPSC frequency following treatment of AMPA in *stg/stg* MLIs, nor was there any change in mIPSC frequency in *stg/stg* mechanically dissociated Purkinke cells. Both observations suggest that presynaptic AMPARs are unable to modulate spontaneous GABA release in the absence of γ-2. A possible explanation for the discrepancy in the data from acute slice recordings of total mIPSC frequency may involve the unresolved influence of somatodendirtic AMPARs. The remaining increase in mIPSC frequency following AMPA treatment in *stg/stg* acute slice recordings could have resulted from sub-threshold depolarisation, which was absent in both the pre-mIPSC and dissociated Purkinje cell measurements. The influence of TARP-association on presynaptic AMPAR function and trafficking will be discussed in greater detail in section 6.1.

3.4.3 | Target dependent, inter-bouton, differences in CNQX sensitivity

In the absence of the AMPAR channel potentiator cyclothiazide, CNQX enhanced mIPSC frequency at MLI – MLI, but not MLI – Purkinje cell synapses. A differential ability of CNQX to evoke responses has been described in the hippocampus, where CNQX depolarised stratum radiatum interneurons, but not CA1 pyramidal neurons, to firing threshold (Maccaferri and Dingledine, 2002). Indeed, unlike this situation in CA1 interneurons, CNQX produced a whole-cell current in pyramidal cells only when the cells were treated with the AMPA channel potentiatior trichloromethiazide (Menuz et al., 2007). Importantly, AMPAR potentiators do not simply reveal a response to CNQX in all cells. For example, Lee et al. (2010b) demonstrate that, unlike thalamic reticular nucleus relay neurons, AMPARs in ventrobasal thalamic relay neurons do not respond to

CNQX even in the presence of trichloromethiazide.

Reasons for the differences in sensitivity to CNQX between cells (Lee et al., 2010b; Maccaferri and Dingledine, 2002; Menuz et al., 2007), and here between axonal boutons, are unresolved. Lee et al. (2010b) suggested differences in AMPAR subunit expression may play a role. Indeed, in the cerebellum, whilst AMPARs at MLI – Purkinje cell axonal boutons are thought to contain the GluA2 subunit, AMPARs at MLI – MLI axonal boutons do not (Rossi et al., 2008; Satake et al., 2006) (Figure 5.5). In heterologous systems, ultrafast application of CNQX produced currents with equivalent CNQX-to-glutamate ratios (for peak amplitude) when GluA1, 3 or 4 were co-expressed with γ-2 (Bats et al., 2012). However, the efficacy of CNQX at γ-2-associated GluA2-containing receptors has not been tested. For arguments sake, if CNQX were to elicit a relatively weak response at homomeric GluA2 AMPARs, CNQX could preferentially activate CP-AMPARs. Indeed, this theory could explain the aforementioned observations by Maccaferri and Dingledine (2002) and Menuz et al. (2007) in the hippocampus. Studies have found 90-92% of synaptic AMPARs (Lu et al., 2009; Rozov et al., 2012) and a majority of extrasynaptic AMPARs (Colquhoun et al., 1992) in CA1 pyramidal neurons contain GluA2, whereas CA1 interneurons have a greater proportion of GluA2-lacking AMPARs (Szabo et al., 2012). However, data from cerebellar Golgi cells does not support a reduced efficacy of CNQX at GluA2-containing AMPARs. Golgi cells are thought to contain only GluA2 and 3 subunits (Coombs and Cull-Candy, 2009), consistent with a linear current-voltage relationship of mEPSC amplitude (Menuz et al., 2008). In contrast to hippocampal pyramidal cells, CNQX produced a marked increase in Golgi cell firing (Brickley et al., 2001). Though a potential difference in regulation of AMPAR subunits by γ-2 has not been tested, the ability of TARPs to differentially regulate CP- and CI-AMPARs is not without precedent. Recently, Studniarczyk et al. (2013) suggest γ-7 reduced the expression of CI-AMPARs at synaptic sites, yet its association with CP-AMPARs increased their number at the PSD.

Besides differences in subunits, variation in AMPAR subunit splicing may underlie the target-dependent heterogeneity in CNQX sensitivity. Menuz et al. (2007) speculated that the limited efficacy of CNQX to evoke a whole-cell current in hippocampal pyramidal

cells compared to cerebellar Golgi cells may have arisen due to the expression of the flip AMPAR subunit splice variant. However, their assertion that this was because the flip variant desensitises more quickly than flop seems erroneous (Mosbacher et al., 1994). Rather, given information on the relative steady-state current remaining following desensitisation of GluA1/2 heteromers, it seems more plausible that when associated with γ-2, flip AMPAR variants would pass greater charge than γ-2-associated flop AMPAR variants (Turetsky et al., 2005).

Considering the similar dependence on γ-2 of the AMPAR-mediated modulation of GABA release at both MLI – MLI and MLI – Purkinje cell boutons, a differential presence of TARPs is unlikely to explain the heterogenous response to CNQX. However, additional influences of untested auxiliary proteins cannot be ruled out (Schwenk et al., 2009, 2012). This will be discussed in greater detail in section 6.3. In conclusion, though I cannot be certain of the underlying cause of differences in CNQX efficacy, the increase in mIPSC frequency recorded in both Purkinje cells and MLIs suggest that presynaptic AMPARs are associated with TARPs at both synapses. Given the absent effects in *stg/stg* mice, I propose that the TARP γ-2 associates with presynaptic AMPARs and is absolutely required for their modulation of spontaneous GABA release.

4 | Presynaptic AMPAR-mediated modulation of action potential-driven GABA release is dependent on TARP γ-2

4.1 | Summary

To examine the potential physiological relevance of the results presented in chapter 3, I next sought to determine if γ-2 is required for the modulation of evoked GABA release by presynaptic AMPARs activated by synaptically released glutamate. Presynaptic AMPARs on cerebellar basket cell boutons are normally activated by glutamate spillover during climbing fibre activity. I found that repetitive climbing fibre stimulation reduced the amplitude of both extracellularly evoked and spontaneously occurring IPSCs recorded from Purkinje cells. This effect on evoked release was accompanied by an increase in paired pulse ratio and coefficient of variation. All effects were strongly attenuated in *stg/stg* mice.

To rule out the possibility that the reduced modulation of GABA release might result from defective glutamate release in *stg/stg* mice, climbing fibre stimulation was replaced with CNQX treatment. CNQX produced equivalent effects on IPSC amplitude and measures of release probability that were also abolished in *stg/stg* mice. Such effects were similarly observed in recordings from synaptically paired MLIs, suggesting that γ-2 regulation of evoked release had no target neuron-dependent differences. Such paired recordings also reduced concerns that inconsistencies associated with extracellular stimulation contributed to the climbing fibre- and CNQX-induced reduction of IPSC amplitude.

Finally, the effects of CNQX on evoked release were replicated in mechanically dissociated Purkinje cells. This reduced preparation provided strong confirmation that TARP-associated AMPARs were located in MLI axonal boutons, and ruled out the possibility that an increase in MLI firing was exclusively responsible for the reduction in GABA release probability. Together, these results extend those of the previous chapter and

establish that γ-2 associates with presynaptic AMPARs and is required for suppression of action potential-evoked GABA release.

4.2 | Introduction

I have established that γ-2 associates with presynaptic AMPARs thereby regulating the AMPAR agonist-induced changes in spontaneous quantal release (chapter 3). However, my results still leave open the contribution of γ-2 to AMPAR-mediated modulation of GABA release in response to synaptically released glutamate. Thus, I sought to determine the role of γ-2 in regulating release following endogenous activation of presynaptic AMPARs. Presynaptic AMPARs present at basket cell terminals are activated following repetitive (5-50 Hz) climbing fibre stimulation (Satake et al., 2000), where glutamate overwhelms the local glial EAAT1 and neuronal EAAT4 glutamate transporters and diffuses to basket cell terminals (Satake et al., 2006, 2010).

Measures of evoked IPSC amplitude can be used as a proxy for changes in release probability. To establish changes in amplitude represent a change in release probability, several criteria should be satisfied. Firstly, when a stimulus is directly followed by a second within a short time interval, either paired-pulse facilitation or paired-pulse depression can occur (Zucker and Regehr, 2002) (subsection 1.5.1). A difference in the PPR is thought to reflect the sum of the changes in release probability experienced at individual release sites onto the same postsynaptic cell. According to the residual Ca^{2+} hypothesis (Katz and Miledi, 1968), an increase in the PPR of successive postsynaptic responses would represent a greater number of release sites where release probability is reduced. This is because terminals which experience a decrease in release probability would accumulate relatively more residual Ca^{2+} to prime a greater number of vesicles for release in response to the second stimulus. As discussed in subsection 1.5.1, this may be explained through saturation of Ca^{2+} buffers (Blatow et al., 2003), or through the existence of an alternative, high-affinity, Ca^{2+} sensor (Atluri and Regehr, 1996). Following an increase in release probability, a decrease in the paired-pulse ratio would be expected. This is thought to mainly reflect a greater depletion of the readily releasable vesicles following the first stimulus, which leaves relatively fewer vesicles available for release following the second stimulus (Schneggenburger et al., 2002). Changes in PPR may alternatively be explained through the Ca^{2+}-mediated inactivation (Forsythe et al., 1998; Xu and Wu, 2005), or

activation (Ishikawa et al., 2005) of VGCCs. In addition, short-term depression may also occur as a result of postsynaptic receptor desensitisation (Kirischuk et al., 2002; Mennerick and Zorumski, 1995; Trussell et al., 1993).

Fluctuation analysis of postsynaptic response amplitude can provide information on the quantal parameters N (number of quanta available for release), p (release probability) and q (quantal size) (Clements and Silver, 2000; Silver et al., 1998; Scheuss et al., 2002). As described by Katz (1969) the average evoked EPSC peak amplitude (I) is given by equation 1.1:

$$I = Npq$$

From the first description of quantal theory (equation 3.1) we can calculate the average number of released vesicles (m):

$$m = Np = \frac{I}{q} \tag{4.1}$$

Assuming binomial statistics, the variance (σ^2) of amplitudes is obtained from:

$$\sigma^2 = Nq^2p(1-p) \tag{4.2}$$

Dividing σ^2 by I gives:

$$\frac{\sigma^2}{I} = q(1-p) \tag{4.3}$$

In order to compare between different neurons, a normalised measure of variance is required. The coefficient of variation (CV) is given as the standard deviation divided by the mean. By substituting I for Npq we get the formula:

$$CV^2 = \frac{\sigma^2}{\mu^2} = \frac{(1-p)}{Np} \tag{4.4}$$

According to this equation, any alteration in CV must occur through changes in presynaptic function (Faber and Korn, 1991; Malinow and Tsien, 1990). The problem with this

measure are the concerns over the validity of using classical binomial methods of quantal analysis at central synapses, where the number of release sites needs to remain constant (Kuno, 1971). As I have no way of controlling for changes in N, further measures of release probability may be required. It is possible to use the number of synaptic failures over a given time as a measure of changes in release probability. Allen and Stevens (1994) demonstrated that the failure of a stimulus to evoke a synaptic current was not due to changes in stimulation or impulse conduction failure, but result of the probabilistic nature of release mechanisms. This analysis can be complicated if the synaptic transmission is evoked from more than one presynaptic input, as a failure rate in one neuron could be masked by release from another. Thus, this analysis is only suitable for recordings where synaptic currents unambiguously originate from a single cell.

In comparison to the increased spontaneous release (Bureau and Mulle, 1998; Rossi et al., 2008) (Chapter 3), the activation of presynaptic AMPARs by both climbing fibre-release glutamate and exogenous AMPAR agonists, acts to reduce action potential-driven GABA release from basket cells (Satake et al., 2000; Rusakov et al., 2005). Divergent effects on the two forms of GABA release are not unique to presynaptic AMPARs on cerebellar basket cells, but are observed, for example with presynaptic NMDARs at the same MLI boutons (Glitsch and Marty, 1999), presynaptic AMPARs at GABAergic dorsal horn neurons in the spinal cord (Engelman et al., 2006), and kainate receptors at MF boutons in the CA3 region of the hippocampus (Contractor et al., 2000).

To investigate if TARP regulation further adds to the divergent regulation of evoked and spontaneous release, or whether, like quantal transmission, γ-2 is required for effective presynaptic AMPAR-mediated modulation of evoked release, I studied action potential-driven GABA release from MLIs in wild-type mice and *stg/stg* mice following either climbing fibre stimulation or application of CNQX.

4.3 | Results

4.3.1 | Evoked inhibitory currents in Purkinje cells

In voltage-clamp recordings from Purkinje cells, IPSCs were evoked by extracellular stimulation. An electrode placed in the lower third of the molecular layer (where basket cells reside) was repositioned until stimulation consistently gave rise to an outward synaptic current. In Purkinje cells, a high background activity of sIPSCs was typically observed with similar amplitudes to the evoked IPSCs (Figure 4.1 *A*). 15 individual responses to stimulation are overlaid in Figure 4.1 *B* to demonstrate the large range in evoked IPSC amplitude, and examples where extracellular stimulation failed to evoke an IPSC.

4.3.2 | Climbing fibre-induced inhibition of evoked IPSCs is reduced in *stg/stg* animals

High frequency activity of climbing fibres has been shown to attenuate the evoked release of GABA from MLIs onto Purkinje cells through the activation of AMPARs on MLI axons (Satake et al., 2000). To investigate the possible role of TARPs in the function of presynaptic AMPARs, I made voltage-clamp recordings from Purkinje cells and compared the effect of climbing fibre stimulation (Figure 4.3*A* & *B*; S1) on MLI-evoked IPSCs in slices from wild-type and *stg/stg* mice (Figure 4.3*A* & *B*; S2).

Climbing fibres were stimulated extracellularly by a pipette placed in the granule cell layer close to the voltage-clamped Purkinje cell (typically within 100 μm). Large EPSCs were evoked that exhibited paired-pulse depression (Figure 4.2 *A*). These features are characteristic of climbing fibre inputs (Silver et al., 1998). Given the position of the stimulation electrode, it was possible that parallel fibres contributed to the evoked EPSC. This appeared unlikely as no small amplitude EPSCs were seen at stimulation voltages just below the threshold required to evoke large currents (Figure 4.2 *B*). In addition, unlike the short term depression observed (Figure 4.2 *A*), parallel fibre – Purkinje cell synapses typically facilitate (Bergerot et al., 2013). Further evidence of the sole climbing fibre origin of the EPSC was provided by the all-or-nothing nature of the response with increasing

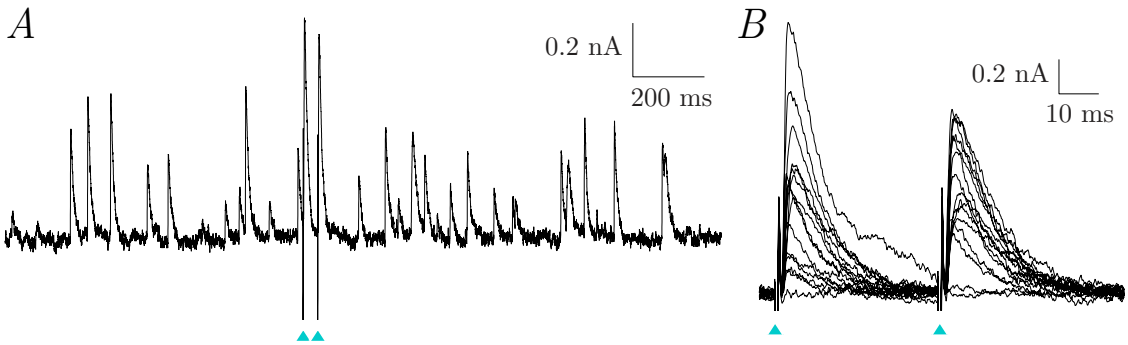

Figure 4.1: General features of inhibitory synaptic currents in Purkinje cell recordings (*A*) Slow time scale recording of spontaneous synaptic currents and a pair of synaptic currents evoked by extracellular stimulation (triangles; pulses of 10-40 V and 20 μs duration separated by 35 ms) in the lower molecular layer. (*B*) Fifteen superimposed traces on a faster time scale demonstrate the variety of responses to identical consecutive presynaptic stimulations (triangles). A trace where no synaptic response was obtained to either stimuli, and another where a response was obtained only following the first pulse, demonstrate the failures of transmission.

stimulation voltage, a characteristic of climbing fibre EPSCs (Figure 4.2 *C*). Alternatively, if parallel fibre transmission was involved, a graded increase in amplitude would have been expected , reflecting the increased recruitment of parallel fibres (Konnerth et al., 1990; Llano et al., 1991). Unlike in the adult, in young animals multiple climbing fibres can innervate Purkinje cells (Bosman and Konnerth, 2009). Thus, to ensure stimulation of only one climbing fibre, the response to increasing stimulation voltages was determined in every experiment.

To distinguish climbing fibre-mediated EPSCs (inward currents) from MLI-evoked IPSCs (outward currents), recordings were made at a holding potential of –30 mV. The amplitudes of 5 consecutive pairs of IPSCs were measured before and after climbing fibre stimulation (40 stimuli at 50 Hz) (Figure 4.3 *C*). In agreement with (Satake et al., 2000), I observed a pronounced reduction in the IPSC amplitude (from 1.00 ± 0.13 nA to 0.54 ± 0.07 nA, $n = 13$; $P = 0.00024$) (Figure 4.3 *C*,*D* & *E*). In slices from *stg*/*stg* mice the climbing fibre-induced suppression of IPSCs was not abolished but was markedly attenuated (Figure 4.3 *F* & *G*; 10.94 ± 0.32%, $P = 0.031$, $n = 6$; $P = 0.00088$ versus wild-type). This suggests that whilst effective AMPAR-mediated modulation of evoked GABA release is dependent on γ-2, a population of AMPARs may be able to function in the absence of this TARP.

4.3.3 | sIPSC amplitude is reduced following climbing fibre stimulation

Glutamate release from climbing fibres is likely to act at several MLI axonal boutons, even those that contact Purkinje cells which do not receive direct input from the stimulated climbing fibre (Coddington et al., 2013). Records of evoked IPSCs were typically accompanied by spontaneously occurring IPSCs (sIPSCs) (Figure 4.1 *A* and Figure 4.4 *A*). Such currents likely represented a mixture of spontaneous single vesicle fusion events (as observed in chapter 3), and GABA release resulting from spontaneous MLI firing, which can occur even in the absence of excitatory synaptic inputs (Häusser and Clark, 1997). At MLI – MLI synapses, Llano and Gerschenfeld (1993) showed in one experiment that 89% of IPSCs resulted from action potential driven release. Although here I am

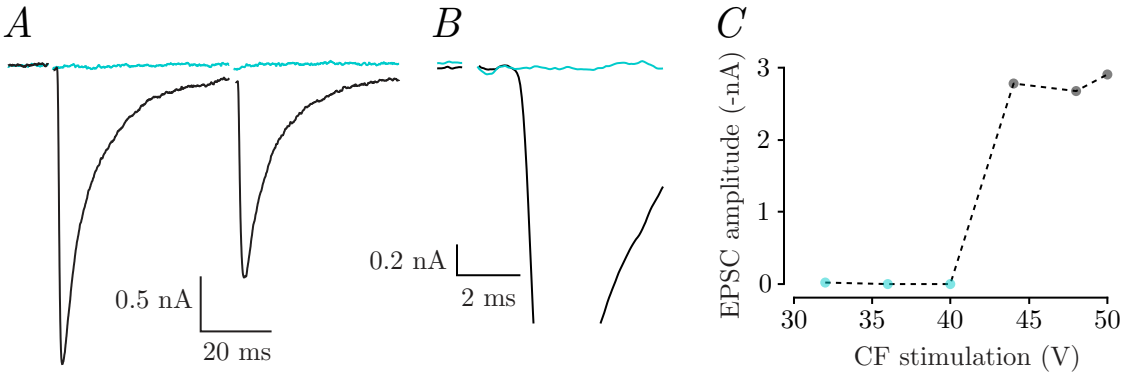

Figure 4.2: Characteristics of climbing fibre-evoked EPSCs in Purkinje cells from wild-type and *stg/stg* mice.

(*A*) Representative records of climbing fibre-evoked EPSCs recorded in a Purkinje cell from a wild-type mouse (P10). Failures (light blue) were seen with 40 V stimuli, while successes were seen with 44 V stimuli. The currents showed characteristic paired-pulse depression. (*B*) Evoked EPSC and failure seen just above and just below the stimulation threshold. The scale is enlarged to check that no parallel fibre responses were present. (*C*) Plot of peak amplitude shows all-or-nothing responses with increasing stimulus voltage.

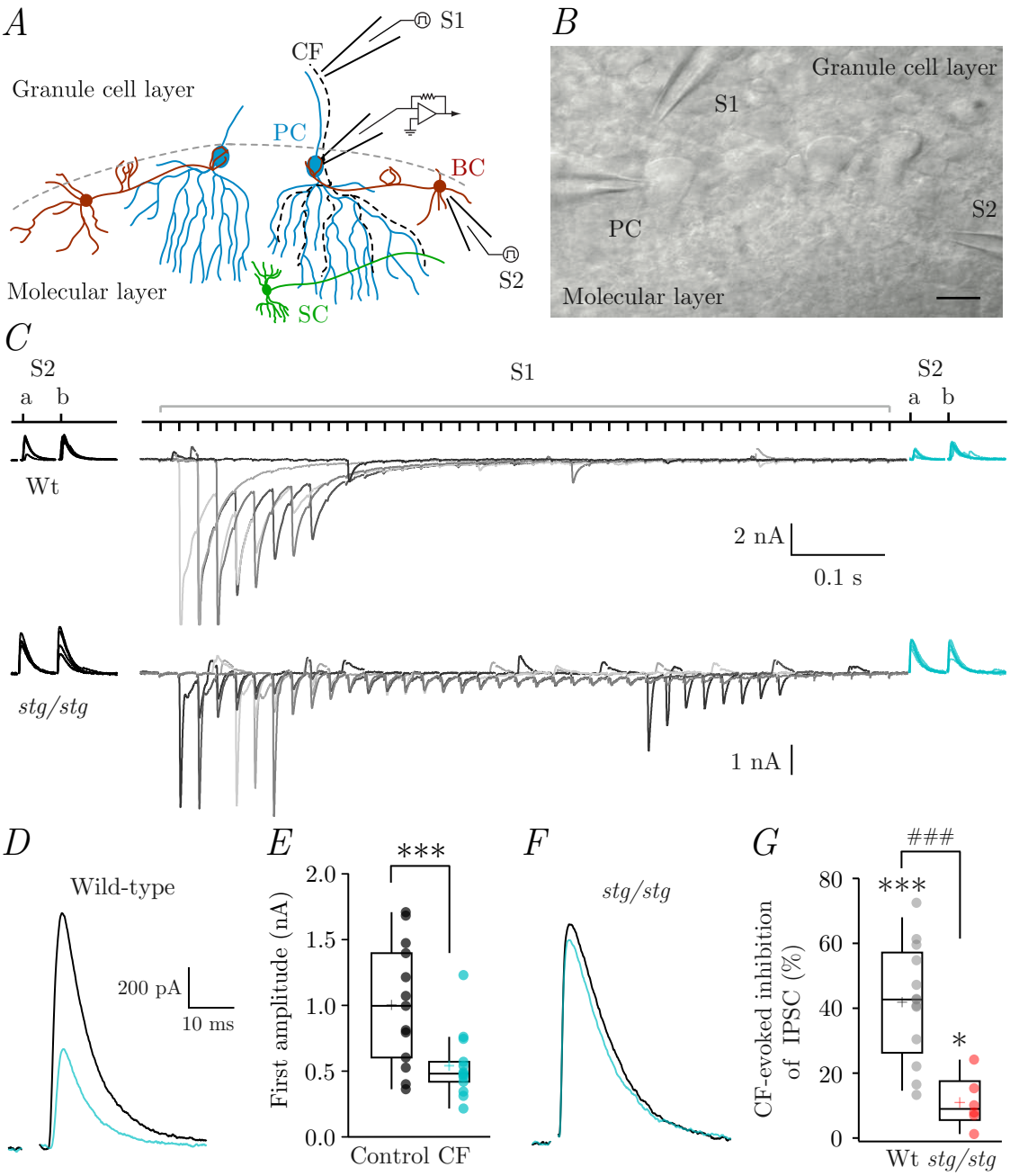

Figure 4.3: Climbing fibre stimulation-induced inhibition of evoked IPSCs is attenuated in Purkinje cells from *stg/stg* mice.

(*A* & *B*) Schematic drawing and bright field image of a sagital cerebellar slice (P11) showing the position of pipettes used for climbing fibre and MLI stimulation (S1, granule cell layer; S2, inner molecular layer). The recording electrode is seen on the soma of the Purkinje cell (PC). Scale bar 20 μm. (*C*) Representative currents from a Purkinje cell in a slice from a P11 wild-type mouse (top) and a P12 *stg/stg* mouse (below) showing IPSCs evoked by paired-pulse MLI stimulation, before (S2, i and ii; black) and after (S2, i and ii; blue) climbing fibre stimulation (S1; 40 stimuli at 50 Hz). The protocol was repeated 5 times and responses overlaid; climbing fibre-evoked EPSCs are shown as different shades of grey. (*D* & *F*) Representative averaged IPSCs are magnified

Figure 4.3 continued: from wild-type and *stg/stg* recordings shown in *C*. Trace identification and colouring as in *C*. (*E*) Pooled data showing IPSC amplitude before and after climbing fibre (CF) stimulation in wild-type mice. Box-and-whisker plots indicate the median (line), the 25-75$^{\text{th}}$ percentiles (box) and the 10-90$^{\text{th}}$ percentiles (whiskers); circles and crosses represent individual and mean values, respectively. *** $P < 0.001$ (Wilcoxon signed-rank test versus zero). (*G*) Pooled data showing the climbing fibre (CF)-induced inhibition of IPSC peak amplitude (calculated as 100-[S2 i post-CF/S2 i pre-CF]) in wild-type and *stg/stg* Purkinje cells. Box-and-whisker plots are as described in (*E*) *** $P < 0.001$, * $P < 0.05$ (Wilcoxon signed-rank test versus zero). ### $P < 0.001$, Wt versus *stg/stg* (Mann-Whitney *U*-test).

studying a different MLI synapse, it could be reasonably assumed that the majority of sIPSCs recorded from Purkinje cells reflect spontaneous MLI firing, and therefore, like the extracellularly evoked IPSCs (Figure 4.3), should display a reduction in amplitude following climbing fibre stimulation. To test this hypothesis I detected IPSCs with a sliding template matching algorithm (subsection 2.5.1) and removed those resulting from extracellular stimulation in the molecular layer (distinguished by the stimulation artefact). This analysis was performed in 6 of the 13 wild-type Purkinje cell recordings that had an appropriate length of recording between repeated climbing fibre stimulations. Continuous current records (Figure 4.4 *B*) and the corresponding cumulative probability plot of sIPSC amplitude (Figure 4.4 *C*) from a representative P11 wild-type Purkinje cell, show a reduction in sIPSC amplitude following climbing fibre stimulation. On average there was a significant reduction in sIPSC amplitude following climbing fibre stimulation (from 238.94 ± to 183.97 pA; Figure 4.4 *C*, $n = 6$, $P = 0.031$), with no change in sIPSC frequency (Figure 4.4 *D*; 1.43 ± 0.28 Hz in control and 2.30 ± 0.8 Hz following climbing fibre stimulation, $n = 6$, $P = 0.69$). In recordings from *stg/stg* mice there was no significant effect of climbing fibre stimulation on sIPSC amplitude (Figure 4.4 *D*; normalised ratio; 0.92 ± 0.05, $n = 6$, $P = 0.16$); however, this was not significantly different from the effect of climbing fibre stimulation on normalised sIPSC amplitude in wild-type mice ($P = 0.13$, Mann-Whitney *U*-test). In *stg/stg* mice, the absence of climbing fibre-induced suppression of sIPSC amplitude is in contrast to the suppression of extracellular evoked IPSCs (Figure 4.3 *F* & *G*). Thus, the earlier suggestion that a population of AMPARs can function in the absence of γ-2, albeit with a markedly reduced effect on release probability, is not supported by the sIPSC amplitude data.

4.3.4 | Climbing fibre stimulation reduced measures of MLI release probability

In wild-type animals the reduction in evoked IPSC amplitude was accompanied by a 1.65 ± 0.041 fold increase in the PPR (Figure 4.5 *AB* & *C*; $n = 13$, $P = 0.00024$; Wilcoxon matched-pairs test). In *stg/stg* animals there was no significant change in the PPR of evoked IPSCs (Figure 4.5 *B* & *C*; normalised values; 1.00 ± 0.05, $n = 6$, $P = 1.00$), which

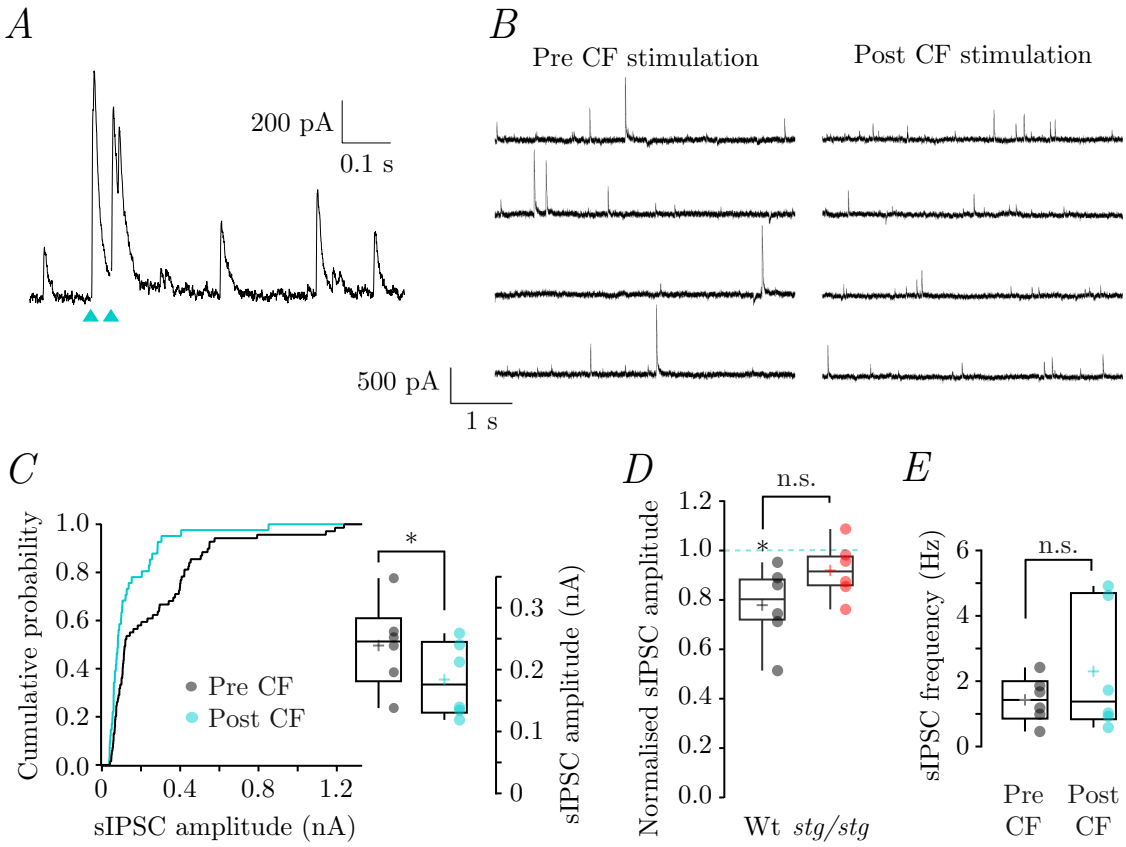

Figure 4.4: The amplitude of spontaneous IPSCs decreased after repetitive climbing-fibre stimulation

(*A*) A recording of evoked IPSCs with background spontaneous IPSC activity. Blue arrow heads indicate IPSCs evoked by extracellular stimulation. (*B*) sIPSCs recorded from a representative Purkinje cell showed a decreased amplitude but unaltered frequency following high-frequency climbing-fibre (CF) stimulation. (*C*) From the same cell as in *A* & *B*, cumulative probability plots of sIPSC amplitude with corresponding summary data from the 6 out of 13 cells that had sufficient length of recording between CF stimulation. Cumulative probability plots show amplitudes are shifted to lower values. Inset shows the pooled sIPSC amplitude data from all 6 cells, box-and-whisker plots indicate the median (line), 25-75$^{\text{th}}$ percentiles (box) and the 10-90$^{\text{th}}$ percentiles (whiskers); circles and crosses represent individual and mean values, respectively. * $P < 0.05$ (Wilcoxon matched-pairs test). (*D*) Summary data showing the effect of climbing fibre stimulation of sIPSC amplitude (ratio of post CF stimulation/pre CF stimulation) for both wild-type (Wt) and *stg*/*stg* mice. Box-and-whisker plots as in *C*. * $P < 0.05$ (Wilcoxon signed-rank test versus one; dotted line), n.s. $P > 0.05$ wild-type (Wt) versus *stg*/*stg* groups (Mann-Whitney *U* test). (*E*) Pooled data from wild-type mice showing no effect of climbing fibre (CF) stimulation on sIPSC frequency (Hz). Box-and-whisker plots as in *C*. n.s. $P > 0.05$ before CF stimulation versus after CF stimulation (Wilcoxon matched-pairs test).

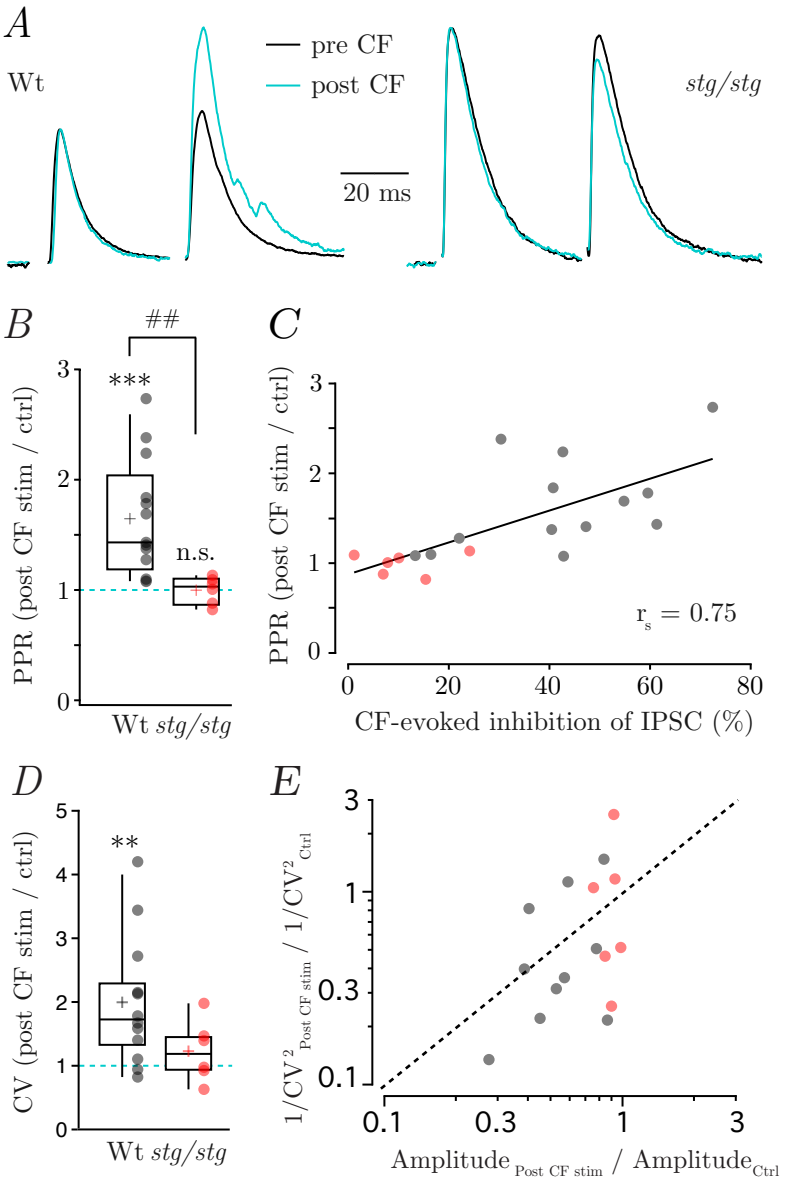

Figure 4.5: Climbing fibre stimulation reduces measures of GABA release probability (*A*) Representative averaged IPSCs from the P11 wild-type recording and P12 *stg/stg* recording shown in Figure 4.3 *C* & *D*. For each condition, the second IPSC was scaled and to the first. (*B*) Pooled data showing IPSC PPR before and after climbing fibre (CF) stimulation in wild-type mice. Box-and-whisker plots indicate the median (line), the 25-75$^{\text{th}}$ percentiles (box) and the 10-90$^{\text{th}}$ percentiles (whiskers); circles and crosses represent individual and mean values, respectively. *** $P < 0.001$, n.s. $P > 0.05$ (Wilcoxon signed-rank test versus one; dotted line), ## $P < 0.01$, wild-type (Wt) versus *stg/stg* (Mann-Whitney *U*-test). (*C*) Scatterplot showing the relationship between the climbing fibre-evoked change in PPR and the degree of IPSC inhibition (Spearman's rank-order correlation $r_s = 0.75$, $P = 0.0003$). (*D*) Pooled data showing the climbing fibre (CF)-induced suppression of CV of peak IPSC amplitude in wild-type (Wt) and *stg/stg* Purkinje

Figure 4.5 continued: cells. Box-and-whisker plots as in *B*. *** $P < 0.001$, n.s. $P > 0.05$ (Wilcoxon signed-rank test versus one; dotted line), n.s. $P > 0.05$, wild-type (Wt) versus *stg*/*stg* (Mann-Whitney U-test). (*E*) Plot data showing the ratio of $1/\mathrm{CV}^2$ as a function of relative IPSC amplitude pre and post climbing fibre stimulation. Black and red symbols represent wild-type and *stg*/*stg* Purkinje cell recordings respectively. The majority of wild-type Purkinje cells fall below the diagonal, whereas a greater proportion of *stg*/*stg* cells lie above the diagonal.

was significantly different from the effect observed in wild-type mice ($P = 0.0014$; Mann-Whitney U-test). Across all recordings, the magnitude of the climbing fibre-induced inhibition correlated significantly with the change in PPR (Figure 4.5 C; $n = 19$, $P = 0.0003$), further suggesting that a reduction in release probability was responsible for the inhibition of GABA release observed in Figures 4.3 and 4.4.

In addition, the CV was significantly increased in recordings from wild-type mice (normalised CV; 2.86 ± 0.91, $n = 13$, $P = 0.0017$) but not in *stg/stg* Purkinje cell recordings (normalised CV; 1.26 ± 0.20, $n = 6$, $P = 0.44$) (Figure 4.5 C). With a significant difference in normalised effects of CNQX between wild-type and *stg/stg* recordings ($P = 0.05$). To further assess the site of modulation I constructed a plot of the ratio of (CV^2 $_{\text{Post climbing fibre stimulation}}/CV^2$ $_{\text{control}}$) as a function of the relative IPSC amplitude (Amplitude $_{\text{Post climbing fibre stimulation}}$/Amplitude $_{\text{control}}$) (Figure 4.5 E). Whilst post-synaptic changes produce a change in amplitude without affecting the CV, a presynaptic site of action would be expected to alter both parameters (Faber and Korn, 1991). When compared to the diagonal line of identity, of the wild-type cells (black markers) which exhibited a reduced IPSC amplitude following climbing-fibre stimulation, a majority also exhibited a marked reduction in the CV. These results suggest that AMPARs associated with γ-2 are expressed presynaptically within MLIs, where they respond to climbing fibre-released glutamate to reduce the release probability of GABAergic synapses on Purkinje cells.

4.3.5 | Climbing fibre release is reduced in *stg/stg* mice

It is possible that the attenuated climbing fibre-induced suppression of IPSC amplitude in *stg/stg* Purkinje cells compared to wild-type Purkinje cells, may have resulted from deficient release of glutamate, rather than a reduced activity of γ-2-associated AMPARs. In Purkinje cell recordings from *stg/stg* mice, climbing fibre EPSCs displayed markedly faster rise and decay kinetics without any difference in amplitude, and thus a reduced charge transfer, compared to wild-type recordings, (Figure 4.6 A & B). Such features contrast to previous studies in older mice, which reported a smaller EPSC amplitude in *stg/stg* compared to wild-type mice and did not comment on any differences in kinetics

(Menuz and Nicoll, 2008; Yamazaki et al., 2010; Yan et al., 2013). Despite this, in one study climbing fibre EPSC kinetics do appear relatively faster in *stg/stg* mice (Yan et al., 2013). The altered decay kinetics, in the absence of changes in amplitude, raises the possibility that, rather than a specific loss of presynaptic γ-2, the reduced climbing fibre-induced inhibition of IPSC amplitude reflected an altered release and/or clearance of glutamate (subsection 4.4.3). To obviate any confounding differences in glutamate release, I next examined the effect of an exogenous AMPAR agonist.

4.3.6 | Effects of CNQX are consistent with the activation of presynaptic γ-2 associated AMPARs

As discussed earlier (subsection 1.3.2), CNQX is traditionally characterised as a competitive AMPAR antagonist. However, when AMPARs are associated with TARPs γ-2, γ-3, γ-4 or γ-8, CNQX acts as a partial agonist, with effects that are potentiated in the presence of a positive allosteric modulator such as cyclothiazide (Bats et al., 2012; Menuz et al., 2007). I reasoned that if presynaptic AMPARs in MLIs were associated with γ-2, as suggested by the loss of climbing fibre effects in slices from *stg/stg* mice, CNQX should reduce MLI-evoked IPSCs. I recorded IPSCs in Purkinje cells employing a paired-pulse protocol (30 ms interval). Application of 2 μM CNQX plus 50 μM cyclothiazide produced a 54 ± 6% reduction in the amplitude of the first evoked IPSC (Figure 4.7 *A* & *B*), a 35 ± 5 % increase in the PPR (Figure 4.7 *C* & *D*), and a 44 ± 21 % increase in the CV of IPSC amplitude (Figure 3.7 *D*; all measures $n = 6$, $P = 0.031$, Wilcoxon signed-rank test). By contrast, in cells from P10-14 *stg/stg* mice CNQX had no effect on IPSC amplitude, PPR or CV (Figure 4.7 *D*; $n = 6$, $P = 1.00$, 0.31 and 1.00, respectively). These results are consistent with the view that the activation of γ-2-associated AMPARs on MLIs attenuates action potential-driven GABA release.

A

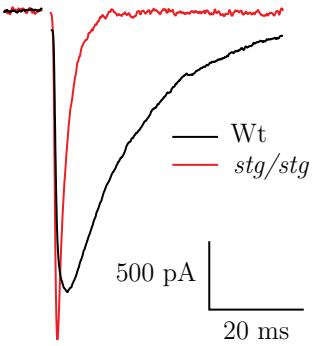

B

	Wild-type ($n = 7$)	*stg/stg* ($n = 4$)	P
Amplitude (-nA)	2.27 ± 0.46	1.68 ± 0.48	0.53
10-90% Rise Time (ms)	0.97 ± 0.10	0.58 ± 0.04	0.0061
37% Decay time (ms)	10.02 ± 1.78	2.65 ± 0.34	0.0061
Charge (pS)	21.30 ± 3.97	6.65 ± 1.76	0.042

CF-EPSC properties in wild-type and *stg/stg* mice

Figure 4.6: Faster climbing fibre-evoked EPSC kinetics in Purkinje cells from *stg/stg* mice

(*A*) Representative averaged climbing fibre-evoked EPSC from a P11 *stg/stg* mouse (red) overlaid on an averaged current from a P10 wild-type mouse (black). (*B*) Properties of climbing fibre-evoked EPSCs from wild-type and *stg/stg* Purkinje cells. Data presented as mean ± SEM (from n cells) show that *stg/stg* EPSCs exhibited significantly faster rise and decay compared to those from wild-type mice, although EPSC amplitude remained unchanged. The EPSCs analysed were the first in any pair or train of stimuli. P values between wild-type and *stg/stg* Purkinje cell values were calculated using Mann-Whitney U-tests.

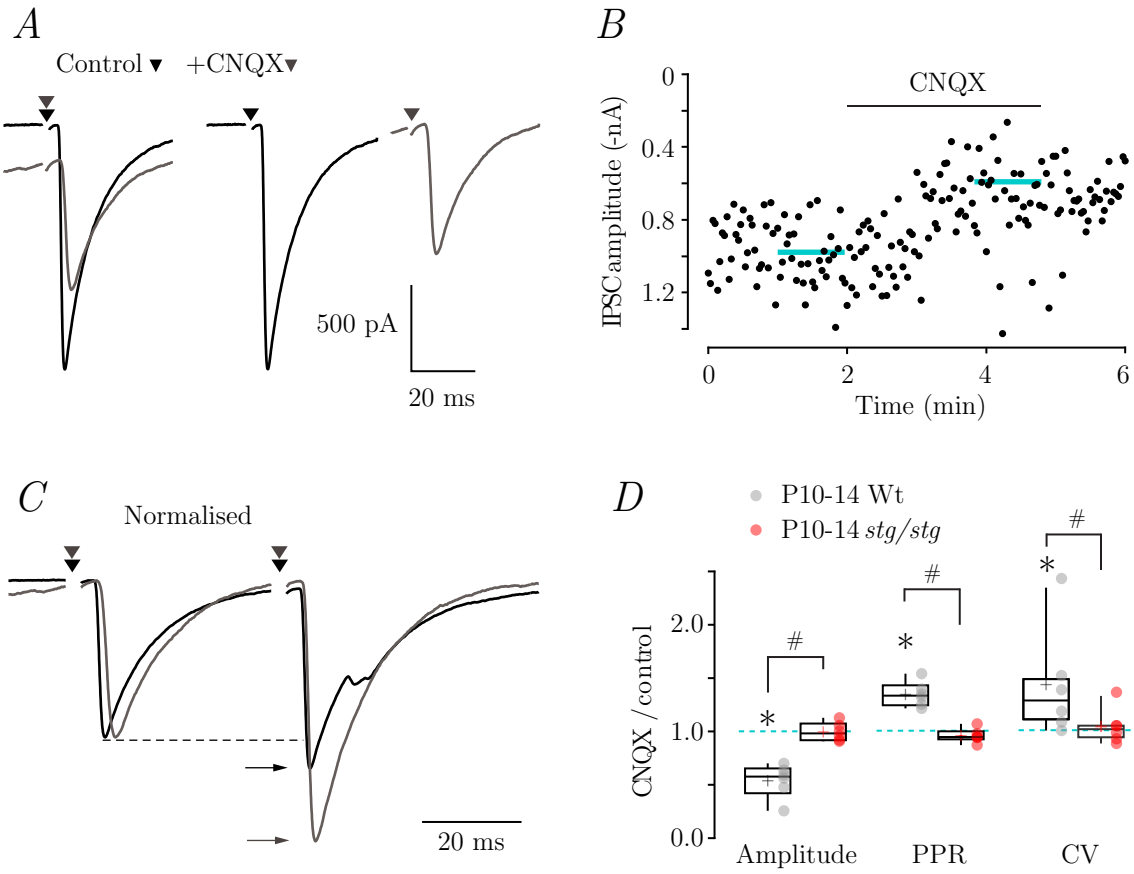

Figure 4.7: CNQX reduces evoked IPSC amplitude and release probability

(*A*) Averaged evoked IPSCs from a representative P10 wild-type Purkinje cell. Superimposed traces (left) were aligned to a common baseline (right) to illustrate the reduced IPSC amplitude in 2 μM CNQX (grey) compared to control (black). (*B*) Representative time course of CNQX-induced reduction in evoked IPSC peak amplitude in a wild-type Purkinje cell (P10). Horizontal blue bars indicate the time periods over which average IPSC amplitudes were calculated. (*C*) Paired evoked IPSCs scaled to the first IPSC show a pronounced increase in PPR in 2 μM CNQX (grey) compared to control (black). (*D*) Pooled data showing inhibition of IPSC peak amplitude, enhancement of PPR, and increased CV of the first IPSC by 2 μM CNQX in wild type Purkinje cells (grey). * $P < 0.05$ (Wilcoxon signed-rank test versus one). These effects were absent in *stg*/*stg* neurons (red). # $P < 0.05$ wild-type versus *stg*/*stg* (Mann-Whitney U-test). Box-and-whisker plots indicate the median (line), 25-75$^{\text{th}}$ percentiles (box) and the 10-90$^{\text{th}}$ percentiles (whiskers); circles and crosses represent individual and mean values, respectively.

4.3.7 | CNQX reduced unitary IPSC amplitude and increased failure rate in paired MLI – MLI recordings

As well as forming synapses with Purkinje cells, MLIs synapse with each other. To investigate potential target-dependent differences in TARP regulation of presynaptic AMPARs I next made dual recordings from synaptically coupled MLIs (Figure 4.8 *A*). After achieving a stable whole-cell voltage-clamp recording from an MLI, a second electrode filled with external solution was used to obtain a loose cell-attached recording (3-5 MΩ) from a neighbouring MLI (Figure 4.8 *A*). The process of finding paired MLIs was initially tiresome, with only 9 out of 56 MLI pairs being connected. However, after I switched the slicing solution from a high sucrose to a Kgluconate based solution (section 2.2), the success rate was approximately doubled to 19 from 60 MLI pairs. It has been suggested that the Kgluconate based solution minimises the flow of Ca^{2+} and other extracellular ions into neurons whose processes were cut, thereby reducing excitotoxicity (Dugué et al., 2005). This ∼30% connection rate was similar to the 20% level of connectivity previously reported (Kondo and Marty, 1998). Akin to recordings from Purkinje cells (Figure 4.4), frequent sIPSCs were observed in recordings from MLIs, representing GABAergic transmission from a number of presynaptic cells. Synaptically paired MLIs were identified based on a high likelihood of an IPSC occurring within 3-4 ms following an action potential recorded from the presynaptic cell (Figure 4.8 *A*; blue triangles). Both the frequency of action potentials and amplitude of paired IPSCs remained stable over time, and in the example shown, very few failures were seen (Figure 4.8 *B*).

Figure 4.8 *C* shows the amplitude histograms of all IPSCs recorded from a single cell compared to those originating from the activity in the identified presynaptic cell. IPSCs originating from activity in the recorded presynaptic MLI accounted for 24.9% of the total IPSCs, and exhibited a relatively Gaussian distribution. In comparison, the amplitude histogram of all sIPSCs was skewed towards larger values, characteristic of central neurons (Bekkers, 1994). A gaussian amplitude distribution of IPSCs has been previously argued to result from a synapse with a single functional release site, branded as a a 'simple' connection (Kondo and Marty, 1998; Auger and Marty, 1997) (Table 4.2; cell pair 5). This particular individual release site produced relatively large IPSCs compared to the

other synapses formed onto the recorded MLI (mean amplitude of the two distributions were 343.24 pA and 149.81 pA, respectively).

Table 4.2 summarises the properties of each of the 6 MLI – MLI paired recordings, and provides information on the type of synapse. In addition to the simple synapse in Figure 4.8, several types of MLI – MLI synaptic connections can be distinguished on the basis of the shape of the IPSC amplitude distribution (Kondo and Marty, 1998). Two '3 component' connections were observed, which are thought to represent a combination of two or three synaptic connections, with each exhibiting a gaussian IPSC amplitude histogram. Where the amplitude histogram could not be separated into gaussian peaks, these connections were referred to as 'multiple' connections (Kondo and Marty, 1998).

In paired MLI recordings from P10-14 wild-type mice, 10 μM CNQX increased the failure rate (Figure 4.9 *B* & *C*; from 0.30 ± 0.15 to 0.73 ± 0.07, $n = 6$, $P = 0.031$) and decreased paired IPSC amplitude (Figure 4.9 *B* & *D*; from 203.57 ± 49.26 pA to 109.82 ± 23.13 pA, $n = 6$; $P = 0.031$). CNQX had no significant impact on the latency between presynaptic action potentials and paired IPSC onsets (Figure 4.9 *E*; from 1.91 ± 0.06 ms to 2.21 ± 0.08 ms, $P = 0.063$).

4.3.8 | CNQX increased spike frequency in paired MLI – MLI recordings

Although the observed effects of CNQX on failure rate and amplitude are consistent with reduced release probability (Kondo and Marty, 1998), they were clearly associated with an increase in MLI firing rate (Figure 4.10 *A* & *B*; from 1.43 ± 0.44 Hz to 12.67 ± 4.55 Hz, $n = 6$, $P = 0.031$). This itself can lead to a reduction in the probability of release (Kondo and Marty, 1998). In order to avoid CNQX-induced somatic depolarisation leading to increased MLI firing, it would have been preferable to voltage-clamp both MLIs. However, a previous study has suggested the amplitude of evoked IPSCs to 'run down' over time, possibly due to dialysis of presynaptic factors required for vesicle release (Kondo and Marty, 1998). To control for the possibility that changes in firing rate, rather that activation of presynaptic AMPARs led to reduced GABA release, I next made recordings from Purkinje cells which had been mechanically dissociated from acute

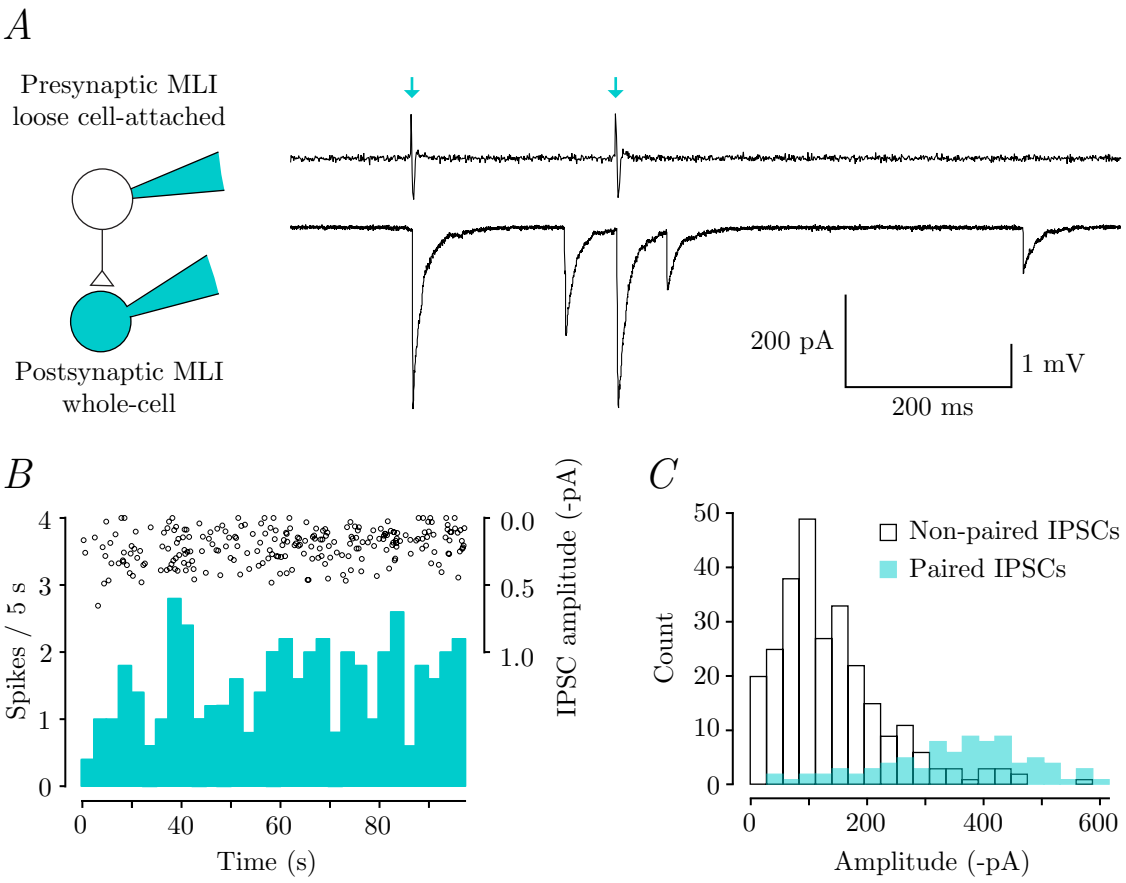

Figure 4.8: A paired-recording experiment from a simple MLI – MLI connection

(*A*) Schematic drawing of the recording configuration and representative paired presynaptic voltage and postsynaptic current recordings on a slow time scale. Arrowheads indicate presynaptic action potentials that elicited a postsynaptic response. (*B*) From the same representative MLI pair as in (A), paired-IPSC amplitudes and number of action potentials every 5 s remained stable over the duration of the experiment under control conditions. (*C*) Histogram shows superimposed amplitude distributions for successful paired IPSCs (light blue) and for spontaneous IPSCs (white) resulting from activity in MLIs other than the single presynaptic ell recorded. The paired-IPSC distribution could be fitted to a single Gaussian with mean value of 343.24 pA.

Cell pair	Action potential frequency (Hz)	Failure rate	Amplitude (-pA)	Latency (ms)	Rise time (ms)	Decay time (ms)	Category
1	1.16	0.90	86.2 9	1.75	0.35	12.68	Simple
2	2.8 9	0.0 7	301.2 7	2.04	0.83	8.58	Multiple
3	0.07	0.03	41.20	1.88	0.75	5.02	3 component
4	0.52	0.06	343.2 4	2.02	0.53	10.25	Multiple
5	1.6 0	0.08	261.72	1.73	0.76	11.47	Simple
6	2.36	0.6 3	187.68	2.03	0.51	6.05	3 component

Table 4.1: Features of paired MLI recordings

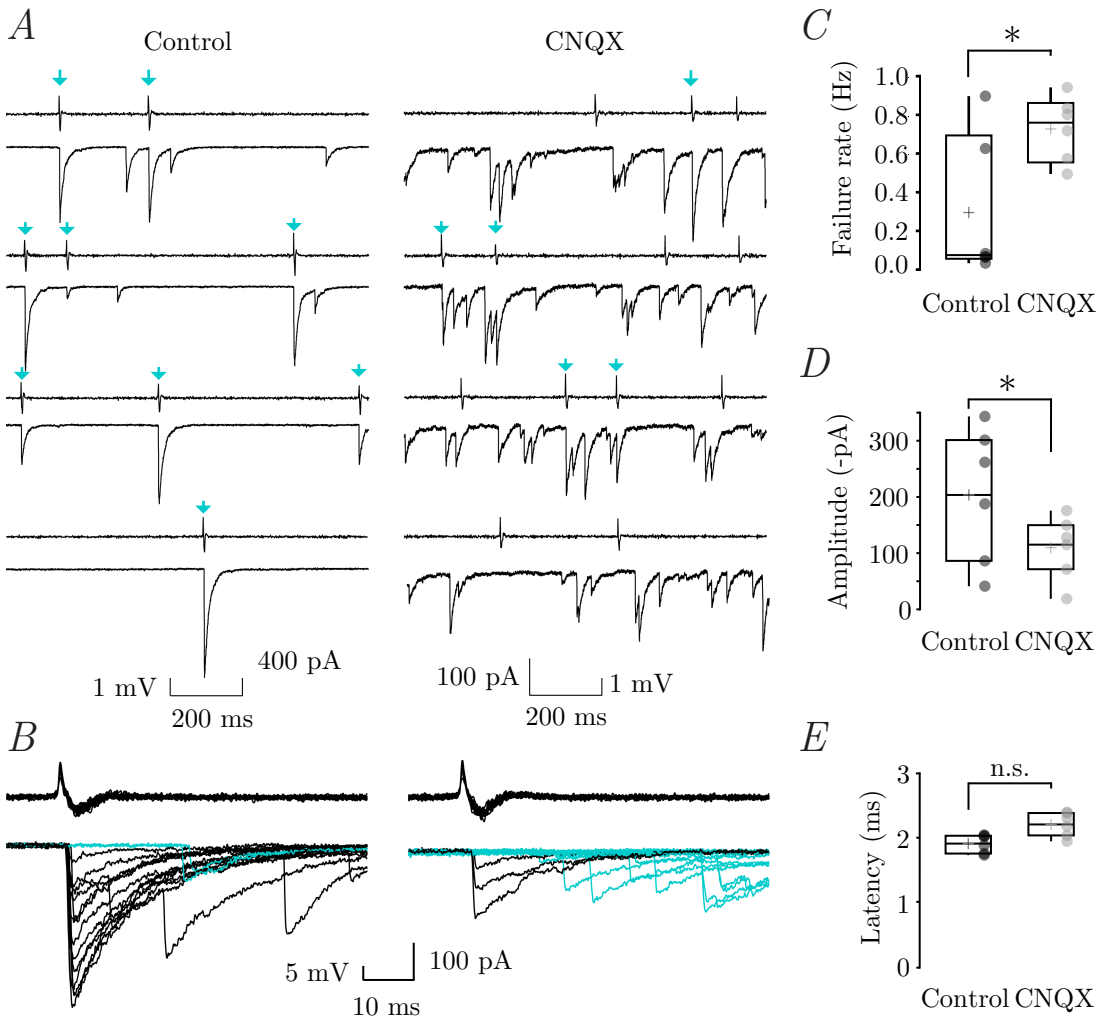

Figure 4.9: CNQX reduced unitary IPSC amplitude and increased failure rate

(*A*) Representative pre- and postsynaptic recordings from an MLI – MLI pair (P11 wild-type mouse). Action potentials in the presynaptic MLI were recorded in the loose cell-attached configuration (upper sweeps) and IPSCs in the postsynaptic MLI (lower sweeps). Blue arrows indicate action potentials triggering unitary IPSCs in the postsynaptic MLI with a latency of $<$ 3 ms. CNQX (10 μM) increased spontaneous IPSC frequency and the number of failures. (*B*) Selected sweeps from the recording in *A*, showing successes (black) and failures (blue). (*C*–*E*) Pooled data showing the effect of CNQX on failure rate, unitary IPSC amplitude and latency. Box-and-whisker plots indicate the median (line), the 25-75$^{\text{th}}$ percentiles (box) and the 10-90$^{\text{th}}$ percentiles (whiskers); filled circles and crosses represent individual and mean values, respectively. * $P < 0.05$ (Wilcoxon matched-pairs test).

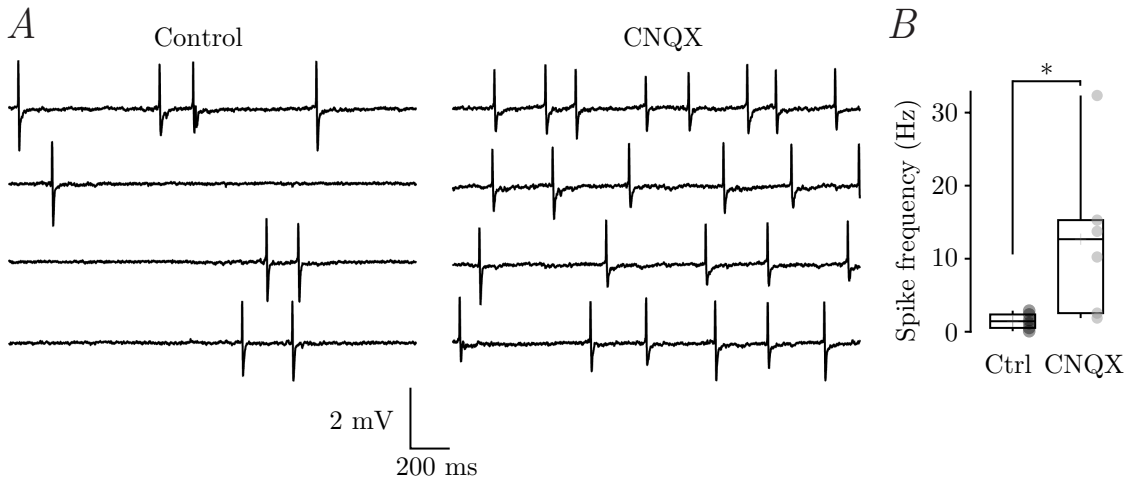

Figure 4.10: CNQX increases MLI firing rate

(*A*) Representative records of MLI firing obtained in the loose cell-attached configuration, before and during application of 10 μM CNQX (P11 wild-type mouse). (*B*) Pooled data showing effect of CNQX on spike frequency. * $P < 0.05$ (Wilcoxon matched-pairs test). Box-and-whisker plots indicate the median (line), 25-75$^{\text{th}}$ percentiles (box) and the 10-90$^{\text{th}}$ percentiles (whiskers); circles and crosses represent individual and mean values, respectively.

cerebellar slices.

4.3.9 | CNQX reduces IPSC amplitude in mechanically dissociated Purkinje cells

To rule out the effects of MLI cell firing on release probability, I examined the effect of CNQX on the amplitude of evoked IPSCs in mechanically dissociated Purkinje cells. In addition to spontaneous events (Figure 3.11), the adherent boutons on dissociated cells can be stimulated to produce evoked currents similar to those observed in acute slices (Akaike et al., 2002) (Figure 4.11 *B*). Unlike the corresponding experiment in acute slices (Figure 4.7), I chose not to apply paired pulses. First, release from MLI adherent boutons can run down with high activity (Guy Moss, personal communication; Duguid et al. (2007)), which would have been perpetuated by high frequency stimulation. Second, as I was confident that only a single bouton was stimulated (Akaike et al., 2002), I was able to apply failure rate analysis as an additional measure of release probability, instead of examining the PPR. Direct stimulation of an adherent bouton triggered IPSCs that required activation of voltage-gated Na^+ channels and were mediated by postsynaptic $GABA_A$Rs, as they were completely blocked by TTX (1 μM) and SR 95531 (20 μM) (Figure 4.11 *B* & *C*). In a representative recording from Purkinje cells, IPSC amplitude was decreased following treatment with 2 μM CNQX plus 50 μM cyclothiazide (Figure 4.11 *B*). A greater density of points around zero during CNQX treatment demonstrates an increase in failure rate (Figure 4.11 *B*). Both effects were visible in probability density histograms (Figure 4.11 *C*), where in response to CNQX, a greater proportion of stimulations produced responses that grouped around 0 pA, corresponding to failed synaptic transmission. the amplitude distribution was shifted to lower values. On average, there was a 30 ± 4% reduction in the amplitude of the evoked IPSCs and a 3.08 ± 0.59 fold increase in the failure rate (Figure 4.11 *E*; both measures; $n = 7$, $P = 0.016$). In addition, the CV of the first IPSC amplitude was increased by 1.38 ± 0.09 fold ($n = 7$, $P = 0.016$) (Figure 4.11 *E*; Table 4.2). This result demonstrates that AMPAR-mediated suppression of evoked GABA release can occur independently of changes in MLI firing rate. The combination of the TARP-dependent agonism of CNQX, and the advantages

of the dissociated Purkinje cell preparation, provide strong evidence that γ-2 is required for presynaptic AMPAR-mediated modulation of evoked GABA release.

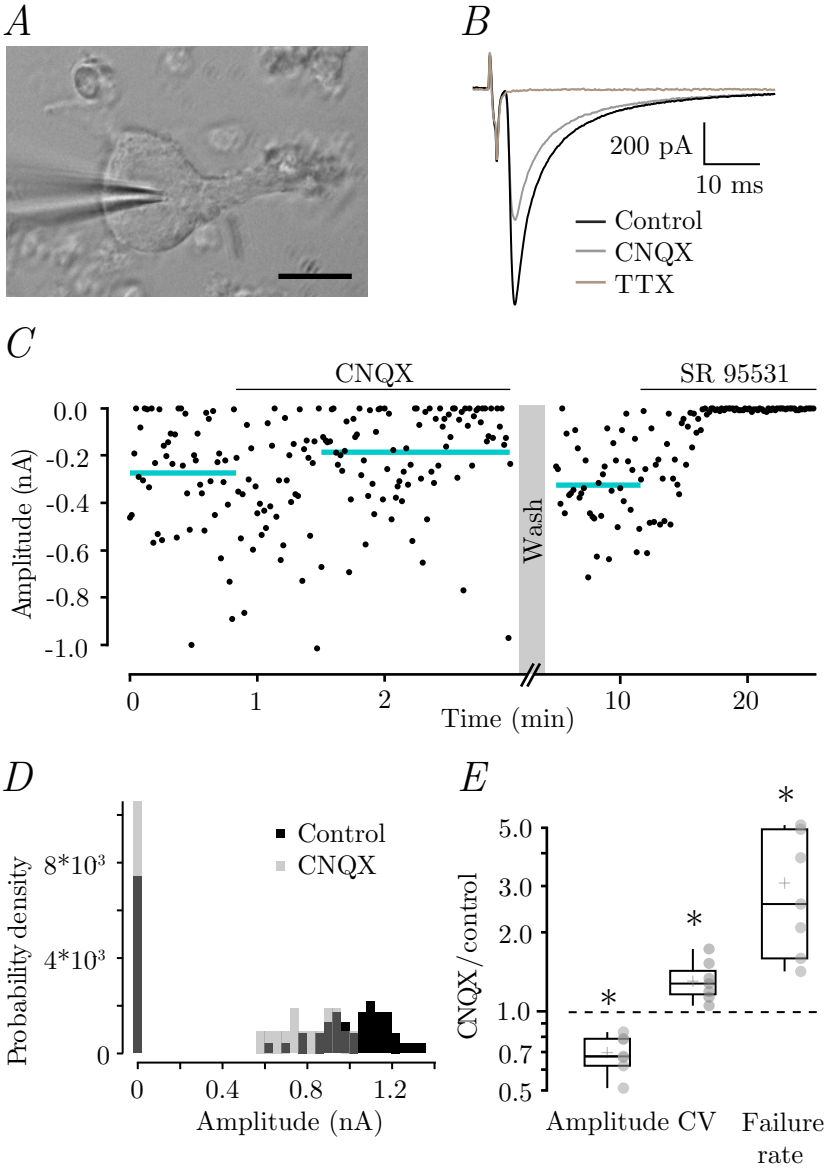

Figure 4.11: CNQX effects on evoked release are preserved in Purkinje cells dissociated from P10-14 mice

(*A*) Image of an acutely dissociated cell, illustrating the large soma and truncated proximal dendritic tree. Scale bar 20 μm. (*B*) Stimulation of a single adherent MLI bouton on an acutely dissociated P12 Purkinje cell evoked IPSCs that were blocked by 1 μM TTX (brown trace). The amplitude of the average IPSC waveform decreased in 2 μM CNQX (plus 50 μM cyclothiazide). (*C*) Sample time course of CNQX-induced reduction in evoked IPSC peak amplitude from a different dissociated Purkinje cell (P13). The amplitude recovered to original values following removal of CNQX, and events were abolished completely by application of the $GABA_AR$ blocker SR 95531 (20 μM). Horizontal grey bars indicate the time periods from which IPSC measurements were averaged. (*D*) Probability density histogram of evoked-IPSC amplitudes; a greater proportion of failures (bar at 0 pA) and a shift to lower amplitude was

Figure 4.11 continued: observed in CNQX (grey bars), compared to control (black bars). (*E*) Pooled data showing inhibition of IPSC peak amplitude, increased CV of IPSC amplitude and increased failure rate in the presence of CNQX. * $P < 0.05$ (Wilcoxon signed-rank test versus one). Box- and-whisker plots indicate the median (line), 25-75$^{\text{th}}$ percentiles (box) and the 10-90$^{\text{th}}$ percentiles (whiskers); circles and crosses represent individual and mean values, respectively.

		Measures of action potential-driven IPSCs											
		Amplitude (nA)			Paired-pulse ratio			Coefficient of variation			Failure rate		
	n	Control	Treatment (normalised)	*P*	Control	Treatment (normalised)	*P*	Control	Treatment (normalised)	*P*	Control	Treatment (normalised)	*P*
Acute slices													
P10-14 WT PCs													
CF-stimulation	*13*	1.00 ± 0.13	0.54 ± 0.07	0.00024	0.97 ± 0.05	1.61 ± 0.17	0.00024	0.21 ± 0.03	0.42 ± 0.06	0.0012			
			0.58 ± 0.05	*0.00024*		*1.65 ± 0.15*	*0.00024*		*2.86 ± 0.91*	*0.0017*			
CNQX	*6*	1.22 ± 0.40	0.56 ± 0.11	0.031	1.05 ± 0.06	1.41 ± 0.08	0.031	0.26 ± 0.03	0.38 ± 0.09	0.031			
			0.54 ± 0.06	*0.031*		*1.35 ± 0.05*	*0.031*		*1.44 ± 0.21*	*0.031*			
P10-14 stg /stg PCs													
CF-stimulation	*6*	0.88 ± 0.06	0.78 ± 0.06	0.031	0.80 ± 0.09	0.79 ± 0.09	1.00	0.11 ± 0.01	0.12 ± 0.02	0.69			
			0. 89 ± 0.03	*0.031*		*1.00 ± 0.05*	*1.00*		*1.26 ± 0.20*	*0.44*			
CNQX[1]	*6*	0.97 ± 0.59	0.92 ± 0.54	0.69	1.32 ± 0.15	1.26 ± 0.13	0.22	0.39± 0.08	0.41 ± 0.09	1.00			
			1.00 ± 0.03	*1.00*		*0.96 ± 0.03*	*0.31*		*1.05 ± 0.07*	*1.00*			
P10-14 WT MLIs													
CNQX[2]	*6*	0.20 ± 0.05	0.11 ± 0.02	0.031							0.30 ± 0.15	0.73 ± 0.07	0.031
			0.59 ± 0.10	*0.031*								*8.31 ± 3.05*	*0.031*
Dissociated cells													
P10-14 WT PCs													
CNQX	*7*	0.62 ± 0.14	0.44 ± 0.01	0.016				0.50 ± 0.08	0.65 ± 0.08	0.016	0.11 ± 0.04	0.21 ± 0.05	0.016
			0.70 ± 0.04	*0.016*					*1.38 ± 0.09*	*0.016*		*3.08 ± 0.59*	*0.016*

Table 4.2: Collated measures of action potential-driven IPSCs.

Raw values were compared using a two-sample Wilcoxon matched-pairs test; normalised values (italicised) were compared against 1 using a one-sample Wilcoxon signed-rank test. P values < 0.05 are shown in red. CF; climbing fibre.

[1] evoked IPSCs; 2 μM CNQX plus 50 μM cyclothiazide.

[2] unitary IPSCs; 10 μM CNQX without cyclothiazide.

4.4 | Discussion

Activation of γ-2-associated presynaptic AMPARs resulted in a pronounced reduction in climbing fibre- and CNQX-induced suppression of evoked GABA release. It is unlikely that an increased MLI firing rate exclusively reduced release probability (Kondo and Marty, 1998), as a TARP-dependent reduction in IPSC amplitude was observed in recordings from mechanically dissociated Purkinje cells. Thus, together with those of chapter 3, these results suggest effective presynaptic AMPAR-mediated modulation of GABA release from MLI axonal varicosities requires γ-2, irrespective of the evoked or spontaneous nature of release, and with no clear target neuron differences.

4.4.1 | Somatodendritic AMPARs modulate release probability and promote feedforward inhibition

Consistent with a residual effect of AMPA in recordings from *stg/stg* MLIs and Purkinje cells (Figure 3.5), an attenuated but significant reduction of IPSC amplitude remained following climbing fibre stimulation in *stg/stg* mice. As raised in chapter 3, such a residual effect may reflect a population of presynaptic AMPARs either associated with γ-7, or TARP-less. However, the loss of effect of climbing fibre stimulation on sIPSC amplitude in recordings from *stg/stg* Purkinje cells argues against this hypothesis. Alternatively, all presynaptic AMPARs may require γ-2 to function, and the remaining effect of climbing fibre stimulation on evoked IPSCs in *stg/stg* Purkinje cells would then reflect spillover-mediated activation of somatodendritic AMPARs (Szapiro and Barbour, 2007). In *stg/stg* mice, such somatodendritic AMPARs are likely to be a combination of γ-7-associated extrasynaptic CI-AMPARs, and TARPless CP-AMPARs at MLI postsynaptic densities (Bats et al., 2012; Jackson and Nicoll, 2011a). Depolarisation resulting from their activation would enhance MLI firing, and even in the absence of γ-2-associated presynaptic AMPARs, would reduce GABA release (Kondo and Marty, 1998). As somatodendritic MLI NMDARs are also expected to mediate parasynaptic signalling following climbing fibre activation (Szapiro and Barbour, 2007), the residual effect may have been greater if D-APV was absent from recordings.

Since climbing fibre-mediated glutamate release would not only increase the firing of the stimulated MLI, but other MLIs within the diffusion limit, a reduction in sIPSC amplitude in *stg/stg* mice would be predicted. Given the heterogenous activation and inhibition of spatially segregated MLI populations following climbing fibre stimulation (Coddington et al., 2013), the absence of any change in sIPSC amplitude shown in *stg/stg* recordings, is not necessarily irreconcilable with the residual suppression on evoked IPSCs in recordings from these mice. It was recently found that MLIs which reside within the domain of spillover diffusion inhibit MLIs outside the climbing fibre glutamate diffusion limit (Coddington et al., 2013). In effect, the population of MLIs with enhanced firing rates would reduce the firing rate of connected MLIs and, because MLIs fire spontaneously (Häusser and Clark, 1997), would reduce their release probability (Kondo and Marty, 1998). Thus, the unaltered sIPSC amplitude, and frequency, in *stg/stg* recordings could reflect a combination of MLIs with an enhanced spike rate and other MLIs with reduced firing rates, depending on their proximity to the stimulated climbing fibre. The absence of effect in *stg/stg* recordings could suggest that all presynaptic AMPARs require γ-2 to modulate evoked GABA release. This is in agreement with the pre-mIPSC data and mechanically dissociated Purkinje cell recordings from *stg/stg* mice shown in chapter 3.

4.4.2 | Extent of presynaptic AMPAR activation by climbing fibre-released glutamate

Herein, I suggest γ-2 associated presynaptic AMPARs can be activated by endogenous glutamate spillover from climbing fibre – Purkinje cell synapses. Climbing fibres form hundreds of synapses upon Purkinje cell dendrites, that exhibit a relatively high probability of release and can release multiple vesicles in response to a single action potential (Wadiche and Jahr, 2001; Rudolph et al., 2011). Consequentially, large and prolonged synaptic glutamate concentrations are thought to saturate adjacent synaptic AMPARs to produce the characteristically large amplitude EPSC (Harrison and Jahr, 2003). In combination with a slow clearance rate, the high glutamate concentration also results in a relatively prolonged EPSC decay (Barbour et al., 1994; Wadiche and Jahr, 2001). In spite

of high expression of glutamate transporters on surrounding Bergmann glial processes that form a tripartite synapse (Lehre and Danbolt, 1998; Tzingounis and Wadiche, 2007), spillover of glutamate from climbing fibre – Purkinje cell synapses exclusively mediates the transmission with MLIs. This is not only true for glutamate receptors at axonal boutons (Satake et al., 2000, 2006, 2010), but also for glutamaterigc transmission onto somatodendritic sites, both in acute slices (Szapiro and Barbour, 2007) and *in vivo* (Jörntell and Ekerot, 2003). In addition, spillover transmission has been shown to activate glutamate receptors at extrasynaptic Purkinje cell sites (Brasnjo and Otis, 2001; Wadiche and Jahr, 2005), and on Bergmann glia (Bergles et al., 1997), but spillover between neighbouring climbing fibre – Purkinje cell synapses does not seem to occur (Wadiche and Jahr, 2001).

Although there is good evidence for spillover-mediated transmission, it is unclear whether the 'volume' of parasynaptic signalling required to activate presynaptic AMPARs occurs in response to normal rates of climbing fibre firing. Satake et al. (2000) reported that 5-50 Hz climbing fibre stimulation reduced evoked GABA release. However, they did not test frequencies between 1 and 2.5 Hz at which climbing fibres in the cat were found to fire *in vivo* (Armstrong and Rawson, 1979). Thus, the ∼40% suppression of IPSC amplitude I observed is likely to be an overestimate of presynaptic AMPAR influence on evoked GABA release, rather the 20% suppression resulting from 5 Hz stimulation may be more realistic (Satake et al., 2000). It would have been interesting to test if any residual effect of climbing fibre stimulation on evoked GABA release occurred in *stg/stg* mice following 1-2.5 Hz climbing fibre stimulation. Low frequency climbing fibre stimulation is thought to be capable of activating somatodendritic AMPARs (Szapiro and Barbour, 2007), it may have been that the artificially elevated glutamate concentration resulting from 50 Hz stimulation caused a large MLI depolarisation that increased MLI firing and contributed to the reduction in GABA release probability.

4.4.3 | Potential changes in climbing fibre released glutamate in *stg/stg* mice

The significance of γ-2 for climbing fibre stimulation-induced suppression of GABA release may be questioned. Though control experiments using CNQX established that γ-2 regulates the presynaptic AMPAR suppression of evoked release, this is subtly different from claiming that γ-2 is important for the suppression of GABA release following climbing fibre stimulation. Given the altered climbing fibre EPSC kinetics I observed in Purkinje cell recordings from *stg/stg* mice, a reduction in glutamate release, and not the absence of γ-2, could have been responsible for the attenuated IPSC suppression in this experiment.

The faster decay, yet unaltered amplitude, of climbing fibre-mediated EPSCs in *stg/stg* Purkinje cell recordings suggests that whilst the glutamate concentration was sufficient to saturate synaptic AMPARs, the concentration was nonetheless reduced compared to wild-type. From previous studies, lower glutamate concentrations would be expected to clear from the synapse at a faster rate, and be less likely to activate extrasynaptic AMPARs, thus speeding the rate of EPSC decay (Wadiche and Jahr, 2001). At parallel fibre presynaptic terminals in *stg/stg* mice, Richardson and Leitch (2005) observed a reduced number of vesicles docked in close proximity to active zones, as well as reduced levels of glutamate immunoreactivity. If such findings are transferable to climbing fibre varicosities, then there is a possibility that the release of glutamate is reduced in *stg/stg* animals.

Alternatively, the difference in EPSC kinetics may reflect an altered morphology of climbing fibre – Purkinje cell synapses in *stg/stg* mice. A reduced crowding of synaptic structures would lead to a greater rate of diffusion out of the cleft, similar to that observed at the cerebellar mossy fibre-to-granule cell synapse at younger ages (Cathala et al., 2005). However, there is little evidence in *stg/stg* mice to suggest that gross synaptic structure is altered compared to wild-type. For example, whilst the thickness of the PSD of MF-to-granule cell and parallel fibre-to-Purkinje cell synapses is reduced, the number and length of such synapses are unchanged (Richardson and Leitch, 2005). Thus, γ-2-associated

AMPARs are present at basket cell boutons where they act to reduce evoked GABA release. However, the potentially confounding differences in neurotransmitter release in *stg/stg* mice make it difficult to unambiguously determine the precise basis of the reduced climbing fibre-induced suppression of release seen in these animals.

5 | Presynaptic AMPARs promote Ca^{2+} entry to modulate the probability of GABA release from MLIs

5.1 | Summary

This chapter is concerned with mechanisms which may mediate the effects of presynaptic AMPARs on release probability.

Incubation with $CdCl_2$ markedly reduced the effect of TARP-associated AMPARs on mIPSC frequency in both MLI and Purkinje cell recordings. In mechanically dissociated Purkinje cells a specific role of P/Q- and N-type VGCCs was revealed using the selective blocker Agatoxin.

In the presence of Ca^{2+} chelators, treatment with AMPA had no effect on either mIPSC frequency or evoked IPSC amplitude recorded from mechanically dissociated Purkinje cells. Inhibition of AMPAR action by the slow Ca^{2+} chelator EGTA, suggests that VGCCs which mediate AMPAR effects form a population distinct from those at the active zone required for action potential-driven release.

In recordings from Purkinje cells in acute cerebellar slices, application of AMPA increased mIPSC amplitude, consistent with the sensitisation of CICR from ryanodine-sensitive stores. In contrast, the application of AMPA to mechanically dissociated Purkinje cells recordings produced a significant reduction of mIPSC amplitude, which suggests that CICR does not contribute to effects mediated solely by presynaptic AMPARs.

These results suggest that presynaptic AMPARs at MLI boutons predominantly regulate GABA release through P/Q- or N- type VGCCs coupled to active zones in the microdomain. At MLI – MLI boutons, direct Ca^{2+} influx through CP-AMPARs may provide an additional source of Ca^{2+} to modulate release. At basket cell – Purkinje cell boutons, a reduction in mIPSC amplitude is inconsistent with the theory that presynaptic AMPARs enhance release partly through the sensitisation of internal Ca^{2+} stores.

5.2 | Introduction

From initial experiments at the frog NMJ, Katz and Miledi demonstrated that Ca^{2+} was essential to trigger exocytosis of synaptic vesicles (Katz and Miledi, 1965, 1967). At the active zone, highly localised and concentrated Ca^{2+} domains result from VGCC openings to sharply evoke transmitter release within less than a millisecond of action potential invasion (Borst and Sakmann, 1996; Südhof, 2012). At MLI (basket cell) boutons that synapse onto Purkinje cells, between 100 and 200 VGCCs are activated by a single action potential, producing a 3-5 μM Ca^{2+} transient which decays to approximately 115-130 nM over hundreds of milliseconds before reverting to resting levels ($\sim$ 100 nM) (Rusakov et al., 2005). At these axonal varicosities, it is thought that P/Q channels predominantly mediate action potential-dependent release with a smaller contribution from N-type VGCCs (Forti et al., 2000). In addition, ryanodine-sensitive internal Ca^{2+} stores have been proposed to contribute to action potential-evoked release by enhancing depolarisation-induced Ca^{2+} elevation (Galante and Marty, 2003).

In contrast to the absolute requirement of Ca^{2+} for action potential-dependent release, the role of Ca^{2+} in driving spontaneous release depends on the particular synapse examined (section 1.4.4). At MLI boutons that contact other MLIs, spontaneous release occurs independently of extracellular Ca^{2+} levels and is not affected by the antagonism of VGCCs (Llano and Gerschenfeld, 1993). At MLI – Purkinje cell synapses, spontaneous release is similarly unaffected by Ca^{2+} entry via VGCCs. At basket cell boutons that synapse on to Purkinje cells, presynaptically located ryanodine-sensitive stores, which mobilise large Ca^{2+} concentrations, have been proposed to provide an additional source of Ca^{2+} to underlie the largest mIPSCs through the initiation of multivesicular release (Llano et al., 2000).

Mechanisms that mediate presynaptic iGluR effects on action potential-driven release

The mechanism by which presynaptic iGluRs modulate action potential-evoked release at MLI – Purkinje cell boutons varies depending on receptor subtype. NMDARs have been

proposed to enhance action potential-dependent release by direct Ca^{2+} influx through the NMDAR channel and subsequent sensitisation of ryanodine-sensitive Ca^{2+} stores (Duguid and Smart, 2004). Presynaptic AMPAR-mediated reduction of evoked release from basket cell boutons that synapse onto Purkinje cells has been suggested to involve G-protein inhibition of P/Q-type VGCCs, without involvement of ryanodine Ca^{2+} stores (Satake et al., 2004). However, the assertions regarding mechanisms of action of presynaptic AMPARs may be erroneous given the methods employed. Firstly, the use of N-ethylmaleimide to block the G-protein/VGCC interaction would potentially have non-specific effects, including the disruption of the NSF-dependent trafficking of presynaptic AMPARs (Pittaluga et al., 2006), and the inhibition of NSF-mediated dissociation of SNAREs, which is normally required for vesicle fusion (Söllner et al., 1993). Both effects could explain the attenuated suppression of evoked release by AMPARs (Satake et al., 2004). Moreover, application of specific blockers of P/Q VGCCs would alter the baseline of evoked release (Forti et al., 2000), reducing any potential effects of AMPAR activation.

Mechanisms that mediate presynaptic iGluR effects on spontaneous release

Presynaptic iGluRs exert their control over spontaneous release through a number of mechanisms that almost always involve regulating axon terminal free Ca^{2+} concentrations (Pinheiro and Mulle, 2008). The exact mechanism by which presynaptic iGluRs at MLI terminals regulate GABA release depends on the target neuron and the subtype of iGluR. At both MLI – MLI and MLI – Purkinje cell boutons, the activation of presynaptic NMDARs enhances release via direct Ca^{2+} influx through the NMDAR channel, without increasing VGCC openings (Duguid and Smart, 2004; Glitsch, 2008a; Rossi et al., 2012). Direct Ca^{2+} influx may subsequently mobilise Ca^{2+} from ryanodine-sensitive internal stores to further augment GABA release (Duguid and Smart, 2004; Rossi et al., 2012), though there is conflicting evidence which suggests this does not occur at MLI – Purkinje cell varicosities (Glitsch, 2008a).

At MLI – MLI synapses, AMPAR-mediated enhancement of spontaneous release appears

to be predominantly mediated by Ca^{2+} permeable forms of the receptor (Rossi et al., 2008). Their activation depolarises the membrane to induce VGCC opening, which largely accounts for the effect on release probability (Bureau and Mulle, 1998). In the presence of the broad VGCC blocker $CdCl_2$ some potentiation of mIPSC frequency remains (Bureau and Mulle, 1998), raising the possibility that direct Ca^{2+} influx through CP-AMPARs may directly stimulate release. By contrast, MLI – Purkinje cell boutons mainly express GluA2 containing CI-AMPARs. Besides the proposed involvement of P/Q-type VGCCs in AMPAR-mediated inhibition of evoked release (Satake et al., 2004), the contribution of VGCCs to AMPAR-mediated modulation of spontaneous release has not been specifically investigated at this subset of axonal varicosities. Rather, AMPAR effects on mIPSC frequency and amplitude were increased by pre-incubation with ryanodine, and decreased by the internal store inhibitor dantrolene, to suggest internal Ca^{2+} stores may contribute to the AMPAR-mediated modulation of spontaneous release (Rossi et al., 2008).

The efficacy and speed of transmitter release is in part determined by the proximity of VGCCs to Ca^{2+} sensors on synaptic vesicles (Eggermann et al., 2012). VGCCs that drive action potential-evoked release are often located close to the active zone, within 10 and 20 nms (Bucurenciu et al., 2008). Such nanodomain coupling (< 100 nm) produces rapidly activating and decaying localised Ca^{2+} transients of large magnitude. This limits any synaptic delay and promotes efficacious transmitter release (Bucurenciu et al., 2008). At other terminals, it is possible that VGCCs involved in evoked release are coupled to the active zone over distances in excess of 100 nm (Hefft and Jonas, 2005; Ohana and Sakmann, 1998). Such microdomain coupling between VGCCs and the Ca^{2+} sensor substrate exhibits relatively prolonged global increases in Ca^{2+} levels at axonal varicosities, which have much slower kinetics than nanodomain Ca^{2+} transients (Atluri and Regehr, 1996; Eggermann et al., 2012).

In this chapter I attempt to further elucidate features of Ca^{2+} influx mechanisms that meditate AMPAR effects on release probability. Given the requirement for VGCCs in the mediation of presynaptic AMPAR effects on spontaneous release at MLI boutons that synapse onto other MLIs, I aimed to investigate if this was also true for MLI – Purkinje cell varicosities. Through the use of specific toxins, and Ca^{2+} chelators with differing binding

rates, it was possible to determine to what extent the VGCCs that mediated AMPAR effects resemble those at the active zone that support action potential-dependent release. Besides addressing the contribution of VGCCs, I present data to suggest that at MLI – MLI boutons, direct Ca^{2+} influx through CP-AMPARs may contribute to the effects on spontaneous release. Finally, following application of AMPA, I observed a reduction in mIPSC amplitude recorded from mechanically dissociated Purkinje cells, calling into question the role of CICR in mediating AMPAR effects on spontaneous release.

5.3 | Results

5.3.1 | VGCCs predominantly mediate presynaptic AMPAR effects on release probability

Voltage-clamp recordings from MLIs have demonstrated that VGCCs are required for AMPAR-mediated potentiation of mIPSC frequency (Bureau and Mulle, 1998). However, the contribution of VGCCs to the enhanced spontaneous release following AMPA treatment has not been determined at MLI boutons that contact Purkinje cells. I examined the effect of Cd^{2+}, a broad-spectrum blocker of VGCCs, on CNQX-induced potentiation of mIPSC frequency (Figure 3.3). Addition of Cd^{2+} had no significant effect on mIPSC frequency in recordings from MLIs (from 0.75 ± 0.23 in control to 0.62 ± 0.19 in Cd^{2+}; $n = 7$; $P = 0.16$; Wilcoxon matched-pairs test), nor from Purkinje cells where a control period was recorded (2.18 ± 0.70 in control to 2.39 ± 0.53 in Cd^{2+}; $n = 6$; $P = 0.84$; Wilcoxon matched-pairs test). This is in agreement with previous reports describing the Ca^{2+}-independent nature of spontaneous release from MLIs (Bureau and Mulle, 1998; Llano and Gerschenfeld, 1993). In the presence of 100 μM Cd^{2+}, the effects of CNQX were significantly reduced (normalised frequency 1.32 ± 0.05 and 1.24 ± 0.15, $n = 7$ and 11, respectively; $P = 0.0047$ and 0.00057 versus CNQX alone, Figure 5.1 *D*). In the presence of Cd^{2+} the residual effect of CNQX was significant in MLIs ($P = 0.016$) but not in Purkinje cells ($P = 0.15$) (Figure 5.1 *D*). These data suggest that activation of VGCCs underlies the action of γ-2-associated presynaptic AMPARs at both MLI-to-MLI and MLI-to-Purkinje cell synapses. The incomplete block by Cd^{2+} at MLI-to-MLI

synapses may reflect an additional direct influx of Ca^{2+} through CP-AMPARs (Bureau and Mulle, 1998; Rossi et al., 2008).

Several types of VGCCs have been shown to be present at presynaptic sites to mediate neurotransmitter release (subsection 1.4.1). At basket cell terminals that synapse onto Purkinje cells, action potential-driven Ca^{2+} transients result mainly from the activity of P/Q VGCCs, with some contribution of N-type VGCCs (Forti et al., 2000). To determine if the type(s) of VGCC(s) which mediate AMPAR effects on spontaneous release correspond to those involved in action potential-driven release, I tested the effect of AMPA on mIPSC frequency following incubation with the funnel web spider toxin Agatoxin. At concentrations of 50-100 nM, Agatoxin selectively blocks P/Q channels, whereas above 1 μM it also blocks N-type VGCCs (Sidach and Mintz, 2000). I recorded from mechanically dissociated Purkinje cells, to remove any potentially contaminating effects of somatodendritic depolarisation on release probability (Christie et al., 2011), and examined the contribution of P/Q- and N-type channels on AMPA-induced potentiation of quantal release (previously shown in Figure 3.6).

A 15 minute incubation in 1 μM Agatoxin had no significant effect on mIPSC frequency recorded from acutely dissociated Purkinje cells (from 0.19 $\pm$ 0.06 Hz in control to 0.30 $\pm$ 0.09 Hz following Agatoxin treatment, $n = 6$, $P = 0.063$, Wilcoxon matched-pairs test, data not shown). Thus, in agreement with previous voltage-clamp recordings from MLIs (Llano and Gerschenfeld, 1993) and Purkinje cells (Llano et al., 2000), this data demonstrates that spontaneous release of GABA from MLIs occurs irrespective of stochastic VGCC openings. In the presence of Agatoxin, application of 2 μM AMPA had no effect on mIPSC frequency (relative frequency; 0.91 $\pm$ 0.20, Figure 5.2 *A*, *B* & *D*, $n = 6$, $P = 1$, Wilcoxon matched-pairs test). Moreover, this lack of effect was significantly different from AMPA alone ($P = 0.0017$, Mann-Whitney U-test following a Kruskal-Wallis test between groups described in table 2.1; $\chi^2(5) = 23.39$, $P = 0.00028$). Thus, a combination of P/Q- and N-type VGCCs likely mediate both action potential-driven release (Forti et al., 2000) and presynaptic AMPAR-mediated enhancement of spontaneous release. Whether both actions involve the exact same population of P/Q- and/or N-type VGCCs is unknown.

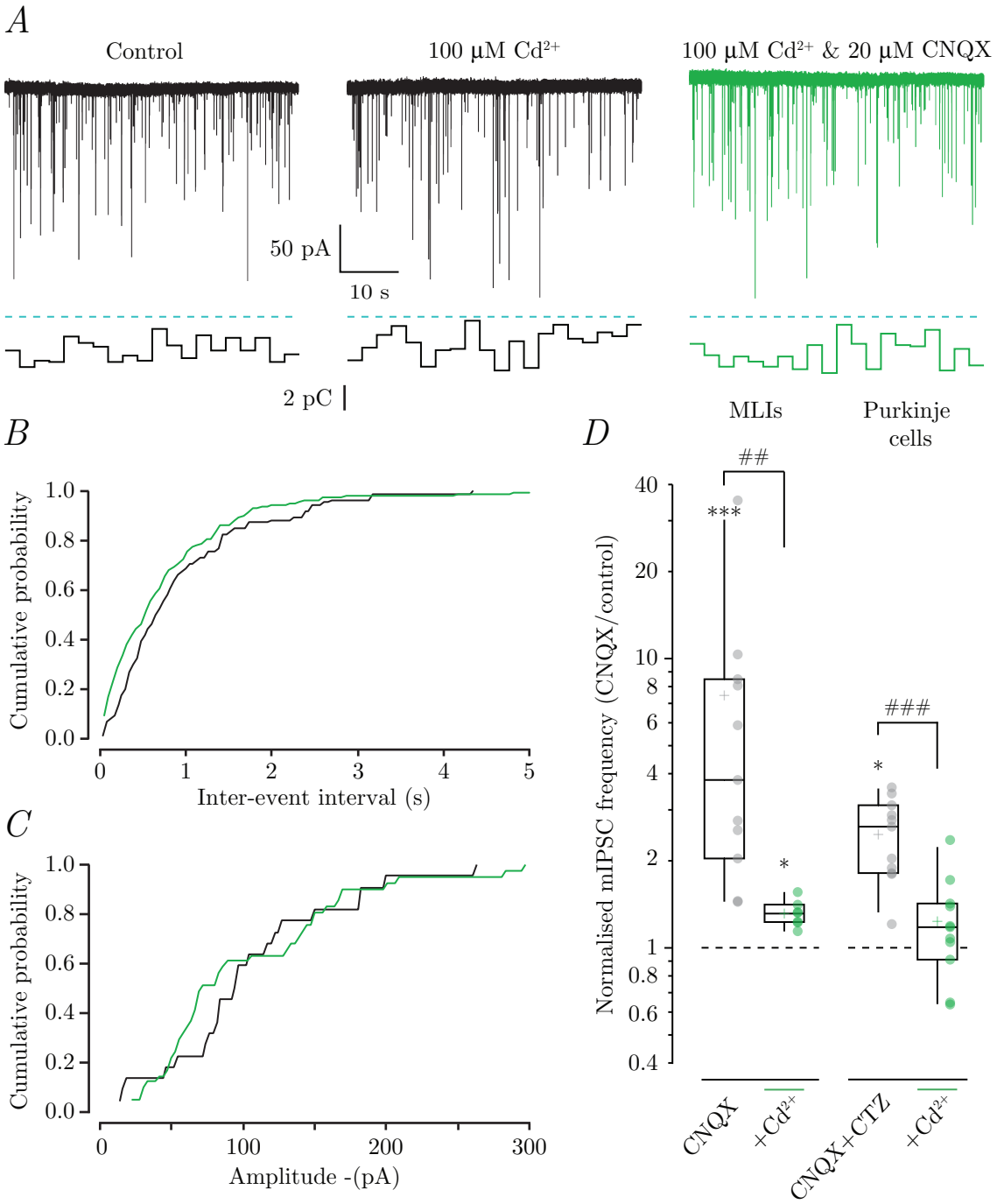

Figure 5.1: $CdCl_2$ strongly inhibits the action of γ-2-associated AMPARs on mIPSC frequency

(*A*) Representative current records and phasic charge transfer measurements from an MLI in a slice from a P11 wild-type mouse incubated in 100 μM $CdCl_2$ for 5 minutes. The effect of 20 μM CNQX is shown in green. Dashed lines refer to 0 charge. (*B* & *C*) Cumulative probability histograms of mIPSC inter-event interval and amplitude, respectively, from sample MLI recordings. (*D*) Pooled data showing the effects of CNQX on mIPSC frequency in the presence (green) and absence (grey) of Cd^{2+} when normalised to control recordings. Data are

Figure 5.1 continued: shown for P10-14 wild-type MLIs (left) and P10-14 wild-type Purkinje cells (right). For Purkinje cell recordings, the effect of 40 μM CNQX was tested in the presence of 50 μM CTZ. Box-and-whisker plots indicate the median (line), the 25-75$^{\text{th}}$ percentiles (box) and the 10-90$^{\text{th}}$ percentiles (whiskers); filled circles and crosses represent individual and mean values, respectively. *, ***, n.s. indicate P values < 0.05, 0.001 and > 0.05, respectively (Wilcoxon signed-rank test versus one). ## P <0.01 and ### P <0.001 (Mann-Whitney U-test versus CNQX in P10-14 cells, following Kruskal-Wallis tests that revealed a significant effect of group (Table 2.1); MLIs $\chi^2(4) = 26.9$, $P = 0.000021$; Purkinje cells $\chi^2(5) = 38.59$, $P = 0.00000029$).

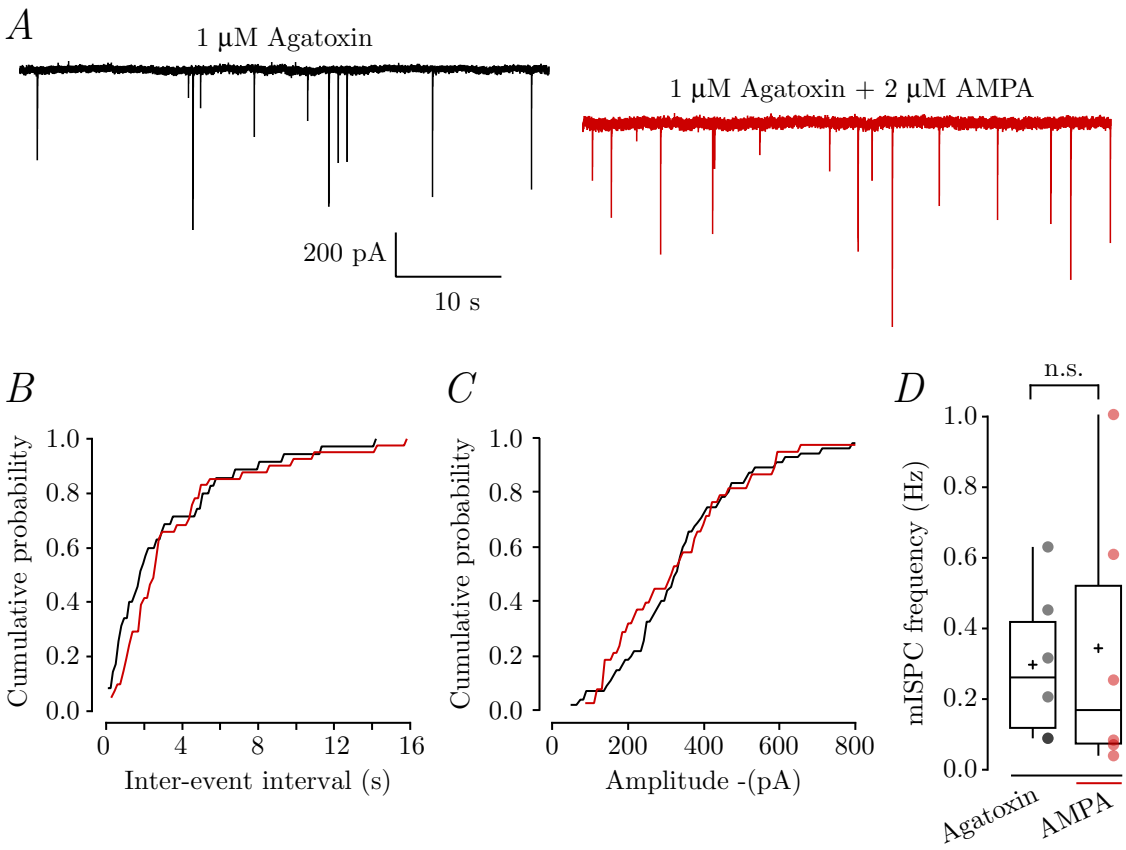

Figure 5.2: Agatoxin blocks AMPAR-mediated effects on mIPSC frequency

(*A*) Sample current records from a P10 wild-type mouse pretreated with 1 μM Agatoxin for 15 minutes, before and after 2 μM AMPA treatment. (*B* & *C*) Cumulative probability histograms of mIPSC inter-event interval and amplitude, respectively, corresponding to the Purkinje cell recording in *B*. (*E*) Pooled data showing the effects of AMPA on mIPSC frequency in P10-14 wild-type mechanically dissociated Purkinje cells. Box-and-whisker plots indicate the median (line), the 25-75$^{\text{th}}$ percentiles (box) and the 10-90$^{\text{th}}$ percentiles (whiskers); filled circles and crosses represent individual and mean values, respectively. n.s. indicate a P value > 0.05 (Wilcoxon matched-pairs test).

5.3.2 | VGCCs that mediate presynaptic AMPAR effects on release are remote from the active zone

At MLI boutons, VGCCs that translate action potential depolarisation into GABA release are coupled to the active zone within the nanodomain (Caillard et al., 2000; Christie et al., 2011) (section 1.4.2). It is not known whether presynaptic AMPARs modulate release probability through the same VGCC population, or act through a separate pool of VGCCs remote from the active zone. The relative binding rates of exogenous Ca^{2+} chelators allow one to distinguish between free Ca^{2+} originating at these two different locations (Adler et al., 1991; Eggermann et al., 2012). BAPTA binds Ca^{2+} very quickly, with a rate constant of 500 $\mu M^{-1} \cdot s^{-1}$ (Naraghi, 1997), and will buffer Ca^{2+} even across the short distances (10-20 nm) between VGCCs and vesicular synaptotagmins in the active zone (Ricci et al., 1998). The binding rate of EGTA is slower (2.7×10^6 $M^{-1} \cdot s^{-1}$; Naraghi (1997)), and thus EGTA is not able to attenuate this fast process, but it will buffer Ca^{2+} that diffuses to the active zone over larger, microdomain-coupled, distances (Eggermann et al., 2012).

To determine if the VGCCs that mediate presynaptic AMPAR effects on spontaneous release were coupled in the nano- or micro-domain, I tested the effects of Ca^{2+} chelators on the presynaptic AMPAR-induced enhancement of mIPSC frequency observed in Figure 3.11. Mechanically dissociated Purkinje cells were incubated with membrane permeable, acetoxymethyl (AM) ester forms of either BAPTA or EGTA $\geqslant$ 30 minutes prior to recording. Once inside a cell membrane, the AM ester is hydrolysed by cellular acetylesterases to a non-membrane-permeable form (Tsien, 1981). In experiments where a control period was recorded prior to BAPTA-AM (100 μM) incubation there was no significant change in basal mIPSC frequency (from 0.93 $\pm$ 0.52 Hz in control to 1.37 $\pm$ 1.01 Hz in BAPTA-AM, $n = 6$, $P = 0.31$, Wilcoxon matched-pairs test). Similarly, no difference was observed in mIPSC frequency between control condition (0.31 $\pm$ 0.06 Hz) and following a 30 minute EGTA-AM (100 μM) treatment (0.33 $\pm$ 0.09 Hz, $n = 10$, $P = 0.77$, Wilcoxon matched-pairs test).

In the presence of either chelator, application of 2 μM AMPA caused no change in mIPSC

frequency. With BAPTA treatment the mIPSC frequency showed no significant change from 1.44 ± 0.76 Hz to 1.86 ± 0.87 Hz ($n = 8$, $P = 0.078$, Wilcoxon matched-pairs test) (Figure 5.3 *A* & *C*). With EGTA pretreatment, mIPSC frequency went from 0.35 ± 0.06 Hz to 0.37 ± 0.05 Hz in AMPA ($n = 15$, $P = 0.42$, Wilcoxon matched pairs test) (Figure 5.3 *B* & *C*). The absence of effect in BAPTA and EGTA incubations was significantly different from treatment with AMPA alone ($P = 0.0079$ and 0.0017, respectively, Figure 5.3 *D*). Thus, presynaptic AMPARs potentiate spontaneous GABA release through the activation of P/Q- and/or N- type VGCCs located in the microdomain, separate to the P/Q- and/or N-type VGCCs at the active zone that meditate action potential-driven release (Christie et al., 2011; Forti et al., 2000).

AMPARs not only modulate spontaneous release, but also reduce the probability of action potential driven release (Figure 4.3, 4.5 and 4.12), potentially through the activation of P/Q-type VGCCs (Rusakov et al., 2005; Satake et al., 2004). It is plausible that such VGCCs either correspond to those distributed in the microdomain (which also mediate AMPAR effects on spontaneous release), or alternatively, are the same VGCCs that evoke action potential-dependent release in the active zone (Christie et al., 2011; Forti et al., 2000). To distinguish between these possibilities, the effect of AMPA was tested on IPSCs evoked from individual adherent boutons on acutely dissociated Purkinje cells (Figure 5.4). Mechanically dissociated Purkinje cells were incubated with 100 μM EGTA-AM for 30 minutes prior to recordings. It has been previously shown that EGTA-AM has no significant effect on evoked IPSC amplitude (Christie et al., 2011). In the presence of EGTA, AMPA had no significant effect on either IPSC peak amplitude (104 % of control value, $n = 6$, $P = 1$, Wilcoxon signed-rank test) (Figure 5.4 *A*, *B* & *C*), or measures of release probability (failure rate and CV were insignificantly increased by 11 and 2 %, respectively; $P = 0.56$ and 1, respectively; Wilcoxon signed-rank test, $n = 6$ for both measures) (Figure 5.4 *C*).

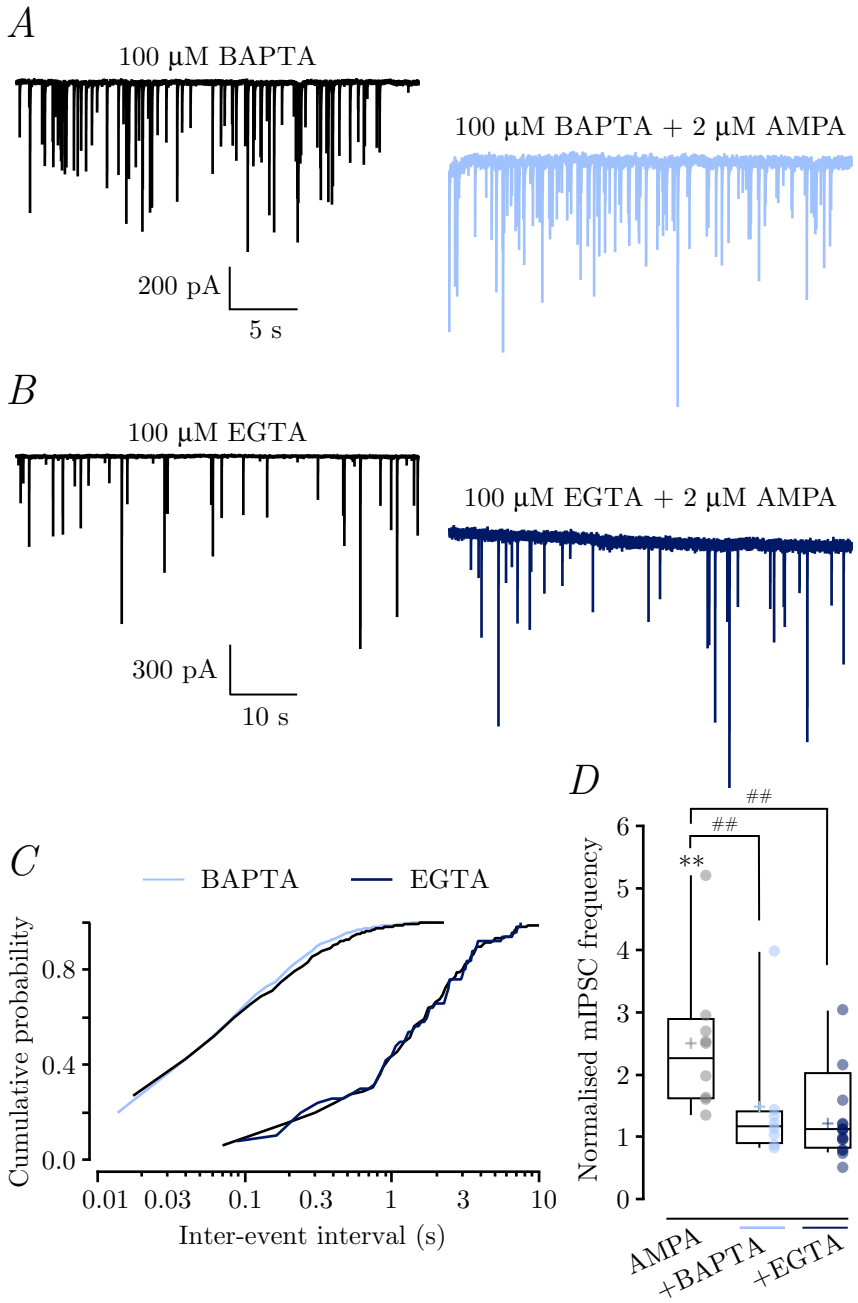

Figure 5.3: Fast and slow Ca^{2+} chelators block AMPAR-mediated modulation of spontaneous release

Representative recordings from mechanically dissociated Purkinje cells pre-incubated with either 100 μM BAPTA-AM (*A*) or 100 μM EGTA-AM (*B*), before and after 2 μM AMPA treatment. (*C*) Cumulative probability histograms of mIPSC inter-event interval corresponding to the Purkinje cell recording in *A* (left) and *B* (right). (*D*) Pooled data comparing the effects of AMPA on normalised mIPSC frequency in P10-14 wild-type mechanically dissociated Purkinje cells incubated with BAPTA-AM (light blue), EGTA-AM (dark blue) or neither (grey). Box-and-whisker plots indicate the median (line), the 25-75th percentiles (box) and the 10-90th percentiles

Figure 5.3 continued: (whiskers); filled circles and crosses represent individual and mean values, respectively. ** indicates $P < 0.05$ (Wilcoxon signed-rank test versus one). ## P <0.01, (Mann-Whitney U-test versus AMPA in P10-14 mechanically dissociated Purkinje cells, following a Kruskal-Wallis test (Table 2.1) that revealed a significant difference between groups; $\chi^2(5) = 23.39$, $P = 0.00028$).

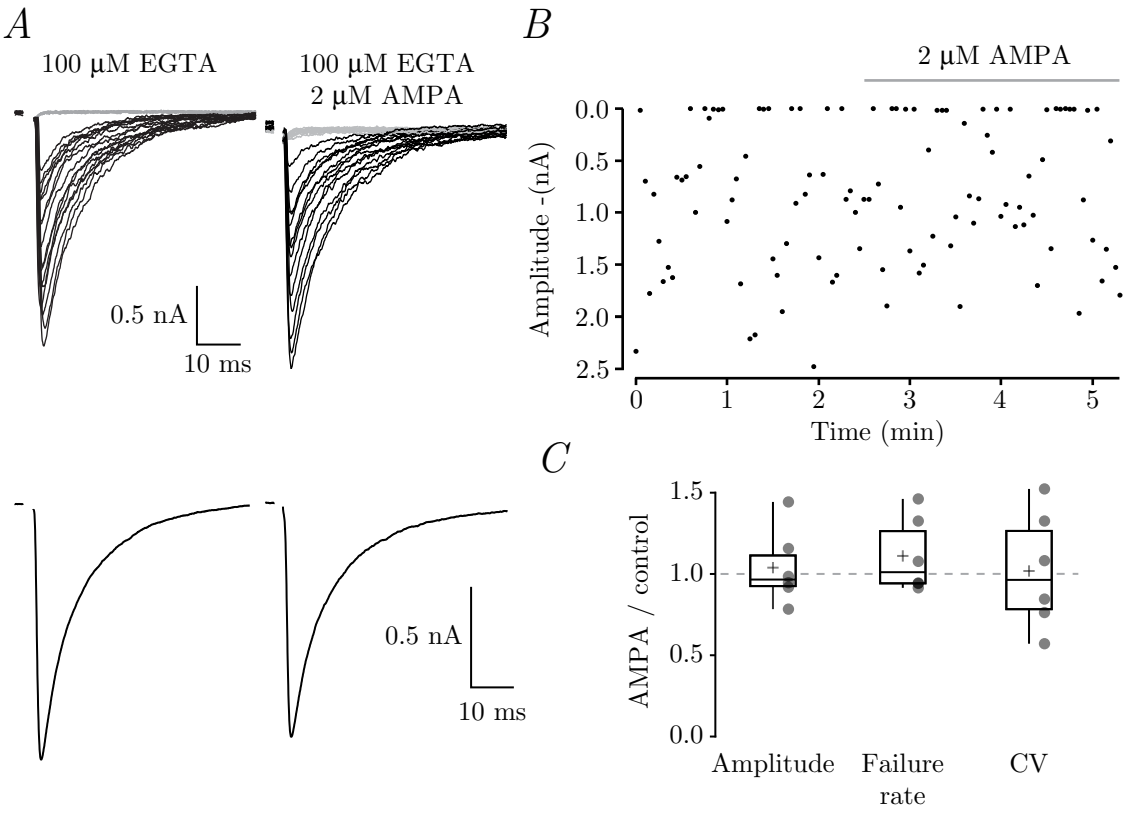

Figure 5.4: EGTA-AM abolishes the AMPAR-mediated reduction in evoked release (*A*) Top panels show selected sweeps from a sample P13 wild-type mechanically dissociated Purkinje cell, with success and failures of evoked release (in black and grey, respectively). Bottom panels show corresponding averaged evoked IPSCs. The effect of 2 μM AMPA was tested in the presence (right), and absence (left) of 100 μM EGTA-AM. (*B*) Time course of evoked IPSC peak amplitude from the same wild-type Purkinje cell as in *A*. Horizontal grey bar indicates the time period over which 2 μM AMPA was applied. (*C*) Pooled data showing application of AMPA did not alter IPSC peak amplitude, failure rate, or the CV of IPSC amplitude compared to control period. Box-and-whisker plots are as described in Figure 5.1.

5.3.3 | Presynaptic CP-AMPARs are associated with γ-2 at MLI – MLI boutons

In the presence of Cd^{2+}, a residual CNQX-induced increase in mIPSC frequency was observed in recordings from MLIs, but not Purkinje cells (Figure 5.1). This observation is consistent with the results of an earlier study in which slices were treated with the partial AMPA and kainate receptor agonist domoate (Bureau and Mulle, 1998). These authors originally speculated that the residual increase in mIPSC frequency may result from direct Ca^{2+} influx through CP-AMPARs. Indeed, it was subsequently found that MLI boutons which contact other MLIs contain predominantly CP- AMPARs whilst MLI – Purkinje cell boutons contain mostly CI-AMPARs (Rossi et al., 2008; Satake et al., 2006). Bats et al. (2012) have shown previously that CP- and CI-AMPARs can be differentially regulated by γ-2, which is required for efficient postsynaptic clustering of CI- but not CP-AMPARs in MLIs. To determine if CP-AMPARs are associated with γ-2, I examined the effect of CNQX on mIPSC frequency in the presence of PhTx-433, an open-channel blocker selective for CP-AMPARs. When wild-type slices were incubated in PhTx-433 (6 μM, 10 min), CNQX (20 μM) no longer produced a significant increase in MLI mIPSC frequency (normalised frequency 1.37 ± 0.25, $n = 7$, $P = 0.47$) or charge transfer (normalised charge 1.49 ± 0.23, n = 7, $P = 1.00$) (Figure 5.5 *A*, *B* & *D*). By contrast, PhTx-433 did not block the CNQX-induced increase in mIPSC frequency or charge transfer recorded in Purkinje cells (40 μM CNQX plus 50 μM cyclothiazide) (normalised frequency 2.82 ± 0.54, $n = 9$, $P = 0.0039$; normalised charge 2.46 ± 0.51, $P = 0.020$) (Figure 5.5 *D*).

5.3.4 | Presynaptic AMPARs preferentially increase the frequency of small mIPSCs at basket cell terminals

The application of 1 μM AMPA not only increased the frequency of mIPSCs from acute slice Purkinje cell recordings (Figure 3.6), but also their amplitude (2.11 ± 0.14 relative to control, $n = 10$, $P = 0.0020$, Wilcoxon signed-rank test). This result is consistent with an earlier study by Rossi et al. (2008) who report a ∼1.6 fold increase in amplitude. In this study they reasoned that Ca^{2+} influx through AMPARs sensitises ryanodine-sensitive

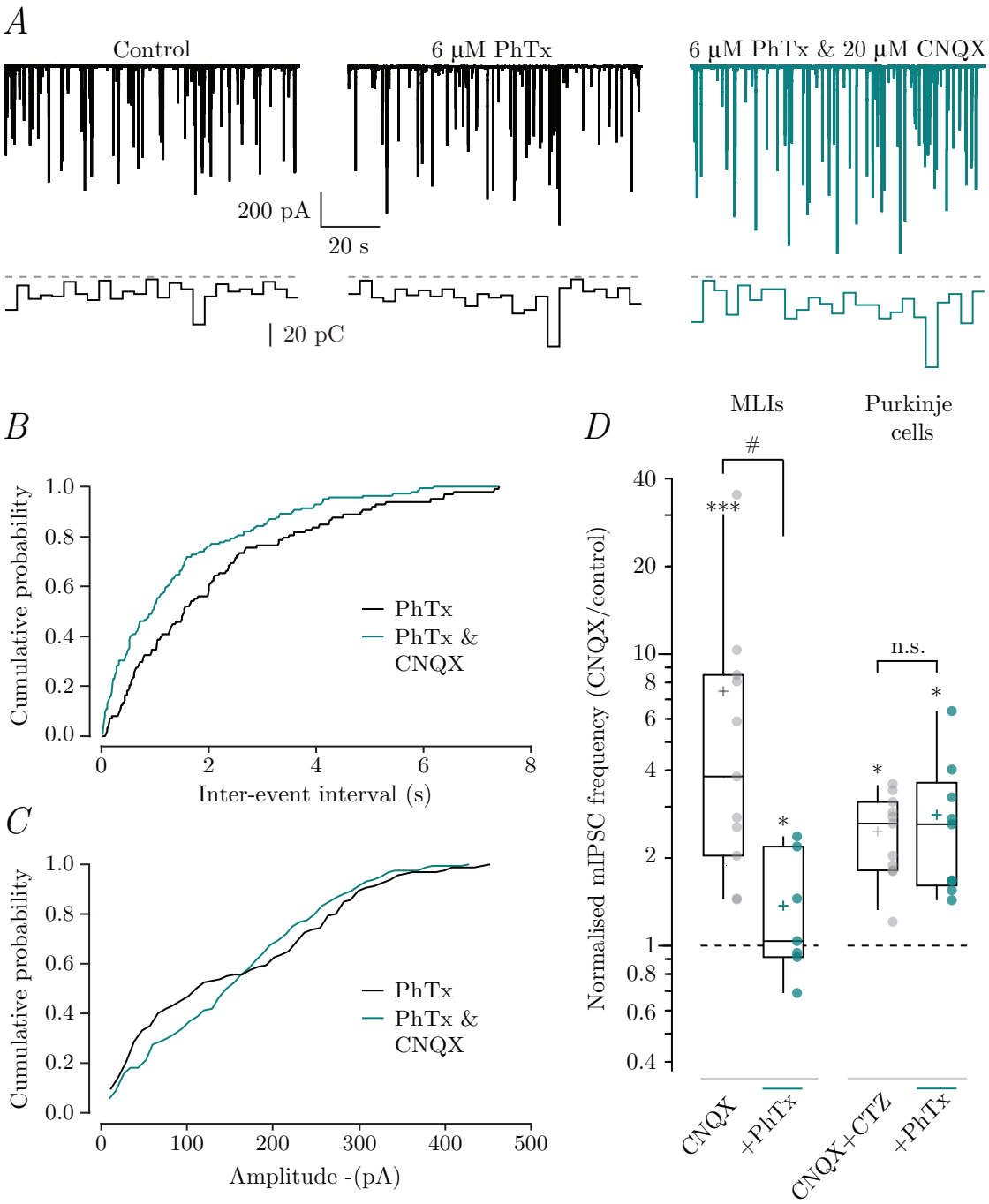

Figure 5.5: PhTx-433 inhibits AMPAR-induced potentiation of spontaneous release depending on postsynaptic neuron

(*A*) Representative current records and phasic charge transfer measurements from a MLI in a slice from a P13 wild-type mouse incubated in 6 μM PhTx-433 for 10 minutes. The effect of 20 μM CNQX in the presence (dashed lines indicate zero charge). (*B* & *C*) Cumulative probability histograms of mIPSC inter-event interval and amplitude, respectively, from sample MLI recordings. (*D*) Pooled data showing the effects of CNQX on mIPSC frequency when normalised to control recordings in P10-14 wild-type MLIs (left) and P10-14 wild-type Purkinje

Figure 5.5 continued: cells (right) within acute cerebellar slices. For Purkinje cell recordings, the effect of 40 μM CNQX was tested in the presence of 50 μM CTZ. Box-and-whisker plots indicate the median (line), the 25-75$^{\text{th}}$ percentiles (box) and the 10-90$^{\text{th}}$ percentiles (whiskers); filled circles and crosses represent individual and mean values, respectively. *, ***, n.s. indicate P values of < 0.05, 0.001 and > 0.05, respectively (Wilcoxon signed-rank test versus one). # P $<$0.05, (Mann-Whitney U-test versus CNQX in P10-14 cells, following a Kruskal-Wallis test that revealed a significant effect of group (Table 2.1); MLIs $\chi^2(4) = 26.9$, $P = 0.000021$; Purkinje cells $\chi^2(5) = 38.59$, $P = 0.00000029$).

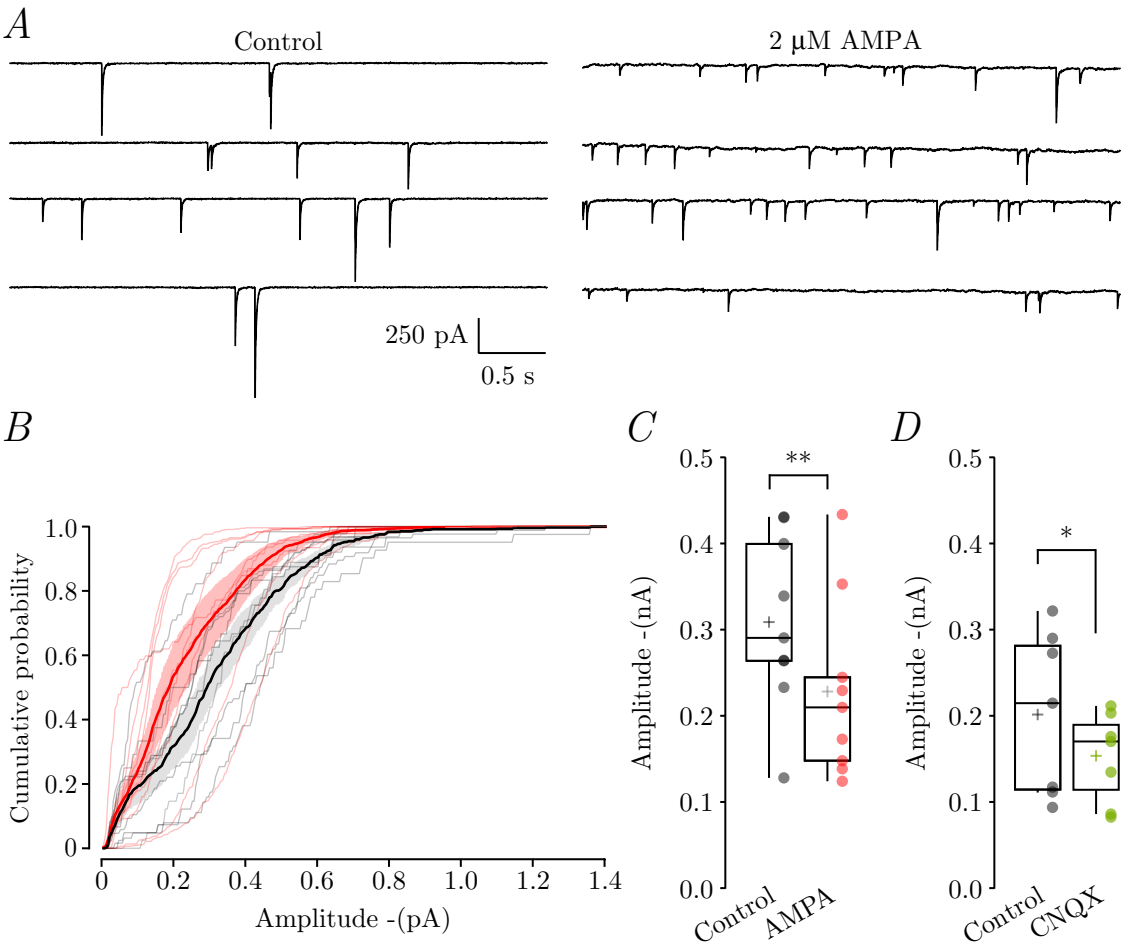

Figure 5.6: AMPAR agonists reduce mIPSC amplitude in mechanically dissociated Purkinje cells

(*A*) Representative recordings taken from a P10 Purkinje cell mechanically dissociated from a wild-type cerebellar slices before and after treatment with 2 μM AMPA. (*B*) Averaged cumulative probability histogram of mIPSC amplitude from ten cells; individual cells illustrated by feint black (control) and red (AMPA) lines. Thick lines and shaded regions represent the averages and SEMs, respectively. (*C* & *D*) Pooled data showing the effects of 2 μM AMPA and 40 μM CNQX (+ 40 μM cyclothiazide) on mIPSC amplitude in P10-14 wild-type mechanically dissociated Purkinje cells. Box-and-whisker plots indicate the median (line), the 25-75$^{\text{th}}$ percentiles (box) and the 10-90$^{\text{th}}$ percentiles (whiskers); filled circles and crosses represent individual and mean values, respectively. ** and * indicate P values < 0.01 and < 0.05, respectively (Wilcoxon matched-pairs test).

Ca^{2+} stores to promote CICR. As Ca^{2+} release from ryanodine-sensitive stores was thought to underlie the large amplitude mIPSCs observed in Purkinje cells by promoting multivesicular GABA release (Llano et al., 2000), Rossi et al. (2008) proposed that CICR was responsible for the AMPAR-mediated enhancement in mIPSC amplitude.

By comparison, mIPSCs recorded from mechanically dissociated Purkinje cells were reduced in amplitude following application of 2 μM AMPA (from 308.78 ± 33.65 pA in control to 228.17 ± 34.71 pA in AMPA, $n = 9$, $P = 0.0078$) (Figure 5.6 *A*, *B* & *C*), and 40 μM CNQX (plus 50 μM cyclothiazide) (from 203.06 ± 151.96 pA in control to 151.96 ± 19.86 pA following CNQX treatment, $n = 9$, $P = 0.047$) (Figure 5.6 *D*). Contrary to evidence from acute slices, the dissociated preparation suggests that presynaptic AMPAR-mediated potentiation of spontaneous release occurs independently of CICR. By enhancing the frequency of small amplitude mIPSCs that result from VGCC activation, without affecting the frequency of large amplitude IPSCs resulting from CICR, this could explain the overall reduction in average mIPSC amplitude from acutely dissociated Purkinje cell recordings.

5.4 | Discussion

In this chapter, I have examined the mechanisms that contribute to the effects of presynaptic AMPARs on release probability. I extend previous findings to suggest, akin to the MLI – MLI varicosities, γ-2-associated AMPARs at MLI boutons that synapse onto Purkinje cells predominantly mediate their effects on spontaneous release through VGCCs. In addition, I identify this population of VGCCs as containing P/Q and/or N subtypes, but unlike VGCCs which transform action potential invasion into transmitter release at the active zone, they reside as a separate population in the microdomain. I provide evidence that γ-2 regulates both CP- and CI-AMPARs, and that Ca^{2+} influx directly through CP-AMPARs may contribute to the enhanced spontaneous release. Finally, by investigating the amplitude of mIPSCs in mechanically dissociated Purkinje cells following treatment of AMPAR agonists, I question the hypothesis that ryanodine-sensitive Ca^{2+} stores are mechanistically involved in presynaptic AMPAR potentiation of spontaneous release at basket cell boutons.

5.4.1 | Presynaptic AMPARs activate microdomain coupled P/Q- and/or N-type VGCCs

P/Q- and N-type VGCCs have been shown to play a major role in action potential-driven Ca^{2+} signals within MLI axons (Forti et al., 2000). By testing the contribution of specific VGCC blockers on the AMPA-induced reduction in evoked IPSC amplitude, Satake et al. (2004) suggested presynaptic AMPARs mainly reduced release through regulation of P/Q VGCCs. However, the dramatic shift in IPSC amplitude baseline in the presence of Agatoxin observed in this study invalidated their further examination of the contribution of P/Q VGCCs to AMPAR function (Satake et al., 2004). As VGCCs are not normally involved in spontaneous GABA release, I avoided this experimental ambiguity to demonstrate presynaptic AMPARs activate P/Q- and/or N-type VGCCs to modulate release probability. Despite confirming previous suppositions, the relative contributions of P/Q- and N-type VGCCs were not tested. Neither were the exact subtypes of VGCCs involved in presynaptic AMPAR effects examined at MLI boutons that target other MLIs.

VGCCs that mediate AMPAR effects on both spontaneous and evoked release reside in the microdomain, distinct from the population of VGCCs that mediate action potential driven release at the active zone (Christie et al., 2011; Forti et al., 2000). Compared to nanodomain-coupled VGCCs, the activation of VGCCs loosely coupled to the active zone is likely to initiate a relatively slow rise in global terminal Ca^{2+} concentration with a prolonged decay (Atluri and Regehr, 1996; Eggermann et al., 2012).

Presynaptic NMDARs are also present at MLI – Purkinje cell boutons (Duguid and Smart, 2004; Duguid et al., 2007; Glitsch and Marty, 1999; Huang and Bordey, 2004). Given the role of VGCCs in AMPAR-mediated effects on release, it is surprising that NMDARs enhance both spontaneous and evoked release without modulating VGCC activity (Duguid and Smart, 2004). The conductance of AMPARs typically lies between 5 and 30 pS (Traynelis et al., 2010), and in cerebellar stellate cells, Liu and Cull-Candy (2005) reported conductances values of 5.5 and 7 pS. By comparison, NMDARs exhibit larger conductances between 20-60 pS (Traynelis et al., 2010), and in stellate cells

mean slope conductances of 57.2 pS and 50.2 pS were reported for synaptic and extra synaptic NMDARs, respectively (Clark et al., 1997). Given the respective single-channel conductances, one might expect NMDARs to elicit a greater membrane depolarisation than AMPARs and thus would be more likely to activate axonal VGCCs within MLI boutons.

The positioning of NMDARs within close proximity to the active zone could potentially explain this paradox. At nanodomain ranges, direct Ca^{2+} influx through the NMDAR channel could potentially sensitise Ca^{2+} sensors that initiate vesicular release. However, due to the presence of VGCCs in MLI active zones (Christie et al., 2011), NMDARs would likely increase their openings and thus their effect on release would show sensitivity to VGCC blockers. A more parsimonious explanation might be that presynaptic NMDARs, like presynaptic AMPARs, are coupled to the active zone in the microdomain, but do not closely associate with VGCCs. This theory would suggest a non-uniform distribution of VGCCs in the terminal, that functionally complex with AMPARs, but not NMDARs. Such a theory would assume that membrane depolarisation following iGluR activation was spatially limited. One way to determine whether AMPAR-activated VGCCs at MLI boutons are uniformly distributed, or occur in clusters, would be to test the effect of presynaptic AMPAR activation at various EGTA concentrations (Eggermann et al., 2012). If the block of AMPAR-potentiated release by EGTA was independent of concentration, it would suggest such VGCCs are non-uniformly clustered (Meinrenken et al., 2002).

5.4.2 | The role of alternative Ca^{2+} sources in mediating presynaptic AMPAR control on release

The presence of CP-AMPARs at MLI – MLI axonal boutons potentially provides an additional source of Ca^{2+} entry to promote spontaneous GABA release. This is not without precedent. AMPARs present at glutamate release sites on amacrine cell dendrites in the retina, have previously been shown to modulate release probability by direct Ca^{2+} entry through the AMPAR channel (Chávez et al., 2006). Moreover, direct Ca^{2+} entry through presynaptic NMDARs on lamprey reticulospinal axons has been proposed to contribute to the enhancement of action potential-driven release (Cochilla and Alford,

1999).

At basket cell boutons that synapse onto Purkinje cells, presynaptic AMPARs have been suggested to promote spontaneous release through the sensitisation of ryanodine-sensitive ER Ca^{2+} stores (Rossi et al., 2008). Following AMPAR activation, CICR from such stores would in theory be activated by the increased Ca^{2+} levels resulting from VGCC activity. This idea was supported by observations from Purkinje cell recordings in acute slices, where the treatment of ryanodine could further amplify the effect of AMPA on mIPSC frequency (Rossi et al., 2008). As CICR from ryanodine-sensitive stores is thought to underlie the large amplitude mIPSCs recorded from Purkinje cells (Llano et al., 2000), this mechanism provides an explanation as to why the amplitude of mIPSCs recorded from Purkinje cells in acute slices is enhanced following application of AMPA, shown in both my data (referred to in subsection 1.3.4), and as initially reported by Rossi et al. (2008). However, in my recordings from mechanically dissociated Purkinje cells, application of AMPA reduced mIPSC amplitude. This would suggest that the Ca^{2+} entering the bouton following presynaptic AMPAR activation is insufficient to evoke CICR. Thus, the number of mIPSCs resulting from VGCC Ca^{2+} entry is increased, yet the frequency of large amplitude mIPSCs that result from Ca^{2+} release from ryanodine-sensitive stores (known to occur spontaneously (Llano et al., 2000)), is unaltered. This would reduce the number of large-mIPSCs as a proportion of the total mIPSCs and have the net effect of reducing the average amplitude of mIPSCs.

The fact that both Rossi et al. (2008) and myself saw an increase in mIPSC amplitude in acute slice recordings may indicate that there was an unavoidable activation of somatodendritic MLI AMPARs with bath application of AMPA (that was obviously absent from dissociated Purkinje cell recordings). Recordings from MLIs in the presence of TTX, demonstrate a somatic depolarisation of $\geqslant$ 20 mV can passively spread down MLI axons to increase release probability (Christie et al., 2011). It could be argued that in slice experiments, application of AMPA promoted the passive spread of somatodendritic depolarisation to basket cell boutons (see section 3.4.1). The membrane depolarisation may have been large enough to trigger an influx of Ca^{2+} through VGCCs of sufficient magnitude to evoke CICR, thereby enhancing the frequency of large amplitude mIPSCs.

Indeed, in the dendrites of hippocampal pyramidal cells, subthreshold membrane depolarisation has been revealed to prime ryanodine-sensitive Ca^{2+} stores for release (Manita et al., 2007). Thus, my data suggest that at basket cell boutons, AMPAR activation enhances the entry of Ca^{2+} through VGCCs. The resulting increase in bouton Ca^{2+} levels promote the spontaneous release of GABA, but is of insufficient magnitude to drive CICR from ryanodine-sensitive stores.

6 | General Discussion

This thesis has addressed regulatory and mechanistic aspects of presynaptic AMPAR function, specifically in regard to the modulation of release probability in cerebellar molecular layer interneurons. In chapters 3 and 4, I established that TARP γ-2 can associate with presynaptic CI- and CP-AMPARs, and play a key role in the modulation of both evoked and spontaneous transmitter release. This was readily apparent from the attenuated effects of AMPAR activation on evoked- and miniature IPSCs in *stg/stg* mice, and by the TARP-dependent actions of CNQX. Importantly, the actions of CNQX could be replicated in mechanically dissociated cells, demonstrating that they arose from direct activation of TARPed presynaptic AMPARs. This contrasts with the situation for presynaptic KARs, where the analogous transmembrane auxiliary protein NETO-1 does not appear necessary for either their presynaptic localisation or function (Copits and Swanson, 2012; Straub et al., 2011). Chapter 5 addressed the mechanism of presynaptic AMPAR function. Spontaneous release from MLI boutons was potentiated by AMPARs mainly through the activation of P/Q- and/or N-type VGCCs. Recordings from Purkinje cells, pre-incubated with the slow binding Ca^{2+} chelator EGTA, suggests that such VGCCs are remote from the active zone and distinct from the nanodomain-coupled VGCCs that couple spike invasion to GABA release.

6.1 | Impact of TARP association for presynaptic AMPARs

For postsynaptic AMPARs, TARPs are known to promote their dendrite-selective sorting (Matsuda et al., 2008b), cell surface delivery (Tomita et al., 2003; Vandenberghe et al., 2005) and synaptic accumulation (Bats et al., 2007; Chen et al., 2000; Howard et al., 2010). Although little is known about the targeting and stabilisation of presynaptic AMPARs, my findings indicate that this may involve similar TARP-dependent processes. In hippocampal neurons and Purkinje cells, following AMPAR export from the Golgi apparatus, TARP interaction with the μ4 subunit of the clathrin-based AP-4 is necessary

for their somatodendritic targeting (Matsuda et al., 2008b). Axonal targeting could involve suppression of this interaction, potentially through phosphorylation of serine or threonine residues in the TARP C-terminal (Matsuda et al., 2008b). At the PSD, interactions of the C-tail of γ-2, γ-3, γ-4 and γ-8 with MAGUKs such as PSD-95 and SAP-97 are important for AMPAR accumulation and stability (Bats et al., 2007; Chen et al., 2000; Howard et al., 2010). At presynaptic sites, similar interactions with SAP-97 or SAP-90, both of which are present in terminals (Kistner et al., 1993; Klöcker et al., 2002), could be important for AMPAR accumulation and stabilisation.

Irrespective of their precise influence on AMPAR number and stability at axonal boutons, TARPs are known to affect AMPAR functional properties, and would thus lead to increased charge transfer and, for CP-AMPARs, greater direct Ca^{2+} influx. In MLIs, the loss of γ-2 in *stg/stg* mice is known to reduce the weighted mean single-channel conductance of synaptic AMPARs by ∼50% (Bats et al., 2012). Correspondingly, the conductance of recombinant CP- (homomeric GluA1, GluA3 and GluA4) and CI-AMPARs (GluA1/A2) is increased by 50-70% when expressed with γ-2 (Bats et al., 2012; Coombs et al., 2012; Soto et al., 2009). In addition, γ-2 slows desensitisation by 20-100% (Coombs et al., 2012; Soto et al., 2009; Milstein et al., 2007; Suzuki et al., 2008; Turetsky et al., 2005) and increases glutamate potency (for homomeric GluA1 the EC50 is reduced by ∼3-6-fold Kott et al. (2007); Priel et al. (2005); Tomita et al. (2005); Yamazaki et al. (2004)). For CP-AMPARs, γ-2 also attenuates (and speeds recovery from) the voltage-dependent block by endogenous intracellular polyamines (Soto et al., 2007) and enhances relative Ca^{2+} permeability (Coombs et al., 2012; Kott et al., 2009).

Together, these effects are expected to increase glutamate potency to broaden the spatial extent over which glutamate spillover is capable of influencing GABA release and thus potentially increase the number of MLI boutons affected. At each bouton, γ-2 association will serve to enhance charge transfer via presynaptic CI- and CP-AMPARs as well as increase direct Ca^{2+} entry via CP-AMPARs. The greater charge transfer conferred by γ-2 association would produce a correspondingly larger terminal depolarisation and thus enhance VGCC activation. This amplification may allow modulation of release by a small number of AMPARs, which could be potentially important given the spatially constrained

environment of a presynaptic site.

6.2 | Presynaptic γ-2-associated AMPARs potentially promote a prolonged waveform of residual Ca^{2+}

γ-2-associated AMPARs predominantly promote spontaneous GABA release from MLIs through the activation of VGCCs. Data in chapter 5 suggest that P/Q- and/or N-type VGCCs activated by presynaptic AMPARs are coupled to MLI active zones in the microdomain. If we assume the Ca^{2+} flux following AMPAR and VGCC activation experiences similar regulation as the Ca^{2+} signals resulting from an action potential, the elevated Ca^{2+} levels will potentially exhibit a biphasic exponential decay (Collin et al., 2005a; Rusakov et al., 2005). At rest, Ca^{2+} concentrations of 40 and 100 nM have been reported in MLI terminals (Collin et al., 2005a; Eggermann and Jonas, 2012; Rusakov et al., 2005). Following AMPAR and VGCC activation, there is likely to be a relatively high and brief Ca^{2+} transient, although the peak concentration is unknown. This will rapidly decay as a result of Ca^{2+} extrusion mechanisms (Ca^{2+}-ATPase, Na^{+}/Ca^{2+} exchangers), diffusion, and binding of fast Ca^{2+} buffers (Collin et al., 2005a; Eggermann and Jonas, 2012; Rusakov et al., 2005), to leave a reduced level of Ca^{2+} which decays at a slower rate. Due to the microdomain proximity of the VGCCs from the active zone, the facilitation of GABA release by presynaptic AMPARs is likely to be mainly dependent on this remaining residual Ca^{2+} concentration (Atluri and Regehr, 1996). Indeed, a computational model of microdomain coupled VGCCs in hippocampal interneuron boutons suggests that the Ca^{2+} sensors which initiate release would be exposed to a slow rising and prolonged waveform of residual Ca^{2+} concentration (Goswami et al., 2012). At a coupling distance of 200 nm, spontaneous VGCC openings in response to a 1.5 s, 20 mV, depolarisation took $\sim$ 500 ms to have a noticeable effect on release rate, which slowly increased until depolarisation ceased. This contrasts to the nanodomain coupled Ca^{2+} transients which had relatively immediate effects on release rate lasting $<$ 50 ms (Goswami et al., 2012). Thus, it is plausible that activation of presynaptic AMPARs in MLI boutons produces a relatively slow build up of residual Ca^{2+}, perhaps akin to that which follows an action potential to evoke asynchronous release.

A number of mechanisms regulate Ca^{2+} concentration within MLI boutons. The exponential decay of residual Ca^{2+} concentration is thought to be strongly modulated by mobile Ca^{2+} buffers such as parvalbumin (Collin et al., 2005a). MLIs contain high concentrations of parvalbumin with estimates ranging from 0.15 and 1 mM (Caillard et al., 2000; Collin et al., 2005a; Eggermann and Jonas, 2012; Rusakov et al., 2005). During development, parvalbumin levels rise, whereas the influence of an unidentified fast Ca^{2+} buffer decreases (Collin et al., 2005a). At the P10-14 age range examined here, parvalbumin is present at higher levels in basket cell boutons, than stellate cell boutons (Collin et al., 2005a). The presence of parvalbumin acts to accelerate the initial decay phase of Ca^{2+} concentration, aided by its binding to Mg^{2+} which preserves its free concentration levels (Eggermann and Jonas, 2012). However, during the exponential decay of residual Ca^{2+}, the dissociation of Ca^{2+} from parvalbumin prolongs its terminal concentration above resting values (with a time constant of 0.6 s) (Collin et al., 2005a), thus exposing the release machinery to more extended periods of residual Ca^{2+}.

The prolongation of residual Ca^{2+} levels by parvalbumin may be of crucial importance for AMPAR-mediated effects on spontaneous release at basket cell terminals. Recent evidence from cholecystokinin-containing interneurons in the hippocampus suggests that microdomain coupling of VGCCs may produce conditions more favourable for higher levels of spontaneous activity than nanodomain coupled VGCCs, especially when the Ca^{2+} extrusion rate and buffer levels are low and the Ca^{2+} sensor affinity is high (Goswami et al., 2012). Moreover, asynchronous neurotransmitter release from MLI boutons was found to be reduced in the absence of parvalbumin (Collin et al., 2005a). If the waveform of Ca^{2+} resulting from presynaptic AMPAR activation is indeed similar to that which promotes asynchronous release, then it is plausible that parvalbumin may be crucial for the effects of AMPARs on GABA release from MLIs.

Accurate knowledge of the number of VGCCs activated by presynaptic AMPARs and the resulting Ca^{2+} waveform experienced by the exocytotic Ca^{2+} sensors requires values of Ca^{2+} concentrations resulting from presynaptic AMPAR and subsequent VGCC activation. Ca^{2+} imaging experiments of basket cell axonal boutons using the Ca^{2+} indicator OGB-1 demonstrated that whilst action potentials evoked a $\sim$20% change

in fluorescence (corresponding to a intraterminal concentration between 3-5 μM), puff application of AMPA or glutamate had no significant effect (Rusakov et al., 2005). This result was surprising given the clear dependence on VGCCs for AMPAR-mediated effects on spontaneous release, but could suggest that AMPARs elicit a relatively low Ca^{2+} influx, below the noise of the recording. Indeed, estimates of residual levels of Ca^{2+} following an action potential range between 115-130 nM (Rusakov et al., 2005), less than the K_d of OGB-1 $\approx$ 0.2 μM (Collin et al., 2005a; Hendel et al., 2008). It is likely that the number of VGCCs opened by presynaptic AMPAR activation is far below the 100-200 channels estimated to give rise to the action potential driven Ca^{2+} transient at basket cell terminals (Rusakov et al., 2005). Rather, the activity of a small number of presynaptic AMPARs and associated VGCCs may raise inter-terminal Ca^{2+} concentrations only by nanomolar concentrations, below the sensitivity of Ca^{2+} indicators. Sparse levels of AMPARs and/or associated VGCCs in MLI varicosities would place greater weight on the charge transfer through an individual AMPAR, potentially further highlighting the importance of γ-2 association for effects on release probability.

6.3 | Differential regulation of CP- and CI-AMPARs

MLIs express both CP- and CI-AMPARs. Bats et al. (2012) have shown previously that these can be differentially regulated by γ-2, which is required for efficient postsynaptic clustering of CI- but not CP-AMPARs. MLI boutons that contact other MLIs contain predominantly CP- AMPARs whilst MLI-Purkinje cell boutons contain mostly CI-AMPARs (Figure 4) (Rossi et al., 2008). If the differential TARP regulation of postsynaptic CP- and CI-AMPARs seen in MLIs were conserved at presynaptic sites, one might have expected CI-AMPARs at MLI – Purkinje cell boutons to be disproportionately affected by the loss of γ-2 in *stg/stg* mice. Paradoxically, the AMPA-induced increase in mIPSC frequency was similarly reduced at both types of synapse. This may suggest that CI- and CP-AMPARs in boutons are equally reliant on γ-2 for their accumulation, unlike the situation described at postsynaptic sites (Bats et al., 2012). Alternatively, at MLI – MLI boutons in *stg/stg* mice, CP-AMPARs lacking γ-2 may be present but their conductance reduced such that it is insufficient to depolarise the membrane and activate VGCCs.

Evidence from mechanically dissociated Purkinje cells suggest that presynaptic AMPARs were unable to modulate GABA release in the absence of γ-2. Thus, although MLIs also express the atypical TARP γ-7 (Fukaya et al., 2005; Yamazaki et al., 2010), it appears unlikely that a population of presynaptic AMPARs exclusively associates with γ-7. Similarly, it seems unlikely that the cornichons (CNIH-2 and CNIH-3) modulate presynaptic AMPARs in MLIs; despite their expression in the molecular layer (Schwenk et al., 2009), they do not appear to reach the surface of cerebellar cells (Gill et al., 2011). Both CKAMP44 (von Engelhardt et al., 2010) and synDIG1 (Kalashnikova et al., 2010) are present in the cerebellum, but there is currently little detailed information about their cellular location. Moreover, there is conflicting evidence as to whether synDIG1 is a bonafide auxiliary protein (Lovero et al., 2013). It is unknown whether GSG1L (Schwenk et al., 2012; Shanks et al., 2012) is present in the cerebellum.

6.4 | Significance of presynaptic auxiliary proteins for synaptic function

It seems likely that under normal circumstances all somatodendritic AMPARs associate with auxiliary transmembrane proteins. My findings raise the possibility that such proteins may play a universal role in the modulation of presynaptic AMPARs. In so doing they may influence a variety of functions known to be regulated by the activation of presynaptic AMPARs, including the transmission of sensorimotor information in the cerebellum (Satake et al., 2000), noxious and non-noxious sensory signals in the spinal cord (Engelman et al., 2006; Lee et al., 2002) and auditory information in the brainstem (Takago et al., 2005). The importance of auxiliary protein association and VGCC mediation for presynaptic AMPAR function may not be limited to the direct modulation of neurotransmitter release at established synapses. For example, activation of AMPARs on axonal growth cones both inhibits the motility of filopodia (Chang and Camilli, 2001) and enhances synaptic vesicle cycling (Schenk et al., 2005), potentially facilitating synaptogenesis. The influence of presynaptic AMPARs also extends to the modulation of action potential propagation; when activated by astrocytic glutamate release, AMPARs on CA3 pyramidal cell axons bring about depolarisation that inactivates

potassium channels, broadening the action potential waveform (Sasaki et al., 2011).

In conclusion, my work suggests that MLI γ-2-associated AMPARs predominantly modulate GABA release through the activation of microdomain coupled P/Q-type and/or N-type VGCCs. Loss of γ-2 in *stg/stg* mice prevents the normal function of presynaptic AMPARs in MLIs. This provides direct evidence that auxiliary transmembrane proteins can associate with presynaptic iGluRs and suggests that, for TARPs at least, their influence extends to all neuronal domains.

6.5 | Future directions

Whilst I have determined that γ-2 is essential for presynaptic AMPAR function, I have not addressed the exact molecular or biophysical mechanisms by which γ-2 plays a role. Assuming that γ-2 physically associates with presynaptic AMPARs, one wonders whether γ-2 regulates the biophysical properties of presynaptic AMPARs, or whether γ-2 regulates the localisation and trafficking of AMPARs, or, as with postsynaptic AMPARs, regulates both trafficking *and* gating. Antibody labelling of axonal AMPARs in cerebellar slices from wild-type and *stg/stg* mice may provide one way to address if TARPs promote presynaptic AMPAR trafficking. To determine if the gating of presynaptic AMPARs is modulated by γ-2 association, outside-out patches could be pulled from cerebellar basket cell boutons from acute slices (Southan and Robertson, 1998), or cultured cerebellar interneurons (Fiszman et al., 2007). Ultrafast application of AMPA or glutamate would provide information on the desensitisation and deactivation kinetics of presynaptic AMPARs, as well as their mean single-channel conductance. The influence of γ-2 would be determined by comparing between currents from wild-type and *stg/stg* mice. If presynaptic AMPARs are dependent on γ-2 for their trafficking to presynaptic sites, it could be possible that no currents are observed from outside-out patches from *stg/stg* MLI boutons.

At the PSD, it is understood that AMPARs constitutively recycle to and from the membrane through well characterised mechanisms (Anggono and Huganir, 2012). The corresponding endocytic and exocytic processes that control AMPAR surface expression

at the presynaptic membrane are poorly characterised. One study, of hippocampal growth cones, suggests that presynaptic AMPARs are trafficked to and from the membrane via synaptic vesicles (Schenk et al., 2003). Synaptic vesicles typically fuse with the membrane at active zones, yet data from chapter 5 suggest that presynaptic AMPARs are located in the microdomain. Does this discrepancy reflect a difference between growth cones and established synapses? Or, do AMPARs exhibit significant lateral movement away from active zones following membrane incorporation? Synaptic vesicles are thought to primarily endocytose at locations coupled to the active zone within the nanodomain (Teng and Wilkinson, 2000; Yamashita et al., 2010). Does this then require presynaptic AMPARs to move laterally back towards active zones to be internalised? The lateral mobility of AMPARs could be tested through real-time imaging of AMPARs tagged with a fluorescent marker. Single-molecule imaging through small and stable fluorophores such as quantum dots may provide a useful measure of AMPAR membrane mobility. This technique may further allow one to determine if presynaptic AMPARs are stabilised within the presynaptic membrane through interactions between the TTPV C-tail motif of γ-2 and MAGUKs, as observed at the PSD (Bats et al., 2007; Sainlos et al., 2011).

At a general level, it may be interesting to know what processes promote the sorting of AMPARs to the axon rather than the dendrite. More specifically, the processes that dictate the selective sorting of CP-AMPARs to MLI – MLI boutons and CI-AMPARs to MLI – Purkinje cell axonal boutons are unknown. It may be conceivable that this inter-bouton heterogeneity relies on specific retrograde signals from distinct postsynaptic target neurons. Such knowledge would be interesting given the target-dependent expression of presynapitc iGluRs observed in a number of neurons (Figure 1.7; subsection 1.3.2). As mentioned, an interaction between AP-4 and TARPs in the ER has been described to promote the dendritic sorting of AMPARs (Matsuda et al., 2008b). Could it be possible that this signalling is suppressed during development and turned on around P15 when the effects of presynaptic AMPAR activation are lost? The reasons for the developmental loss of presynaptic AMPARs at MLI axonal varicosities is unknown, but it may not be a coincidence that they are lost around the same time that the molecular layer stops expanding. Consistent with their role in synapse formation (Chang and Camilli,

2001), their developmental expression may reflect a role in the formation of GABAergic innervation in the molecular layer.

The mechanism that mediates presynaptic AMPAR suppression of action potential-driven release from MLIs remains contentious. As described earlier, assertions that a direct interaction between presynaptic AMPARs and the $G_{i/o}$-protein was responsible for the suppression of release, were complicated by the use of N-ethylmaleimide to block G-protein binding (Satake et al., 2004) (subsection 5.2). Recordings of mIPSC frequency from Purkinje cells incubated with pertussis toxin, may allow for a more valid test of a potential G-protein interaction. However, pertussis toxin experiments are time-consuming, often requiring long incubations that are unsuitable for acute slice recordings. To overcome this difficultly, a protocol to maintain mechanically dissociated Purkinje cells in cell culture media could be attempted. This would have the additional advantage of removing the potentially confounding influence of somatodendritic AMPARs. Other mechanisms that may have accounted for the presynaptic AMPAR-induced suppression of evoked GABA release include shunting inhibition as a result of the combined conductance through AMPARs and VGCCs positioned at microdomain (Segev, 1990), or a depolarisation-evoked inactivation of Na^+ channels (Graham and Redman, 1994). To differentiate between these two alternatives, it may be informative to test the effect of an equivalent conductance in a computer simulation of action potential invasion at MLI boutons. However, this model may require more accurate information on the number, conductance and location of both AMPARs and subsequently activated VGCCs present in MLIs axonal varicosities. One might predict that a mechanism which involves the inactivation of Na^{2+} channels would slow the rising phase of the action potential, thus reducing the speed of neurotransmission. Though there was no significant difference in the latency of IPSC onset in paired MLI–MLI recordings in control and CNQX conditions (Figure 4.10 *E*), there was a trend to increase, which may have been revealed to be significant with a more powerful statistical test, or a greater number of recordings ($n = 6$).

The contribution of ryanodine-sensitive Ca^{2+} stores to presynaptic AMPAR effects requires further study. In chapter 5, I suggest that the activation of somatodendritic AMPARs, but not presynaptic AMPARs, may have been responsible for the increased

amplitude of mIPSCs in acute slice recordings, as well as the previously reported effects of ryanodine and dantrolene on mIPSC frequency (Rossi et al., 2008). By examining the effect of AMPA on mIPSC frequency from mechanically dissociated Purkinje cells in the presence of ryanodine or dantrolene, it might be possible to confirm or reject the contribution of CICR to presynaptic AMPAR effects on spontaneous release.

Both AMPARs and NMDARs are expressed at MLI boutons, yet following the synaptic release of glutamate, their coincidental activation has never been described. For example, parallel fibre stimulation evoked Ca^{2+} transients were observed in axons of MLIs, likely to be stellate cells (Rossi et al., 2008). Such currents were blocked by GYKI 53556 but not D-APV, to suggest that presynaptic AMPARs, but not preysnaptic NMDARs were activated. Parallel fibre stimulation was further shown to reduce the autaptic/autoreceptor current in stellate cells (Liu, 2007). This effect was blocked by AMPAR antagonists, but not NMDAR blockers. However, another study found parallel fibre stimulation could activate presynaptic NMDARs to produce a long-term enhancement of the autaptic/autoreceptor current (Liu and Lachamp, 2006). At basket cell terminals, the reduction of evoked GABA release following spillover of climbing fibre glutamate was unaltered in the presence of D-APV, but markedly suppressed by the AMPAR blocker GYKI 53655 (Satake et al., 2000). In another study, climbing fibre-released glutamate was found to enhance mIPSC frequency in Purkinje cells, an effect that was attributed to the activation of NMDARs (Duguid and Smart, 2004). This study found that climbing fibre glutamate did not spillover to MLI boutons to activate presynaptic NMDARs, but rather depolarised Purkinje cell dendrites to elicit a retrograde release of glutamate. Although one would expect a concomitant effect of climbing fibre glutamate on presynaptic AMPARs, there was no mention to their involvement in the modulation on GABA release in these experiments. Do these experiments suggest that presynaptic iGluRs are targeted to separate MLI boutons and are differentially activated according to the specific waveform of spillover or retrograde glutamate? Or can both iGluRs exist at the same MLI bouton and simultaneously contribute to effects on GABA release? To differentiate between these two possibilities, the effect of glutamate could be tested on evoked GABA release stimulated from a single MLI bouton in the dissociated

Purkinje cell preparation. The effects on release in the presence and absence of AMPAR and NMDAR blockers may reveal if both iGluRs occur at the same bouton, and if so, will allow one to determine the net effect of their simultaneous activation.

References

Abrahamsson, T., Cathala, L., Matsui, K., Shigemoto, R. and DiGregorio, D. A. (2012). Thin dendrites of cerebellar interneurons confer sublinear synaptic integration and a gradient of short-term plasticity. Neuron *73*, 1159–72.

Adesnik, H., Nicoll, R. A. and England, P. M. (2005). Photoinactivation of native AMPA receptors reveals their real-time trafficking. Neuron *48*, 977–85.

Adler, E. M., Augustine, G. J., Duffy, S. N. and Charlton, M. P. (1991). Alien intracellular calcium chelators attenuate neurotransmitter release at the squid giant synapse. The Journal of Neuroscience *11*, 1496–507.

Akaike, N. and Moorhouse, A. J. (2003). Techniques: applications of the nerve-bouton preparation in neuropharmacology. Trends in Pharmacological Sciences *24*, 44–7.

Akaike, N., Murakami, N., Katsurabayashi, S., Jin, Y.-H. and Imazawa, T. (2002). Focal stimulation of single GABAergic presynaptic boutons on the rat hippocampal neuron. Neuroscience Research *42*, 187–95.

Alle, H. and Geiger, J. R. P. (2006). Combined analog and action potential coding in hippocampal mossy fibers. Science *311*, 1290–3.

Allen, C. and Stevens, C. F. (1994). An evaluation of causes for unreliability of synaptic transmission. Proceedings of the National Academy of Sciences of the United States of America *91*, 10380–3.

Allison, D. W., Gelfand, V. I., Spector, I. and Craig, A. M. (1998). Role of actin in anchoring postsynaptic receptors in cultured hippocampal neurons: differential attachment of NMDA versus AMPA receptors. The Journal of Neuroscience *18*, 2423–36.

Anderson, D., Mehaffey, W. H., Iftinca, M., Rehak, R., Engbers, J. D. T., Hameed, S., Zamponi, G. W. and Turner, R. W. (2010). Regulation of neuronal activity by Cav3-Kv4 channel signaling complexes. Nature Neuroscience *13*, 333–7.

Angelotti, T. P. and Macdonald, R. L. (1993). Assembly of GABAA receptor subunits: alpha 1 beta 1 and alpha 1 beta 1 gamma 2S subunits produce unique ion channels with dissimilar single-channel properties. The Journal of Neuroscience *13*, 1429–40.

Anggono, V. and Huganir, R. L. (2012). Regulation of AMPA receptor trafficking and synaptic plasticity. Current Opinion in Neurobiology *22*, 461–9.

Ango, F., Wu, C., der Want, J. J. V., Wu, P., Schachner, M. and Huang, Z. J. (2008). Bergmann glia and the recognition molecule CHL1 organize GABAergic axons and direct innervation of Purkinje cell dendrites. PLoS Biology *6*, e103.

Araki, K., Meguro, H., Kushiya, E., Takayama, C., Inoue, Y. and Mishina, M. (1993). Selective expression of the glutamate receptor channel delta 2 subunit in cerebellar Purkinje cells. Biochemical and Biophysical Research Communications *197*, 1267–76.

Araki, Y., Lin, D.-T. and Huganir, R. L. (2010). Plasma membrane insertion of the AMPA receptor GluA2 subunit is regulated by NSF binding and Q/R editing of the ion pore. Proceedings of the National Academy of Sciences of the United States of America *107*, 11080–5.

Arena, J. P., Liu, K. K., Paress, P. S. and Cully, D. F. (1991). Avermectin-sensitive chloride currents induced by Caenorhabditis elegans RNA in Xenopus oocytes. Molecular Pharmacology *40*, 368–74.

Ariel, P., Hoppa, M. B. and Ryan, T. A. (2012). Intrinsic variability in Pv, RRP size, Ca(2+) channel repertoire, and presynaptic potentiation in individual synaptic boutons. Frontiers in Synaptic Neuroscience *4*.

Armstrong, D. M. and Rawson, J. A. (1979). Activity patterns of cerebellar cortical neurones and climbing fibre afferents in the awake cat. The Journal of Physiology *289*, 425–48.

Armstrong, N. and Gouaux, E. (2000). Mechanisms for activation and antagonism of an AMPA-sensitive glutamate receptor: crystal structures of the GluR2 ligand binding core. Neuron *28*, 165–81.

Armstrong, N., Jasti, J., Beich-Frandsen, M. and Gouaux, E. (2006). Measurement of conformational changes accompanying desensitization in an ionotropic glutamate receptor. Cell *127*, 85–97.

Armstrong, N., Sun, Y., Chen, G. Q. and Gouaux, E. (1998). Structure of a glutamate-receptor ligand-binding core in complex with kainate. Nature *395*, 913–7.

Aroniadou-Anderjaska, V., Pidoplichko, V. I., Figueiredo, T. H., Almeida-Suhett, C. P., Prager, E. M. and Braga, M. F. M. (2012). Presynaptic facilitation of glutamate release in the basolateral amygdala: a mechanism for the anxiogenic and seizurogenic function of GluK1 receptors. Neuroscience *221*, 157–69.

Ascher, P. and Nowak, L. (1988a). The role of divalent cations in the N-methyl-D-aspartate responses of mouse central neurones in culture. The Journal of Physiology *399*, 247–66.

Ascher, P. and Nowak, L. (1988b). Quisqualate- and kainate-activated channels in mouse central neurones in culture. The Journal of Physiology *399*, 227–45.

Atasoy, D., Ertunc, M., Moulder, K. L., Blackwell, J., Chung, C., Su, J. and Kavalali, E. T. (2008). Spontaneous and evoked glutamate release activates two populations of NMDA receptors with limited overlap. The Journal of Neuroscience *28*, 10151–66.

Atluri, P. P. and Regehr, W. G. (1996). Determinants of the time course of facilitation at the granule cell to Purkinje cell synapse. The Journal of Neuroscience *16*, 5661–71.

Atluri, P. P. and Regehr, W. G. (1998). Delayed release of neurotransmitter from cerebellar granule cells. The Journal of Neuroscience *18*, 8214–27.

Atwood, H. L. and Bittner, G. D. (1971). Matching of excitatory and inhibitory inputs to crustacean muscle fibers. Journal of Neurophysiology *34*, 157–70.

Atwood, H. L. and Karunanithi, S. (2002). Diversification of synaptic strength: presynaptic elements. Nature Reviews Neuroscience *3*, 497–516.

Auger, C., Kondo, S. and Marty, A. (1998). Multivesicular release at single functional synaptic sites in cerebellar stellate and basket cells. The Journal of Neuroscience *18*, 4532–47.

Auger, C. and Marty, A. (1997). Heterogeneity of functional synaptic parameters among single release sites. Neuron *19*, 139–50.

Augustin, I., Rosenmund, C., Südhof, T. C. and Brose, N. (1999). Munc13-1 is essential for fusion competence of glutamatergic synaptic vesicles. Nature *400*, 457–61.

Augustine, G. J., Adler, E. M. and Charlton, M. P. (1991). The calcium signal for transmitter secretion from presynaptic nerve terminals. Annals of the New York Academy of Sciences *635*, 365–81.

Ayalon, G., Segev, E., Elgavish, S. and Stern-Bach, Y. (2005). Two regions in the N-terminal domain of ionotropic glutamate receptor 3 form the subunit oligomerization interfaces that control subtype-specific receptor assembly. The Journal of Biological Chemistry *280*, 15053–60.

Ayalon, G. and Stern-Bach, Y. (2001). Functional assembly of AMPA and kainate receptors is mediated by several discrete protein-protein interactions. Neuron *31*, 103–13.

Banke, T. G., Bowie, D., Lee, H., Huganir, R. L., Schousboe, A. and Traynelis, S. F. (2000). Control of GluR1 AMPA receptor function by cAMP-dependent protein kinase. The Journal of Neuroscience *20*, 89–102.

Bannister, R. A., Melliti, K. and Adams, B. A. (2004). Differential modulation of CaV2.3 Ca2+ channels by Galphaq/11-coupled muscarinic receptors. Molecular Pharmacology *65*, 381–8.

Barbour, B. (1993). Synaptic currents evoked in Purkinje cells by stimulating individual granule cells. Neuron *11*, 759–69.

Barbour, B., Keller, B. U., Llano, I. and Marty, A. (1994). Prolonged presence of glutamate during excitatory synaptic transmission to cerebellar Purkinje cells. Neuron *12*, 1331–43.

Bardoni, R., Torsney, C., Tong, C.-K., Prandini, M. and MacDermott, A. B. (2004). Presynaptic NMDA receptors modulate glutamate release from primary sensory neurons in rat spinal cord dorsal horn. The Journal of Neuroscience *24*, 2774–81.

Barmack, N. H. and Yakhnitsa, V. (2008). Functions of interneurons in mouse cerebellum. The Journal of Neuroscience *28*, 1140–52.

Barmack, N. H. and Yakhnitsa, V. (2011). Topsy turvy: functions of climbing and mossy fibers in the vestibulo-cerebellum. Neuroscientist *17*, 221–36.

Barria, A., Derkach, V. and Soderling, T. (1997a). Identification of the Ca2+/calmodulin-dependent protein kinase II regulatory phosphorylation site in the alpha-amino-3-hydroxyl-5-methyl-4-isoxazole-propionate-type glutamate receptor. The Journal of Biological Chemistry *272*, 32727–30.

Barria, A., Muller, D., Derkach, V., Griffith, L. C. and Soderling, T. R. (1997b). Regulatory phosphorylation of AMPA-type glutamate receptors by CaM-KII during long-term potentiation. Science *276*, 2042–5.

Batchelor, A. M., Madge, D. J. and Garthwaite, J. (1994). Synaptic activation of metabotropic glutamate receptors in the parallel fibre-Purkinje cell pathway in rat cerebellar slices. Neuroscience *63*, 911–5.

Bats, C., Groc, L. and Choquet, D. (2007). The interaction between stargazin and PSD-95 regulates AMPA receptor surface trafficking. Neuron *53*, 719–34.

Bats, C., Soto, D., Studniarczyk, D., Farrant, M. and Cull-Candy, S. G. (2012). Channel properties reveal differential expression of TARPed and TARPless AMPARs in stargazer neurons. Nature Neuroscience *15*, 853.

Baumert, M., Maycox, P. R., Navone, F., Camilli, P. D. and Jahn, R. (1989). Synaptobrevin: an integral membrane protein of 18,000 daltons present in small synaptic vesicles of rat brain. The EMBO Journal *8*, 379–84.

Bean, A. J., Zhang, X. and Hökfelt, T. (1994). Peptide secretion: what do we know? Federation of American Societies for Experimental Biology Journal *8*, 630–8.

Bean, B. P. (2007). The action potential in mammalian central neurons. Nature Reviews Neuroscience *8*, 451–465.

Bedoukian, M. A., Weeks, A. M. and Partin, K. M. (2006). Different domains of the AMPA receptor direct stargazin-mediated trafficking and stargazin-mediated modulation of kinetics. The Journal of Biological Chemistry *281*, 23908–21.

Bedoukian, M. A., Whitesell, J. D., Peterson, E. J., Clay, C. M. and Partin, K. M. (2008). The stargazin C terminus encodes an intrinsic and transferable membrane sorting signal. The Journal of Biological Chemistry *283*, 1597–600.

Beech, D. J., Bernheim, L. and Hille, B. (1992). Pertussis toxin and voltage dependence distinguish multiple pathways modulating calcium channels of rat sympathetic neurons. Neuron *8*, 97–106.

Bekkers, J. M. (1994). Quantal analysis of synaptic transmission in the central nervous system. Current Opinion in Neurobiology *4*, 360–5.

Bell, C. C. (2002). Evolution of cerebellum-like structures. Brain, Behavior and Evolution *59*, 312–26.

Bell, C. C. and Grimm, R. J. (1969). Discharge properties of Purkinje cells recorded on single and double microelectrodes. Journal of Neurophysiology *32*, 1044–55.

Bender, V. A., Bender, K. J., Brasier, D. J. and Feldman, D. E. (2006). Two coincidence detectors for spike timing-dependent plasticity in somatosensory cortex. The Journal of Neuroscience *26*, 4166–77.

Bennett, M. K., Calakos, N. and Scheller, R. H. (1992). Syntaxin: a synaptic protein implicated in docking of synaptic vesicles at presynaptic active zones. Science *257*, 255–9.

Beretta, F., Sala, C., Saglietti, L., Hirling, H., Sheng, M. and Passafaro, M. (2005). NSF interaction is important for direct insertion of GluR2 at synaptic sites. Molecular and Cellular Neurosciences *28*, 650–60.

Bergerot, A., Rigby, M., Bouvier, G. and Marcaggi, P. (2013). Persistent posttetanic depression at cerebellar parallel fiber to purkinje cell synapses. PLoS ONE *8*, e70277.

Bergles, D. E., Dzubay, J. A. and Jahr, C. E. (1997). Glutamate transporter currents in bergmann glial cells follow the time course of extrasynaptic glutamate. Proceedings of the National Academy of Sciences of the United States of America *94*, 14821–5.

Berl, S. and Waelsh, H. (1958). Determination of glutamic acid, glutamine, glutathione and gamma-aminobutyric acid and their distribution in brain tissue. Journal of Neurochemistry *3*, 161–9.

Berlucchi, G. (1999). Some aspects of the history of the law of dynamic polarization of the neuron. From William James to Sherrington, from Cajal and van Gehuchten to Golgi. Journal of the History of the Neurosciences *8*, 191–201.

Berretta, N. and Jones, R. S. (1996). Tonic facilitation of glutamate release by presynaptic N-methyl-D-aspartate autoreceptors in the entorhinal cortex. Neuroscience *75*, 339–44.

Betz, A., Okamoto, M., Benseler, F. and Brose, N. (1997). Direct interaction of the rat unc-13 homologue Munc13-1 with the N terminus of syntaxin. The Journal of Biological Chemistry *272*, 2520–6.

Betz, A., Thakur, P., Junge, H. J., Ashery, U., Rhee, J. S., Scheuss, V., Rosenmund, C., Rettig, J. and Brose, N. (2001). Functional interaction of the active zone proteins Munc13-1 and RIM1 in synaptic vesicle priming. Neuron *30*, 183–96.

Bidoret, C., Ayon, A., Barbour, B. and Casado, M. (2009). Presynaptic NR2A-containing NMDA receptors implement a high-pass filter synaptic plasticity rule. Proceedings of the National Academy of Sciences of the United States of America *106*, 14126–31.

Bishop, G. A. (1993). An analysis of HRP-filled basket cell axons in the cat's cerebellum. I. Morphometry and configuration. Anatomy and Embryology *188*, 287–97.

Bisti, S., Iosif, G. and Strata, P. (1971). Suppression of inhibition in the cerebellar cortex by picrotoxin and bicuculline. Brain Research *28*, 591–3.

Bittner, G. D. and Baxter, D. A. (1991). Synaptic plasticity at crayfish neuromuscular junctions: facilitation and augmentation. Synapse *7*, 235–43.

Blanpied, T. A., Scott, D. B. and Ehlers, M. D. (2002). Dynamics and regulation of clathrin coats at specialized endocytic zones of dendrites and spines. Neuron *36*, 435–49.

Blaschke, M., Keller, B. U., Rivosecchi, R., Hollmann, M., Heinemann, S. and Konnerth, A. (1993). A single amino acid determines the subunit-specific spider toxin block of alpha-amino-3-hydroxy-5-methylisoxazole-4-propionate/kainate receptor channels. Proceedings of the National Academy of Sciences of the United States of America *90*, 6528–32.

Blatow, M., Caputi, A., Burnashev, N., Monyer, H. and Rozov, A. (2003). Ca2+ buffer saturation underlies paired pulse facilitation in calbindin-D28k-containing terminals. Neuron *38*, 79–88.

Bleakman, D., Ballyk, B. A., Schoepp, D. D., Palmer, A. J., Bath, C. P., Sharpe, E. F., Woolley, M. L., Bufton, H. R., Kamboj, R. K., Tarnawa, I. and Lodge, D. (1996). Activity of 2,3-benzodiazepines at native rat and recombinant human glutamate receptors in vitro: stereospecificity and selectivity profiles. Neuropharmacology *35*, 1689–702.

Boehm, J., Kang, M.-G., Johnson, R. C., Esteban, J., Huganir, R. L. and Malinow, R. (2006). Synaptic incorporation of AMPA receptors during LTP is controlled by a PKC phosphorylation site on GluR1. Neuron *51*, 213–25.

Bollmann, J. H., Sakmann, B. and Borst, J. G. (2000). Calcium sensitivity of glutamate release in a calyx-type terminal. Science *289*, 953–7.

Bolshakov, V., Gapon, S. A. and Magazanik, L. G. (1991). Different types of glutamate

receptors in isolated and identified neurones of the mollusc Planorbarius corneus. The Journal of Physiology *439*, 15–35.

Bonfardin, V. D. J., Fossat, P., Theodosis, D. T. and Oliet, S. H. R. (2010). Glia-dependent switch of kainate receptor presynaptic action. The Journal of Neuroscience *30*, 985–95.

Bonfardin, V. D. J., Theodosis, D. T., Konnerth, A. and Oliet, S. H. R. (2012). Kainate receptor-induced retrograde inhibition of glutamatergic transmission in vasopressin neurons. The Journal of Neuroscience *32*, 1301–10.

Borst, J. G. and Sakmann, B. (1996). Calcium influx and transmitter release in a fast CNS synapse. Nature *383*, 431–4.

Borst, J. G. and Sakmann, B. (1998). Calcium current during a single action potential in a large presynaptic terminal of the rat brainstem. The Journal of Physiology *506*, 143–57.

Bosman, L. W. J. and Konnerth, A. (2009). Activity-dependent plasticity of developing climbing fiber-Purkinje cell synapses. Neuroscience *162*, 612–23.

Bowie, D. and Mayer, M. L. (1995). Inward rectification of both AMPA and kainate subtype glutamate receptors generated by polyamine-mediated ion channel block. Neuron *15*, 453–62.

Braga, M. F. M., Aroniadou-Anderjaska, V., Xie, J. and Li, H. (2003). Bidirectional modulation of GABA release by presynaptic glutamate receptor 5 kainate receptors in the basolateral amygdala. The Journal of Neuroscience *23*, 442–52.

Brager, D. H., Luther, P. W., Erdélyi, F., Szabó, G. and Alger, B. E. (2003). Regulation of exocytosis from single visualized GABAergic boutons in hippocampal slices. The Journal of Neuroscience *23*, 10475–86.

Braithwaite, S. P., Xia, H. and Malenka, R. C. (2002). Differential roles for NSF and GRIP/ABP in AMPA receptor cycling. Proceedings of the National Academy of Sciences of the United States of America *99*, 7096–101.

Branco, T., Marra, V. and Staras, K. (2010). Examining size-strength relationships at hippocampal synapses using an ultrastructural measurement of synaptic release probability. Journal of Structural Biology *172*, 203–10.

Branco, T. and Staras, K. (2009). The probability of neurotransmitter release: variability and feedback control at single synapses. Nature Reviews Neuroscience *10*, 373–83.

Brandt, A., Khimich, D. and Moser, T. (2005). Few CaV1.3 channels regulate the exocytosis of a synaptic vesicle at the hair cell ribbon synapse. The Journal of Neuroscience *25*, 11577–85.

Brasier, D. J. and Feldman, D. E. (2008). Synapse-specific expression of functional presynaptic NMDA receptors in rat somatosensory cortex. The Journal of Neuroscience *28*, 2199–211.

Brasnjo, G. and Otis, T. S. (2001). Neuronal glutamate transporters control activation of postsynaptic metabotropic glutamate receptors and influence cerebellar long-term depression. Neuron *31*, 607–16.

Briatore, F., Patrizi, A., Viltono, L., Sassoè-Pognetto, M. and Wulff, P. (2010). Quantitative organization of GABAergic synapses in the molecular layer of the mouse cerebellar cortex. PLoS ONE *5*, e12119.

Brickley, S. G., Cull-Candy, S. G. and Farrant, M. (1996). Development of a tonic form of synaptic inhibition in rat cerebellar granule cells resulting from persistent activation of GABAA receptors. The Journal of Physiology *497*, 753–9.

Brickley, S. G., Farrant, M., Swanson, G. T. and Cull-Candy, S. G. (2001). CNQX increases GABA-mediated synaptic transmission in the cerebellum by an AMPA/kainate receptor-independent mechanism. Neuropharmacology *41*, 730–6.

Bronk, P., Deák, F., Wilson, M. C., Liu, X., Südhof, T. C. and Kavalali, E. T. (2007). Differential effects of SNAP-25 deletion on Ca2+ -dependent and Ca2+ -independent neurotransmission. Journal of Neurophysiology *98*, 794–806.

Brown, K. M., Sugihara, I., Shinoda, Y. and Ascoli, G. A. (2012). Digital morphometry of rat cerebellar climbing fibers reveals distinct branch and bouton types. The Journal of Neuroscience *32*, 14670–84.

Brown, T. H., Wong, R. K. and Prince, D. A. (1979). Spontaneous miniature synaptic potentials in hippocampal neurons. Brain Research *177*, 194–9.

Brunel, N., Hakim, V., Isope, P., Nadal, J.-P. and Barbour, B. (2004). Optimal information storage and the distribution of synaptic weights: perceptron versus Purkinje cell. Neuron *43*, 745–57.

Buchanan, K. A., Blackman, A. V., Moreau, A. W., Elgar, D., Costa, R. P., Lalanne, T., Jones, A. A. T., Oyrer, J. and Sjöström, P. J. (2012). Target-Specific expression of presynaptic NMDA receptors in neocortical microcircuits. Neuron *75*, 451–66.

Bucurenciu, I., Bischofberger, J. and Jonas, P. (2010). A small number of open Ca2+ channels trigger transmitter release at a central GABAergic synapse. Nature Neuroscience *13*, 19–21.

Bucurenciu, I., Kulik, A., Schwaller, B., Frotscher, M. and Jonas, P. (2008). Nanodomain coupling between Ca2+ channels and Ca2+ sensors promotes fast and efficient transmitter release at a cortical GABAergic synapse. Neuron *57*, 536–45.

Bureau, I. and Mulle, C. (1998). Potentiation of GABAergic synaptic transmission by AMPA receptors in mouse cerebellar stellate cells: changes during development. The Journal of Physiology *509*, 817–31.

Burnashev, N., Monyer, H., Seeburg, P. H. and Sakmann, B. (1992). Divalent ion permeability of AMPA receptor channels is dominated by the edited form of a single subunit. Neuron *8*, 189–98.

Burnashev, N., Villarroel, A. and Sakmann, B. (1996). Dimensions and ion selectivity of recombinant AMPA and kainate receptor channels and their dependence on Q/R site residues. The Journal of Physiology *496*, 165–73.

Cai, C., Coleman, S. K., Niemi, K. and Keinänen, K. (2002). Selective binding of synapse-associated protein 97 to GluR-A alpha-amino-5-hydroxy-3-methyl-4-isoxazole propionate receptor subunit is determined by a novel sequence motif. The Journal of Biological Chemistry *277*, 31484–90.

Caiati, M. D., Sivakumaran, S. and Cherubini, E. (2010). In the developing rat hippocampus, endogenous activation of presynaptic kainate receptors reduces GABA release from mossy fiber terminals. The Journal of Neuroscience *30*, 1750–9.

Caillard, O., Moreno, H., Schwaller, B., Llano, I., Celio, M. R. and Marty, A. (2000). Role of the calcium-binding protein parvalbumin in short-term synaptic plasticity. Proceedings of the National Academy of Sciences of the United States of America *97*, 13372–7.

Callaway, J. C., Lasser-Ross, N. and Ross, W. N. (1995). IPSPs strongly inhibit climbing fiber-activated [Ca2+]i increases in the dendrites of cerebellar Purkinje neurons. The Journal of Neuroscience *15*, 2777–87.

Campbell, S. L., Mathew, S. S. and Hablitz, J. J. (2007). Pre- and postsynaptic effects of kainate on layer II/III pyramidal cells in rat neocortex. Neuropharmacology *53*, 37–47.

Carletti, B. and Rossi, F. (2008). Neurogenesis in the cerebellum. Neuroscientist *14*, 91–100.

Carlos, J. A. D. and Borrell, J. (2007). A historical reflection of the contributions of Cajal and Golgi to the foundations of neuroscience. Brain Res Rev *55*, 8–16.

Carter, A. G. and Regehr, W. G. (2000). Prolonged synaptic currents and glutamate spillover at the parallel fiber to stellate cell synapse. The Journal of Neuroscience *20*, 4423–34.

Carter, A. G. and Regehr, W. G. (2002). Quantal events shape cerebellar interneuron firing. Nature Neuroscience *5*, 1309–18.

Casado, M., Dieudonné, S. and Ascher, P. (2000). Presynaptic N-methyl-D-aspartate receptors at the parallel fiber-Purkinje cell synapse. Proceedings of the National Academy of Sciences of the United States of America *97*, 11593–7.

Casado, M., Isope, P. and Ascher, P. (2002). Involvement of presynaptic N-methyl-D-aspartate receptors in cerebellar long-term depression. Neuron *33*, 123–30.

Cathala, L., Holderith, N. B., Nusser, Z., DiGregorio, D. A. and Cull-Candy, S. G. (2005). Changes in synaptic structure underlie the developmental speeding of AMPA receptor-mediated EPSCs. Nature Neuroscience *8*, 1310–8.

Cattaert, D. and Manira, A. E. (1999). Shunting versus inactivation: analysis of presynaptic inhibitory mechanisms in primary afferents of the crayfish. The Journal of Neuroscience *19*, 6079–89.

Cattaert, D., Manira, A. E. and Clarac, F. (1992). Direct evidence for presynaptic inhibitory mechanisms in crayfish sensory afferents. Journal of Neurophysiology *67*, 610–24.

Chadderton, P., Margrie, T. W. and Häusser, M. (2004). Integration of quanta in cerebellar granule cells during sensory processing. Nature *428*, 856–60.

Chamberlain, S. E. L., Jane, D. E. and Jones, R. S. G. (2012). Pre- and post-synaptic functions of kainate receptors at glutamate and GABA synapses in the rat entorhinal cortex. Hippocampus *22*, 555–76.

Chan-Palay, V. and Palay, S. L. (1970). Interrelations of basket cell axons and climbing fibers in the cerebellar cortex of the rat. Zeitschrift für Anatomie und Entwicklungsgeschichte *132*, 191–227.

Chan-Palay, V. and Palay, S. L. (1972). The stellate cells of the rat's cerebellar cortex. Zeitschrift für Anatomie und Entwicklungsgeschichte *136*, 224–48.

Chang, H.-R. and Kuo, C.-C. (2008). The activation gate and gating mechanism of the NMDA receptor. The Journal of Neuroscience *28*, 1546–56.

Chang, S. and Camilli, P. D. (2001). Glutamate regulates actin-based motility in axonal filopodia. Nature Neuroscience *4*, 787–93.

Chatterton, J. E., Awobuluyi, M., Premkumar, L. S., Takahashi, H., Talantova, M., Shin, Y., Cui, J., Tu, S., Sevarino, K. A., Nakanishi, N., Tong, G., Lipton, S. A. and Zhang, D. (2002). Excitatory glycine receptors containing the NR3 family of NMDA receptor subunits. Nature *415*, 793–8.

Chavas, J. and Marty, A. (2003). Coexistence of excitatory and inhibitory GABA synapses in the cerebellar interneuron network. The Journal of Neuroscience *23*, 2019–31.

Chávez, A. E., Singer, J. H. and Diamond, J. S. (2006). Fast neurotransmitter release triggered by Ca influx through AMPA-type glutamate receptors. Nature *443*, 705–8.

Chen, G. Q., Cui, C., Mayer, M. L. and Gouaux, E. (1999). Functional characterization of a potassium-selective prokaryotic glutamate receptor. Nature *402*, 817–21.

Chen, L., Chetkovich, D. M., Petralia, R. S., Sweeney, N. T., Kawasaki, Y., Wenthold, R. J., Bredt, D. S. and Nicoll, R. A. (2000). Stargazin regulates synaptic targeting of AMPA receptors by two distinct mechanisms. Nature *408*, 936–43.

Cho, C.-H., St-Gelais, F., Zhang, W., Tomita, S. and Howe, J. R. (2007). Two families of TARP isoforms that have distinct effects on the kinetic properties of AMPA receptors and synaptic currents. Neuron *55*, 890–904.

Christie, J. M., Chiu, D. N. and Jahr, C. E. (2011). Ca(2+)-dependent enhancement of release by subthreshold somatic depolarization. Nature Neuroscience *14*, 62–8.

Christie, J. M. and Jahr, C. E. (2008). Dendritic NMDA receptors activate axonal calcium channels. Neuron *60*, 298–307.

Chung, C., Barylko, B., Leitz, J., Liu, X. and Kavalali, E. T. (2010). Acute dynamin inhibition dissects synaptic vesicle recycling pathways that drive spontaneous and evoked neurotransmission. The Journal of Neuroscience *30*, 1363–76.

Chung, H. J., Xia, J., Scannevin, R. H., Zhang, X. and Huganir, R. L. (2000). Phosphorylation of the AMPA receptor subunit GluR2 differentially regulates its interaction with PDZ domain-containing proteins. The Journal of Neuroscience *20*, 7258–67.

Citri, A., Bhattacharyya, S., Ma, C., Morishita, W., Fang, S., Rizo, J. and Malenka, R. C. (2010). Calcium binding to PICK1 is essential for the intracellular retention of AMPA receptors underlying long-term depression. The Journal of Neuroscience *30*, 16437–52.

Clark, B. A. and Cull-Candy, S. G. (2002). Activity-dependent recruitment of extrasynaptic NMDA receptor activation at an AMPA receptor-only synapse. The Journal of Neuroscience *22*, 4428–36.

Clark, B. A., Farrant, M. and Cull-Candy, S. G. (1997). A direct comparison of the single-channel properties of synaptic and extrasynaptic NMDA receptors. The Journal of Neuroscience *17*, 107–16.

Clarke, V. R. J., Ballyk, B. A., Hoo, K. H., Mandelzys, A., Pellizzari, A., Bath, C. P., Thomas, J., Sharpe, E. F., Davies, C. H., Ornstein, P. L., Schoepp, D. D., Kamboj, R. K., Collingridge, G. L., Lodge, D. and Bleakman, D. (1997). A hippocampal GluR5 kainate receptor regulating inhibitory synaptic transmission. Nature *389*, 599.

Clements, J. D. (1990). A statistical test for demonstrating a presynaptic site of action for a modulator of synaptic amplitude. J Neurosci Methods *31*, 75–88.

Clements, J. D. and Bekkers, J. M. (1997). Detection of spontaneous synaptic events with an optimally scaled template. Journal Biophysical *73*, 220–9.

Clements, J. D., Forsythe, I. D. and Redman, S. J. (1987). Presynaptic inhibition of synaptic potentials evoked in cat spinal motoneurones by impulses in single group Ia axons. The Journal of Physiology *383*, 153–69.

Clements, J. D. and Silver, R. A. (2000). Unveiling synaptic plasticity: a new graphical and analytical approach. Trends in Neurosciences *23*, 105–13.

Cochilla, A. J. and Alford, S. (1999). NMDA receptor-mediated control of presynaptic calcium and neurotransmitter release. The Journal of Neuroscience *19*, 193–205.

Coddington, L. T., Rudolph, S., Lune, P. V., Overstreet-Wadiche, L. and Wadiche, J. I. (2013). Spillover-mediated feedforward inhibition functionally segregates interneuron activity. Neuron *78*, 1050–62.

Cokić, B. and Stein, V. (2008). Stargazin modulates AMPA receptor antagonism. Neuropharmacology *54*, 1062–70.

Collin, T., Chat, M., Lucas, M. G., Moreno, H., Racay, P., Schwaller, B., Marty, A. and Llano, I. (2005a). Developmental changes in parvalbumin regulate presynaptic Ca2+ signaling. The Journal of Neuroscience *25*, 96–107.

Collin, T., Marty, A. and Llano, I. (2005b). Presynaptic calcium stores and synaptic transmission. Current Opinion in Neurobiology *15*, 275–81.

Collingridge, G. L., Olsen, R. W., Peters, J. and Spedding, M. (2008). A nomenclature for ligand-gated ion channels. Neuropharmacology *56*, 2–5.

Colquhoun, D., Jonas, P. and Sakmann, B. (1992). Action of brief pulses of glutamate on AMPA/kainate receptors in patches from different neurones of rat hippocampal slices. The Journal of Physiology *458*, 261–87.

Consalez, G. G. and Hawkes, R. (2012). The compartmental restriction of cerebellar interneurons. Frontiers in Neural Circuits *6*, 123.

Conti, R., Tan, Y. P. and Llano, I. (2004). Action potential-evoked and ryanodine-sensitive spontaneous Ca2+ transients at the presynaptic terminal of a developing CNS inhibitory synapse. The Journal of Neuroscience *24*, 6946–57.

Contractor, A., Mulle, C. and Swanson, G. T. (2011). Kainate receptors coming of age: milestones of two decades of research. Trends in Neurosciences *34*, 154–63.

Contractor, A., Swanson, G. and Heinemann, S. F. (2001). Kainate receptors are involved in short- and long-term plasticity at mossy fiber synapses in the hippocampus. Neuron *29*, 209–16.

Contractor, A., Swanson, G. T., Sailer, A., O'Gorman, S. and Heinemann, S. F. (2000). Identification of the kainate receptor subunits underlying modulation of excitatory synaptic transmission in the CA3 region of the hippocampus. The Journal of Neuroscience *20*, 8269–78.

Coombs, I. D. and Cull-Candy, S. G. (2009). Transmembrane AMPA receptor regulatory proteins and AMPA receptor function in the cerebellum. Neuroscience *162*, 656–665.

Coombs, I. D., Soto, D., Zonouzi, M., Renzi, M., Shelley, C., Farrant, M. and Cull-Candy, S. G. (2012). Cornichons modify channel properties of recombinant and glial AMPA receptors. The Journal of Neuroscience *32*, 9796–804.

Copits, B. A. and Swanson, G. T. (2012). Dancing partners at the synapse: auxiliary subunits that shape kainate receptor function. Nature Reviews Neuroscience *13*, 675–86.

Corlew, R., Wang, Y., Ghermazien, H., Erisir, A. and Philpot, B. D. (2007). Developmental switch in the contribution of presynaptic and postsynaptic NMDA receptors to long-term depression. The Journal of Neuroscience *27*, 9835–45.

Correia, S. S., Bassani, S., Brown, T. C., Lisé, M.-F., Backos, D. S., El-Husseini, A., Passafaro, M. and Esteban, J. A. (2008). Motor protein-dependent transport of AMPA receptors into spines during long-term potentiation. Nature Neuroscience *11*, 457–66.

Cossart, R., Tyzio, R., Dinocourt, C., Esclapez, M., Hirsch, J. C., Ben-Ari, Y. and Bernard, C. (2001). Presynaptic kainate receptors that enhance the release of GABA on CA1 hippocampal interneurons. Neuron *29*, 497–508.

Cowan, W. M. and Kandel, E. R. (2003). "A brief history of synapses and synaptic transmission" in Synapses. 1st edition. WM Cowan, TC Südhof and CF Stevens. The Johns Hopkins University Press.

Crepel, F. (2007). Developmental Changes in Retrograde Messengers Involved in Depolarization-Induced Suppression of Excitation at Parallel Fiber-Purkinje Cell Synapses in Rodents. Journal of Neurophysiology *97*, 824.

Crépel, F. (2009). Role of presynaptic kainate receptors at parallel fiber-purkinje cell synapses in induction of cerebellar LTD: interplay with climbing fiber input. Journal of Neurophysiology *102*, 965–73.

Crepel, F., Mariani, J. and Delhaye-Bouchaud, N. (1976). Evidence for a multiple innervation of Purkinje cells by climbing fibers in the immature rat cerebellum. Journal of Neurobiology *7*, 567–78.

Cuadra, A. E., Kuo, S.-H., Kawasaki, Y., Bredt, D. S. and Chetkovich, D. M. (2004). AMPA receptor synaptic targeting regulated by stargazin interactions with the Golgi-resident PDZ protein nPIST. The Journal of Neuroscience *24*, 7491–502.

Cull-Candy, S., Kelly, L. and Farrant, M. (2006). Regulation of Ca2+-permeable AMPA receptors: synaptic plasticity and beyond. Current Opinion in Neurobiology *16*, 288–97.

Cull-Candy, S. G. and Usherwood, P. N. (1973). Two populations of L-glutamate receptors on locust muscle fibres. Nature New Biology *246*, 62–4.

Curtis, D., Phillis, J. and Watkins, J. C. (1959). Chemical excitation of spinal neurones. Nature *183*, 611–2.

Curtis, D. and Watkins, J. C. (1963). Acidic amino acids with strong excitatory actions on mammalian neurones. The Journal of Physiology *166*, 1–14.

Dale, H. (1914). The action of certain esters and ethers of choline and their relation to muscarine. The Journal of Pharmacology and Experimental Therapeutics *6*, 147–190.

Das, U., Kumar, J., Mayer, M. L. and Plested, A. J. R. (2010). Domain organization and function in GluK2 subtype kainate receptors. Proceedings of the National Academy of Sciences of the United States of America *107*, 8463–8.

Davie, J. T., Clark, B. A. and Häusser, M. (2008). The origin of the complex spike in cerebellar Purkinje cells. The Journal of Neuroscience *28*, 7599–609.

Davies, J. and Watkins, J. C. (1979). Selective antagonism of amino acid-induced and synaptic excitation in the cat spinal cord. The Journal of Physiology *297*, 621–35.

Davies, J. and Watkins, J. C. (1981). Differentiation of kainate and quisqualate receptors in the cat spinal cord by selective antagonism with gamma-D(and L)-glutamylglycine. Brain Research *206*, 172–7.

Davies, J. and Watkins, J. C. (1985). Depressant actions of gamma-D-glutamylaminomethyl sulfonate (GAMS) on amino acid-induced and synaptic excitation in the cat spinal cord. Brain Research *327*, 113–20.

Daw, M. I., Pelkey, K. A., Chittajallu, R. and McBain, C. J. (2010). Presynaptic kainate receptor activation preserves asynchronous GABA release despite the reduction in synchronous release from hippocampal cholecystokinin interneurons. The Journal of Neuroscience *30*, 11202–9.

de Jong, A. P. H., Schmitz, S. K., Toonen, R. F. G. and Verhage, M. (2012). Dendritic position is a major determinant of presynaptic strength. The Journal of Cell Biology *197*, 327–37.

de Lange, R. P. J., de Roos, A. D. G. and Borst, J. G. G. (2003). Two modes of vesicle recycling in the rat calyx of Held. The Journal of Neuroscience *23*, 10164–73.

De-Robertis, E. and Bennett, H. (1955). Some features of the submicroscopic morphology of synapses in frog and earthworm. The Journal of Biophysical and Biochemical Cytology *1*, 47–58.

De-Zeeuw, C., Simpson, J. I., Hoogenraad, C. C., Galjart, N., Koekkoek, S. K. and Ruigrok, T. J. (1998). Microcircuitry and function of the inferior olive. Trends in Neurosciences *21*, 391–400.

Dean, P., Porrill, J., Ekerot, C. and Jörntell, H. (2009). The cerebellar microcircuit as an adaptive filter: experimental and computational evidence. Nature Reviews Neuroscience *11*, 30–43.

Dehnes, Y., Chaudhry, F. A., Ullensvang, K., Lehre, K. P., Storm-Mathisen, J. and Danbolt, N. C. (1998). The glutamate transporter EAAT4 in rat cerebellar Purkinje

cells: a glutamate-gated chloride channel concentrated near the synapse in parts of the dendritic membrane facing astroglia. The Journal of Neuroscience *18*, 3606–19.

del Castillo, J. and Katz, B. (1954). Quantal components of the end-plate potential. The Journal of Physiology *124*, 560–73.

Delaney, A. J. and Jahr, C. E. (2002). Kainate receptors differentially regulate release at two parallel fiber synapses. Neuron *36*, 475–82.

Delvendahl, I., Weyhersmüller, A., Ritzau-Jost, A. and Hallermann, S. (2013). Hippocampal and cerebellar mossy fibre boutons - same name, different function. The Journal of Physiology *591*, 3179–88.

Denker, A., Kröhnert, K. and Rizzoli, S. O. (2009). Revisiting synaptic vesicle pool localization in the Drosophila neuromuscular junction. The Journal of Physiology *587*, 2919–26.

Dietrich, L. E. P. and Ungermann, C. (2004). On the mechanism of protein palmitoylation. EMBO reports *5*, 1053.

DiGregorio, D. A., Nusser, Z. and Silver, R. A. (2002). Spillover of glutamate onto synaptic AMPA receptors enhances fast transmission at a cerebellar synapse. Neuron *35*, 521–33.

Dittman, J. S., Kreitzer, A. C. and Regehr, W. G. (2000). Interplay between facilitation, depression, and residual calcium at three presynaptic terminals. The Journal of Neuroscience *20*, 1374–85.

Dittman, J. S. and Regehr, W. G. (1998). Calcium dependence and recovery kinetics of presynaptic depression at the climbing fiber to Purkinje cell synapse. The Journal of Neuroscience *18*, 6147–62.

Dixon, W. (1924). Nicotin, Coniin, Piperidin, Lupetidin, Cytisin, Lobelin, Spartein, Gelsemin. Mittel, welche auf bestimmte Nervenzellen wirken. Handbook Experimental Pharmacology *2*, 656–736.

Dizon, M. J. and Khodakhah, K. (2011). The role of interneurons in shaping Purkinje cell responses in the cerebellar cortex. The Journal of Neuroscience *31*, 10463–73.

Dobrunz, L. E. and Stevens, C. F. (1997). Heterogeneity of release probability, facilitation, and depletion at central synapses. Neuron *18*, 995–1008.

Dodge, F. A. and Rahamimoff, R. (1967). Co-operative action a calcium ions in transmitter release at the neuromuscular junction. The Journal of Physiology *193*, 419–32.

Donato, R., Rodrigues, R. J., Takahashi, M., Tsai, M. C., Soto, D., Miyagi, K., Villafuertes, R. G., Cunha, R. A. and Edwards, F. A. (2008). GABA release by basket cells onto Purkinje cells, in rat cerebellar slices, is directly controlled by presynaptic purinergic receptors, modulating Ca2+ influx. Cell Calcium *44*, 521–32.

Dudel, J. and Kuffler, S. (1961). Presynaptic inhibition at the crayfish neuromuscular junction. The Journal of Physiology *155*, 543–62.

Dugué, G. P., Dumoulin, A., Triller, A. and Dieudonné, S. (2005). Target-dependent use of co-released inhibitory transmitters at central synapses. The Journal of Neuroscience *25*, 6490–8.

Duguid, I. C., Pankratov, Y., Moss, G. W. J. and Smart, T. G. (2007). Somatodendritic release of glutamate regulates synaptic inhibition in cerebellar Purkinje cells via autocrine mGluR1 activation. The Journal of Neuroscience *27*, 12464–74.

Duguid, I. C. and Smart, T. G. (2004). Retrograde activation of presynaptic NMDA receptors enhances GABA release at cerebellar interneuron-Purkinje cell synapses. Nature Neuroscience *7*, 525–33.

Dumoulin, A., Triller, A. and Dieudonné, S. (2001). IPSC kinetics at identified GABAergic and mixed GABAergic and glycinergic synapses onto cerebellar Golgi cells. The Journal of Neuroscience *21*, 6045–57.

Dzubay, J. A. and Otis, T. S. (2002). Climbing fiber activation of metabotropic glutamate receptors on cerebellar purkinje neurons. Neuron *36*, 1159–67.

Eccles, J. (1945). An electrical hypothesis of synaptic and neuromuscular transmission. Nature *156*, 680–682.

Eccles, J. C. (1967). Circuits in the cerebellar control of movement. Proceedings of the National Academy of Sciences of the United States of America *58*, 336–43.

Eccles, J. C., Llinás, R. and Sasaki (1966). Parallel fibre stimulation and the responses induced thereby in the Purkinje cells of the cerebellum. Experimental Brain Research *1*, 17–39.

Eccles, J. C., Llinás, R. and SASAKI, K. (1964). Golgi cell inhibition in the cerebellar cortex. Nature *204*, 1265–6.

Eccles, J. C., Llinás, R. and Sasaki, K. (1966a). The inhibitory interneurones within the cerebellar cortex. Experimental Brain Research *1*, 1–16.

Eccles, J. C., Llinás, R. and Sasaki, K. (1966b). The excitatory synaptic action of climbing fibres on the purinje cells of the cerebellum. The Journal of Physiology *182*, 268–96.

Eccles, J. C., Sasaki, K. and Strata, P. (1967). Interpretation of the potential fields generated in the cerebellar cortex by a mossy fibre volley. Experimental Brain Research *3*, 58–80.

Eccles, R. M. and Willis, W. D. (1963). Presynaptic inhibition of the monosynaptic reflex pathway in kittens. The Journal of Physiology *165*, 403–20.

Eggermann, E., Bucurenciu, I., Goswami, S. P. and Jonas, P. (2012). Nanodomain coupling between Ca2+ channels and sensors of exocytosis at fast mammalian synapses. Nature Reviews Neuroscience *13*, 7–21.

Eggermann, E. and Jonas, P. (2012). How the 'slow' Ca(2+) buffer parvalbumin affects transmitter release in nanodomain-coupling regimes. Nature Neuroscience *15*, 20–2.

Einstein, A. (1905). On the movement of small particles suspended in stationary liquids required by the molecular-kinetic theory of heat. Annalen der Physik *17*, 16.

Elias, G. M., Funke, L., Stein, V., Grant, S. G., Bredt, D. S. and Nicoll, R. A. (2006). Synapse-specific and developmentally regulated targeting of AMPA receptors by a family of MAGUK scaffolding proteins. Neuron *52*, 307–20.

Engelman, H. S., Anderson, R. L., Daniele, C. and Macdermott, A. B. (2006). Presynaptic

alpha-amino-3-hydroxy-5-methyl-4-isoxazolepropionic acid (AMPA) receptors modulate release of inhibitory amino acids in rat spinal cord dorsal horn. Neuroscience *139*, 539–53.

Engelman, H. S. and Macdermott, A. B. (2004). Presynaptic ionotropic receptors and control of transmitter release. Nature Reviews Neuroscience *5*, 135–45.

Ermolyuk, Y. S., Alder, F. G., Henneberger, C., Rusakov, D. A., Kullmann, D. M. and Volynski, K. E. (2012). Independent regulation of Basal neurotransmitter release efficacy by variable Ca2+ influx and bouton size at small central synapses. PLoS Biology *10*, e1001396.

Ewins, A. J. (1914). Acetylcholine a new active principle of ergot. The Journal of Biochemistry *8*, 44–49.

Faber, D. S. and Korn, H. (1991). Applicability of the coefficient of variation method for analyzing synaptic plasticity. Biophysical Journal *60*, 1288–94.

Farina, A. N., Blain, K. Y., Maruo, T., Kwiatkowski, W., Choe, S. and Nakagawa, T. (2011). Separation of domain contacts is required for heterotetrameric assembly of functional NMDA receptors. The Journal of Neuroscience *31*, 3565–79.

Farrant, M. and Cull-Candy, S. G. (1991). Excitatory amino acid receptor-channels in Purkinje cells in thin cerebellar slices. Proceedings of the Royal Society B Biological Sciences *244*, 179–84.

Farrant, M. and Kaila, K. (2007). The cellular, molecular and ionic basis of GABA(A) receptor signalling. Progress in Brain Research *160*, 59–87.

Fatt, P. and Katz, B. (1952). Spontaneous subthreshold activity at motor nerve endings. The Journal of Physiology *117*, 109–28.

Feligioni, M., Holman, D., Haglerod, C., Davanger, S. and Henley, J. M. (2006). Ultrastructural localisation and differential agonist-induced regulation of AMPA and kainate receptors present at the presynaptic active zone and postsynaptic density. Journal of Neurochemistry *99*, 549–60.

Fiszman, M. L., Barberis, A., Lu, C., Fu, Z., Erdélyi, F., Szabó, G. and Vicini, S. (2005). NMDA receptors increase the size of GABAergic terminals and enhance GABA release. The Journal of Neuroscience *25*, 2024–31.

Fiszman, M. L., Erdélyi, F., Szabó, G. and Vicini, S. (2007). Presynaptic AMPA and kainate receptors increase the size of GABAergic terminals and enhance GABA release. Neuropharmacology *52*, 1631–40.

Forsythe, I. D., Tsujimoto, T., Barnes-Davies, M., Cuttle, M. F. and Takahashi, T. (1998). Inactivation of presynaptic calcium current contributes to synaptic depression at a fast central synapse. Neuron *20*, 797–807.

Forti, L., Pouzat, C. and Llano, I. (2000). Action potential-evoked Ca2+ signals and calcium channels in axons of developing rat cerebellar interneurones. The Journal of Physiology *527*, 33–48.

Foust, A., Popovic, M., Zecevic, D. and McCormick, D. A. (2010). Action potentials initiate in the axon initial segment and propagate through axon collaterals reliably in cerebellar Purkinje neurons. The Journal of Neuroscience *30*, 6891–902.

Frank, K. and Fuortes, M. (1957). Presynaptic and postsynaptic inhibition of neurosynaptic reflex. Federation Proceedings *16*, 39–40.

Fredj, N. B. and Burrone, J. (2009). A resting pool of vesicles is responsible for spontaneous vesicle fusion at the synapse. Nature Neuroscience *12*, 751–8.

Frerking, M., Petersen, C. C. and Nicoll, R. A. (1999). Mechanisms underlying kainate receptor-mediated disinhibition in the hippocampus. Proc Natl Acad Sci USA *96*, 12917–22.

Frerking, M., Schmitz, D., Zhou, Q., Johansen, J. and Nicoll, R. A. (2001). Kainate receptors depress excitatory synaptic transmission at CA3–>CA1 synapses in the hippocampus via a direct presynaptic action. The Journal of Neuroscience *21*, 2958–66.

Freund, T. F. and Buzsáki, G. (1996). Interneurons of the hippocampus. Hippocampus *6*, 347–470.

Fu, A. K. Y., Hung, K.-W., Fu, W.-Y., Shen, C., Chen, Y., Xia, J., Lai, K.-O. and Ip, N. Y. (2011). APC(Cdh1) mediates EphA4-dependent downregulation of AMPA receptors in homeostatic plasticity. Nature Neuroscience *14*, 181–9.

Fujishima, K., Horie, R., Mochizuki, A. and Kengaku, M. (2012). Principles of branch dynamics governing shape characteristics of cerebellar Purkinje cell dendrites. Development *139*, 3442–55.

Fukaya, M., Yamazaki, M., Sakimura, K. and Watanabe, M. (2005). Spatial diversity in gene expression for VDCCgamma subunit family in developing and adult mouse brains. Neuroscience Research *53*, 376–83.

Furshpan, E. and Potter, D. (1959). Transmission at the giant motor synapses of the crayfish. The Journal of Physiology *145*, 289–325.

Furukawa, H., Singh, S. K., Mancusso, R. and Gouaux, E. (2005). Subunit arrangement and function in NMDA receptors. Nature *438*, 185–92.

Galante, M. and Marty, A. (2003). Presynaptic ryanodine-sensitive calcium stores contribute to evoked neurotransmitter release at the basket cell-Purkinje cell synapse. The Journal of Neuroscience *23*, 11229–34.

Galarreta, M., Erdélyi, F., Szabó, G. and Hestrin, S. (2004). Electrical coupling among irregular-spiking GABAergic interneurons expressing cannabinoid receptors. The Journal of Neuroscience *24*, 9770–8.

Gangadharan, V., Wang, R., Ulzhöfer, B., Luo, C., Bardoni, R., Bali, K. K., Agarwal, N., Tegeder, I., Hildebrandt, U., Nagy, G. G., Todd, A. J., Ghirri, A., Häussler, A., Sprengel, R., Seeburg, P. H., Macdermott, A. B., Lewin, G. R. and Kuner, R. (2011). Peripheral calcium-permeable AMPA receptors regulate chronic inflammatory pain in mice. The Journal of Clinical Investigation *121*, 1608–23.

Gao, Y., Zorman, S., Gundersen, G., Xi, Z., Ma, L., Sirinakis, G., Rothman, J. E. and Zhang, Y. (2012). Single reconstituted neuronal SNARE complexes zipper in three distinct stages. Science *337*, 1340–3.

Gardner, S. M., Takamiya, K., Xia, J., Suh, J.-G., Johnson, R., Yu, S. and Huganir, R. L. (2005). Calcium-permeable AMPA receptor plasticity is mediated by subunit-specific interactions with PICK1 and NSF. Neuron *45*, 903–15.

Garduño, J., Galindo-Charles, L., Jiménez-Rodríguez, J., Galarraga, E., Tapia, D., Mihailescu, S. and Hernandez-Lopez, S. (2012). Presynaptic alpha4beta2 nicotinic acetylcholine receptors increase glutamate release and serotonin neuron excitability in the dorsal raphe nucleus. The Journal of Neuroscience *32*, 15148–57.

Gasparini, S., Kasyanov, A. M., Pietrobon, D., Voronin, L. L. and Cherubini, E. (2001). Presynaptic R-type calcium channels contribute to fast excitatory synaptic transmission in the rat hippocampus. The Journal of Neuroscience *21*, 8715–21.

Geiger, J. R. and Jonas, P. (2000). Dynamic control of presynaptic Ca(2+) inflow by fast-inactivating K(+) channels in hippocampal mossy fiber boutons. Neuron *28*, 927–39.

Geiger, J. R., Melcher, T., Koh, D. S., Sakmann, B., Seeburg, P. H., Jonas, P. and Monyer, H. (1995). Relative abundance of subunit mRNAs determines gating and Ca2+ permeability of AMPA receptors in principal neurons and interneurons in rat CNS. Neuron *15*, 193–204.

Gelsomino, G., Menna, E., Antonucci, F., Rodighiero, S., Riganti, L., Mulle, C., Benfenati, F., Valtorta, F., Verderio, C. and Matteoli, M. (2012). Kainate induces mobilization of synaptic vesicles at the growth cone through the activation of Protein Kinase A. Cerebral Cortex *23*, 531–41.

Geppert, M., Goda, Y., Hammer, R. E., Li, C., Rosahl, T. W., Stevens, C. F. and Südhof, T. C. (1994). Synaptotagmin I: a major Ca2+ sensor for transmitter release at a central synapse. Cell *79*, 717–27.

Gibson, H. E., Edwards, J. G., Page, R. S., Hook, M. J. V. and Kauer, J. A. (2008). TRPV1 channels mediate long-term depression at synapses on hippocampal interneurons. Neuron *57*, 746–59.

Gidon, A. and Segev, I. (2012). Principles governing the operation of synaptic inhibition in dendrites. Neuron *75*, 330–41.

Gielen, M., Retchless, B. S., Mony, L., Johnson, J. W. and Paoletti, P. (2009). Mechanism of differential control of NMDA receptor activity by NR2 subunits. Nature *459*, 703–7.

Gill, M. B., Kato, A. S., Roberts, M. F., Yu, H., Wang, H., Tomita, S. and Bredt, D. S. (2011). Cornichon-2 modulates AMPA receptor-transmembrane AMPA receptor regulatory protein assembly to dictate gating and pharmacology. The Journal of Neuroscience *31*, 6928–38.

Glaum, S. R. and Miller, R. J. (1995). Presynaptic metabotropic glutamate receptors modulate omega-conotoxin-GVIA-insensitive calcium channels in the rat medulla. Neuropharmacology *34*, 953–64.

Glitsch, M. (2006). Selective inhibition of spontaneous but not Ca2+ -dependent release machinery by presynaptic group II mGluRs in rat cerebellar slices. Journal of Neurophysiology *96*, 86–96.

Glitsch, M. and Marty, A. (1999). Presynaptic effects of NMDA in cerebellar Purkinje cells and interneurons. The Journal of Neuroscience *19*, 511–9.

Glitsch, M. D. (2008a). Calcium influx through N-methyl-D-aspartate receptors triggers GABA release at interneuron-Purkinje cell synapse in rat cerebellum. Neuroscience *151*, 403–9.

Glitsch, M. D. (2008b). Spontaneous neurotransmitter release and Ca2+–how spontaneous is spontaneous neurotransmitter release? Cell Calcium *43*, 9–15.

Goda, Y. and Stevens, C. F. (1994). Two components of transmitter release at a central synapse. Proceedings of the National Academy of Sciences of the United States of America *91*, 12942–6.

Goossens, H. H. L. M., Hoebeek, F. E., Alphen, A. M. V., Steen, J. V. D., Stahl, J. S., Zeeuw, C. I. D. and Frens, M. A. (2004). Simple spike and complex spike activity of floccular Purkinje cells during the optokinetic reflex in mice lacking cerebellar long-term depression. European Journal of Neuroscience *19*, 687–97.

Goswami, S. P., Bucurenciu, I. and Jonas, P. (2012). Miniature IPSCs in hippocampal granule cells are triggered by voltage-gated Ca2+ channels via microdomain coupling. The Journal of Neuroscience *32*, 14294–304.

Graham, B. and Redman, S. (1994). A simulation of action potentials in synaptic boutons during presynaptic inhibition. Journal of Neurophysiology *71*, 538–49.

Greger, I. H., Akamine, P., Khatri, L. and Ziff, E. B. (2006). Developmentally regulated, combinatorial RNA processing modulates AMPA receptor biogenesis. Neuron *51*, 85–97.

Greger, I. H., Khatri, L., Kong, X. and Ziff, E. B. (2003). AMPA receptor tetramerization is mediated by Q/R editing. Neuron *40*, 763–74.

Greger, I. H., Khatri, L. and Ziff, E. B. (2002). RNA editing at arg607 controls AMPA receptor exit from the endoplasmic reticulum. Neuron *34*, 759–72.

Groemer, T. W. and Klingauf, J. (2007). Synaptic vesicles recycling spontaneously and during activity belong to the same vesicle pool. Nature Neuroscience *10*, 145–7.

Gu, J. G. and Macdermott, A. B. (1997). Activation of ATP P2X receptors elicits glutamate release from sensory neuron synapses. Nature *389*, 749–53.

Gundappa-Sulur, G., Schutter, E. D. and Bower, J. M. (1999). Ascending granule cell axon: an important component of cerebellar cortical circuitry. The Journal of Comparative Neurology *408*, 580–96.

Hallermann, S., Fejtova, A., Schmidt, H., Weyhersmüller, A., Silver, R. A., Gundelfinger, E. D. and Eilers, J. (2010). Bassoon speeds vesicle reloading at a central excitatory synapse. Neuron *68*, 710–23.

Hámori, J. and Somogyi, J. (1983). Differentiation of cerebellar mossy fiber synapses in the rat: a quantitative electron microscope study. The Journal of Comparative Neurology *220*, 365–77.

Han, Y., Kaeser, P. S., Südhof, T. C. and Schneggenburger, R. (2011). RIM determines Ca2+ channel density and vesicle docking at the presynaptic active zone. Neuron *69*, 304–16.

Hanley, J. G., Khatri, L., Hanson, P. I. and Ziff, E. B. (2002). NSF ATPase and alpha-/beta-SNAPs disassemble the AMPA receptor-PICK1 complex. Neuron *34*, 53–67.

Harlow, M. L., Ress, D., Stoschek, A., Marshall, R. M. and McMahan, U. J. (2001). The architecture of active zone material at the frog's neuromuscular junction. Nature *409*, 479–84.

Harmel, N., Cokic, B., Zolles, G., Berkefeld, H., Mauric, V., Fakler, B., Stein, V. and Klöcker, N. (2012). AMPA receptors commandeer an ancient cargo exporter for use as an auxiliary subunit for signaling. PLoS ONE *7*, e30681.

Harrison, J. and Jahr, C. E. (2003). Receptor occupancy limits synaptic depression at climbing fiber synapses. The Journal of Neuroscience *23*, 377–83.

Harvey, R. J. and Napper, R. M. (1991). Quantitative studies on the mammalian cerebellum. Progress in Neurobiology *36*, 437–63.

Hashimoto, K., Fukaya, M., Qiao, X., Sakimura, K., Watanabe, M. and Kano, M. (1999). Impairment of AMPA receptor function in cerebellar granule cells of ataxic mutant mouse stargazer. The Journal of Neuroscience *19*, 6027–36.

Hashimoto, K. and Kano, M. (2003). Functional differentiation of multiple climbing fiber inputs during synapse elimination in the developing cerebellum. Neuron *38*, 785–96.

Hashimoto, K. and Kano, M. (2005). Postnatal development and synapse elimination of climbing fiber to Purkinje cell projection in the cerebellum. Neuroscience Research *53*, 221–8.

Hastie, P., Ulbrich, M. H., Wang, H.-L., Arant, R. J., Lau, A. G., Zhang, Z., Isacoff, E. Y. and Chen, L. (2013). AMPA receptor/TARP stoichiometry visualized by single-molecule subunit counting. Proceedings of the National Academy of Sciences of the United States of America *110*, 5163–8.

Hatton, C. J. and Paoletti, P. (2005). Modulation of triheteromeric NMDA receptors by N-terminal domain ligands. Neuron *46*, 261–74.

Häusser, M. and Clark, B. A. (1997). Tonic synaptic inhibition modulates neuronal output pattern and spatiotemporal synaptic integration. Neuron *19*, 665–78.

Hayashi, T. (1954). Effects of sodium glutamate on the nervous system. Journal of Medicine *3*, 183 – 192.

Hayashi, T. and Huganir, R. L. (2004). Tyrosine phosphorylation and regulation of the AMPA receptor by SRC family tyrosine kinases. The Journal of Neuroscience *24*, 6152–60.

Hayashi, T., Rumbaugh, G. and Huganir, R. L. (2005). Differential regulation of AMPA receptor subunit trafficking by palmitoylation of two distinct sites. Neuron *47*, 709–23.

He, K., Song, L., Cummings, L. W., Goldman, J., Huganir, R. L. and Lee, H.-K. (2009). Stabilization of Ca2+-permeable AMPA receptors at perisynaptic sites by GluR1-S845 phosphorylation. Proceedings of the National Academy of Sciences of the United States of America *106*, 20033–8.

Hefft, S. and Jonas, P. (2005). Asynchronous GABA release generates long-lasting inhibition at a hippocampal interneuron-principal neuron synapse. Nature Neuroscience *8*, 1319–28.

Helmchen, F., Borst, J. G. and Sakmann, B. (1997). Calcium dynamics associated with a single action potential in a CNS presynaptic terminal. Biophysical Journal *72*, 1458–71.

Hendel, T., Mank, M., Schnell, B., Griesbeck, O., Borst, A. and Reiff, D. F. (2008). Fluorescence changes of genetic calcium indicators and OGB-1 correlated with neural activity and calcium in vivo and in vitro. The Journal of Neuroscience *28*, 7399–411.

Herlitze, S., Raditsch, M., Ruppersberg, J. P., Jahn, W., Monyer, H., Schoepfer, R. and Witzemann, V. (1993). Argiotoxin detects molecular differences in AMPA receptor channels. Neuron *10*, 1131–40.

Herring, B. E., Shi, Y., Suh, Y. H., Zheng, C.-Y., Blankenship, S. M., Roche, K. W. and Nicoll, R. A. (2013). Cornichon proteins determine the subunit composition of synaptic AMPA receptors. Neuron *77*, 1083–96.

Hibino, H., Pironkova, R., Onwumere, O., Vologodskaia, M., Hudspeth, A. J. and Lesage, F. (2002). RIM binding proteins (RBPs) couple Rab3-interacting molecules (RIMs) to voltage-gated Ca(2+) channels. Neuron *34*, 411–23.

Higuchi, M., Single, F. N., Köhler, M., Sommer, B., Sprengel, R. and Seeburg, P. H. (1993). RNA editing of AMPA receptor subunit GluR-B: a base-paired intron-exon structure determines position and efficiency. Cell *75*, 1361–70.

Hille, B. (1992). Ionic channels of excitable membranes. Massachusetts: Sinauer Associates Inc.

Hirai, H., Launey, T., Mikawa, S., Torashima, T., Yanagihara, D., Kasaura, T., Miyamoto, A. and Yuzaki, M. (2003). New role of delta2-glutamate receptors in AMPA receptor trafficking and cerebellar function. Nature Neuroscience *6*, 869–76.

Holderith, N., Lorincz, A., Katona, G., Rózsa, B., Kulik, A., Watanabe, M. and Nusser, Z. (2012). Release probability of hippocampal glutamatergic terminals scales with the size of the active zone. Nature Neuroscience *15*, 988–97.

Hollmann, M. and Heinemann, S. (1994). Cloned glutamate receptors. Annual Review of Neuroscience *17*, 31–108.

Hoogenraad, C. C., Popa, I., Futai, K., Martinez-Sanchez, E., Sanchez-Martinez, E., Wulf, P. S., van Vlijmen, T., Dortland, B. R., Oorschot, V., Govers, R., Monti, M., Heck, A. J. R., Sheng, M., Klumperman, J., Rehmann, H., Jaarsma, D., Kapitein, L. C. and van der Sluijs, P. (2010). Neuron specific Rab4 effector GRASP-1 coordinates membrane specialization and maturation of recycling endosomes. PLoS Biology *8*, e1000283.

Hori, Y., Endo, K. and Takahashi, T. (1992). Presynaptic inhibitory action of enkephalin on excitatory transmission in superficial dorsal horn of rat spinal cord. The Journal of Physiology *450*, 673–85.

Howard, M. A., Elias, G. M., Elias, L. A. B., Swat, W. and Nicoll, R. A. (2010). The role of SAP97 in synaptic glutamate receptor dynamics. Proceedings of the National Academy of Sciences of the United States of America *107*, 3805–10.

Hua, Y., Sinha, R., Martineau, M., Kahms, M. and Klingauf, J. (2010). A common origin of synaptic vesicles undergoing evoked and spontaneous fusion. Nature Neuroscience *13*, 1451–1453.

Huang, H. and Bordey, A. (2004). Glial glutamate transporters limit spillover activation of presynaptic NMDA receptors and influence synaptic inhibition of Purkinje neurons. The Journal of Neuroscience *24*, 5659–69.

Huang, Y. H., Ishikawa, M., Lee, B. R., Nakanishi, N., Schluter, O. M. and Dong, Y. (2011a). Searching for Presynaptic NMDA Receptors in the Nucleus Accumbens. The Journal of Neuroscience *31*, 18453–18463.

Huang, Z., Lujan, R., Kadurin, I., Uebele, V. N., Renger, J. J., Dolphin, A. C. and Shah, M. M. (2011b). Presynaptic HCN1 channels regulate Cav3.2 activity and neurotransmission at select cortical synapses. Nature Neuroscience *14*, 478–86.

Huang, Z. J., Cristo, G. D. and Ango, F. (2007). Development of GABA innervation in the cerebral and cerebellar cortices. Nature Reviews Neuroscience *8*, 673–86.

Hubbard, J. I., Jones, S. F. and Landau, E. M. (1968). On the mechanism by which calcium and magnesium affect the spontaneous release of transmitter from mammalian motor nerve terminals. The Journal of Physiology *194*, 355–80.

Hull, C., Adesnik, H. and Scanziani, M. (2009). Neocortical Disynaptic Inhibition Requires Somatodendritic Integration in Interneurons. The Journal of Neuroscience *29*, 8991.

Hull, C. and Regehr, W. G. (2012). Identification of an inhibitory circuit that regulates cerebellar Golgi cell activity. Neuron *73*, 149–58.

Humeau, Y., Shaban, H., Bissière, S. and Lüthi, A. (2003). Presynaptic induction of heterosynaptic associative plasticity in the mammalian brain. Nature *426*, 841–5.

Ishikawa, T., Kaneko, M., Shin, H.-S. and Takahashi, T. (2005). Presynaptic N-type and P/Q-type Ca2+ channels mediating synaptic transmission at the calyx of Held of mice. The Journal of Physiology *568*, 199–209.

Ishikawa, T., Nakamura, Y., Saitoh, N., Li, W.-B., Iwasaki, S. and Takahashi, T. (2003). Distinct roles of Kv1 and Kv3 potassium channels at the calyx of Held presynaptic terminal. The Journal of Neuroscience *23*, 10445–53.

Isope, P. and Barbour, B. (2002). Properties of unitary granule cell–>Purkinje cell synapses in adult rat cerebellar slices. The Journal of Neuroscience *22*, 9668–78.

Ito, M., Yoshida, M. and Obata, K. (1964). Monosynaptic inhibition of the intracerebellar nuclei induced rom the cerebellar cortex. Experientia *20*, 575–6.

Ito-Ishida, A., Miyazaki, T., Miura, E., Matsuda, K., Watanabe, M., Yuzaki, M. and Okabe, S. (2012). Presynaptically released Cbln1 induces dynamic axonal structural changes by interacting with GluD2 during cerebellar synapse formation. Neuron *76*, 549–64.

Ives, J. H., Fung, S., Tiwari, P., Payne, H. L. and Thompson, C. L. (2004). Microtubule-associated protein light chain 2 is a stargazin-AMPA receptor complex-interacting protein in vivo. The Journal of Biological Chemistry *279*, 31002–9.

Jackson, A. C., Milstein, A. D., Soto, D., Farrant, M., Cull-Candy, S. G. and Nicoll, R. A. (2011). Probing TARP modulation of AMPA receptor conductance with polyamine toxins. The Journal of Neuroscience *31*, 7511–20.

Jackson, A. C. and Nicoll, R. A. (2011a). Stargazin (TARP gamma-2) is required for compartment-specific AMPA receptor trafficking and synaptic plasticity in cerebellar stellate cells. The Journal of Neuroscience *31*, 3939–52.

Jackson, A. C. and Nicoll, R. A. (2011b). The expanding social network of ionotropic glutamate receptors: TARPs and other transmembrane auxiliary subunits. Neuron *70*, 178–99.

Jaeger, D. and Bower, J. M. (1999). Synaptic control of spiking in cerebellar Purkinje cells: dynamic current clamp based on model conductances. The Journal of Neuroscience *19*, 6090–101.

Jaeger, D., Schutter, E. D. and Bower, J. M. (1997). The role of synaptic and voltage-gated currents in the control of Purkinje cell spiking: a modeling study. The Journal of Neuroscience *17*, 91–106.

Jakab, R. L. and Hámori, J. (1988). Quantitative morphology and synaptology of cerebellar glomeruli in the rat. Anatomy and Embryology *179*, 81–8.

Jakawich, S. K., Nasser, H. B., Strong, M. J., Mccartney, A. J., Perez, A. S., Rakesh, N., Carruthers, C. J. and Sutton, M. A. (2010). Local Presynaptic Activity Gates Homeostatic Changes in Presynaptic Function Driven by Dendritic BDNF Synthesis. Neuron *68*, 1143–1158.

Ji, Z. and Hawkes, R. (1994). Topography of Purkinje cell compartments and mossy fiber terminal fields in lobules II and III of the rat cerebellar cortex: spinocerebellar and cuneocerebellar projections. Neuroscience *61*, 935–54.

Jiang, L., Xu, J., Nedergaard, M. and Kang, J. (2001). A kainate receptor increases the efficacy of GABAergic synapses. Neuron *30*, 503–13.

Jin, R., Banke, T. G., Mayer, M. L., Traynelis, S. F. and Gouaux, E. (2003). Structural basis for partial agonist action at ionotropic glutamate receptors. Nature Neuroscience *6*, 803–10.

Jin, R., Clark, S., Weeks, A. M., Dudman, J. T., Gouaux, E. and Partin, K. M. (2005). Mechanism of positive allosteric modulators acting on AMPA receptors. The Journal of Neuroscience *25*, 9027–36.

Jin, X.-T. and Smith, Y. (2007). Activation of presynaptic kainate receptors suppresses GABAergic synaptic transmission in the rat globus pallidus. Neuroscience *149*, 338–49.

Johnson, J. W. and Ascher, P. (1987). Glycine potentiates the NMDA response in cultured mouse brain neurons. Nature *325*, 529–31.

Jörntell, H. and Ekerot, C.-F. (2003). Receptive field plasticity profoundly alters the cutaneous parallel fiber synaptic input to cerebellar interneurons in vivo. The Journal of Neuroscience *23*, 9620–31.

Jouhanneau, J.-S., Ball, S. M., Molnár, E. and Isaac, J. T. R. (2011). Mechanisms of bi-directional modulation of thalamocortical transmission in barrel cortex by presynaptic kainate receptors. Neuropharmacology *60*, 832–41.

Jourdain, P., Bergersen, L. H., Bhaukaurally, K., Bezzi, P., Santello, M., Domercq, M., Matute, C., Tonello, F., Gundersen, V. and Volterra, A. (2007). Glutamate exocytosis from astrocytes controls synaptic strength. Nature Neuroscience *10*, 331–9.

Ju, W., Morishita, W., Tsui, J., Gaietta, G., Deerinck, T. J., Adams, S. R., Garner, C. C., Tsien, R. Y., Ellisman, M. H. and Malenka, R. C. (2004). Activity-dependent regulation of dendritic synthesis and trafficking of AMPA receptors. Nature Neuroscience *7*, 244–53.

Kaech, S., Parmar, H., Roelandse, M., Bornmann, C. and Matus, A. (2001). Cytoskeletal microdifferentiation: a mechanism for organizing morphological plasticity in dendrites.

Proceedings of the National Academy of Sciences of the United States of America *98*, 7086–92.

Kakegawa, W., Miyoshi, Y., Hamase, K., Matsuda, S., Matsuda, K., Kohda, K., Emi, K., Motohashi, J., Konno, R., Zaitsu, K. and Yuzaki, M. (2011). D-serine regulates cerebellar LTD and motor coordination through the delta2 glutamate receptor. Nature Neuroscience *14*, 603–11.

Kalashnikova, E., Lorca, R. A., Kaur, I., Barisone, G. A., Li, B., Ishimaru, T., Trimmer, J. S., Mohapatra, D. P. and Díaz, E. (2010). SynDIG1: an activity-regulated, AMPA- receptor-interacting transmembrane protein that regulates excitatory synapse development. Neuron *65*, 80–93.

Kamboj, S. K., Swanson, G. T. and Cull-Candy, S. G. (1995). Intracellular spermine confers rectification on rat calcium-permeable AMPA and kainate receptors. The Journal of Physiology *486*, 297–303.

Kamiya, H. and Ozawa, S. (1998). Kainate receptor-mediated inhibition of presynaptic Ca2+ influx and EPSP in area CA1 of the rat hippocampus. The Journal of Physiology *509*, 833–45.

Kamiya, H., Ozawa, S. and Manabe, T. (2002). Kainate receptor-dependent short-term plasticity of presynaptic Ca2+ influx at the hippocampal mossy fiber synapses. The Journal of Neuroscience *22*, 9237–43.

Kaneda, M., Farrant, M. and Cull-Candy, S. G. (1995). Whole-cell and single-channel currents activated by GABA and glycine in granule cells of the rat cerebellum. The Journal of Physiology *485*, 419–35.

Karakas, E., Simorowski, N. and Furukawa, H. (2009). Structure of the zinc-bound amino-terminal domain of the NMDA receptor NR2B subunit. The EMBO Journal *28*, 3910–20.

Karakossian, M. H. and Otis, T. S. (2004). Excitation of cerebellar interneurons by group I metabotropic glutamate receptors. Journal of Neurophysiology *92*, 1558–65.

Kato, A. S., Gill, M. B., Ho, M. T., Yu, H., Tu, Y., Siuda, E. R., Wang, H., Qian, Y.-W., Nisenbaum, E. S., Tomita, S. and Bredt, D. S. (2010). Hippocampal AMPA Receptor Gating Controlled by Both TARP and Cornichon Proteins. Neuron *68*, 1082–96.

Kato, A. S., Zhou, W., Milstein, A. D., Knierman, M. D., Siuda, E. R., Dotzlaf, J. E., Yu, H., Hale, J. E., Nisenbaum, E. S., Nicoll, R. A. and Bredt, D. S. (2007). New transmembrane AMPA receptor regulatory protein isoform, gamma-7, differentially regulates AMPA receptors. The Journal of Neuroscience *27*, 4969–77.

Katz, B. (1969). The Release of Neural Transmitter Substances. Liverpool University Press, UK.

Katz, B. and Miledi, R. (1965). The effect of calcium on acetylcholine release from motor nerve terminals. Proceedings of the Royal Society of London. Series B, Biological Sciences *161*, 496–503.

Katz, B. and Miledi, R. (1967). The timing of calcium action during neuromuscular transmission. The Journal of Physiology *189*, 535–44.

Katz, B. and Miledi, R. (1968). The role of calcium in neuromuscular facilitation. The Journal of Physiology *195*, 481–92.

Katz, B. and Miledi, R. (1969). Tetrodotoxin-resistant electric activity in presynaptic terminals. The Journal of Physiology *203*, 459–87.

Kay, L., Humphreys, L., Eickholt, B. J. and Burrone, J. (2011). Neuronal activity drives matching of pre- and postsynaptic function during synapse maturation. Nature Neuroscience *14*, 688–90.

Kelly, L., Farrant, M. and Cull-Candy, S. G. (2009). Synaptic mGluR activation drives plasticity of calcium-permeable AMPA receptors. Nature Neuroscience *12*, 593–601.

Kennedy, M. J., Davison, I. G., Robinson, C. G. and Ehlers, M. D. (2010). Syntaxin-4 defines a domain for activity-dependent exocytosis in dendritic spines. Cell *141*, 524–35.

Kerchner, G. A., Wang, G. D., Qiu, C. S., Huettner, J. E. and Zhuo, M. (2001). Direct presynaptic regulation of GABA/glycine release by kainate receptors in the dorsal horn: an ionotropic mechanism. Neuron *32*, 477–88.

Kerchner, G. A., Wilding, T. J., Huettner, J. E. and Zhuo, M. (2002). Kainate receptor subunits underlying presynaptic regulation of transmitter release in the dorsal horn. The Journal of Neuroscience *22*, 8010–7.

Kerchner, G. A., Wilding, T. J., Li, P., Zhuo, M. and Huettner, J. E. (2001). Presynaptic kainate receptors regulate spinal sensory transmission. The Journal of Neuroscience *21*, 59–66.

Khaliq, Z. M., Gouwens, N. W. and Raman, I. M. (2003). The contribution of resurgent sodium current to high-frequency firing in Purkinje neurons: an experimental and modeling study. The Journal of Neuroscience *23*, 4899–912.

Kidd, F. L., Coumis, U., Collingridge, G. L., Crabtree, J. W. and Isaac, J. T. R. (2002). A presynaptic kainate receptor is involved in regulating the dynamic properties of thalamocortical synapses during development. Neuron *34*, 635–46.

Kim, C. H. and Lisman, J. E. (1999). A role of actin filament in synaptic transmission and long-term potentiation. The Journal of Neuroscience *19*, 4314–24.

Kim, C. H. and Lisman, J. E. (2001). A labile component of AMPA receptor-mediated synaptic transmission is dependent on microtubule motors, actin, and N-ethylmaleimide-sensitive factor. The Journal of Neuroscience *21*, 4188–94.

Kim, K. S., Yan, D. and Tomita, S. (2010). Assembly and stoichiometry of the AMPA receptor and transmembrane AMPA receptor regulatory protein complex. The Journal of Neuroscience *30*, 1064–72.

Kim, M.-H., Korogod, N., Schneggenburger, R., Ho, W.-K. and Lee, S.-H. (2005). Interplay between Na+/Ca2+ exchangers and mitochondria in Ca2+ clearance at the calyx of Held. The Journal of Neuroscience *25*, 6057–65.

Kirischuk, S., Clements, J. D. and Grantyn, R. (2002). Presynaptic and postsynaptic mechanisms underlie paired pulse depression at single GABAergic boutons in rat collicular cultures. The Journal of Physiology *543*, 99–116.

Kistner, U., Wenzel, B. M., Veh, R. W., Cases-Langhoff, C., Garner, A. M., Appeltauer, U., Voss, B., Gundelfinger, E. D. and Garner, C. C. (1993). SAP90, a rat presynaptic protein related to the product of the Drosophila tumor suppressor gene dlg-A. The Journal of Biological Chemistry *268*, 4580–3.

Kiyonaka, S., Wakamori, M., Miki, T., Uriu, Y., Nonaka, M., Bito, H., Beedle, A. M., Mori, E., Hara, Y., Waard, M. D., Kanagawa, M., Itakura, M., Takahashi, M., Campbell, K. P. and Mori, Y. (2007). RIM1 confers sustained activity and neurotransmitter vesicle anchoring to presynaptic Ca2+ channels. Nature Neuroscience *10*, 691–701.

Klausberger, T. and Somogyi, P. (2008). Neuronal diversity and temporal dynamics: the unity of hippocampal circuit operations. Science *321*, 53–7.

Klöcker, N., Bunn, R. C., Schnell, E., Caruana, G., Bernstein, A., Nicoll, R. A. and Bredt, D. S. (2002). Synaptic glutamate receptor clustering in mice lacking the SH3 and GK domains of SAP97. European Journal of Neuroscience *16*, 1517–22.

Knoll, J. and Vizi, E. S. (1970). Presynaptic inhibition of acetylcholine release by endogenous and exogenous noradrenaline at high rate of stimulation. British Journal of Pharmacology *40*, 554–555.

Knoll, J. and Vizi, E. S. (1971). Effect of frequency of stimulation on the inhibition by noradrenaline of the acetylcholine output from parasympathetic nerve terminals. British Journal of Pharmacology *42*, 263–72.

Kochubey, O., Lou, X. and Schneggenburger, R. (2011). Regulation of transmitter release by Ca(2+) and synaptotagmin: insights from a large CNS synapse. Trends in Neurosciences *34*, 237–46.

Koenig, J. H. and Ikeda, K. (1999). Contribution of active zone subpopulation of vesicles to evoked and spontaneous release. Journal of Neurophysiology *81*, 1495–505.

Koester, H. J. and Johnston, D. (2005). Target cell-dependent normalization of transmitter release at neocortical synapses. Science *308*, 863–6.

Koh, D. S., Burnashev, N. and Jonas, P. (1995). Block of native Ca(2+)-permeable AMPA receptors in rat brain by intracellular polyamines generates double rectification. The Journal of Physiology *486*, 305–12.

Koike, M., Tsukada, S., Tsuzuki, K., Kijima, H. and Ozawa, S. (2000). Regulation of kinetic properties of GluR2 AMPA receptor channels by alternative splicing. The Journal of Neuroscience *20*, 2166–74.

Kojima, H. and Takahashi, T. (1985). Characterization of miniature inhibitory post-synaptic potentials in rat spinal motoneurones. The Journal of Physiology *368*, 627–40.

Kollo, M., Holderith, N. B. and Nusser, Z. (2006). Novel subcellular distribution pattern of A-type K+ channels on neuronal surface. The Journal of Neuroscience *26*, 2684–91.

Kombian, S. B., Hirasawa, M., Mouginot, D., Chen, X. and Pittman, Q. J. (2000). Short-term potentiation of miniature excitatory synaptic currents causes excitation of supraoptic neurons. Journal of Neurophysiology *83*, 2542–53.

Kondo, S. and Marty, A. (1998). Synaptic currents at individual connections among stellate cells in rat cerebellar slices. The Journal of Physiology *509*, 221–32.

Konnerth, A., Llano, I. and Armstrong, C. M. (1990). Synaptic currents in cerebellar Purkinje cells. Proceedings of the National Academy of Sciences of the United States of America *87*, 2662–5.

Korbo, L., Andersen, B. B., Ladefoged, O. and Møller, A. (1993). Total numbers of various cell types in rat cerebellar cortex estimated using an unbiased stereological method. Brain Research *609*, 262–8.

Kotchabhakdi, N. and Walberg, F. (1978). Cerebellar afferent projections from the vestibular nuclei in the cat: an experimental study with the method of retrograde axonal transport of horseradish peroxidase. Experimental Brain Research *31*, 591–604.

Kott, S., Sager, C., Tapken, D., Werner, M. and Hollmann, M. (2009). Comparative analysis of the pharmacology of GluR1 in complex with transmembrane AMPA receptor regulatory proteins gamma2, gamma3, gamma4, and gamma8. Neuroscience *158*, 78–88.

Kott, S., Werner, M., Körber, C. and Hollmann, M. (2007). Electrophysiological properties of AMPA receptors are differentially modulated depending on the associated member of the TARP family. The Journal of Neuroscience *27*, 3780–9.

Koyama, S., Matsumoto, N., Kubo, C. and Akaike, N. (2000). Presynaptic 5-HT3 receptor-mediated modulation of synaptic GABA release in the mechanically dissociated rat amygdala neurons. The Journal of Physiology *529*, 373–83.

Kristensen, A. S., Jenkins, M. A., Banke, T. G., Schousboe, A., Makino, Y., Johnson, R. C., Huganir, R. and Traynelis, S. F. (2011). Mechanism of Ca2+/calmodulin-dependent kinase II regulation of AMPA receptor gating. Nature Neuroscience *14*, 727–35.

Kumar, J., Schuck, P., Jin, R. and Mayer, M. L. (2009). The N-terminal domain of GluR6-subtype glutamate receptor ion channels. Nature Structural and Molecular Biology *16*, 631–8.

Kumar, J., Schuck, P. and Mayer, M. L. (2011). Structure and assembly mechanism for heteromeric kainate receptors. Neuron *71*, 319–31.

Kuner, T., Seeburg, P. H. and Guy, H. R. (2003). A common architecture for K+ channels and ionotropic glutamate receptors? Trends in Neurosciences *26*, 27–32.

Kuno, M. (1971). Quantum aspects of central and ganglionic synaptic transmission in vertebrates. Physiological Reviews *51*, 647–78.

Langer, S. Z. (1974). Presynaptic regulation of catecholamine release. Biochemical Pharmacology *23*, 1793–800.

Larramendi, L. M. and Lemkey-Johnston, N. (1970). The distribution of recurrent Purkinje collateral synapses in the mouse cerebellar cortex: an electron microscopic study. The Journal of Comparative Neurology *138*, 451–9.

Larsell, O. (1952). The morphogenesis and adult pattern of the lobules and fissures of the cerebellum of the white rat. The Journal of Comparative Neurology *97*, 281–356.

Larsen, R. S., Corlew, R. J., Henson, M. A., Roberts, A. C., Mishina, M., Watanabe, M., Lipton, S. A., Nakanishi, N., Pérez-Otaño, I., Weinberg, R. J. and Philpot,

B. D. (2011). NR3A-containing NMDARs promote neurotransmitter release and spike timing–dependent plasticity. Nature Neuroscience *14*, 338–44.

Lauri, S. E., Bortolotto, Z. A., Bleakman, D., Ornstein, P. L., Lodge, D., Isaac, J. T. and Collingridge, G. L. (2001). A critical role of a facilitatory presynaptic kainate receptor in mossy fiber LTP. Neuron *32*, 697–709.

Lauri, S. E., Bortolotto, Z. A., Nistico, R., Bleakman, D., Ornstein, P. L., Lodge, D., Isaac, J. T. R. and Collingridge, G. L. (2003). A role for Ca2+ stores in kainate receptor-dependent synaptic facilitation and LTP at mossy fiber synapses in the hippocampus. Neuron *39*, 327–41.

Lauri, S. E., Segerstråle, M., Vesikansa, A., Maingret, F., Mulle, C., Collingridge, G. L., Isaac, J. T. R. and Taira, T. (2005). Endogenous activation of kainate receptors regulates glutamate release and network activity in the developing hippocampus. The Journal of Neuroscience *25*, 4473–84.

Lauri, S. E., Vesikansa, A., Segerstråle, M., Collingridge, G. L., Isaac, J. T. R. and Taira, T. (2006). Functional maturation of CA1 synapses involves activity-dependent loss of tonic kainate receptor-mediated inhibition of glutamate release. Neuron *50*, 415–29.

Lee, C. J., Bardoni, R., Tong, C. K., Engelman, H. S., Joseph, D. J., Magherini, P. C. and Macdermott, A. B. (2002). Functional expression of AMPA receptors on central terminals of rat dorsal root ganglion neurons and presynaptic inhibition of glutamate release. Neuron *35*, 135–46.

Lee, H. K., Barbarosie, M., Kameyama, K., Bear, M. F. and Huganir, R. L. (2000). Regulation of distinct AMPA receptor phosphorylation sites during bidirectional synaptic plasticity. Nature *405*, 955–9.

Lee, M.-C., Yasuda, R. and Ehlers, M. D. (2010a). Metaplasticity at single glutamatergic synapses. Neuron *66*, 859–70.

Lee, S.-H., Govindaiah, G. and Cox, C. L. (2010b). Selective excitatory actions of DNQX and CNQX in rat thalamic neurons. Journal of Neurophysiology *103*, 1728–34.

Lee, S. H., Liu, L., Wang, Y. T. and Sheng, M. (2002). Clathrin adaptor AP2 and NSF interact with overlapping sites of GluR2 and play distinct roles in AMPA receptor trafficking and hippocampal LTD. Neuron *36*, 661–74.

Lehre, K. P. and Danbolt, N. C. (1998). The number of glutamate transporter subtype molecules at glutamatergic synapses: chemical and stereological quantification in young adult rat brain. The Journal of Neuroscience *18*, 8751–7.

Lemkey-Johnston, N. and Larramendi, L. M. (1968). Types and distribution of synapses upon basket and stellate cells of the mouse cerebellum: an electron microscopic study. The Journal of Comparative Neurology *134*, 73–112.

Letts, V. A., Felix, R., Biddlecome, G. H., Arikkath, J., Mahaffey, C. L., Valenzuela, A., Bartlett, F. S., Mori, Y., Campbell, K. P. and Frankel, W. N. (1998). The mouse stargazer gene encodes a neuronal Ca2+-channel gamma subunit. Nature Genetics *19*, 340–7.

Li, L., Bischofberger, J. and Jonas, P. (2007). Differential gating and recruitment of P/Q-, N-, and R-type Ca2+ channels in hippocampal mossy fiber boutons. The Journal of Neuroscience *27*, 13420–9.

Li, Y.-H., Han, T.-Z. and Meng, K. (2008). Tonic facilitation of glutamate release by glycine binding sites on presynaptic NR2B-containing NMDA autoreceptors in the rat visual cortex. Neuroscience Letters *432*, 212–6.

Lien, C.-C., Mu, Y., Vargas-Caballero, M. and ming Poo, M. (2006). Visual stimuli-induced LTD of GABAergic synapses mediated by presynaptic NMDA receptors. Nature Neuroscience *9*, 372–80.

Lin, A., Hou, Q., Jarzylo, L., Amato, S., Gilbert, J., Shang, F. and Man, H.-Y. (2011). Nedd4-mediated AMPA receptor ubiquitination regulates receptor turnover and trafficking. Journal of Neurochemistry *119*, 27–39.

Lin, A. W. and Man, H.-Y. (2013). Ubiquitination of neurotransmitter receptors and postsynaptic scaffolding proteins. Neural Plasticity *2013*, 432057.

Lin, D.-T., Makino, Y., Sharma, K., Hayashi, T., Neve, R., Takamiya, K. and Huganir, R. L. (2009). Regulation of AMPA receptor extrasynaptic insertion by 4.1N, phosphorylation and palmitoylation. Nature Neuroscience *12*, 879–87.

Liu, H., Dean, C., Arthur, C. P., Dong, M. and Chapman, E. R. (2009). Autapses and networks of hippocampal neurons exhibit distinct synaptic transmission phenotypes in the absence of synaptotagmin I. The Journal of Neuroscience *29*, 7395–403.

Liu, S. J. (2007). Biphasic modulation of GABA release from stellate cells by glutamatergic receptor subtypes. Journal of Neurophysiology *98*, 550–6.

Liu, S. J. and Cull-Candy, S. G. (2005). Subunit interaction with PICK and GRIP controls Ca2+ permeability of AMPARs at cerebellar synapses. Nature Neuroscience *8*, 768–75.

Liu, S. J. and Lachamp, P. (2006). The activation of excitatory glutamate receptors evokes a long-lasting increase in the release of GABA from cerebellar stellate cells. The Journal of Neuroscience *26*, 9332–9.

Liu, S. Q. and Cull-Candy, S. G. (2000). Synaptic activity at calcium-permeable AMPA receptors induces a switch in receptor subtype. Nature *405*, 454–8.

Llano, I. and Gerschenfeld, H. M. (1993). Inhibitory synaptic currents in stellate cells of rat cerebellar slices. The Journal of Physiology *468*, 177–200.

Llano, I., González, J., Caputo, C., Lai, F. A., Blayney, L. M., Tan, Y. P. and Marty, A. (2000). Presynaptic calcium stores underlie large-amplitude miniature IPSCs and spontaneous calcium transients. Nature Neuroscience *3*, 1256–65.

Llano, I., Marty, A., Armstrong, C. M. and Konnerth, A. (1991). Synaptic- and agonist-induced excitatory currents of Purkinje cells in rat cerebellar slices. J Physiol (Lond) *434*, 183–213.

Llinás, R. and Nicholson, C. (1971). Electrophysiological properties of dendrites and somata in alligator Purkinje cells. Journal of Neurophysiology *34*, 532–51.

Llinás, R., Nicholson, C., Freeman, J. A. and Hillman, D. E. (1968). Dendritic spikes and their inhibition in alligator Purkinje cells. Science *160*, 1132–5.

Llinás, R. and Sugimori, M. (1980). Electrophysiological properties of in vitro Purkinje cell somata in mammalian cerebellar slices. The Journal of Physiology *305*, 171–95.

Llinás, R., Sugimori, M. and Silver, R. B. (1992). Presynaptic calcium concentration microdomains and transmitter release. The Journal of Physiology *86*, 135–8.

Lodge, D. (2009). The history of the pharmacology and cloning of ionotropic glutamate receptors and the development of idiosyncratic nomenclature. Neuropharmacology *56*, 6–21.

Loewenstein, Y., Mahon, S., Chadderton, P., Kitamura, K., Sompolinsky, H., Yarom, Y. and Häusser, M. (2005). Bistability of cerebellar Purkinje cells modulated by sensory stimulation. Nature Neuroscience *8*, 202–11.

Loewi, O. (1921). Über humorale übertragbarkeit der herznervenwirkung. Pflügers Archive European Journal of Physiology *189*, 239–242.

Lomeli, H., Mosbacher, J., Melcher, T., Höger, T., Geiger, J. R., Kuner, T., Monyer, H., Higuchi, M., Bach, A. and Seeburg, P. H. (1994). Control of kinetic properties of AMPA receptor channels by nuclear RNA editing. Science *266*, 1709–13.

Lomeli, H., Sprengel, R., Laurie, D. J., Köhr, G., Herb, A., Seeburg, P. H. and Wisden, W. (1993). The rat delta-1 and delta-2 subunits extend the excitatory amino acid receptor family. FEBS Letters *315*, 318–22.

Lou, X., Scheuss, V. and Schneggenburger, R. (2005). Allosteric modulation of the presynaptic Ca2+ sensor for vesicle fusion. Nature *435*, 497–501.

Lourenço, J., Cannich, A., Carta, M., Coussen, F., Mulle, C. and Marsicano, G. (2010). Synaptic activation of kainate receptors gates presynaptic CB(1) signaling at GABAergic synapses. Nature Neuroscience *13*, 197–204.

Lovero, K. L., Blankenship, S. M., Shi, Y. and Nicoll, R. A. (2013). SynDIG1 Promotes Excitatory Synaptogenesis Independent of AMPA Receptor Trafficking and Biophysical Regulation. PLoS ONE *8*, e66171.

Lu, J., Helton, T. D., Blanpied, T. A., Rácz, B., Newpher, T. M., Weinberg, R. J. and Ehlers, M. D. (2007). Postsynaptic positioning of endocytic zones and AMPA receptor cycling by physical coupling of dynamin-3 to Homer. Neuron *55*, 874–89.

Lu, W., Isozaki, K., Roche, K. W. and Nicoll, R. A. (2010). Synaptic targeting of AMPA receptors is regulated by a CaMKII site in the first intracellular loop of GluA1. Proceedings of the National Academy of Sciences of the United States of America *107*, 22266–71.

Lu, W. and Roche, K. W. (2012). Posttranslational regulation of AMPA receptor trafficking and function. Current Opinion in Neurobiology *22*, 470–9.

Lu, W., Shi, Y., Jackson, A. C., Bjorgan, K., During, M. J., Sprengel, R., Seeburg, P. H. and Nicoll, R. A. (2009). Subunit composition of synaptic AMPA receptors revealed by a single-cell genetic approach. Neuron *62*, 254–68.

Lüscher, C., Xia, H., Beattie, E. C., Carroll, R. C., von Zastrow, M., Malenka, R. C. and Nicoll, R. A. (1999). Role of AMPA receptor cycling in synaptic transmission and plasticity. Neuron *24*, 649–58.

Lussier, M. P., Nasu-Nishimura, Y. and Roche, K. W. (2011). Activity-dependent ubiquitination of the AMPA receptor subunit GluA2. The Journal of Neuroscience *31*, 3077–81.

Lysetskiy, M., Földy, C. and Soltesz, I. (2005). Long- and short-term plasticity at mossy fiber synapses on mossy cells in the rat dentate gyrus. Hippocampus *15*, 691–6.

Maccaferri, G. and Dingledine, R. (2002). Complex effects of CNQX on CA1 interneurons of the developing rat hippocampus. Neuropharmacology *43*, 523–9.

Maier, W., Schemm, R., Grewer, C. and Laube, B. (2007). Disruption of interdomain interactions in the glutamate binding pocket affects differentially agonist affinity and efficacy of N-methyl-D-aspartate receptor activation. The Journal of Biological Chemistry *282*, 1863–72.

Maingret, F., Lauri, S. E., Taira, T. and Isaac, J. T. R. (2005). Profound regulation of neonatal CA1 rat hippocampal GABAergic transmission by functionally distinct kainate receptor populations. The Journal of Physiology *567*, 131–42.

Malinow, R. and Tsien, R. W. (1990). Presynaptic enhancement shown by whole-cell recordings of long-term potentiation in hippocampal slices. Nature *346*, 177–80.

Mameli, M., Carta, M., Partridge, L. D. and Valenzuela, C. F. (2005). Neurosteroid-induced plasticity of immature synapses via retrograde modulation of presynaptic NMDA receptors. The Journal of Neuroscience *25*, 2285–94.

Man, H.-Y., Sekine-Aizawa, Y. and Huganir, R. L. (2007). Regulation of alpha-amino-3-hydroxy-5-methyl-4-isoxazolepropionic acid receptor trafficking through PKA phosphorylation of the Glu receptor 1 subunit. Proceedings of the National Academy of Sciences of the United States of America *104*, 3579–84.

Manita, S., Suzuki, T., Inoue, M., Kudo, Y. and Miyakawa, H. (2007). Paired-pulse ratio of synaptically induced transporter currents at hippocampal CA1 synapses is not related to release probability. Brain Research *1154*, 71–9.

Mann-Metzer, P. and Yarom, Y. (1999). Electrotonic coupling interacts with intrinsic properties to generate synchronized activity in cerebellar networks of inhibitory interneurons. The Journal of Neuroscience *19*, 3298–306.

Mann-Metzer, P. and Yarom, Y. (2002a). Jittery trains induced by synaptic-like currents in cerebellar inhibitory interneurons. Journal of Neurophysiology *87*, 149–56.

Mann-Metzer, P. and Yarom, Y. (2002b). Pre- and postsynaptic inhibition mediated by GABA(B) receptors in cerebellar inhibitory interneurons. Journal of Neurophysiology *87*, 183–90.

Markram, H., Wang, Y. and Tsodyks, M. (1998). Differential signaling via the same axon of neocortical pyramidal neurons. Proceedings of the National Academy of Sciences of the United States of America *95*, 5323–8.

Marra, V., Burden, J. J., Thorpe, J. R., Smith, I. T., Smith, S. L., Häusser, M., Branco, T. and Staras, K. (2012). A preferentially segregated recycling vesicle pool of limited size supports neurotransmission in native central synapses. Neuron *76*, 579–89.

Maruta, J., Hensbroek, R. A. and Simpson, J. I. (2007). Intraburst and interburst signaling by climbing fibers. The Journal of Neuroscience *27*, 11263–70.

Masu, M., Tanabe, Y., Tsuchida, K., Shigemoto, R. and Nakanishi, S. (1991). Sequence and expression of a metabotropic glutamate receptor. Nature *349*, 760–5.

Mathew, S. S. and Hablitz, J. J. (2011). Presynaptic NMDA receptors mediate IPSC potentiation at GABAergic synapses in developing rat neocortex. PLoS ONE *6*, e17311.

Mathews, P. J., Lee, K. H., Peng, Z., Houser, C. R. and Otis, T. S. (2012). Effects of climbing fiber driven inhibition on Purkinje neuron spiking. The Journal of Neuroscience *32*, 17988–97.

Matsuda, K., Fletcher, M., Kamiya, Y. and Yuzaki, M. (2003). Specific assembly with the NMDA receptor 3B subunit controls surface expression and calcium permeability of NMDA receptors. The Journal of Neuroscience *23*, 10064–73.

Matsuda, S., Kamiya, Y. and Yuzaki, M. (2005). Roles of the N-terminal domain on the function and quaternary structure of the ionotropic glutamate receptor. The Journal of Biological Chemistry *280*, 20021–9.

Matsuda, S., Mikawa, S. and Hirai, H. (1999). Phosphorylation of serine-880 in GluR2 by protein kinase C prevents its C terminus from binding with glutamate receptor-interacting protein. Journal of Neurochemistry *73*, 1765–8.

Matsuda, S., Miura, E., Matsuda, K., Kakegawa, W., Kohda, K., Watanabe, M. and Yuzaki, M. (2008a). Accumulation of AMPA receptors in autophagosomes in neuronal axons lacking adaptor protein AP-4. Neuron *57*, 730–45.

Matsuda, S., Miura, E., Matsuda, K., Kakegawa, W., Kohda, K., Watanabe, M. and Yuzaki, M. (2008b). Accumulation of AMPA receptors in autophagosomes in neuronal axons lacking adaptor protein AP-4. Neuron *57*, 730–45.

Maximov, A., Tang, J., Yang, X., Pang, Z. P. and Südhof, T. C. (2009). Complexin controls the force transfer from SNARE complexes to membranes in fusion. Science *323*, 516–21.

McGuinness, L., Taylor, C., Taylor, R. D. T., Yau, C., Langenhan, T., Hart, M. L., Christian, H., Tynan, P. W., Donnelly, P. and Emptage, N. J. (2010). Presynaptic NMDARs in the hippocampus facilitate transmitter release at theta frequency. Neuron *68*, 1109–27.

McKay, B. E. and Turner, R. W. (2004). Kv3 K+ channels enable burst output in rat cerebellar Purkinje cells. European Journal of Neuroscience *20*, 729–39.

McKinney, R. A., Capogna, M., Dürr, R., Gähwiler, B. H. and Thompson, S. M. (1999). Miniature synaptic events maintain dendritic spines via AMPA receptor activation. Nature Neuroscience *2*, 44–9.

Meinrenken, C. J., Borst, J. G. G. and Sakmann, B. (2002). Calcium secretion coupling at calyx of held governed by nonuniform channel-vesicle topography. The Journal of Neuroscience *22*, 1648–67.

Mejia-Gervacio, S., Collin, T., Pouzat, C., Tan, Y. P., Llano, I. and Marty, A. (2007). Axonal speeding: shaping synaptic potentials in small neurons by the axonal membrane compartment. Neuron *53*, 843–55.

Mejia-Gervacio, S. and Marty, A. (2006). Control of interneurone firing pattern by axonal autoreceptors in the juvenile rat cerebellum. The Journal of Physiology *571*, 43–55.

Melcher, T., Maas, S., Herb, A., Sprengel, R., Seeburg, P. H. and Higuchi, M. (1996). A mammalian RNA editing enzyme. Nature *379*, 460–4.

Mennerick, S. and Zorumski, C. F. (1995). Paired-pulse modulation of fast excitatory synaptic currents in microcultures of rat hippocampal neurons. The Journal of Physiology *488*, 85–101.

Menuz, K. and Nicoll, R. A. (2008). Loss of Inhibitory Neuron AMPA Receptors Contributes to Ataxia and Epilepsy in Stargazer Mice. The Journal of Neuroscience *28*, 10599–10603.

Menuz, K., O'Brien, J. L., Karmizadegan, S., Bredt, D. S. and Nicoll, R. A. (2008). TARP redundancy is critical for maintaining AMPA receptor function. The Journal of Neuroscience *28*, 8740–6.

Menuz, K., Stroud, R. M., Nicoll, R. A. and Hays, F. A. (2007). TARP auxiliary subunits switch AMPA receptor antagonists into partial agonists. Science *318*, 815–7.

Midgett, C. R. and Madden, D. R. (2008). The quaternary structure of a calcium-permeable AMPA receptor: conservation of shape and symmetry across functionally distinct subunit assemblies. Journal of Molecular Biology *382*, 578–84.

Midtgaard, J. (1992). Membrane properties and synaptic responses of Golgi cells and stellate cells in the turtle cerebellum in vitro. The Journal of Physiology *457*, 329–54.

Milstein, A. D., Zhou, W., Karimzadegan, S., Bredt, D. S. and Nicoll, R. A. (2007). TARP subtypes differentially and dose-dependently control synaptic AMPA receptor gating. Neuron *55*, 905–18.

Min, M. Y., Melyan, Z. and Kullmann, D. M. (1999). Synaptically released glutamate reduces gamma-aminobutyric acid (GABA)ergic inhibition in the hippocampus via kainate receptors. Proceedings of the National Academy of Sciences of the United States of America *96*, 9932–7.

Mitchell, S. J. and Silver, R. A. (2003). Shunting inhibition modulates neuronal gain during synaptic excitation. Neuron *38*, 433–45.

Mittmann, W., Koch, U. and Häusser, M. (2005). Feed-forward inhibition shapes the spike output of cerebellar Purkinje cells. The Journal of Physiology *563*, 369–78.

Mochida, S., Few, A. P., Scheuer, T. and Catterall, W. A. (2008). Regulation of presynaptic Ca(V)2.1 channels by Ca2+ sensor proteins mediates short-term synaptic plasticity. Neuron *57*, 210–6.

Monaghan, D. T., Bridges, R. J. and Cotman, C. W. (1989). The excitatory amino acid receptors: their classes, pharmacology, and distinct properties in the function of the central nervous system. Annual Review of Pharmacology and Toxicology *29*, 365–402.

Monsivais, P., Clark, B. A., Roth, A. and Häusser, M. (2005). Determinants of action potential propagation in cerebellar Purkinje cell axons. The Journal of Neuroscience *25*, 464–72.

Monyer, H., Seeburg, P. H. and Wisden, W. (1991). Glutamate-operated channels: developmentally early and mature forms arise by alternative splicing. Neuron *6*, 799–810.

Mortensen, M. and Smart, T. G. (2006). Extrasynaptic alpha/beta subunit GABAA receptors on rat hippocampal pyramidal neurons. The Journal of Physiology *577*, 841–856.

Mosbacher, J., Schoepfer, R., Monyer, H., Burnashev, N., Seeburg, P. H. and Ruppersberg, J. P. (1994). A molecular determinant for submillisecond desensitization in glutamate receptors. Science *266*, 1059–62.

Moser, T. and Beutner, D. (2000). Kinetics of exocytosis and endocytosis at the cochlear inner hair cell afferent synapse of the mouse. Proceedings of the National Academy of Sciences of the United States of America *97*, 883–8.

Mukherjee, K., Yang, X., Gerber, S. H., Kwon, H.-B., Ho, A., Castillo, P. E., Liu, X. and Südhof, T. C. (2010). Piccolo and bassoon maintain synaptic vesicle clustering without directly participating in vesicle exocytosis. Proceedings of the National Academy of Sciences of the United States of America *107*, 6504–9.

Mulle, C., Sailer, A., Swanson, G. T., Brana, C., O'Gorman, S., Bettler, B. and Heinemann, S. F. (2000). Subunit composition of kainate receptors in hippocampal interneurons. Neuron *28*, 475–84.

Murthy, V. N., Schikorski, T., Stevens, C. F. and Zhu, Y. (2001). Inactivity produces increases in neurotransmitter release and synapse size. Neuron *32*, 673–82.

Murthy, V. N., Sejnowski, T. J. and Stevens, C. F. (1997). Heterogeneous release properties of visualized individual hippocampal synapses. Neuron *18*, 599–612.

Murthy, V. N. and Stevens, C. F. (1999). Reversal of synaptic vesicle docking at central synapses. Nature Neuroscience *2*, 503–7.

Nakagawa, T. (2010). The biochemistry, ultrastructure, and subunit assembly mechanism of AMPA receptors. Molecular Neurobiology *42*, 161–84.

Nakagawa, T., Cheng, Y., Ramm, E., Sheng, M. and Walz, T. (2005). Structure and different conformational states of native AMPA receptor complexes. Nature *433*, 545–9.

Napper, R. M. and Harvey, R. J. (1988). Number of parallel fiber synapses on an individual Purkinje cell in the cerebellum of the rat. The Journal of Comparative Neurology *274*, 168–77.

Naraghi, M. (1997). T-jump study of calcium binding kinetics of calcium chelators. Cell Calcium *22*, 255–68.

Neher, E. (1998). Usefulness and limitations of linear approximations to the understanding of Ca++ signals. Cell Calcium *24*, 345–57.

Neher, E. and Sakaba, T. (2008). Multiple roles of calcium ions in the regulation of neurotransmitter release. Neuron *59*, 861–72.

Ng, D., Pitcher, G. M., Szilard, R. K., Sertié, A., Kanisek, M., Clapcote, S. J., Lipina, T., Kalia, L. V., Joo, D., McKerlie, C., Cortez, M., Roder, J. C., Salter, M. W. and McInnes, R. R. (2009). Neto1 is a novel CUB-domain NMDA receptor-interacting protein required for synaptic plasticity and learning. PLoS Biology *7*, e41.

Nicholson, C., ten Bruggencate, G., Stöckle, H. and Steinberg, R. (1978). Calcium and potassium changes in extracellular microenvironment of cat cerebellar cortex. Journal of Neurophysiology *41*, 1026–39.

Nicoletti, F., Wroblewski, J. T., Novelli, A., Alho, H., Guidotti, A. and Costa, E. (1986). The activation of inositol phospholipid metabolism as a signal-transducing system for

excitatory amino acids in primary cultures of cerebellar granule cells. The Journal of Neuroscience *6*, 1905–11.

Nikishi, T. I. and Augustine, G. J. (2004). Synaptotagmin I synchronizes transmitter release in mouse hippocampal neurons. The Journal of Neuroscience *24*, 6127–32.

Noebels, J. L., Qiao, X., Bronson, R. T., Spencer, C. and Davisson, M. T. (1990). Stargazer: a new neurological mutant on chromosome 15 in the mouse with prolonged cortical seizures. Epilepsy Research *7*, 129–35.

Nusser, Z., Cull-Candy, S. G. and Farrant, M. (1997). Differences in synaptic GABA(A) receptor number underlie variation in GABA mini amplitude. Neuron *19*, 697–709.

Nusser, Z., Naylor, D. and Mody, I. (2001). Synapse-specific contribution of the variation of transmitter concentration to the decay of inhibitory postsynaptic currents. Biophysical Journal *80*, 1251–1261.

O'Brien, R. J., Xu, D., Petralia, R. S., Steward, O., Huganir, R. L. and Worley, P. (1999). Synaptic clustering of AMPA receptors by the extracellular immediate-early gene product Narp. Neuron *23*, 309–23.

Ohana, O. and Sakmann, B. (1998). Transmitter release modulation in nerve terminals of rat neocortical pyramidal cells by intracellular calcium buffers. The Journal of Physiology *513*, 135–48.

O'Hara, P. J., Sheppard, P. O., Thøgersen, H., Venezia, D., Haldeman, B. A., McGrane, V., Houamed, K. M., Thomsen, C., Gilbert, T. L. and Mulvihill, E. R. (1993). The ligand-binding domain in metabotropic glutamate receptors is related to bacterial periplasmic binding proteins. Neuron *11*, 41–52.

Ohno-Shosaku, T., Maejima, T. and Kano, M. (2001). Endogenous cannabinoids mediate retrograde signals from depolarized postsynaptic neurons to presynaptic terminals. Neuron *29*, 729–38.

Oldfield, C. S., Marty, A. and Stell, B. M. (2010). Interneurons of the cerebellar cortex toggle Purkinje cells between up and down states. Proceedings of the National Academy of Sciences of the United States of America *107*, 13153–8.

Oliva, A. A., Jiang, M., Lam, T., Smith, K. L. and Swann, J. W. (2000). Novel hippocampal interneuronal subtypes identified using transgenic mice that express green fluorescent protein in GABAergic interneurons. The Journal of Neuroscience *20*, 3354–68.

Opazo, P., Labrecque, S., Tigaret, C. M., Frouin, A., Wiseman, P. W., Koninck, P. D. and Choquet, D. (2010). CaMKII Triggers the Diffusional Trapping of Surface AMPARs through Phosphorylation of Stargazin. Neuron *67*, 239–252.

Oyler, G. A., Higgins, G. A., Hart, R. A., Battenberg, E., Billingsley, M., Bloom, F. E. and Wilson, M. C. (1989). The identification of a novel synaptosomal-associated protein, SNAP-25, differentially expressed by neuronal subpopulations. The Journal of Cell Biology *109*, 3039–52.

Paillart, C., Li, J., Matthews, G. and Sterling, P. (2003). Endocytosis and vesicle recycling at a ribbon synapse. The Journal of Neuroscience *23*, 4092–9.

Palade, G. E. and Palay, S. L. (1954). Electron microscope observations of interneuronal and neuromuscular synapses. The Anatomical Record *118*, 335–336.

Palay, S. L. and Chan-Palay, V. (1974). Cerebellar Cortex: Cytology and organization. Berlin: Springer-Verlag.

Palkovits, M., Magyar, P. and Szentágothai, J. (1972). Quantitative histological analysis of the cerebellar cortex in the cat. IV. Mossy fiber-Purkinje cell numerical transfer. Brain Research *45*, 15–29.

Palmer, L. M., Clark, B. A., Gründemann, J., Roth, A., Stuart, G. J. and Häusser, M. (2010). Initiation of simple and complex spikes in cerebellar Purkinje cells. The Journal of Physiology *588*, 1709–17.

Pan, Z. H., Hu, H. J., Perring, P. and Andrade, R. (2001). T-type Ca(2+) channels mediate neurotransmitter release in retinal bipolar cells. Neuron *32*, 89–98.

Partin, K. M., Patneau, D. K. and Mayer, M. L. (1994). Cyclothiazide differentially modulates desensitization of alpha-amino-3-hydroxy-5-methyl-4-isoxazolepropionic acid receptor splice variants. Molecular Pharmacology *46*, 129–38.

Partovi, D. and Frerking, M. (2006). Presynaptic inhibition by kainate receptors converges mechanistically with presynaptic inhibition by adenosine and GABAB receptors. Neuropharmacology *51*, 1030–7.

Pasternack, A., Coleman, S. K., Jouppila, A., Mottershead, D. G., Lindfors, M., Pasternack, M. and Keinänen, K. (2002). Alpha-amino-3-hydroxy-5-methyl-4-isoxazolepropionic acid (AMPA) receptor channels lacking the N-terminal domain. The Journal of Biological Chemistry *277*, 49662–7.

Paton, W. (1958). Central and synaptic transmission in the nervous system; pharmacological aspects. Annual Review of Physiology *20*, 431–70.

Paukert, M., Huang, Y. H., Tanaka, K., Rothstein, J. D. and Bergles, D. E. (2010). Zones of enhanced glutamate release from climbing fibers in the mammalian cerebellum. The Journal of Neuroscience *30*, 7290–9.

Pei, W., Huang, Z., Wang, C., Han, Y., Park, J. S. and Niu, L. (2009). Flip and flop: a molecular determinant for AMPA receptor channel opening. Biochemistry *48*, 3767–77.

Pelkey, K. A. and McBain, C. J. (2007). Differential regulation at functionally divergent release sites along a common axon. Current Opinion in Neurobiology *17*, 366–73.

Pelkey, K. A., Topolnik, L., Lacaille, J.-C. and McBain, C. J. (2006). Compartmentalized Ca(2+) channel regulation at divergent mossy-fiber release sites underlies target cell-dependent plasticity. Neuron *52*, 497–510.

Perin-Dureau, F., Rachline, J., Neyton, J. and Paoletti, P. (2002). Mapping the binding site of the neuroprotectant ifenprodil on NMDA receptors. The Journal of Neuroscience *22*, 5955–65.

Perkel, D. J., Hestrin, S., Sah, P. and Nicoll, R. A. (1990). Excitatory synaptic currents in Purkinje cells. Proceedings of the Royal Society London, Biological Sciences *241*, 116–21.

Perrais, D., Pinheiro, P. S., Jane, D. E. and Mulle, C. (2009). Antagonism of recombinant and native GluK3-containing kainate receptors. Neuropharmacology *56*, 131–40.

Persohn, E., Malherbe, P. and Richards, J. G. (1992). Comparative molecular neuroanatomy of cloned GABAA receptor subunits in the rat CNS. The Journal of Comparative Neurology *326*, 193–216.

Pfenninger, K., Akert, K., Moor, H. and Sandri, C. (1972). The fine structure of freeze-fractured presynaptic membranes. Journal of Neurocytology *1*, 129–49.

Piccolino, M. (1997). Luigi Galvani and animal electricity: two centuries after the foundation of electrophysiology. Trends in Neurosciences *20*, 443–8.

Pickart, C. M. and Eddins, M. J. (2004). Ubiquitin: structures, functions, mechanisms. Biochimica et Biophysica Acta *1695*, 55–72.

Pijpers, A. and Ruigrok, T. J. H. (2006). Organization of pontocerebellar projections to identified climbing fiber zones in the rat. The Journal of Comparative Neurology *496*, 513–28.

Pinheiro, P. S. and Mulle, C. (2008). Presynaptic glutamate receptors: physiological functions and mechanisms of action. Nature Reviews Neuroscience *9*, 423–36.

Pinheiro, P. S., Perrais, D., Coussen, F., Barhanin, J., Bettler, B., Mann, J. R., Malva, J. O., Heinemann, S. F. and Mulle, C. (2007). GluR7 is an essential subunit of presynaptic kainate autoreceptors at hippocampal mossy fiber synapses. Proceedings of the National Academy of Sciences of the United States of America *104*, 12181–6.

Piochon, C., Irinopoulou, T., Brusciano, D., Bailly, Y., Mariani, J. and Levenes, C. (2007). NMDA receptor contribution to the climbing fiber response in the adult mouse Purkinje cell. The Journal of Neuroscience *27*, 10797–809.

Pittaluga, A., Feligioni, M., Longordo, F., Luccini, E. and Raiteri, M. (2006). Trafficking of presynaptic AMPA receptors mediating neurotransmitter release: neuronal selectivity and relationships with sensitivity to cyclothiazide. Neuropharmacology *50*, 286–96.

Pouzat, C. and Marty, A. (1998). Autaptic inhibitory currents recorded from interneurones in rat cerebellar slices. The Journal of Physiology *509*, 777–83.

Pouzat, C. and Marty, A. (1999). Somatic recording of GABAergic autoreceptor current in cerebellar stellate and basket cells. The Journal of Neuroscience *19*, 1675–90.

Praefcke, G. J. K. and McMahon, H. T. (2004). The dynamin superfamily: universal membrane tubulation and fission molecules? Nature Reviews Molecular Cell Biology *5*, 133–47.

Priel, A., Kolleker, A., Ayalon, G., Gillor, M., Osten, P. and Stern-Bach, Y. (2005). Stargazin reduces desensitization and slows deactivation of the AMPA-type glutamate receptors. The Journal of Neuroscience *25*, 2682–6.

Quiocho, F. A. and Ledvina, P. S. (1996). Atomic structure and specificity of bacterial periplasmic receptors for active transport and chemotaxis: variation of common themes. Molecular Microbiology *20*, 17–25.

Quirk, J. C., Siuda, E. R. and Nisenbaum, E. S. (2004). Molecular determinants responsible for differences in desensitization kinetics of AMPA receptor splice variants. The Journal of Neuroscience *24*, 11416–20.

Rakic, P. (1972). Extrinsic cytological determinants of basket and stellate cell dendritic pattern in the cerebellar molecular layer. The Journal of Comparative Neurology *146*, 335–354.

Rall, W., Burke, R. E., Smith, T. G., Nelson, P. G. and Frank, K. (1967). Dendritic location of synapses and possible mechanisms for the monosynaptic EPSP in motoneurons. Journal of Neurophysiology *30*, 1169–93.

Raman, I. M. and Bean, B. P. (1997). Resurgent sodium current and action potential formation in dissociated cerebellar Purkinje neurons. The Journal of Neuroscience *17*, 4517–26.

Ramirez, D. M. O., Khvotchev, M., Trauterman, B. and Kavalali, E. T. (2012). Vti1a identifies a vesicle pool that preferentially recycles at rest and maintains spontaneous neurotransmission. Neuron *73*, 121–34.

Rancillac, A. and Barbara, J. G. (2005). Frequency-dependent recruitment of inhibition mediated by stellate cells in the rat cerebellar cortex. Journal of Neuroscience Research *80*, 414–23.

Rancz, E. A. and Häusser, M. (2010). Dendritic spikes mediate negative synaptic gain control in cerebellar Purkinje cells. Proceedings of the National Academy of Sciences of the United States of America *107*, 22284–9.

Rancz, E. A., Ishikawa, T., Duguid, I., Chadderton, P., Mahon, S. and Häusser, M. (2007). High-fidelity transmission of sensory information by single cerebellar mossy fibre boutons. Nature *450*, 1245–8.

Ren, M., Yoshimura, Y., Takada, N., Horibe, S. and Komatsu, Y. (2007). Specialized inhibitory synaptic actions between nearby neocortical pyramidal neurons. Science *316*, 758–61.

Renzi, M., Farrant, M. and Cull-Candy, S. G. (2007). Climbing-fibre activation of NMDA receptors in Purkinje cells of adult mice. The Journal of Physiology *585*, 91–101.

Reyes, A., Lujan, R., Rozov, A., Burnashev, N., Somogyi, P. and Sakmann, B. (1998). Target-cell-specific facilitation and depression in neocortical circuits. Nature Neuroscience *1*, 279–85.

Ricci, A. J., Wu, Y. C. and Fettiplace, R. (1998). The endogenous calcium buffer and the time course of transducer adaptation in auditory hair cells. The Journal of Neuroscience *18*, 8261–77.

Richards, D. A., Guatimosim, C. and Betz, W. J. (2000). Two endocytic recycling routes selectively fill two vesicle pools in frog motor nerve terminals. Neuron *27*, 551–9.

Richards, D. A., Guatimosim, C., Rizzoli, S. O. and Betz, W. J. (2003). Synaptic vesicle pools at the frog neuromuscular junction. Neuron *39*, 529–41.

Richardson, C. A. and Leitch, B. (2005). Phenotype of cerebellar glutamatergic neurons is altered in stargazer mutant mice lacking brain-derived neurotrophic factor mRNA expression. The Journal of Comparative Neurology *481*, 145–59.

Riker, W., Roberts, J., Standaert, F. and Fujimori, H. (1957). The motor nerve terminal as the primary focus for drug-in-duced facilitation of neuromuscular transmission. The Journal of Pharmacology and Experimental Therapeutics *121*, 286–312.

Rinzel, J. and Rall, W. (1974). Transient response in a dendritic neuron model for current injected at one branch. Biophysical Journal *14*, 759–90.

Rizzoli, S. O. and Betz, W. J. (2004). The structural organization of the readily releasable pool of synaptic vesicles. Science *303*, 2037–9.

Rizzoli, S. O. and Betz, W. J. (2005). Synaptic vesicle pools. Nature Reviews Neuroscience *6*, 57–69.

Robert, A., Armstrong, N., Gouaux, J. E. and Howe, J. R. (2005). AMPA receptor binding cleft mutations that alter affinity, efficacy, and recovery from desensitization. The Journal of Neuroscience *25*, 3752–62.

Rocca, D. L., Amici, M., Antoniou, A., Suarez, E. B., Halemani, N., Murk, K., McGarvey, J., Jaafari, N., Mellor, J. R., Collingridge, G. L. and Hanley, J. G. (2013). The Small GTPase Arf1 Modulates Arp2/3-Mediated Actin Polymerization via PICK1 to Regulate Synaptic Plasticity. Neuron *79*, 293–307.

Rocca, D. L., Martin, S., Jenkins, E. L. and Hanley, J. G. (2008). Inhibition of Arp2/3-mediated actin polymerization by PICK1 regulates neuronal morphology and AMPA receptor endocytosis. Nature Cell Biology *10*, 259–71.

Roche, K. W., O'Brien, R. J., Mammen, A. L., Bernhardt, J. and Huganir, R. L. (1996). Characterization of multiple phosphorylation sites on the AMPA receptor GluR1 subunit. Neuron *16*, 1179–88.

Rodríguez-Moreno, A., Herreras, O. and Lerma, J. (1997). Kainate receptors presynaptically downregulate GABAergic inhibition in the rat hippocampus. Neuron *19*, 893–901.

Rodríguez-Moreno, A. and Lerma, J. (1998). Kainate receptor modulation of GABA release involves a metabotropic function. Neuron *20*, 1211–8.

Rodríguez-Moreno, A. and Paulsen, O. (2008). Spike timing-dependent long-term depression requires presynaptic NMDA receptors. Nature Neuroscience *11*, 744–5.

Rokni, D., Llinas, R. and Yarom, Y. (2007). Stars and stripes in the cerebellar cortex: a voltage sensitive dye study. Frontiers in Systems Neuroscience *1*, 1.

Rosahl, T. W., Spillane, D., Missler, M., Herz, J., Selig, D. K., Wolff, J. R., Hammer, R. E., Malenka, R. C. and Südhof, T. C. (1995). Essential functions of synapsins I and II in synaptic vesicle regulation. Nature *375*, 488–93.

Rossi, B., Maton, G. and Collin, T. (2008). Calcium-permeable presynaptic AMPA receptors in cerebellar molecular layer interneurones. The Journal of Physiology *586*, 5129–5145.

Rossi, B., Ogden, D., Llano, I., Tan, Y. P., Marty, A. and Collin, T. (2012). Current and Calcium Responses to Local Activation of Axonal NMDA Receptors in Developing Cerebellar Molecular Layer Interneurons. PLoS ONE *7*, e39983.

Rossi, D. J. and Hamann, M. (1998). Spillover-mediated transmission at inhibitory synapses promoted by high affinity alpha6 subunit GABA(A) receptors and glomerular geometry. Neuron *20*, 783–95.

Rossmann, M., Sukumaran, M., Penn, A. C., Veprintsev, D. B., Babu, M. M. and Greger,

I. H. (2011). Subunit-selective N-terminal domain associations organize the formation of AMPA receptor heteromers. The EMBO Journal *30*, 959.

Roth, A. and Häusser, M. (2001). Compartmental models of rat cerebellar Purkinje cells based on simultaneous somatic and dendritic patch-clamp recordings. The Journal of Physiology *535*, 445–72.

Rozas, J. L., Paternain, A. V. and Lerma, J. (2003). Noncanonical signaling by ionotropic kainate receptors. Neuron *39*, 543–53.

Rozov, A., Burnashev, N., Sakmann, B. and Neher, E. (2001). Transmitter release modulation by intracellular Ca2+ buffers in facilitating and depressing nerve terminals of pyramidal cells in layer 2/3 of the rat neocortex indicates a target cell-specific difference in presynaptic calcium dynamics. The Journal of Physiology *531*, 807–26.

Rozov, A., Sprengel, R. and Seeburg, P. H. (2012). GluA2-lacking AMPA receptors in hippocampal CA1 cell synapses: evidence from gene-targeted mice. Frontiers in Molecular Neuroscience *5*, 22.

Rubin, R. P. (2007). A brief history of great discoveries in pharmacology: in celebration of the centennial anniversary of the founding of the American Society of Pharmacology and Experimental Therapeutics. Pharmacological Reviews *59*, 289–359.

Rudolph, S., Overstreet-Wadiche, L. and Wadiche, J. I. (2011). Desynchronization of multivesicular release enhances Purkinje cell output. Neuron *70*, 991–1004.

Ruigrok, T. J. H., Hensbroek, R. A. and Simpson, J. I. (2011). Spontaneous activity signatures of morphologically identified interneurons in the vestibulocerebellum. The Journal of Neuroscience *31*, 712–24.

Rusakov, D. A., Saitow, F., Lehre, K. P. and Konishi, S. (2005). Modulation of presynaptic Ca2+ entry by AMPA receptors at individual GABAergic synapses in the cerebellum. The Journal of Neuroscience *25*, 4930–40.

Saglietti, L., Dequidt, C., Kamieniarz, K., Rousset, M.-C., Valnegri, P., Thoumine, O., Beretta, F., Fagni, L., Choquet, D., Sala, C., Sheng, M. and Passafaro, M. (2007). Extracellular interactions between GluR2 and N-cadherin in spine regulation. Neuron *54*, 461–77.

Sainlos, M., Tigaret, C., Poujol, C., Olivier, N. B., Bard, L., Breillat, C., Thiolon, K., Choquet, D. and Imperiali, B. (2011). Biomimetic divalent ligands for the acute disruption of synaptic AMPAR stabilization. Nature Chemical Biology *7*, 81–91.

Sakaba, T. (2008). Two Ca(2+)-dependent steps controlling synaptic vesicle fusion and replenishment at the cerebellar basket cell terminal. Neuron *57*, 406–19.

Sallert, M., Malkki, H., Segerstråle, M., Taira, T. and Lauri, S. E. (2007). Effects of the kainate receptor agonist ATPA on glutamatergic synaptic transmission and plasticity during early postnatal development. Neuropharmacology *52*, 1354–65.

Sallert, M., Rantamäki, T., Vesikansa, A., Anthoni, H., Harju, K., Yli-Kauhaluoma, J., Taira, T., Castren, E. and Lauri, S. E. (2009). Brain-derived neurotrophic factor controls activity-dependent maturation of CA1 synapses by downregulating tonic activation of presynaptic kainate receptors. The Journal of Neuroscience *29*, 11294–303.

Salussolia, C. L., Corrales, A., Talukder, I., Kazi, R., Akgul, G., Bowen, M. and Wollmuth,

L. P. (2011a). Interaction of the M4 segment with other transmembrane segments is required for surface expression of mammalian alpha-amino-3-hydroxy-5-methyl-4-isoxazolepropionic acid (AMPA) receptors. The Journal of Biological Chemistry *286*, 40205–18.

Salussolia, C. L., Prodromou, M. L., Borker, P. and Wollmuth, L. P. (2011b). Arrangement of subunits in functional NMDA receptors. The Journal of Neuroscience *31*, 11295–304.

Sans, N., Racca, C., Petralia, R. S., Wang, Y. X., McCallum, J. and Wenthold, R. J. (2001). Synapse-associated protein 97 selectively associates with a subset of AMPA receptors early in their biosynthetic pathway. The Journal of Neuroscience *21*, 7506–16.

Sara, Y., Bal, M., Adachi, M., Monteggia, L. M. and Kavalali, E. T. (2011). Use-dependent AMPA receptor block reveals segregation of spontaneous and evoked glutamatergic neurotransmission. The Journal of Neuroscience *31*, 5378–82.

Sara, Y., Virmani, T., Deák, F., Liu, X. and Kavalali, E. T. (2005). An isolated pool of vesicles recycles at rest and drives spontaneous neurotransmission. Neuron *45*, 563–73.

Sasaki, T., Matsuki, N. and Ikegaya, Y. (2011). Action-potential modulation during axonal conduction. Science *331*, 599–601.

Satake, S., Saitow, F., Rusakov, D. and Konishi, S. (2004). AMPA receptor-mediated presynaptic inhibition at cerebellar GABAergic synapses: a characterization of molecular mechanisms. European Journal of Neuroscience *19*, 2464–74.

Satake, S., Saitow, F., Yamada, J. and Konishi, S. (2000). Synaptic activation of AMPA receptors inhibits GABA release from cerebellar interneurons. Nature Neuroscience *3*, 551–8.

Satake, S., Song, S.-Y., Cao, Q., Satoh, H., Rusakov, D. A., Yanagawa, Y., Ling, E.-A., Imoto, K. and Konishi, S. (2006). Characterization of AMPA receptors targeted by the climbing fiber transmitter mediating presynaptic inhibition of GABAergic transmission at cerebellar interneuron-Purkinje cell synapses. The Journal of Neuroscience *26*, 2278–89.

Satake, S., Song, S.-Y., Konishi, S. and Imoto, K. (2010). Glutamate transporter EAAT4 in Purkinje cells controls intersynaptic diffusion of climbing fiber transmitter mediating inhibition of GABA release from interneurons. European Journal of Neuroscience *32*, 1843–1853.

Saviane, C. and Silver, R. A. (2006). Fast vesicle reloading and a large pool sustain high bandwidth transmission at a central synapse. Nature *439*, 983–7.

Scanziani, M., Capogna, M., Gähwiler, B. H. and Thompson, S. M. (1992). Presynaptic inhibition of miniature excitatory synaptic currents by baclofen and adenosine in the hippocampus. Neuron *9*, 919–27.

Scanziani, M., Gahwiler, B. H. and Thompson, S. M. (1995). Presynaptic inhibition of excitatory synaptic transmission by muscarinic and metabotropic glutamate receptor activation in the hippocampus: are Ca2+ channels involved? Neuropharmacology *34*, 1549–57.

Sceniak, M. P. and Sabo, S. L. (2010). Modulation of firing rate by background synaptic noise statistics in rat visual cortical neurons. J Neurophysiol *104*, 2792–805.

Schenk, U., Menna, E., Kim, T., Passafaro, M., Chang, S., Camilli, P. D. and Matteoli, M. (2005). A novel pathway for presynaptic mitogen-activated kinase activation via AMPA receptors. The Journal of Neuroscience *25*, 1654–63.

Schenk, U., Verderio, C., Benfenati, F. and Matteoli, M. (2003). Regulated delivery of AMPA receptor subunits to the presynaptic membrane. The EMBO Journal *22*, 558–68.

Scheuss, V., Schneggenburger, R. and Neher, E. (2002). Separation of presynaptic and postsynaptic contributions to depression by covariance analysis of successive EPSCs at the calyx of held synapse. The Journal of Neuroscience *22*, 728–39.

Schicker, K. W., Dorostkar, M. M. and Boehm, S. (2008). Modulation of transmitter release via presynaptic ligand-gated ion channels. Current Molecular Pharmacology *1*, 106–29.

Schikorski, T. and Stevens, C. F. (2001). Morphological correlates of functionally defined synaptic vesicle populations. Nature Neuroscience *4*, 391–5.

Schilling, K., Oberdick, J., Rossi, F. and Baader, S. L. (2008). Besides Purkinje cells and granule neurons: an appraisal of the cell biology of the interneurons of the cerebellar cortex. Histochemistry and Cell Biology *130*, 601–15.

Schmitz, D., Mellor, J., Breustedt, J. and Nicoll, R. A. (2003). Presynaptic kainate receptors impart an associative property to hippocampal mossy fiber long-term potentiation. Nature Neuroscience *6*, 1058–63.

Schmitz, D., Mellor, J. and Nicoll, R. A. (2001). Presynaptic kainate receptor mediation of frequency facilitation at hippocampal mossy fiber synapses. Science *291*, 1972–6.

Schmolesky, M. T., Weber, J. T., Zeeuw, C. I. D. and Hansel, C. (2002). The making of a complex spike: ionic composition and plasticity. Annals of the New York Academy of Sciences *978*, 359–90.

Schneggenburger, R. and Neher, E. (2000). Intracellular calcium dependence of transmitter release rates at a fast central synapse. Nature *406*, 889–93.

Schneggenburger, R., Sakaba, T. and Neher, E. (2002). Vesicle pools and short-term synaptic depression: lessons from a large synapse. Trends in Neurosciences *25*, 206–12.

Schoch, S., Deák, F., Königstorfer, A., Mozhayeva, M., Sara, Y., Südhof, T. C. and Kavalali, E. T. (2001). SNARE function analyzed in synaptobrevin/VAMP knockout mice. Science *294*, 1117–22.

Scholz, R., Berberich, S., Rathgeber, L., Kolleker, A., Köhr, G. and Kornau, H.-C. (2010). AMPA receptor signaling through BRAG2 and Arf6 critical for long-term synaptic depression. Neuron *66*, 768–80.

Schwarz, L. A., Hall, B. J. and Patrick, G. N. (2010). Activity-dependent ubiquitination of GluA1 mediates a distinct AMPA receptor endocytosis and sorting pathway. The Journal of Neuroscience *30*, 16718–29.

Schwenk, J., Harmel, N., Brechet, A., Zolles, G., Berkefeld, H., Müller, C. S., Bildl, W.,

Baehrens, D., Hüber, B., Kulik, A., Klöcker, N., Schulte, U. and Fakler, B. (2012). High-resolution proteomics unravel architecture and molecular diversity of native AMPA receptor complexes. Neuron *74*, 621–33.

Schwenk, J., Harmel, N., Zolles, G., Bildl, W., Kulik, A., Heimrich, B., Chisaka, O., Jonas, P., Schulte, U., Fakler, B. and Klöcker, N. (2009). Functional proteomics identify cornichon proteins as auxiliary subunits of AMPA receptors. Science *323*, 1313–9.

Scott, R., Lalic, T., Kullmann, D. M., Capogna, M. and Rusakov, D. A. (2008). Target-cell specificity of kainate autoreceptor and Ca2+-store-dependent short-term plasticity at hippocampal mossy fiber synapses. The Journal of Neuroscience *28*, 13139–49.

Segev, I. (1990). Computer study of presynaptic inhibition controlling the spread of action potentials into axonal terminals. Journal of Neurophysiology *63*, 987–98.

Semyanov, A. and Kullmann, D. M. (2001). Kainate receptor-dependent axonal depolarization and action potential initiation in interneurons. Nature Neuroscience *4*, 718–23.

Setou, M., Seog, D.-H., Tanaka, Y., Kanai, Y., Takei, Y., Kawagishi, M. and Hirokawa, N. (2002). Glutamate-receptor-interacting protein GRIP1 directly steers kinesin to dendrites. Nature *417*, 83–7.

Shahrezaei, V., Cao, A. and Delaney, K. R. (2006). Ca2+ from one or two channels controls fusion of a single vesicle at the frog neuromuscular junction. The Journal of Neuroscience *26*, 13240–9.

Shanks, N. F., Savas, J. N., Maruo, T., Cais, O., Hirao, A., Oe, S., Ghosh, A., Noda, Y., Greger, I. H., Yates, J. R. and Nakagawa, T. (2012). Differences in AMPA and kainate receptor interactomes facilitate identification of AMPA receptor auxiliary subunit GSG1L. Cell Reports *1*, 590–8.

Shapovalov, A. I., Shiriaev, B. I. and Tamarova, Z. A. (1979). Synaptic activity in motoneurons of the immature cat spinal cord in vitro. Effects of manganese and tetrodotoxin. Brain Research *160*, 524–8.

Shelley, C., Farrant, M. and Cull-Candy, S. G. (2012). TARP-associated AMPA receptors display an increased maximum channel conductance and multiple kinetically distinct open states. The Journal of Physiology *590*, 5723–38.

Shen, L., Liang, F., Walensky, L. D. and Huganir, R. L. (2000). Regulation of AMPA receptor GluR1 subunit surface expression by a 4.1N-linked actin cytoskeletal association. The Journal of Neuroscience *20*, 7932–40.

Sheng, J., He, L., Zheng, H., Xue, L., Luo, F., Shin, W., Sun, T., Kuner, T., Yue, D. T. and Wu, L.-G. (2012). Calcium-channel number critically influences synaptic strength and plasticity at the active zone. Nature Neuroscience *15*, 998–1006.

Sheperd, G. (2009). Creating modern neuroscience: the evolutionary 1950s. Oxford University Press USA.

Shi, Y., Lu, W., Milstein, A. D. and Nicoll, R. A. (2009). The stoichiometry of AMPA receptors and TARPs varies by neuronal cell type. Neuron *62*, 633–40.

Shi, Y., Suh, Y. H., Milstein, A. D., Isozaki, K., Schmid, S. M., Roche, K. W. and Nicoll, R. A. (2010). Functional comparison of the effects of TARPs and cornichons on AMPA

receptor trafficking and gating. Proceedings of the National Academy of Sciences of the United States of America *107*, 16315–9.

Shin, H., Wyszynski, M., Huh, K.-H., Valtschanoff, J. G., Lee, J.-R., Ko, J., Streuli, M., Weinberg, R. J., Sheng, M. and Kim, E. (2003). Association of the kinesin motor KIF1A with the multimodular protein liprin-alpha. The Journal of Biological Chemistry *278*, 11393–401.

Shinoda, Y., Sugiuchi, Y., Futami, T. and Izawa, R. (1992). Axon collaterals of mossy fibers from the pontine nucleus in the cerebellar dentate nucleus. Journal of Neurophysiology *67*, 547–60.

Shinozaki, H. and Konishi, S. (1970). Actions of several anthelmintics and insecticides on rat cortical neurones. Brain Research *24*, 368–71.

Shinozaki, H. and Shibuya, I. (1974). A new potent excitant, quisqualic acid: effects on crayfish neuromuscular junction. Neuropharmacology *13*, 665–72.

Shu, Y., Hasenstaub, A., Duque, A., Yu, Y. and McCormick, D. A. (2006). Modulation of intracortical synaptic potentials by presynaptic somatic membrane potential. Nature *441*, 761–5.

Sidach, S. S. and Mintz, I. M. (2000). Low-affinity blockade of neuronal N-type Ca channels by the spider toxin omega-agatoxin-IVA. The Journal of Neuroscience *20*, 7174–82.

Silver, R. A. (2010). Neuronal arithmetic. Nature Reviews Neuroscience *11*, 474–89.

Silver, R. A., Momiyama, A. and Cull-Candy, S. G. (1998). Locus of frequency-dependent depression identified with multiple-probability fluctuation analysis at rat climbing fibre-Purkinje cell synapses. The Journal of Physiology *510*, 881–902.

Sjöström, P. J., Turrigiano, G. G. and Nelson, S. B. (2003). Neocortical LTD via coincident activation of presynaptic NMDA and cannabinoid receptors. Neuron *39*, 641–54.

Sladeczek, F., Pin, J. P., Récasens, M., Bockaert, J. and Weiss, S. (1985). Glutamate stimulates inositol phosphate formation in striatal neurones. Nature *317*, 717–9.

Smart, T. G. and Paoletti, P. (2012). Synaptic neurotransmitter-gated receptors. Cold Spring Harb Perspect Biol *4*.

Smith, S. M., Chen, W., Vyleta, N. P., Williams, C., Lee, C.-H., Phillips, C. and Andresen, M. C. (2012). Calcium regulation of spontaneous and asynchronous neurotransmitter release. Cell Calcium *52*, 226–33.

Sobolevsky, A. I., Rosconi, M. P. and Gouaux, E. (2009). X-ray structure, symmetry and mechanism of an AMPA-subtype glutamate receptor. Nature *462*, 745–56.

Söllner, T., Bennett, M. K., Whiteheart, S. W., Scheller, R. H. and Rothman, J. E. (1993). A protein assembly-disassembly pathway in vitro that may correspond to sequential steps of synaptic vesicle docking, activation, and fusion. Cell *75*, 409–18.

Sommer, B., Keinänen, K., Verdoorn, T. A., Wisden, W., Burnashev, N., Herb, A., Köhler, M., Takagi, T., Sakmann, B. and Seeburg, P. H. (1990). Flip and flop: a cell-specific functional switch in glutamate-operated channels of the CNS. Science *249*, 1580–5.

Sommer, B., Köhler, M., Sprengel, R. and Seeburg, P. H. (1991). RNA editing in brain controls a determinant of ion flow in glutamate-gated channels. Cell *67*, 11–9.

Somogyi, P., Fritschy, J. M., Benke, D., Roberts, J. D. and Sieghart, W. (1996). The gamma 2 subunit of the GABAA receptor is concentrated in synaptic junctions containing the alpha 1 and beta 2/3 subunits in hippocampus, cerebellum and globus pallidus. Neuropharmacology *35*, 1425–44.

Sotelo, C. (2004). Cellular and genetic regulation of the development of the cerebellar system. Progress in Neurobiology *72*, 295–339.

Sotelo, C. and Llinás, R. (1972). Specialized membrane junctions between neurons in the vertebrate cerebellar cortex. The Journal of Cell Biology *53*, 271–89.

Soto, D., Coombs, I. D., Kelly, L., Farrant, M. and Cull-Candy, S. G. (2007). Stargazin attenuates intracellular polyamine block of calcium-permeable AMPA receptors. Nature Neuroscience *10*, 1260–7.

Soto, D., Coombs, I. D., Renzi, M., Zonouzi, M., Farrant, M. and Cull-Candy, S. G. (2009). Selective regulation of long-form calcium-permeable AMPA receptors by an atypical TARP, gamma-5. Nature Neuroscience *12*, 277–85.

Southan, A. P., Morris, N. P., Stephens, G. J. and Robertson, B. (2000). Hyperpolarization-activated currents in presynaptic terminals of mouse cerebellar basket cells. The Journal of Physiology *526*, 91–7.

Southan, A. P. and Robertson, B. (1998). Patch-clamp recordings from cerebellar basket cell bodies and their presynaptic terminals reveal an asymmetric distribution of voltage-gated potassium channels. The Journal of Neuroscience *18*, 948–55.

Southan, A. P. and Robertson, B. (2000). Electrophysiological characterization of voltage-gated K(+) currents in cerebellar basket and purkinje cells: Kv1 and Kv3 channel subfamilies are present in basket cell nerve terminals. The Journal of Neuroscience *20*, 114–22.

Spruston, N., Jaffe, D. B., Williams, S. H. and Johnston, D. (1993). Voltage- and space-clamp errors associated with the measurement of electrotonically remote synaptic events. Journal of Neurophysiology *70*, 781–802.

Stanley, E. F. (1993). Single calcium channels and acetylcholine release at a presynaptic nerve terminal. Neuron *11*, 1007–11.

Steiner, P., Alberi, S., Kulangara, K., Yersin, A., Sarria, J.-C. F., Regulier, E., Kasas, S., Dietler, G., Muller, D., Catsicas, S. and Hirling, H. (2005). Interactions between NEEP21, GRIP1 and GluR2 regulate sorting and recycling of the glutamate receptor subunit GluR2. The EMBO Journal *24*, 2873–84.

Stern-Bach, Y., Bettler, B., Hartley, M., Sheppard, P. O., O'Hara, P. J. and Heinemann, S. F. (1994). Agonist selectivity of glutamate receptors is specified by two domains structurally related to bacterial amino acid-binding proteins. Neuron *13*, 1345–57.

Stöckle, H. and ten Bruggencate, G. (1980). Fluctuation of extracellular potassium and calcium in the cerebellar cortex related to climbing fiber activity. Neuroscience *5*, 893–901.

Straub, C., Hunt, D. L., Yamasaki, M., Kim, K. S., Watanabe, M., Castillo, P. E. and

Tomita, S. (2011). Distinct functions of kainate receptors in the brain are determined by the auxiliary subunit Neto1. Nature Neuroscience *14*, 866.

Straub, C. and Tomita, S. (2012). The regulation of glutamate receptor trafficking and function by TARPs and other transmembrane auxiliary subunits. Current Opinion in Neurobiology *22*, 488–95.

Strømgaard, K., Jensen, L. S. and Vogensen, S. B. (2005). Polyamine toxins: development of selective ligands for ionotropic receptors. Toxicon *45*, 249–54.

Stuart, G. and Häusser, M. (1994). Initiation and spread of sodium action potentials in cerebellar Purkinje cells. Neuron *13*, 703–12.

Stuart, G. J. and Redman, S. J. (1992). The role of GABAA and GABAB receptors in presynaptic inhibition of Ia EPSPs in cat spinal motoneurones. The Journal of Physiology *447*, 675–92.

Studniarczyk, D., Coombs, I., Cull-Candy, S. G. and Farrant, M. (2013). TARP gamma-7 selectively enhances synaptic expression of calcium-permeable AMPARs. Nature Neuroscience *16*.

Suárez, L. M. and Solís, J. M. (2006). Taurine potentiates presynaptic NMDA receptors in hippocampal Schaffer collateral axons. The European Journal of Neuroscience *24*, 405–18.

Suárez, L. M., Suárez, F., Olmo, N. D., Ruiz, M., González-Escalada, J. R. and Solís, J. M. (2005). Presynaptic NMDA autoreceptors facilitate axon excitability: a new molecular target for the anticonvulsant gabapentin. The European Journal of Neuroscience *21*, 197–209.

Südhof, T. C. (2012). The presynaptic active zone. Neuron *75*, 11–25.

Sugihara, I., Wu, H. and Shinoda, Y. (1999). Morphology of single olivocerebellar axons labeled with biotinylated dextran amine in the rat. The Journal of Comparative Neurology *414*, 131–48.

Sugihara, I., Wu, H. S. and Shinoda, Y. (2001). The entire trajectories of single olivocerebellar axons in the cerebellar cortex and their contribution to Cerebellar compartmentalization. The Journal of Neuroscience *21*, 7715–23.

Sugiyama, H., Ito, I. and Hirono, C. (1987). A new type of glutamate receptor linked to inositol phospholipid metabolism. Nature *325*, 531–3.

Suh, Y. H., Terashima, A., Petralia, R. S., Wenthold, R. J., Isaac, J. T. R., Roche, K. W. and Roche, P. A. (2010). A neuronal role for SNAP-23 in postsynaptic glutamate receptor trafficking. Nature Neuroscience *13*, 338–43.

Sultan, F. and Bower, J. M. (1998). Quantitative Golgi study of the rat cerebellar molecular layer interneurons using principal component analysis. The Journal of Comparative Neurology *393*, 353–73.

Sun, H. Y., Bartley, A. F. and Dobrunz, L. E. (2009). Calcium-permeable presynaptic kainate receptors involved in excitatory short-term facilitation onto somatostatin interneurons during natural stimulus patterns. Journal of Neurophysiology *101*, 1043–55.

Sun, H. Y. and Dobrunz, L. E. (2006). Presynaptic kainate receptor activation is a novel mechanism for target cell-specific short-term facilitation at Schaffer collateral synapses. The Journal of Neuroscience *26*, 10796–807.

Sun, J., Pang, Z. P., Qin, D., Fahim, A. T., Adachi, R. and Südhof, T. C. (2007). A dual-Ca2+-sensor model for neurotransmitter release in a central synapse. Nature *450*, 676–82.

Sun, L. and Liu, S. J. (2007). Activation of extrasynaptic NMDA receptors induces a PKC-dependent switch in AMPA receptor subtypes in mouse cerebellar stellate cells. The Journal of Physiology *583*, 537–53.

Suter, K. J. and Jaeger, D. (2004). Reliable control of spike rate and spike timing by rapid input transients in cerebellar stellate cells. Neuroscience *124*, 305–17.

Sutton, M. A., Wall, N. R., Aakalu, G. N. and Schuman, E. M. (2004). Regulation of dendritic protein synthesis by miniature synaptic events. Science *304*, 1979–83.

Sutton, R. B., Fasshauer, D., Jahn, R. and Brunger, A. T. (1998). Crystal structure of a SNARE complex involved in synaptic exocytosis at 2.4 A resolution. Nature *395*, 347–53.

Suzuki, E., Kessler, M. and Arai, A. C. (2008). The fast kinetics of AMPA GluR3 receptors is selectively modulated by the TARPs gamma4 and gamma8. Molecular and Cellular Neuroscience *38*, 117–23.

Swanson, G. T., Kamboj, S. K. and Cull-Candy, S. G. (1997). Single-channel properties of recombinant AMPA receptors depend on RNA editing, splice variation, and subunit composition. The Journal of Neuroscience *17*, 58–69.

Swanson, G. T. and Sakai, R. (2009). Ligands for ionotropic glutamate receptors. Progress in Molecular and Subcellular Biology *46*, 123–57.

Sylwestrak, E. L. and Ghosh, A. (2012). Elfn1 regulates target-specific release probability at CA1-interneuron synapses. Science *338*, 536–40.

Szabo, A., Somogyi, J., Cauli, B., Lambolez, B., Somogyi, P. and Lamsa, K. P. (2012). Calcium-permeable AMPA receptors provide a common mechanism for LTP in glutamatergic synapses of distinct hippocampal interneuron types. The Journal of Neuroscience *32*, 6511–6.

Szapiro, G. and Barbour, B. (2007). Multiple climbing fibers signal to molecular layer interneurons exclusively via glutamate spillover. Nature Neuroscience *10*, 735–42.

Szatkowski, M., Barbour, B. and Attwell, D. (1990). Non-vesicular release of glutamate from glial cells by reversed electrogenic glutamate uptake. Nature *348*, 443–6.

Takago, H., Nakamura, Y. and Takahashi, T. (2005). G protein-dependent presynaptic inhibition mediated by AMPA receptors at the calyx of Held. Proceedings of the National Academy of Sciences of the United States of America *102*, 7368–73.

Takahashi, T., Forsythe, I. D., Tsujimoto, T., Barnes-Davies, M. and Onodera, K. (1996). Presynaptic calcium current modulation by a metabotropic glutamate receptor. Science *274*, 594–7.

Takasu, M. A., Dalva, M. B., Zigmond, R. E. and Greenberg, M. E. (2002). Modulation of

NMDA receptor-dependent calcium influx and gene expression through EphB receptors. Science *295*, 491–5.

Takayasu, Y., Iino, M., Kakegawa, W., Maeno, H., Watase, K., Wada, K., Yanagihara, D., Miyazaki, T., Komine, O., Watanabe, M., Tanaka, K. and Ozawa, S. (2005). Differential roles of glial and neuronal glutamate transporters in Purkinje cell synapses. The Journal of Neuroscience *25*, 8788–93.

Takayasu, Y., Iino, M., Shimamoto, K., Tanaka, K. and Ozawa, S. (2006). Glial glutamate transporters maintain one-to-one relationship at the climbing fiber-Purkinje cell synapse by preventing glutamate spillover. The Journal of Neuroscience *26*, 6563–72.

Takechi, H., Eilers, J. and Konnerth, A. (1998). A new class of synaptic response involving calcium release in dendritic spines. Nature *396*, 757–60.

Takeuchi, A. and Takeuchi, N. (1964). The effect on crayfish muscle of iontophoretically applied glutamate. The Journal of Physiology *170*, 296–317.

Takeuchi, T., Miyazaki, T., Watanabe, M., Mori, H., Sakimura, K. and Mishina, M. (2005). Control of synaptic connection by glutamate receptor delta2 in the adult cerebellum. The Journal of Neuroscience *25*, 2146–56.

Tank, D. W., Sugimori, M., Connor, J. A. and Llinás, R. R. (1988). Spatially resolved calcium dynamics of mammalian Purkinje cells in cerebellar slice. Science *242*, 773–7.

Tashiro, A., Dunaevsky, A., Blazeski, R., Mason, C. A. and Yuste, R. (2003). Bidirectional regulation of hippocampal mossy fiber filopodial motility by kainate receptors: a two-step model of synaptogenesis. Neuron *38*, 773–84.

Tedford, H. W. and Zamponi, G. W. (2006). Direct G protein modulation of Cav2 calcium channels. Pharmacological Reviews *58*, 837–62.

Teng, H. and Wilkinson, R. S. (2000). Clathrin-mediated endocytosis near active zones in snake motor boutons. The Journal of Neuroscience *20*, 7986–93.

Thach, W. T. (1968). Discharge of Purkinje and cerebellar nuclear neurons during rapidly alternating arm movements in the monkey. Journal of Neurophysiology *31*, 785–97.

Tichelaar, W., Safferling, M., Keinänen, K., Stark, H. and Madden, D. R. (2004). The Three-dimensional Structure of an Ionotropic Glutamate Receptor Reveals a Dimer-of-dimers Assembly. Journal of Molecular Biology *344*, 435–42.

Tikhonov, D. B. and Magazanik, L. G. (2009). Origin and molecular evolution of ionotropic glutamate receptors. Neuroscience and Behavioral Physiology *39*, 763–73.

Todd, K. J., Slatter, C. A. B. and Ali, D. W. (2004). Activation of ionotropic glutamate receptors on peripheral axons of primary motoneurons mediates transmitter release at the zebrafish NMJ. Journal of Neurophysiology *91*, 828–40.

Tomita, S., Adesnik, H., Sekiguchi, M., Zhang, W., Wada, K., Howe, J. R., Nicoll, R. A. and Bredt, D. S. (2005). Stargazin modulates AMPA receptor gating and trafficking by distinct domains. Nature *435*, 1052–8.

Tomita, S., Chen, L., Kawasaki, Y., Petralia, R. S., Wenthold, R. J., Nicoll, R. A. and Bredt, D. S. (2003). Functional studies and distribution define a family of

transmembrane AMPA receptor regulatory proteins. The Journal of Cell Biology *161*, 805–16.

Tomita, S., Sekiguchi, M., Wada, K., Nicoll, R. A. and Bredt, D. S. (2006). Stargazin controls the pharmacology of AMPA receptor potentiators. Proceedings of the National Academy of Sciences of the United States of America *103*, 10064–7.

Toth, K., Suares, G., Lawrence, J. J., Philips-Tansey, E. and McBain, C. J. (2000). Differential mechanisms of transmission at three types of mossy fiber synapse. The Journal of Neuroscience *20*, 8279–89.

Traynelis, S. F., Wollmuth, L. P., Mcbain, C. J., Menniti, F. S., Vance, K. M., Ogden, K. K., Hansen, K. B., Yuan, H., Myers, S. J. and Dingledine, R. (2010). Glutamate Receptor Ion Channels: Structure, Regulation, and Function. Pharmacological Reviews *62*, 405–496.

Trendelenburg, U. (1957). The action of morphine on the superior cervical ganglion and on the nictitating membrane of the cat. British Journal of Pharmacology and Chemotherapy *12*, 79–85.

Tretter, V., Ehya, N., Fuchs, K. and Sieghart, W. (1997). Stoichiometry and assembly of a recombinant GABAA receptor subtype. The Journal of Neuroscience *17*, 2728–37.

Trigo, F. F., Bouhours, B., Rostaing, P., Papageorgiou, G., Corrie, J. E. T., Triller, A., Ogden, D. and Marty, A. (2010). Presynaptic miniature GABAergic currents in developing interneurons. Neuron *66*, 235–47.

Trigo, F. F., Chat, M. and Marty, A. (2007). Enhancement of GABA release through endogenous activation of axonal GABA(A) receptors in juvenile cerebellum. The Journal of Neuroscience *27*, 12452–63.

Trimble, W. S., Cowan, D. M. and Scheller, R. H. (1988). VAMP-1: a synaptic vesicle-associated integral membrane protein. Proceedings of the National Academy of Sciences of the United States of America *85*, 4538–42.

Trussell, L. O., Zhang, S. and Raman, I. M. (1993). Desensitization of AMPA receptors upon multiquantal neurotransmitter release. Neuron *10*, 1185–96.

Tsien, R. Y. (1981). A non-disruptive technique for loading calcium buffers and indicators into cells. Nature *290*, 527–8.

Tsuji, S. (2006). René Couteaux (1909-1999) and the morphological identification of synapses. Biology of the Cell *98*, 503–9.

Turecek, R. and Trussell, L. O. (2001). Presynaptic glycine receptors enhance transmitter release at a mammalian central synapse. Nature *411*, 587–90.

Turetsky, D., Garringer, E. and Patneau, D. K. (2005). Stargazin modulates native AMPA receptor functional properties by two distinct mechanisms. The Journal of Neuroscience *25*, 7438–48.

Tzingounis, A. V. and Wadiche, J. I. (2007). Glutamate transporters: confining runaway excitation by shaping synaptic transmission. Nature Reviews Neuroscience *8*, 935–47.

Ulbrich, M. H. and Isacoff, E. Y. (2008). Rules of engagement for NMDA receptor subunits. Proceedings of the National Academy of Sciences of the United States of America *105*, 14163–8.

Vandenberghe, W., Nicoll, R. A. and Bredt, D. S. (2005). Stargazin is an AMPA receptor auxiliary subunit. Proceedings of the National Academy of Sciences of the United States of America *102*, 485–90.

Varela, J. A., Sen, K., Gibson, J., Fost, J., Abbott, L. F. and Nelson, S. B. (1997). A quantitative description of short-term plasticity at excitatory synapses in layer 2/3 of rat primary visual cortex. The Journal of Neuroscience *17*, 7926–40.

Verhage, M., Maia, A. S., Plomp, J. J., Brussaard, A. B., Heeroma, J. H., Vermeer, H., Toonen, R. F., Hammer, R. E., van den Berg, T. K., Missler, M., Geuze, H. J. and Südhof, T. C. (2000). Synaptic assembly of the brain in the absence of neurotransmitter secretion. Science *287*, 864–9.

Vesikansa, A., Sakha, P., Kuja-Panula, J., Molchanova, S., Rivera, C., Huttunen, H. J., Rauvala, H., Taira, T. and Lauri, S. E. (2012). Expression of GluK1c underlies the developmental switch in presynaptic kainate receptor function. Scientific Reports *2*, 310.

Vincent, P. and Marty, A. (1996). Fluctuations of inhibitory postsynaptic currents in Purkinje cells from rat cerebellar slices. The Journal of Physiology *494*, 183–99.

Vizi, E. S. (1979). Presynaptic modulation of neurochemical transmission. Progress in Neurobiology *12*, 181–290.

von Engelhardt, J., Mack, V., Sprengel, R., Kavenstock, N., Li, K. W., Stern-Bach, Y., Smit, A. B., Seeburg, P. H. and Monyer, H. (2010). CKAMP44: a brain-specific protein attenuating short-term synaptic plasticity in the dentate gyrus. Science *327*, 1518–22.

Voogd, J., Gerrits, N. M. and Ruigrok, T. J. (1996). Organization of the vestibulocerebellum. Annals of the New York Academy of Sciences *781*, 553–79.

Voogd, J. and Glickstein, M. (1998). The anatomy of the cerebellum. Trends in Neurosciences *21*, 370–5.

Vorobjev, V. S. (1991). Vibrodissociation of sliced mammalian nervous tissue. The Journal of Neuroscience Methods *38*, 145–50.

Vyleta, N. P. and Smith, S. M. (2011). Spontaneous glutamate release is independent of calcium influx and tonically activated by the calcium-sensing receptor. The Journal of Neuroscience *31*, 4593–606.

Wadiche, J. I. and Jahr, C. E. (2001). Multivesicular release at climbing fiber-Purkinje cell synapses. Neuron *32*, 301–13.

Wadiche, J. I. and Jahr, C. E. (2005). Patterned expression of Purkinje cell glutamate transporters controls synaptic plasticity. Nature Neuroscience *8*, 1329–34.

Wall, M. J. and Usowicz, M. M. (1997). Development of action potential-dependent and independent spontaneous GABAA receptor-mediated currents in granule cells of postnatal rat cerebellum. European Journal of Neuroscience *9*, 533–48.

Wang, L.-Y., Neher, E. and Taschenberger, H. (2008). Synaptic vesicles in mature calyx of Held synapses sense higher nanodomain calcium concentrations during action potential-evoked glutamate release. The Journal of Neuroscience *28*, 14450–8.

Wang, P. Y., Petralia, R. S., Wang, Y.-X., Wenthold, R. J. and Brenowitz, S. D. (2011).

Functional NMDA Receptors at Axonal Growth Cones of Young Hippocampal Neurons. The Journal of Neuroscience *31*, 9289–97.

Wang, Z., Edwards, J. G., Riley, N., Provance, D. W., Karcher, R., Li, X.-D., Davison, I. G., Ikebe, M., Mercer, J. A., Kauer, J. A. and Ehlers, M. D. (2008). Myosin Vb mobilizes recycling endosomes and AMPA receptors for postsynaptic plasticity. Cell *135*, 535–48.

Washbourne, P., Thompson, P. M., Carta, M., Costa, E. T., Mathews, J. R., Lopez-Benditó, G., Molnár, Z., Becher, M. W., Valenzuela, C. F., Partridge, L. D. and Wilson, M. C. (2002). Genetic ablation of the t-SNARE SNAP-25 distinguishes mechanisms of neuroexocytosis. Nature Neuroscience *5*, 19–26.

Watkins, J. C. and Jane, D. E. (2006). The glutamate story. British Journal of Pharmacology *147*, 100–8.

Weber, J. P., Reim, K. and Sørensen, J. B. (2010). Opposing functions of two sub-domains of the SNARE-complex in neurotransmission. The EMBO Journal *29*, 2477–90.

Wilhelm, B. G., Groemer, T. W. and Rizzoli, S. O. (2010). The same synaptic vesicles drive active and spontaneous release. Nature Neuroscience *13*, 1454–1456.

Williams, C., Chen, W., Lee, C.-H., Yaeger, D., Vyleta, N. P. and Smith, S. M. (2012). Coactivation of multiple tightly coupled calcium channels triggers spontaneous release of GABA. Nature Neuroscience *15*, 1195–97.

Williams, S. R. and Mitchell, S. J. (2008). Direct measurement of somatic voltage clamp errors in central neurons. Nature Neuroscience *11*, 790–8.

Wilson, R. I., Kunos, G. and Nicoll, R. A. (2001). Presynaptic specificity of endocannabinoid signaling in the hippocampus. Neuron *31*, 453–62.

Wisden, W. and Seeburg, P. H. (1993). A complex mosaic of high-affinity kainate receptors in rat brain. The Journal of Neuroscience *13*, 3582–98.

Woodhall, G., Evans, D. I., Cunningham, M. O. and Jones, R. S. (2001). NR2B-containing NMDA autoreceptors at synapses on entorhinal cortical neurons. Journal of Neurophysiology *86*, 1644–51.

Wyszynski, M., Kim, E., Dunah, A. W., Passafaro, M., Valtschanoff, J. G., Serra-Pagès, C., Streuli, M., Weinberg, R. J. and Sheng, M. (2002). Interaction between GRIP and liprin-alpha/SYD2 is required for AMPA receptor targeting. Neuron *34*, 39–52.

Xu, H., Wu, L.-J., Zhao, M.-G., Toyoda, H., Vadakkan, K. I., Jia, Y., Pinaud, R. and Zhuo, M. (2006). Presynaptic regulation of the inhibitory transmission by GluR5-containing kainate receptors in spinal substantia gelatinosa. Molecular Pain *2*, 29.

Xu, J., Mashimo, T. and Südhof, T. C. (2007). Synaptotagmin-1, -2, and -9: Ca(2+) sensors for fast release that specify distinct presynaptic properties in subsets of neurons. Neuron *54*, 567–81.

Xu, J. and Wu, L.-G. (2005). The decrease in the presynaptic calcium current is a major cause of short-term depression at a calyx-type synapse. Neuron *46*, 633–45.

Xu-Friedman, M. A., Harris, K. M. and Regehr, W. G. (2001). Three-dimensional comparison of ultrastructural characteristics at depressing and facilitating synapses onto cerebellar Purkinje cells. The Journal of Neuroscience *21*, 6666–72.

Yamada, K., Fukaya, M., Shibata, T., Kurihara, H., Tanaka, K., Inoue, Y. and Watanabe, M. (2000). Dynamic transformation of Bergmann glial fibers proceeds in correlation with dendritic outgrowth and synapse formation of cerebellar Purkinje cells. The Journal of Comparative Neurology *418*, 106–20.

Yamasaki, M., Hashimoto, K. and Kano, M. (2006). Miniature Synaptic Events Elicited by Presynaptic Ca2+ Rise Are Selectively Suppressed by Cannabinoid Receptor Activation in Cerebellar Purkinje Cells. The Journal of Neuroscience *26*, 86.

Yamashita, T., Eguchi, K., Saitoh, N., von Gersdorff, H. and Takahashi, T. (2010). Developmental shift to a mechanism of synaptic vesicle endocytosis requiring nanodomain Ca2+. Nature Neuroscience *13*, 838–44.

Yamazaki, M., Araki, K., Shibata, A. and Mishina, M. (1992). Molecular cloning of a cDNA encoding a novel member of the mouse glutamate receptor channel family. Biochemical and Biophysical Research Communications *183*, 886–92.

Yamazaki, M., Fukaya, M., Hashimoto, K., Yamasaki, M., Tsujita, M., Itakura, M., Abe, M., Natsume, R., Takahashi, M., Kano, M., Sakimura, K. and Watanabe, M. (2010). TARPs gamma-2 and gamma-7 are essential for AMPA receptor expression in the cerebellum. European Journal of Neuroscience *31*, 2204–20.

Yamazaki, M., Ohno-Shosaku, T., Fukaya, M., Kano, M., Watanabe, M. and Sakimura, K. (2004). A novel action of stargazin as an enhancer of AMPA receptor activity. Neuroscience Research *50*, 369–74.

Yan, D., Yamasaki, M., Straub, C., Watanabe, M. and Tomita, S. (2013). Homeostatic control of synaptic transmission by distinct glutamate receptors. Neuron *78*, 687–99.

Yang, J., Woodhall, G. L. and Jones, R. S. G. (2006). Tonic facilitation of glutamate release by presynaptic NR2B-containing NMDA receptors is increased in the entorhinal cortex of chronically epileptic rats. The Journal of Neuroscience *26*, 406–10.

Yang, J. H., Sklar, P., Axel, R. and Maniatis, T. (1997). Purification and characterization of a human RNA adenosine deaminase for glutamate receptor B pre-mRNA editing. Proceedings of the National Academy of Sciences of the United States of America *94*, 4354–9.

Yang, Y.-M. and Wang, L.-Y. (2006). Amplitude and kinetics of action potential-evoked Ca2+ current and its efficacy in triggering transmitter release at the developing calyx of held synapse. The Journal of Neuroscience *26*, 5698–708.

Yao, J., Gaffaney, J. D., Kwon, S. E. and Chapman, E. R. (2011). Doc2 is a Ca2+ sensor required for asynchronous neurotransmitter release. Cell *147*, 666–77.

Yao, Y., Harrison, C. B., Freddolino, P. L., Schulten, K. and Mayer, M. L. (2008). Molecular mechanism of ligand recognition by NR3 subtype glutamate receptors. The EMBO Journal *27*, 2158–70.

Yoon, T.-Y., Lu, X., Diao, J., Lee, S.-M., Ha, T. and Shin, Y.-K. (2008). Complexin and Ca2+ stimulate SNARE-mediated membrane fusion. Nature Structural and Molecular Biology *15*, 707–13.

Youn, D.-H. and Randic, M. (2004). Modulation of excitatory synaptic transmission in the spinal substantia gelatinosa of mice deficient in the kainate receptor GluR5 and/or GluR6 subunit. The Journal of Physiology *555*, 683–98.

Yuan, H., Hansen, K. B., Vance, K. M., Ogden, K. K. and Traynelis, S. F. (2009). Control of NMDA receptor function by the NR2 subunit amino-terminal domain. The Journal of Neuroscience *29*, 12045–58.

Yudowski, G. A., Puthenveedu, M. A., Leonoudakis, D., Panicker, S., Thorn, K. S., Beattie, E. C. and von Zastrow, M. (2007). Real-time imaging of discrete exocytic events mediating surface delivery of AMPA receptors. The Journal of Neuroscience *27*, 11112–21.

Zenisek, D. (2008). Vesicle association and exocytosis at ribbon and extraribbon sites in retinal bipolar cell presynaptic terminals. Proceedings of the National Academy of Sciences of the United States of America *105*, 4922–7.

Zhang, W., St-Gelais, F., Grabner, C. P., Trinidad, J. C., Sumioka, A., Morimoto-Tomita, M., Kim, K. S., Straub, C., Burlingame, A. L., Howe, J. R. and Tomita, S. (2009). A transmembrane accessory subunit that modulates kainate-type glutamate receptors. Neuron *61*, 385–96.

Zhao, H. M., Wenthold, R. J., Wang, Y. X. and Petralia, R. S. (1997). Delta-glutamate receptors are differentially distributed at parallel and climbing fiber synapses on Purkinje cells. Journal of Neurochemistry *68*, 1041–52.

Zorumski, C. F., Yang, J. and Fischbach, G. D. (1989). Calcium-dependent, slow desensitization distinguishes different types of glutamate receptors. Cellular and Molecular Neurobiology *9*, 95–104.

Zucker, R. S. and Regehr, W. G. (2002). Short-term synaptic plasticity. Annual Reviews Physiology *64*, 355–405.